Solid Mechanics and Its Applications

Sohrob Mottaghi
Rene Gabbai
Haym Benaroya

An Analytical Mechanics Framework for Flow-Oscillator Modeling of Vortex-Induced Bluff-Body Oscillations

Springer

Solid Mechanics and Its Applications

Volume 260

The fundamental questions arising in mechanics are: Why?, How?, and How much? The aim of this series is to provide lucid accounts written by authoritative researchers giving vision and insight in answering these questions on the subject of mechanics as it relates to solids. The scope of the series covers the entire spectrum of solid mechanics. Thus it includes the foundation of mechanics; variational formulations; computational mechanics; statics, kinematics and dynamics of rigid and elastic bodies; vibrations of solids and structures; dynamical systems and chaos; the theories of elasticity, plasticity and viscoelasticity; composite materials; rods, beams, shells and membranes; structural control and stability; soils, rocks and geomechanics; fracture; tribology; experimental mechanics; biomechanics and machine design. The median level of presentation is the first year graduate student. Some texts are monographs defining the current state of the field; others are accessible to final year undergraduates; but essentially the emphasis is on readability and clarity.

Springer and Professors Barber and Klarbring welcome book ideas from authors. Potential authors who wish to submit a book proposal should contact Dr. Mayra Castro, Senior Editor, Springer Heidelberg, Germany, e-mail: mayra.castro@springer.com

Indexed by SCOPUS, Ei Compendex, EBSCO Discovery Service, OCLC, ProQuest Summon, Google Scholar and SpringerLink.

More information about this series at http://www.springer.com/series/6557

Sohrob Mottaghi · Rene Gabbai ·
Haym Benaroya

An Analytical Mechanics Framework for Flow-Oscillator Modeling of Vortex-Induced Bluff-Body Oscillations

Springer

Sohrob Mottaghi
FAA William J. Hughes Technical Center
Atlantic City International Airport
Atlantic City, NJ, USA

Rene Gabbai
Pratt & Whitney
East Hartford, CT, USA

Haym Benaroya
Mechanical and Aerospace Engineering
Rutgers University
Piscataway, NJ, USA

ISSN 0925-0042 ISSN 2214-7764 (electronic)
Solid Mechanics and Its Applications
ISBN 978-3-030-26131-3 ISBN 978-3-030-26133-7 (eBook)
https://doi.org/10.1007/978-3-030-26133-7

This Springer imprint is published by the registered company Springer Nature Switzerland AG
The registered company address is: Gewerbestrasse 11, 6330 Cham, Switzerland

We dedicate this book as follows:

I would like to dedicate this book to my sister Sarah Mottaghi.
—Sohrob Mottaghi

I would like dedicate this book to my family: to my wife Jessica and children Miriam and Isabelle for keeping me grounded, and to my parents Jacques and Mary for instilling in me a sense of wonder and intellectual curiosity.
—Rene Gabbai

I would like to dedicate this book to my family: my wife Shelley, my mother Esther, my children Adam, Ana, Liz, and Tiffany, my sister Dahlia and her husband Ron, my nephew Max, and to the memory of my father Alfred.
—Haym Benaroya

Preface

It is a pleasure to complete this book that is devoted to the fundamental study of vortex-induced oscillations. This study is borne of the desire to understand such fluid–structure interactions at a fundamental level, and to derive mathematical models within the framework of the flow-oscillator paradigm.

This monograph is a compendium of the efforts of the authors over two decades. We view it as a preliminary effort that has many opportunities for extensions and added insights by others who are so interested.

We find that the variational framework for such modeling efforts provides certain advantages for the derivation of the governing equations, but these equations are not unique. Rather, the derived equations depend on the physical assumptions made initially and throughout the analysis. Our primary goal has been to create a modeling framework within which flow-oscillators can reside, and to show how a number of well-known flow-oscillators, formulated by others, can be viewed as being a part of this framework. An advantage of this framework is that assumptions are explicit and can be removed or changed. Other assumptions can be added. Each of these alterations leads to different governing equations, as one would expect. But the assumptions are explicit, physical, understood, and open to debate.

We appreciate the work of many of our colleagues on this problem of vortex-induced oscillations, and from whom we have learned much. We hope that this effort by us resulting in a new perspective proves to be interesting and useful.

Piscataway, USA
June 2019

Haym Benaroya

Acknowledgements

We are pleased to acknowledge the following people. Dr. Tom Swean, while he was a program manager at ONR, supported our work for many years. We discussed the science and engineering of vortex-induced vibration as colleagues, and we will always be grateful for his insights and his support.

We thank Dr. Yuriy Gulak for our discussions on this subject, as well as many other subjects, over the past decades. His deep insights and knowledge, and friendship, are gratefully and warmly appreciated.

We thank Dr. Joey Sanchez for his valuable assistance with the integration of the various documents that represented our work of over two decades, over multiple computer systems and TEX operating systems, that led to this monograph.

SM wishes to express his gratitude to Prof. Haym Benaroya for his continuous mentorship in the field of vortex-induced vibration. He is also thankful to RDG since SM's studies were, in part, inspired by RDG's earlier work in this field.

RDG would like to express his sincere gratitude to his coauthors. In particular, he would like to thank Prof. Haym Benaroya for introducing him to the fascinating field that is vortex-induced vibration.

HB would like to acknowledge Dr. Timothy Wei for our early collaborations in this research area. HB also sincerely acknowledges the great pleasure of working with his two coauthors, who are very talented researchers as well as being kind and generous persons, from whom much has been learned.

Contents

Chapter 1
Introduction

Abstract This chapter introduces the focus problem of this monograph, vortex-induced oscillations, which is within the fluid–structure interaction class of problems. The organization of the monograph is provided.

1.1 Background and Overview

The problem of fluid–structure interaction (FSI) has long been one of the great challenges in engineering. It is a crucial consideration in the design of many bluff-body engineering structures, such as offshore structures, skyscrapers, aircraft, and bridges. It is also a serious design consideration for aerodynamic bodies, such as wings, but this is beyond our scope. While the importance of the subject has been understood for well over a century, it has been only in the past few decades that efforts have been made to analytically model the general behavior of such systems. Parallel to analytical attempts, many experiments have been devoted to gathering data and interpreting such interactions. Consequently, analytical dynamics-based modeling of such problems has evolved with coupling to experimental data resulting in various semi-analytical representations. Generally, attempts have been made to model vortex-induced vibration (VIV) problems as few degrees-of-freedom (DOF) oscillatory models; therefore, they are referred to as *reduced-order* models.

Due to the complexity of the interactions between fluid and structure, in particular for vortex-induced vibration, a variety of efforts have been undertaken to explain the physics of this coupling. Initially, the efforts were experimental so that "reality" could be visualized, and then explained. Tremendous efforts have led to impressive results by numerous experimentalists along with an extensive phenomenological understanding of this behavior. The practical needs of industry required more than just understanding; it required designs of structures and machines that could operate safely for long periods of time in fluid environments where complex interactions occur. For vortex-induced oscillations, this led to the need for design equations that were representative of the experimental data, as well as technologies to minimize the effects of shedding vortices. Physical theory lagged experimental data, of course, but the need for governing design equations was there, resulting in the formulation

S. Mottaghi et al., *An Analytical Mechanics Framework for Flow-Oscillator Modeling of Vortex-Induced Bluff-Body Oscillations*, Solid Mechanics and Its Applications 260,
https://doi.org/10.1007/978-3-030-26133-7_1

of governing equations that qualitatively mimicked the data and could be made to fit the data in specific instances by the use of nonphysical "arbitrary" parameters. Such semi-empirical equations have formed the backbone of reduced-order modeling for VIV.

Our monograph represents a line of work with the goal of laying a fundamental foundation for such reduced-order modeling. This effort is based on the variational principles of mechanics. Before we go to that work in Chap. 4 and subsequent chapters, we review the efforts of the community. In Chap. 2, we provide a representative review of the literature for bluff bodies. In Chap. 3, we summarize variational mechanics. In Chaps. 4–7, we provide detailed derivations of a sequence of our analytical dynamics modeling efforts of VIV.

1.2 Introduction to the Model Problem

For experimental studies of VIV, certain types of structural configurations have been preferred in the literature, where a rigid solid body with one or two degree(s)-of-freedom is immersed in a flow. While the experiments have been conducted on a variety of solid shapes (and occasionally on flexible bodies), *reduced-order semi-analytical models* have been generally developed for single DOF rigid bluff bodies, specifically for circular cylinders. The most commonly used model, called the *model problem* [5], is a type of inverted solid pendulum that is immersed in a flow, rests on elastic supports and can only move transversely to the flow direction. A second model is the translating cylinder. Schematic diagrams of elements of two representative configurations of the *model problem* are shown in Figs. 1.1 and 1.2. The *model problem* has been widely used since it possesses a simple geometric configuration, and yet, it exhibits the majority of the nonlinear behaviors observed in VIV systems. Consequently, the majority of VIV experiments have been conducted based on the *model problem*. Both in experimental and analytical studies, the flow is controlled or considered to be two dimensional for all time, as are the shedding vortices.

The purpose of this work is to present our theoretical studies that derive reduced-order models from first principles, where assumptions are explicitly stated. Therefore, experimental observations are not the main focus of this research work. However, a few key features observed in the experimental studies are summarized for those who are not familiar with the subject. An in-depth review of experimental studies of VIV can be found in [4].

Starting with the stagnant fluid, if the speed of the flow past a bluff-body cylinder is increased, three different behavioral regimes are identified: *pre-synchronization*, *resonant synchronization*, and *classical lock-in*. Pre-synchronization is the first regime where the structure starts oscillating and vortices are first observed. The amplitudes of the structural oscillations are low and the vortices' strength are weak to moderate. Observed in this region is a beating behavior, that is, the peak amplitudes of structural response increase and decrease gradually as the structure oscillates. Moreover, the flow drives the structure in this region.

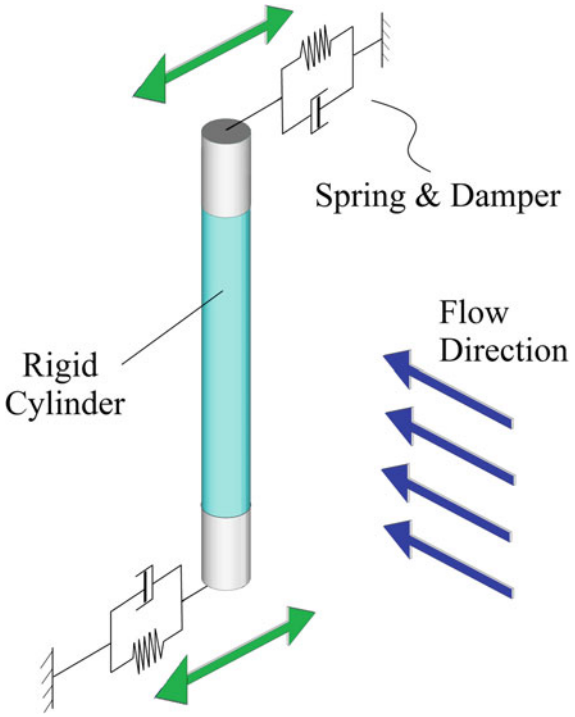

Fig. 1.1 A representative configuration of the model problem: translating cylinder

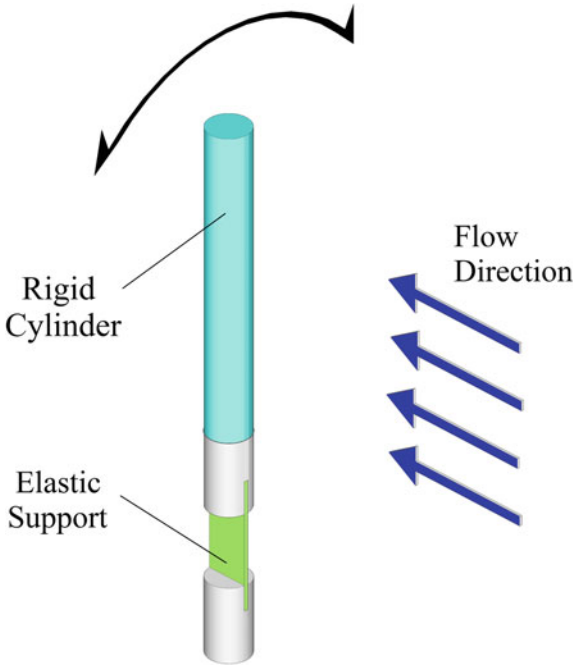

Fig. 1.2 A representative configuration of the model problem: inverted pendulum

As the average velocity of the flow is increased, vortices become stronger until the frequency of the vortex shedding reaches the natural frequency of the structure, where near-resonant behavior is observed. Thus, the structural response reaches a maximum and this is called the *resonant synchronization* region. Similar to the *pre-synchronization* region, beating behavior is noticeable but weaker, and the structure remains driven by the flow.

If the flow velocity is increased further, constant structural oscillation amplitude and frequency are observed for a range of flow velocities. This phenomenon is called *classical lock-in*. Unlike the other two regions, the flow is modulated by the structure and the observed vortices are the least organized. The existence of three distinct regimes in the frequency–amplitude response curves of an inverted pendulum is shown in Fig. 1.3. As in Fig. 2.1, many experiments show the existence of hysteretic behavior, where the maximum amplitude of the oscillations are larger as the velocity is increased than when it is decreased. VIV is a complicated phenomenon. The structural response depends on many factors, such as shedding frequency, Reynolds number, material damping, structural stiffness, surface roughness, cylinder length, density of the fluid, and mass of the cylinder, [4, 8]. Therefore,

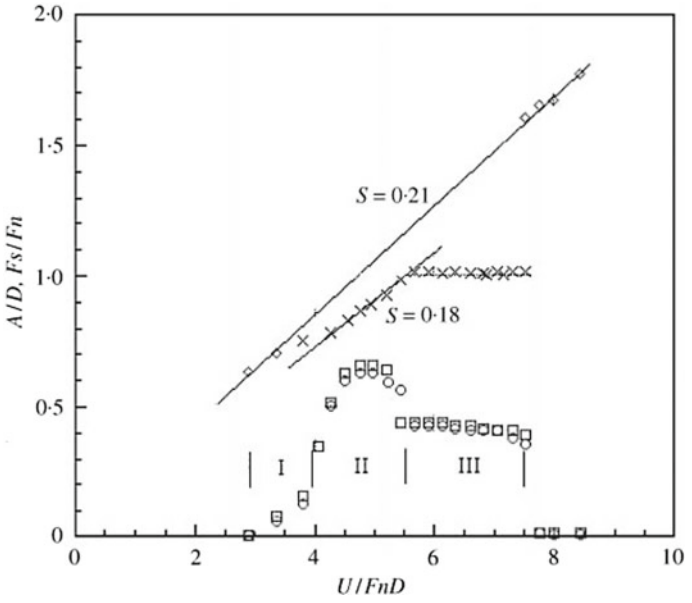

Fig. 1.3 The frequency–amplitude response curves of an inverted pendulum, where A is the amplitude of oscillation, D is the diameter of the cylinder, F_s is the frequency of oscillation, F_n is the natural frequency of the cylinder, U represents the fluid velocity; □, ◯ amplitude of oscillation for two independent but identical experimental runs; × frequency of oscillation and vortex shedding frequency in which VIV was observed; ◇ frequency of vortex shedding where the cylinder was stationary; *I* pre-synchronization; *II* resonant synchronization; *III* classic lock-in [2]. Reprinted with permission

reduced-order modeling of VIV has evolved in parallel to experiments in order to quantify our understanding of this phenomenon.

Efforts to model VIV as reduced-order systems can be divided into two categories: empirical models and first-principles models. Moreover, the empirical models can be divided into two subcategories: wake-oscillator (wake-body) models and experimental force-coefficient models. The wake-oscillator models are based on the assumption that an immersed structure in a flow experiences nonlinear oscillator-like hydrodynamic forces. Therefore, the aim is to obtain nonlinear fluid force equations from the experimentally acquired data that can be coupled with the structural equation of motion. One of the early models is the one proposed by Hartlen and Currie [6]. They used a van der Pol-type fluid oscillator to model the fluid–structure system,

$$\ddot{x} + 2\zeta\dot{x} + x = a\omega_0^2 C_L \tag{1.1}$$

$$\ddot{C}_L - \alpha\omega_0\dot{C}_L + \frac{\gamma}{\omega_0}\dot{C}_L^3 + \omega_0^2 C_L = \beta\dot{x}, \tag{1.2}$$

where a, ω_0, and ζ are the known structural parameters, and the fluid parameters α, β, and γ are found experimentally.

The experimental force-coefficient models are single degree-of-freedom models. They only include a single forcing function obtained experimentally. Generally, the empirical models have relative success in capturing the features of VIV. However, these models neglect the dynamic coupling between the flow and the structure by only considering the forces as they are seen by the structure. Therefore, they do not provide much understanding of the physics of the problem, as the fluid and structure exchange energy. These *ad hoc* methods are outside the scope of this work that is focused on first-principles models, specifically, using variational principles. Useful reviews of the empirical models can be found in [1, 3, 4]. While variational principles have been known for well over a century, it was not until 1973 that McIver was among the first researchers to propose the use of variational methods in modeling fluid–structure interaction problems [7]. Also, the work by Benaroya and Wei in 2000 is one of the earliest attempts to use such methods for VIV problems [2]. Consequently, the literature on the subject is very limited.

In the next chapter, we provide an overview of the literature on VIV. The field is vast and our review should be considered to be representative rather than comprehensive. This review is intended to provide the reader a feel for the physics of the dynamic behavior, and a summary of relevant modeling efforts.

References

1. Benaroya H, Gabbai RD (2008) Modelling vortex-induced fluid structure interaction. Philos Trans Math Phys Eng Sci 366(1868):1231–1274
2. Benaroya H, Wei T (2000) Hamilton's principle for external viscous fluid structure interactions. J Sound Vib 238(1):113–145

3. Gabbai RD (2006) Hamilton's principle for fluid-structure interaction and applications to the free-vibration of an elastically-mounted cylinder. PhD dissertation, Rutgers, the State University of New Jersey, New Brunswick, NJ
4. Gabbai RD, Benaroya H (2005) An overview of modeling and experiments of vortex-induced vibration of circular cylinders. J Sound Vib 282:575–616
5. Gabbai RD, Benaroya H (2008) A first-principles derivation procedure for wake-body models in vortex-induced vibration: proof-of-concept. J Sound Vib 312:19–38
6. Hartlen RT, Currie IG (1970) Lift-oscillator model of vortex induced vibration. J Eng Mech 96(5):577–591
7. McIver DB (1973) Hamilton's principle for systems of changing mass. J Eng Mech 7(3):249–261
8. Sarpkaya T (2004) A critical review of the intrinsic nature of vortex-induced vibrations. J Fluids Struct 19(4):389–447

Chapter 2
Literature in Vortex-Induced Oscillations

Abstract A literature review is provided in this chapter of vortex-induced oscillations. While the literature is vast, our review is selective but representative of the field. Reviewed are: (i) experimental studies on: fluid forces, three-dimensionality and free-surface effects, vortex-shedding modes and synchronization regions, frequency dependence of the added mass, the dynamics of cylinders with low mass-damping; (ii) semi-empirical models: wake-oscillator, single degree-of-freedom, force decomposition; (iii) variational approaches; and (iv) numerical approaches.

2.1 Introduction

Vortex-induced vibration (VIV) occurs when shedding vortices (a von Kármán vortex street) exert oscillatory forces on a cylinder in the direction perpendicular to both the flow and the structure. The structure starts to oscillate due to these forces if it is not fixed. For fixed cylinders, the frequency of shedding is related to the nondimensional Strouhal number, defined as $S = f_v D/U$, where f_v is the frequency of vortex shedding, U is the steady velocity of the flow, and D is the diameter of the circular cylinder. The Strouhal number is found to be nearly constant with a value of 0.2 for a large range of Reynolds numbers. This range is often called the subcritical range and spans the Reynolds number range from 300 to 2×10^5 [19].

For flow past cylinders that are free to vibrate, the phenomenon of synchronization or lock-in is observed. For low flow speeds, the cylinder will initially respond at the frequency f_v. This frequency is fixed by the Strouhal number. As the flow speed is increased, the shedding frequency approaches the fundamental natural frequency of the cylinder, f_n. In this regime of flow speeds, the vortex-shedding frequency no longer follows the Strouhal relationship. Rather, the shedding frequency becomes "locked-in" to the natural frequency of the cylinder. Within the lock-in regime large body motions are observed (the structure undergoes near-resonance vibration).

It is also well known that a hysteresis behavior may exist in the amplitude variation and frequency capture depending on the approach to the resonance range—whether from a low velocity or from a high velocity [88]. As will be discussed later, the two branches of this hysteresis loop are associated with different vortex-shedding

S. Mottaghi et al., *An Analytical Mechanics Framework for Flow-Oscillator Modeling of Vortex-Induced Bluff-Body Oscillations*, Solid Mechanics and Its Applications 260,
https://doi.org/10.1007/978-3-030-26133-7_2

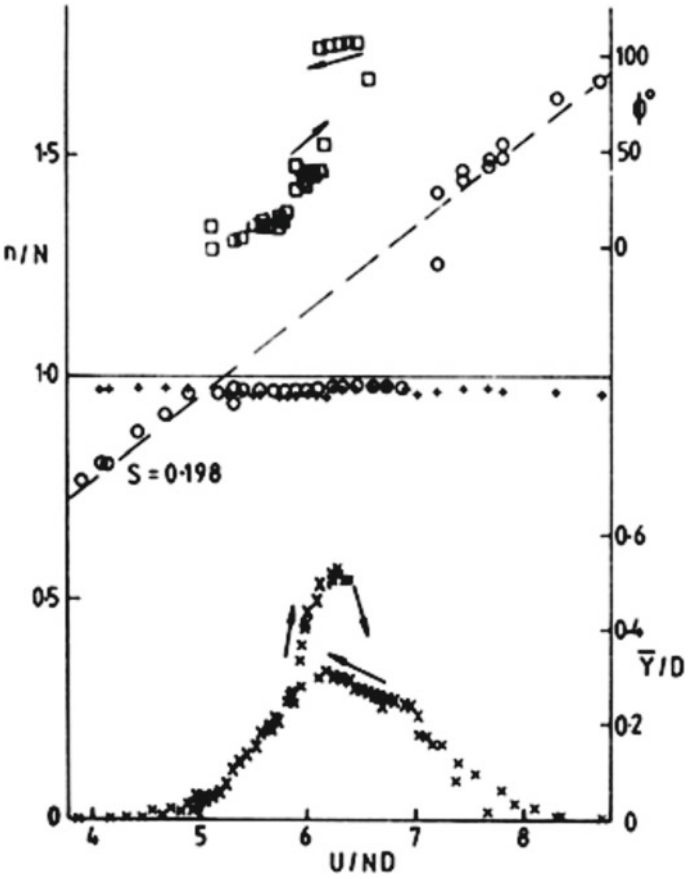

Fig. 2.1 Oscillation characteristics for a freely vibrating circular cylinder with light damping. N is the body oscillation frequency, n is the vortex-shedding frequency, $\overline{V} = D$ is the normalized maximum amplitude of oscillation measured at a particular value of the reduced velocity, and ϕ^o is the phase angle between the fluid force and the cylinder displacement. O, vortex-shedding frequency; +, cylinder frequency; □, phase angle; x, oscillation amplitude [4]. Reprinted with permission of the author

modes and transition between these branches is associated with a phase jump of $\sim 180°$ [65]. Shown in Fig. 2.1 is a typical response in the lock-in region of a freely vibrating circular cylinder with light damping. The hysteresis effect is clearly seen, with higher amplitudes achieved when the reduced velocity is increased over a certain range. Here, N is the body oscillation frequency, n is the vortex-shedding frequency, $\bar{Y}$ is the maximum amplitude of oscillation measured at a particular value of the reduced velocity, and $\phi°$ is the phase angle between the fluid force and the cylinder displacement. The straight line $S = 0.198$ is the line of constant Strouhal number.

The amplitude of the structural response during lock-in and the band of fluid velocities over which the lock-in phenomenon exists is strongly dependent on a reduced damping parameter expressing the ratio of the damping force to the excitation force. The Scruton number, $Sc = 4\pi m\zeta/\rho D^2$, is but one of many representations for this reduced damping parameter found in the literature. As the reduced damping parameter increases, lock-in becomes characterized by a decreasing peak structural amplitude and occurs over a decreasing band of velocities. It is also worth noting that different phenomena are seen in structures with high and low structure–fluid density ratios $M^* = m/\rho D^2$, where m is the cylinder mass per unit length and ρ is the fluid density. For systems with high M^*, the vortex-shedding frequency is entrained by the structural frequency. For systems with low M^*, it is the fluid oscillation which sets the frequency, and the entrainment frequency instead tends toward the shedding frequency f_v.

The engineering implications of VIV have been well documented in the literature. Structures such as tall buildings, chimneys, stacks, and long-span bridges develop pronounced vibrations when exposed to fluid flow. For example, studies focusing on the VIV of these structures are found in references [18, 22, 59, 74]. The length and higher flexibility of some of these structures further aggravates the problem. In offshore applications, VIV of long slender structures such as pipelines, risers, tendons, and spar platforms challenge engineering designers [17]. Some examples of fundamental studies on the nature of the VIV of marine structures are included in references [25, 30, 50, 100, 105]. Extensive research has also been done in the area of VIV assessment [21, 69, 72] and suppression [3, 49] .

In this review, both experimental and theoretical investigations of the fundamental aspects of vortex-induced vibration of circular cylinders are discussed in some detail. The goal has been to be thorough without being exhaustive. The main focus is on the semi-empirical models used to predict the response of the cylinder to the forces from the flow. These models are not rigorous and generally provide minimal insights into the flow field. To understand the flow effect on a structure, it is important that the actual flow field be described. Consequently, a secondary focus of this review is to discuss the flow characteristics around the cylinder. The flow field generated by flow separation around a body is a very complex fluid dynamics problem. However, much progress has been made toward the understanding of flow around bluff bodies. This is especially true in the field of computational fluid dynamics (CFD), and in keeping with the primary focus of this review, only selected papers highlighting this progress have been included.

Many reviews of the subject have been written that primarily focused on the experimental data [4, 7, 8, 64, 73, 88]. A recent one is by Sarpkaya [92]. While there continues to be extensive work on VIV, this work is still an excellent representation of our understanding. At about the same time, a review paper by two of us [34] focused on semi-empirical, reduced-order, modeling efforts. Since that time, additional review papers have appeared: Williamson and Govardhan [109], Bearman [5], and Wu et al. [111].

While VIV continues to be the subject of intensive research efforts and is quickly evolving, the need for reduced-order models continues to this day. Among their

attractions is the fact that they can be used in higher Reynolds number flows than CFD models and they have been solved in both the time and frequency domains. In addition, an alternative new method for the modeling of VIV is discussed, an approach that is the basis for this monograph. The method is based on the variational principles of mechanics and leads to a more fundamental (without ad hoc assumptions) derivation of the reduced-order equations of motion, yet remains inexorably linked to physical data. Experimental data helps to verify the model predictions, thus leading to the most advantageous model framework.

2.2 Experimental Studies

There are innumerable experimental studies on the vortex-induced vibration of bluff bodies, especially circular cylinders. These studies have examined a multitude of phenomena, from vortex shedding from a stationary bluff body to vortex shedding from an elastic body. The vibration caused by vortices generated by the flow past a structure depends on several factors. The correlation of the force components, the Reynolds number, the shedding frequencies, and the added mass effects are just a few of these. The literature is rich with experiments in which many of these factors have been considered, usually by varying one or two factors and holding the rest fixed. Here, key papers highlighting the influences of some of these factors on the structural response are discussed. Attention is focused mostly on results pertaining to the structural response. However, since VIV is indeed a coupled phenomena, some mention must be made of the hydrodynamics.

Before proceeding, it is worthwhile to define those variables that consistently appear in the equations developed in this section of the review. The outer diameter of a circular cylinder is designated by D, the length of the cylinder by L, the free-stream velocity of the flow by U, and the fluid density by ρ. The Strouhal number, S, is defined as $S = f_v D/U$, where f_v is taken to be the natural vortex-shedding frequency of a fixed cylinder. The reduced velocity is defined as $V_r = U/f_n D$, where f_n is the natural frequency of the structure. The normalized damping is defined as $\zeta = c_{sys}/c_{crit}$, where c_{sys} is the system damping, and c_{crit} is the critical damping.

Bearman [4] presents a comprehensive review of experimental studies related to vortex shedding from bluff bodies. He addresses the important question of the role of afterbody shape in vortex-induced vibration and results pertaining to a variety of afterbody shapes are included. Bearman first examines the mechanism of vortex shedding from a fixed bluff body. The presence of two shear layers is primarily responsible for vortex shedding. The presence of the body does not directly cause the vortex shedding, but it instead modifies the vortex- shedding process by allowing feedback between the wake and the shedding of circulation at the separation points.

Another important point discussed is the absence of two-dimensionality in the vortices shed from a two-dimensional bluff body in uniform flow. The spanwise coupling between the two shear layers that lead to the generation of vortex shedding is generally weak. This implies that unsteady quantities related to vortex shedding (e.g.,

surface pressure) are not constant along the span of the body. However, continuous regions of similar properties are characterized in terms of correlation lengths. Small departures from two-dimensionality, in the form of a taper along the axis of the bluff body or the presence of shear flow, leads to significant reductions in the vortex-shedding correlation length.

Bearman also examines vortex shedding from oscillating bluff bodies. The fundamental difference between fixed and oscillating bluff bodies is that the motion of the cylinder can take control of the instability mechanism that leads to vortex shedding. This is manifested in the capture of the vortex-shedding frequency by the body natural frequency over a range of reduced velocities. The vortex-shedding correlation length is significantly increased when the vortex-shedding frequency coincides with the body oscillation frequency. The range of reduced velocities over which the vortex-shedding frequency coincides with the natural frequency of the body depends on the oscillation amplitude. Larger ranges of frequency capture result from larger oscillation amplitudes.

It is worth pointing out that the capture range will always include the reduced velocity value corresponding to the inverse Strouhal number, and that maximum amplitude is attained near to (but not exactly) this value. In other words, the reduced velocity for maximum amplitude is close to $1/S$. The location of this resonant point within the capture range depends on the shape of the afterbody.

In the capture range, flow conditions around a bluff body change rapidly. The fluctuating lift coefficient increases due to the improved two dimensionality of the flow. This improved two dimensionality (increased correlation length) increases the strength of the shed vortices. The increase in the lift coefficient can also be attributed to the influence of the body motion, which manifests itself through the reduction of the length of the vortex-formation region and the formation of stronger vortices near the base of the body. The mechanism governing the phase of the vortex-induced force relative to the body motion has also been explored by Bearman. The changes in phase angle through the capture range occur in a progressive and not discontinuous fashion. In the lower end of the lock-in range, a vortex formed on one side of the cylinder is shed when the cylinder is near to attaining its maximum amplitude on the opposite side (Mode 1). As the reduced velocity is increased, the timing of vortex shedding suddenly changes, and the same vortex is now shed when the cylinder reaches its maximum amplitude on the same side (Mode 2). Clearly, the point in an oscillation cycle at which the cylinder receives its maximum transverse thrust changes drastically over a narrow range of reduced velocities. Zdravkovich [113] discusses in detail the modification of vortex shedding in the synchronization range. The existence of the two modes, Mode 1 and Mode 2, is used to explain the existence of the hysteresis effect.

Bearman [4] discusses free versus forced vibrations in experiments. Forced vibration experiments offer the advantage that the reduced velocity and amplitude ratios can be independently varied. In free vibration experiments, these two parameters are inseparable, since varying the reduced velocity leads to changes in the amplitude ratio. The major disadvantage of forced vibration experiments is that only a very limited range of reduced velocities and amplitude ratios studied will actually

correspond to those encountered in a free vibration. Bearman states that free and forced vibration flows are the same, provided that one assumes that the exact history of motion is inconsequential.

2.2.1 Fluid Forces on an Oscillating Cylinder

Vortex shedding from a circular cylinder produces alternating forces on the cylinder and it is these forces that cause the cylinder to vibrate if it is free to do so. Experiments by Sarpkaya [87] determine the in-phase and out-of-phase components of the time-dependent force acting on a rigid circular cylinder undergoing forced transverse oscillations in a uniform stream. These force components are used in the prediction of the dynamic response of an elastically mounted cylinder in the synchronization range. The details of this aspect of the investigation are relegated to the section of this review describing semi-empirical models. Preliminary experimental work measures the mean fluid-induced force on the cylinder in the direction of flow for various amplitudes and frequencies of cylinder oscillation in the transverse direction. The in-line force is found to increase as A/D increases, where A is the transverse oscillation amplitude. For a given value of A/D, the in-line force reaches a maximum for $D = \overline{V}T$ (mathematically similar to a Strouhal number) in the range 0.18–0.20, where T is the oscillation period and $\overline{V}$ has the same meaning as U. Furthermore, synchronization is found to occur at a frequency slightly lower than the Strouhal frequency for a stationary cylinder, 0.21, corresponding to the range of Reynolds numbers considered by Sarpkaya, 5000–25,000.

In considering the transverse force on the cylinder, the lift coefficient C_L is expressed in terms of an in-phase inertia force and an out-of-phase drag force. The inertia coefficient C_{ml} characterizes the in-phase force, while the out-of-phase force is characterized by the drag coefficient C_{dl}. The drag and inertia coefficients are assumed independent of the Reynolds number in the range considered, 5000–25,000. Synchronization is manifested by a rapid decrease in the inertia coefficient and a rapid increase in the absolute value of the drag coefficient. The experiments also confirm that the net effect of the cylinder–flow interaction near synchronization, for $A/D < 1$, is the same as for periodic flow over a cylinder at rest. This suggests that the fluid becomes the oscillator under these conditions.

The major implication is then that use of the maximum inertia coefficient obtained by oscillating the cylinder in a fluid otherwise at rest, $C_{ml} = 1$, does not give the correct results since C_{ml} has been shown to reach a value of about 2 near synchronization. There is a range of $V_r = \overline{V}T/D$ near perfect synchronization, $V_r \sim 5$, where the drag coefficient is found to be in-phase (negative) with the direction of motion of the cylinder. In this range, the drag coefficient actually helps to magnify the oscillations, and for this reason the range is often referred to as the negative damping region.

Gopalkrishnan [36] measures the vortex-induced lift and drag forces on a smooth circular cylinder undergoing forced sinusoidal oscillations transverse to the free stream. The measurements are conducted in water. The lift force phase angle (defined

in the same way as ϕ^o in Fig. 2.1) is found to be very different for large oscillation amplitudes than for small oscillation amplitudes. This is partially responsible for the amplitude-limited nature of VIV. The range of reduced velocities where the cylinder is excited into oscillations by the flow (the lift coefficient excitation region) is found to not coincide with the lock-in region. Furthermore, the excitation region is found to be dependent on the phase, while lock-in is found to be a frequency-dependent effect. The author also measures the lift and drag forces on a cylinder subjected to an amplitude-modulated force causing beating motions. The presence of beating is found to cause a reduction in the mean drag coefficient, an increase in the rms oscillating drag coefficient, and increased extent of the primary excitation regions (vs. sinusoidal excitation). The overall magnitude of the lift coefficient was comparable to that corresponding to sinusoidal forcing.

2.2.2 Three-Dimensionality and Free-Surface Effects

Three-dimensional features naturally arise in the VIV problem, where elastic structures are characterized by their eigenmodes and wake flows show secondary instabilities [30]. The transition to three dimensionality in the near wake of a circular cylinder is discussed by Williamson [106]. Three-dimensional structures in the wake were found to occur for Reynolds numbers greater than about 178. These three-dimensional structures are attributed directly to the deformation of the primary wake vortices, and were not the result of any secondary (Kelvin–Helmholtz) vortices caused by high-frequency oscillations within the separating shear layers. The transition to three dimensionality is found to involve two successive transitions, each characterized by a discontinuity in the Strouhal–Reynolds number relationship. These discontinuities can be seen in Fig. 2.2. The first discontinuity (Re: 170–180) is associated with the transition from periodic and laminar vortex shedding to shedding involving the formation of vortex loops. The second discontinuity (Re: 225–270) is related to the transition from the vortex loops to finer scale streamwise vortices. The first discontinuity is found to be hysteretic, while the second discontinuity is not. A more comprehensive discussion on these discontinuities (so-called Mode *A* and Mode *B* secondary 3*D* instabilities), and vortex dynamics in bluff body wakes in general, can be found in two review papers by Williamson [107, 108]. Specifically, comparisons of measurements and theoretical predictions of spanwise instabilities for modes "A" and "B" are given in Fig. 10 of Williamson [108].

The question of three dimensionality in the wake of a surface-piercing rigid cylinder mounted as an inverted pendulum is examined in detail by Voorhees and Wei [102]. The cylinder is characterized by a low mass ratio, $m^* = 1.90$, and high mass-damping, $m^*\zeta = 0.103$. The mass ratio is defined as the mass of the cylinder assembly divided by the mass of water displaced by the cylinder, $m^* = m/\rho\pi r^2 L$. The ratio of mechanical to critical damping is represented by ζ. This study, for Re: 2300–6800, found that the response characteristics of the cylinder are similar to those seen in elastically mounted cylinders of similar m^* and $m^*\zeta$. Strong axial flows

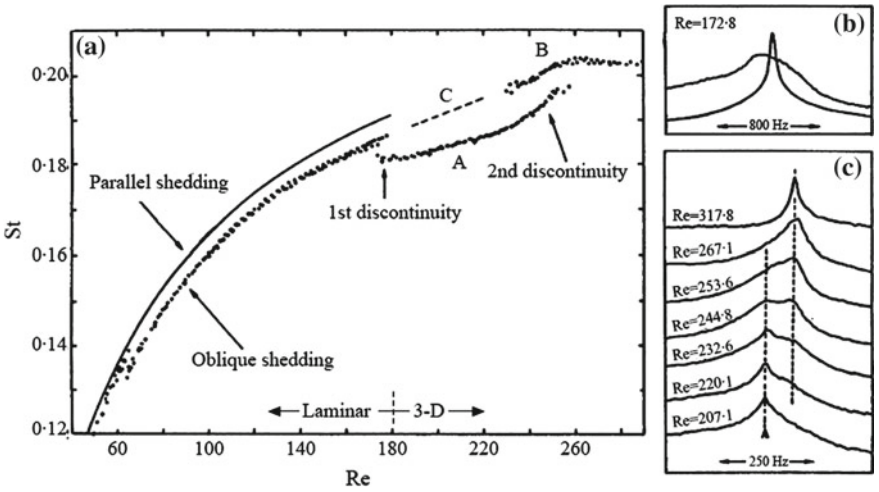

Fig. 2.2 **a** Variation in Strouhal number as a function of Reynolds number; **b** frequency spectra at first discontinuity; **c** frequency spectra at second discontinuity [114]. Reprinted with permission

associated with the Kármán vortices are observed, and these flows are generally directed upwards toward the free surface. Below the free surface, these axial flows can be predominantly attributed to the linearly increasing oscillation amplitude along the span. Near the free surface, however, there is an equal probability of upflow and downflow. These upflows and downflows are shown to be well correlated to the quasi-periodic beating of the cylinder amplitude at the reference reduced velocity $U^* = 4.9$ (Re: 3400) in the synchronization range. In essence, the effect of the free surface is to disrupt the primary upflow mechanism and also to induce lateral spreading of the top portions of the Kármán vortices.

Regarding free surfaces, several fundamental aspects of vortex-formation are found to depend on the gap between the cylinder and the free surface, as discussed by Lin and Rockwell [71] for the case of a fully submerged cylinder oriented parallel to the free surface. The influence of a free surface on the wake structure has also been investigated by Sheridan et al. [94, 95].

2.2.3 Vortex-Shedding Modes and Synchronization Regions

The character of the vortex shedding is important in that it influences lift force phase and, consequently, the energy transfer between the fluid and the body. Williamson and Roshko [110] explore the existence of regions of vortex synchronization in the wavelength–amplitude plane. From the outset, the Reynolds number is not treated as an independent parameter in this study. The Reynolds number is kept within a certain range, $30 < \mathrm{Re} < 1000$, but is never held fixed. The amplitude ratio equals

A/D. The wavelength ratio is $\lambda/D = UT_e/D$, where $T_e = 1/f_e$ is the period of cylinder oscillation in the transverse direction. The wavelength ratio is equivalent to the reduced velocity, but has the distinct advantage that it introduces the trajectory along which the body travels relative to the fluid. Within the fundamental lock-in region ($\lambda/D \approx 5$ or $T_e \approx T_s$, where T_s is the period of vortex shedding for a non-oscillating cylinder), the acceleration of the cylinder at the start of each half-cycle induces the rolling-up of each of the separating shear layers into a new pair of vortices. Consequently, the cylinder sheds four regions of vorticity in each cycle. The authors find that below a critical trajectory wavelength (for a given amplitude ratio), each half-cycle results in the coalescence of a pair of like-signed vortices. Consequently, two regions of opposite vorticity are fed into the downstream wake per cycle. The resulting formation is similar to the classic von Kármán vortex street wake and is called the 2S mode. Above the critical trajectory wavelength, the like-sign vortices are found to convect away from each other. Each of these vortices is then paired up with a vortex of opposite sign. The resulting formation is two vortex pairs (of opposite signs) convecting laterally away from the centerline. This mode is called the $2P$ mode.

At exactly the critical wavelength, four regions are no longer formed. Only two vortices are formed in each cycle, and the resulting shed vorticity is more concentrated than at other wavelengths. This condition is called the resonant synchronization. The resonant synchronization is important because it coincides (approximately) with the peak in the lift forces seen in experimental results. The conclusion is that the larger forces are being induced by the shedding of more concentrated vorticity. Figure 2.3 is a map of vortex synchronization patterns near the fundamental lock-in region. The critical curve represents the transition from one mode of vortex formation to another. Curves *I* and *II* represent locations, where the forces on the body show a sharp jump.

The transition from the $2S$ mode to the $2P$ mode can be sudden, and it is this abrupt change in the dynamics of the vortex wake that is a plausible explanation for the sharp changes in the character of the body forces through the primary lock-in. The jump in the phase angle ϕ between the lift force and the body motion seen near the natural shedding frequency ($T_e \approx T_s$) can be attributed to the process of pairing in the $2P$ mode, which causes a sharp change in the timing of the shedding. Since it is possible that in a certain small range of wavelength either one of the two modes can exist, hysteresis will result. The $2P \rightarrow 2S$ (decreasing wavelength) jump occurs for a lower wavelength than does the $2S \rightarrow 2P$ (increasing wavelength) jump. This is illustrated in Fig. 2.4.

A more general approach for categorizing the vortex-shedding modes is taken by Zdravkovich [114]. Vortex shedding from a cylinder is classified as either low-speed mode or high-speed mode. The low-speed mode is related to laminar wake instability, while the high-speed mode is related to vortex formation and shedding. The transition state between the low- and high-speed modes is characterized by "fingers" or distortions of eddy filaments in the near wake. These "fingers" cause irregular vortex filaments to appear along the span. Zdravkovich also describes two modes in the streamwise oscillation of a cylinder in an oscillatory flow. Near the synchronization frequency, which would, in this case, be approximately twice the

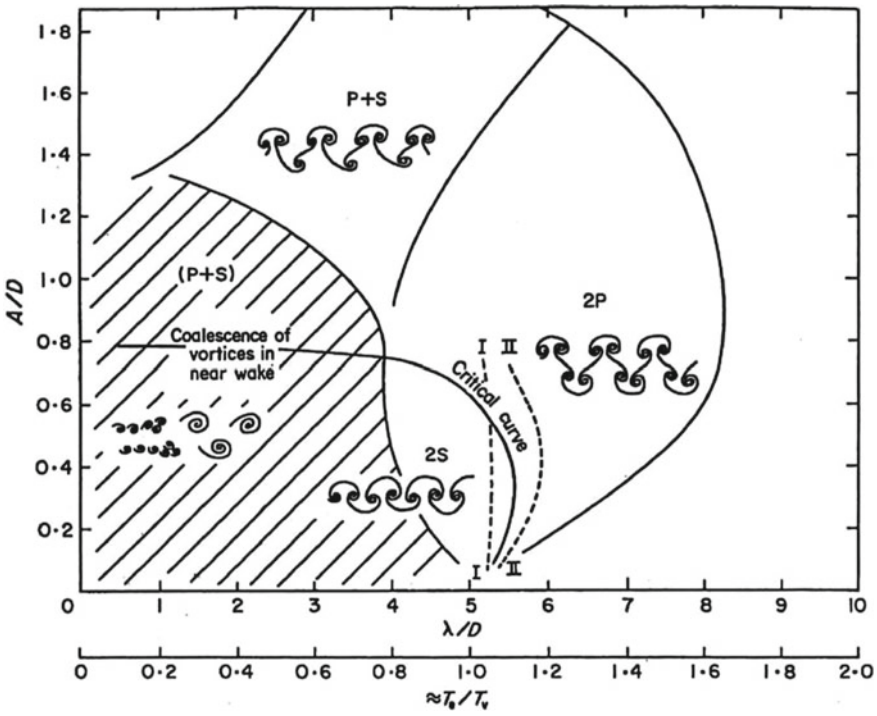

Fig. 2.3 Map of vortex synchronization near the fundamental lock-in. A/D is the amplitude ratio and λ/D is the wavelength ratio. The "critical curve" represents the transition from one mode of vortex formation to another. Curves I and II represent locations where the forces on the body show a sharp jump [110]. Reprinted with permission

natural shedding frequency, the following modes are found: One vortex formed per half-cycle and two vortices formed per half-cycle. Interestingly, the transition state from the first mode to the second mode is characterized by one vortex formed in odd half-cycles and two vortices formed in even half-cycles.

2.2.4 The Frequency Dependence of the Added Mass

The added mass is not the same for a body oscillating at a given frequency in a still fluid as for a body oscillating at the same frequency in a moving fluid. The relationship between added mass and response frequency for lightly damped elastically mounted rigid cylinders in uniform flow (Re: $10^4 - 6 \times 10^4$) is examined by Vikestad et al. [101]. The cylinder is allowed to vibrate in the crossflow direction only. Two different experiments are conducted for various values of the reduced velocity: those with no support excitation, and those with support (external) excitation at a given frequency.

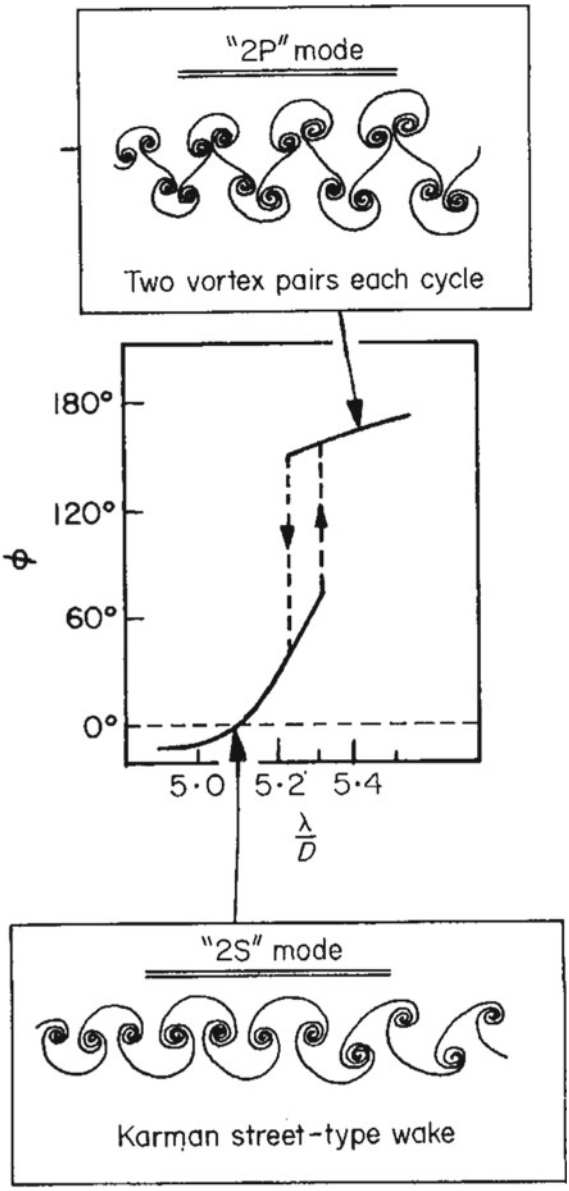

Fig. 2.4 Variation of the lift force phase angle ϕ with wavelength ratio λ/D [110]. Reprinted with permission

The reduced velocity $U_r = U/f_o D$ is defined on the basis of the natural frequency (f_o) measured in still water. Since the natural frequency is generally not constant but depends on the added mass ($f_n = f_n(C_a)$), it is not possible to conduct experiments on the dependence of the oscillation frequency on the added mass without fixing the reduced velocity. This follows from the fact that the oscillation frequency is itself

dependent on the reduced velocity, leading to a "circular" problem. The added mass coefficient is estimated from

$$C_a = -\frac{8}{nT\rho\pi D^2 L(\omega^2 x_o)^2}\int_t^{t+nT} F_v \ddot{x}\,dt, \tag{2.1}$$

where F_v is the crossflow component of the total hydrodynamic force, $\ddot{x}$ is the cylinder acceleration, T is the period of cylinder oscillation, $\omega^2 x_o$ is the acceleration amplitude, and n is the number of periods over which integration is performed.

For experiments conducted without support excitation, two different calculations are performed using Eq. 2.1: an average C_a over many periods, and a time-dependent C_a obtained by averaging over a sequence of single periods. For C_a calculated over many periods, the authors define the mean oscillation frequency as $f_{osc} = \sqrt{(\ddot{x}_{rms}/x_{rms})}/2\pi$ and the true natural frequency as

$$f_n(U_r) = \frac{1}{2\pi}\sqrt{\frac{k_{TOT}}{m + \rho V_{cyl} C_a(U_r)}},$$

where m is the cylinder effective dry mass, k_{TOT} is the total stiffness of the oscillatory system, and V_{cyl} is the cylinder volume. The results of plotting f_{osc}/f_o and f_{osc}/f_n versus U_r (Fig. 2.5) show no evidence that the oscillation frequency is locked-in to one fixed natural frequency. Instead, the oscillation frequency is the true natural frequency over a wide range of reduced velocities. In fact, since the added mass coefficient decreases with reduced velocity (see Fig. 4a of [101]), the natural frequency increases (Eq. 2.1) with reduced velocity. According to the authors, this is the reason why low mass ratio cylinders have lock-in regions that extend over a broader range of flow speeds.

For C_a calculated over single periods, the variation in the added mass from one vibration cycle to next is shown to be considerably large. This variation is found to be least in the range of reduced velocities U_r: 4–6. This is the range of reduced velocities for which there is a strong correlation between the added mass coefficient and the cylinder displacement. The variation in the added mass from cycle to cycle is also shown to be closely correlated to the cycle-to-cycle variation in the response frequency. Again, this is attributed to changes in the added mass-dependent natural frequency. The interested reader is referred to the journal paper for details of the experimental results pertaining to support (external) excitation.

2.2.5 *Dynamics of Cylinders with Low Mass-Damping*

Khalak and Williamson [60] study the forces and vortex-induced response of a rigid circular cylinder in an experimental facility characterized by a very low mass ratio m^* and a very low normalized damping ratio ζ. The combined mass-damping parameter $m^*\zeta$ has a value of 0.013, a value at least one order of magnitude lower than any previous study. Initially, the cylinder is held fixed (static) in a uniform flow. The test cylinder has either a free end, which produced oblique vortex shedding, or an

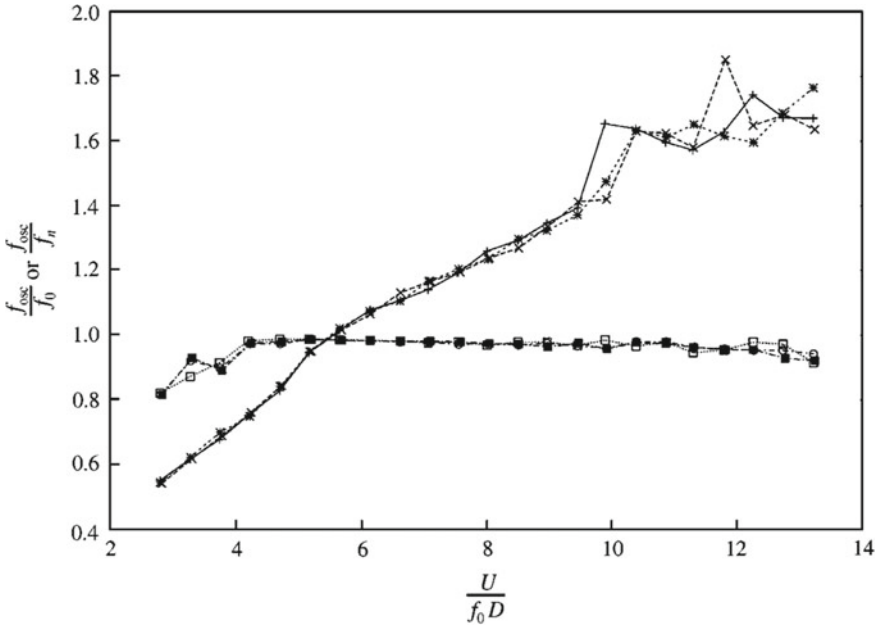

Fig. 2.5 Mean oscillation frequency divided by the natural frequency in still water, $f_{osc} = f_0$; shown by the sloped lines. Mean oscillation frequency divided by the true natural frequency, $f_{osc} = f_n$; shown by the horizontal lines. Both are shown as functions of the reduced velocity U_r [101]. Reprinted with permission

end-cylinder (a larger cylinder placed coaxially) which produces parallel shedding. The total fluctuating lift and drag forces on the cylinder are measured for both end conditions as a function of the Reynolds number. The time-averaged drag coefficient is found to be consistently higher in the case of parallel shedding and this result is essentially independent of Reynolds number. The RMS lift coefficient is also found to be higher in the case of parallel shedding, but the difference is not Reynolds number independent. Spectral analysis indicates that the lift force is dominated by a single peak at the shedding frequency in the case of parallel shedding, while in the case of oblique shedding two smaller peaks are present.

The transverse response of the elastically mounted cylinder is also examined in the same work. The response of the cylinder is found to have two distinct resonant branches. Hysteresis results from moving between these branches, and the jump between the branches can be interpreted as a change in the vortex-shedding mode. These two resonant branches, called the upper (very high amplitude response) and lower branches (moderate amplitude response), can be seen in Fig. 2.6. Note that the reduced velocity is formed using the natural frequency in air f_n, $U^* = U/f_n D$. Also shown is data from Feng [32], which is obtained for a much higher mass-damping parameter of $m^* \zeta = 0.36$. Clearly, there is a substantial increase in both the amplitude and range of the response for lower values of mass-damping. Note that the values of

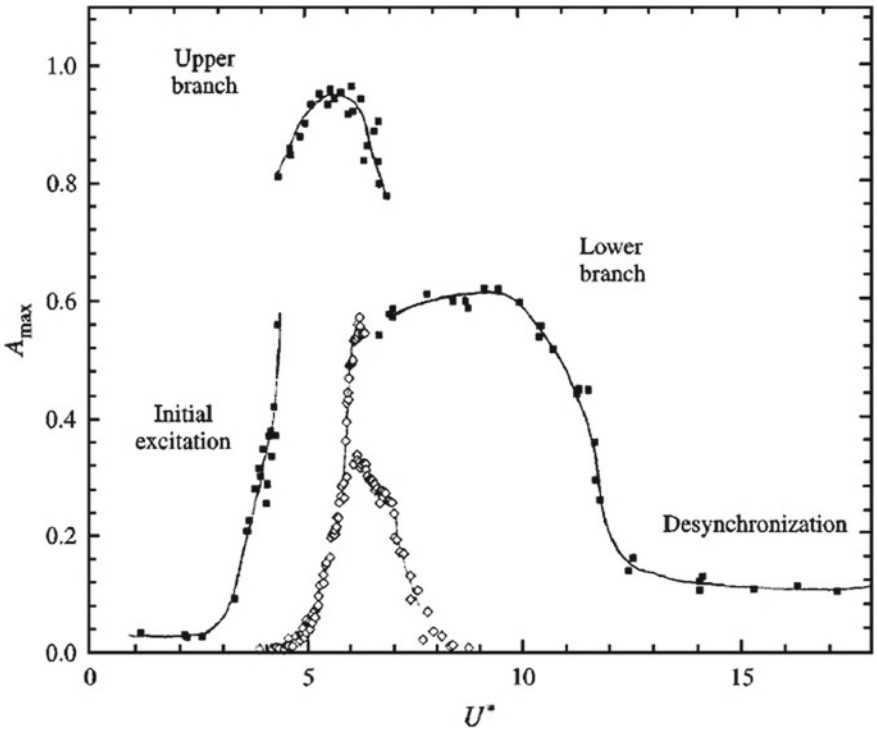

Fig. 2.6 Maximum response amplitudes Amax as functions of the reduced velocity U^* for $m^* = 2.4$ (□) and $m^* = 248$ (◇) [61]. Reprinted with permission

m^* and ζ did not include the effects of added mass. Also shown in Fig. 2.6 are the initial excitation region and the desynchronization region as described in [61]. The classical experiments of Feng (high $m^*\,\zeta$) show the absence of the upper branch and only two response branches exist. The initial branch has been shown to be associated with the 2S mode of vortex formation, while the lower branch corresponds with the $2P$ mode [63].

The mass ratio m^* and the normalized damping ζ are found to independently affect the response of the system. By maintaining the value of $m^*\,\zeta$ constant, the value of m^* is independently adjusted. Lower values of m^* are manifested in the form of higher response amplitudes and a larger range of response in the lower resonance branch. However, changes to m^* do not significantly alter the characteristics of the upper branch. The level of maximum excitation in the upper branch is found to be well characterized by the combined mass-damping parameter $m^*\zeta$ [62, 63]. Most importantly, these effects cannot be explained by including the added mass. Presumably, for low mass ratios the inertia of the fluid being accelerated by the cylinder is important. A linear equation of motion is developed with the inclusion of an inviscid added mass force. The failure of the added mass to explain the mass dependence of

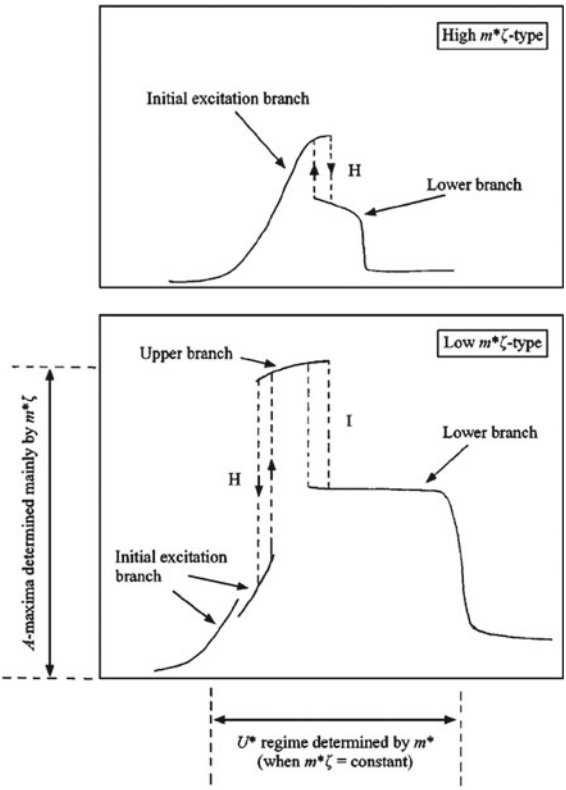

Fig. 2.7 The two distinct types of amplitude response: high $m^*\zeta$ and low $m^*\zeta$: The mode transitions are either hysteretic (H) or intermittently switching (I) [63]. Reprinted with permission

the response led the authors to conjecture that it is instead the phase angle ϕ which is responsible. The classical "mass-damping" parameter $(m^* + C_A)\zeta$ has been shown to collapse peak amplitude data over a wide range of mass ratios. The use of the combined parameter is valid down to at least $(m^* + C_A)\zeta \sim 0.006$ [63].

In their subsequent paper [63], Khalak and Williamson show that as the normalized velocity is increased, the transition from the initial excitation region to the upper branch is hysteretic. The transition from the upper branch to the lower branch also involves a jump but is followed by intermittent switching. This intermittence is clearly seen in the instantaneous phase measurements between the lift force and the displacement in the transition region. Both of the transitions are associated with jumps in response amplitude and frequency, but only the transition from the upper to the lower branch is associated with a 180° jump in the phase angle. Figure 2.7 is a schematic of the differences between high-$m^*\zeta$ and low-$m^*\zeta$ amplitude response. Perhaps the most interesting result is that in the excitation regime, the frequency of cylinder oscillation is significantly higher than the structural natural frequency. It is also below the natural vortex shedding frequency of a non-oscillating cylinder (see Fig. 4 of [63]). These characteristics are not what would be expected from a

classical lock-in. Other investigations by Williamson's group at Cornell can be found in references [39–41].

As part of a new paradigm to support the reduced-order analytical modeling of fluid–structure interactions, Dong et al. [23] use high-resolution Digital Particle Image Velocimetry (DPIV) to measure fluid energy transport terms. The terms form part of the equation of motion for a rigid circular cylinder with a low mass-damping ($m^*\zeta = 0.0377$) mounted like an inverted pendulum. The equation of motion is derived using a form of Hamilton's Principle appropriately developed for systems of changing mass. More specifically, the governing equation is formulated using the control volume (CV) approach. It is worth mentioning here that, except for the quasi-two dimensionality of the flow, no empirical assumptions are incorporated into the model. The assumption made is reasonable in light of the fact that Voorhees and Wei [102] show that three-dimensional effects are dominant near the free surface. The fluid energy terms that are calculated from the DPIV velocity vectors are the time rate change of the fluid kinetic energy within the CV, the net flux of fluid kinetic energy across the boundaries of the CV, and the work done on the CV boundaries by pressure and viscous forces. These terms are calculated for a single value of the reduced velocity U^* corresponding to a Reynolds number of 2300. This corresponds to the resonant synchronization regime, where the cylinder response exhibits a beating behavior (i.e., large-amplitude modulated oscillations).

The results of the study indicate that the choice of a CV is crucial to obtaining energy transport traces that are more easily interpreted.

2.2.6 Additional Studies

There have been many additional more specialized studies of vortex-induced vibration. Huera-Huarte and Bearman [51, 52] considered the wake structures and vortex-induced vibrations of a long flexible cylinder. Fujarra et al. [33] studied the vortex-induced oscillations of a flexible cantilever beam. Branković and Bearman [13] studied the vortex-induced vibration of a straked cylinder, noting that the familiar phase jump did not occur.

When circular cylinders are allowed to oscillate with two degrees- of-freedom rather than just in a transverse direction, in addition to the figure eight motion, characteristics of the flow and shedding change. Jeon and Gharib [58] note a dramatic increase in phase coherence and the disappearance of the $2P$ mode, and that the transverse motion sets the frequency of shedding and the streamwise motion the relative phase. Laneville [68] concurs with these results. Jauvits and Williamson [57] studied the response of an elastically mounted cylinder free to move in two degrees-of-freedom, which has low mass and damping. They find that the transverse motion, the modes of vibration and the vortex wake dynamics change very little with the added freedom to move in two directions. Their principle conclusion is that results from experiments where only transverse oscillations are allowed are valid for those structures that undergo two degree-of-freedom oscillations.

Bourdier and Chaplin [12] studied vortex-induced vibration of a rigid cylinder on elastic supports with end-stops. Cagney and Balabani [15] studied wake modes of a cylinder undergoing free streamwise vortex-induced vibration, which tend to be an order of magnitude lower that those in the transverse direction. Lam and Liu [66] studied large-amplitude transverse oscillations in a slow uniform cross flow.

2.3 Semi-empirical Models

In this review chapter, every attempt has been made to preserve the notation of the governing equations as given in the references. This facilitates the reader's ability to correspond between this review and a given paper. Work with structures undergoing vortex-induced vibration can be classified into three main types. The first class consists of wake-body (wake-oscillator) coupled models, in which the body and the wake oscillations are coupled through common terms in equations for both. The second class, the single degree-of-freedom (SDOF) models, use a single dynamic equation with aeroelastic forcing terms on the right-hand side of the equation. The third class, the force-decomposition models, rely on experimental measurements of certain components of the forces on the structure.

2.3.1 Wake-Oscillator Models

Several wake-oscillator models have been proposed in the literature. The models generally have the following characteristics: The oscillator is self-exciting and self-limiting, the natural frequency of the oscillator is proportional to the free stream velocity such that the Strouhal relationship is satisfied, and the cylinder motion interacts with the oscillator. The latter essentially says that the cylinder motion strongly affects the lift forces, which in turn influence the cylinder motion. Also, the models assume that the flow around the cylinder is two dimensional (i.e., the flow is fully correlated). Consequently, the models are limited to moderate to large response amplitudes. These models often do not include any analysis of the flow field and their value is at best to explain and simulate experimental results. For this reason, these models are often referred to as *phenomenological*. The modeler's desire is to obtain the equations of the cylinder oscillator and the fluid oscillator by independent means and then use them together to predict the response of the combined fluid-elastic system [24]. Parkinson [83] presents a comprehensive review of the modeling of flow-induced vibrations in bluff bodies.

2.3.1.1 Rigid Cylinders

Bishop and Hassan [9] are credited with first suggesting the idea of using a van der Pol-type oscillator to represent the time-varying forces on a cylinder due to vortex shedding. Their work is noteworthy for linking experimental results to possible classes of dynamic behavior and in this way they laid the foundation for reduced-order mathematical modeling of vortex-induced vibration. They characterized the regimes of behavior, including that there is a synchronization region—entrainment—when shedding frequency is close to structural natural frequency, and that there is a hysteretic behavior—a jump in response—depending on whether the driving frequency is increasing or decreasing. Their experiments showed that the wake could be entrained to oscillate as well at 1/2 and 1/3 the natural frequency. Another important conclusion drawn from the data was that the wake behaves under external forcing as a nonlinear self-excited oscillator. This led to the use of van der Pol equations for the mathematical modeling of the "flow oscillator".

Hartlen and Currie [47] formulated the most noteworthy of the oscillator models. In their model, a van der Pol soft nonlinear oscillator for the lift force is coupled to the cylinder motion by a linear dependence on the cylinder velocity. The cylinder motion is restricted to pure translation in the transverse direction, perpendicular to both the flow direction and the cylinder axis. The cylinder is restrained by linear springs and is linearly damped. The model is given by the pair of coupled nondimensional differential equations,

$$x_r^{''} + 2\zeta x_r^{'} + x_r = a\omega_o^2 c_L \tag{2.2}$$

$$c_L^{''} - \alpha\omega_o c_L^{'} + \frac{\gamma}{\omega_o}(c_L^{'})^3 + \omega_o^2 c_L = \beta x_r^{'}, \tag{2.3}$$

where primes denote time derivatives with respect to the nondimensional time $\tau = \omega_n t$, x_r is the dimensionless cylinder displacement, c_L is the lift coefficient, ω_o is the ratio of the Strouhal shedding frequency to the natural frequency of the cylinder, $\omega_o = f_o/f_n$, and ζ is the material damping factor. The parameter a is a known dimensionless constant. Of the undetermined parameters α, γ, and β, only two must be chosen to provide the best fit to experimental data. This follows from the fact that α and γ are related to each other by the expression $C_{Lo} = (4\alpha/3\ \gamma)^{1/2}$, where C_{Lo} is the amplitude of the fluctuation of c_L on a fixed cylinder. It is worth noting that the second term on the left-hand side of Eq. 2.3 provides the growth of the lift coefficient c_L, while the third term on the left-hand side of the same equation prevents its unlimited growth. These terms are important to the success of the model because the large-amplitude oscillations characteristic of VIV are accompanied by a significant (yet finite) increase in the lift coefficient.

With the appropriate choice of parameters, the Hartlen and Currie model qualitatively captures many of the features seen in experimental results [81, 88]. For instance, a large cylinder oscillation amplitude resonance region occurs when the vortex shedding frequency is near the natural frequency of the cylinder. The frequency of oscillation in this region is nearly constant at a value close to the cylinder

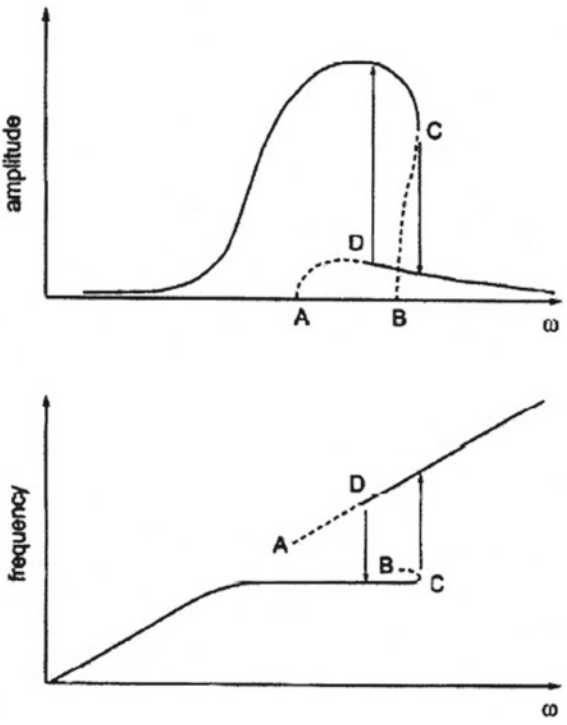

Fig. 2.8 Amplitude and frequency response of the Hartlen–Currie model. ω is proportional to the flow velocity. Solid lines represent stable branches of the periodic motions, while dotted lines represent unstable branches. Arrows show jumps in amplitude and frequency corresponding to sweeps of ω [81]. Reprinted with permission

natural frequency. The hysteresis effects seen in the experimental results of Feng [32] are also seen in the analysis of the Hartlen and Currie model by Ng et al. [81] using multiple scales and bifurcation analyses. Figure 2.8 is an illustration of the amplitude and frequency responses of the Hartlen and Currie model with $\zeta = 0.0015$, $\alpha = 0.02$, $\gamma = 2/3$, $a = 0.002$ and $\beta = 0.4$. The horizontal axis ω is proportional to the flow velocity. Solid lines represent stable branches of the periodic motions, while dotted lines represent unstable branches. Arrows show jumps in amplitude and frequency corresponding to sweeps of ω.

Skop and Griffin [98] develop a model to resolve what they felt were inadequacies of the Hartlen and Currie model, including the fact that the model parameters are not related to any physical parameters of the system. A modified van der Pol equation is again employed as the governing equation of the lift, and an equation is presented for the oscillatory motion of the body. The equations are

$$\frac{\ddot{X}}{D} + 2\zeta\omega_n\frac{\dot{X}}{D} + \omega_n^2\frac{X}{D} = (\rho V^2 L/2M)C_L = \mu\omega_s^2 C_L \tag{2.4}$$

$$\ddot{C}_L - \omega_s G\left[C_{Lo}^2 - \frac{4}{3}\left(\frac{\dot{C}_L}{\omega_s}\right)^2\right]\dot{C}_L + \omega_s^2\left[1 - \frac{4}{3}H\dot{C}_L^{\,2}\right]C_L = \omega_s F\left(\frac{\dot{X}}{D}\right), \tag{2.5}$$

where ω_s is the shedding frequency, C_L is the oscillating lift coefficient, C_{Lo} is the fluctuating lift amplitude from a stationary cylinder, ω_n is the undamped natural frequency of the spring–mass system, and ζ is the sum of the structural, fluid, and externally applied damping. M is the mass of the cylinder and $\mu = \rho LD^2 \big/ 8\pi^2 S^2 M$ is a parameter representing the ratio of the displaced mass of fluid to the mass of the cylinder. The parameters G, H, and F are to be determined from experimental data.

Solutions to these governing equations in the lock-in state (frequency entrainment) are sought using the method of van der Pol, in which one seeks solutions of the form $X/D = aC_{Lo} \sin \omega t$ and $C_L = AC_{Lo} \sin(\omega t + \varphi)$, where φ is the phase difference between the fluctuating lift coefficient and the cylinder displacement. Substitution of the assumed solutions into the governing equations results in relationships between the various model parameters. Relationships between the two independent model parameters G and H and the physical mass and damping parameters μ and ζ are formulated by considering a variety of experimental results from the literature and then using a best-fit line. For instance, the relation for G is given as $\log_{10} G = 0.23 - 0.19(\zeta/\mu)$. However, the fact that the parameters G and H are obtained for each experimental value of ζ and μ by trial and error is an inherent flaw in this model. The value of the third empirical constant is given as $F = 4G\zeta^2 \big/ \mu H$.

Using these relationships, the authors are able to quantitatively predict the results of a different set of resonant vibration experiments found in the literature with reasonable accuracy. The question can, of course, be raised of how much predictive value to assign a model which has been "tweaked" from the beginning.

In a subsequent paper, Griffin et al. [44] compare the results of their own experiments with spring-mounted cylinders in a wind tunnel and the results predicted by their wake-oscillator model. Measurements are made of the vibration amplitude and frequency under a variety of flow conditions at Reynolds numbers between 350 and 1000. All measurements are conducted under conditions of synchronization between the vortex-shedding frequency and the cylinder oscillation frequency. The major conclusions of the study are as follows, with (E) denoting experimental results, (T) denoting theoretical results and (E-T) denoting compared results:

- The magnitude and location of the peak resonant amplitude and the detuning between the vibration and cylinder natural frequencies are quantitatively predicted by the model (E-T).
- The maximum lift occurs at a flow speed somewhat less than that which produces the largest amplitude (T).
- The maximum energy transfer to the cylinder occurs at the flow speed which produces the largest amplitude (E-T).
- There is a substantial change in the phase angle φ between lift and the cylinder motion in the synchronization regime (T).
- The energy transfer to the cylinder per vibration cycle will be positive if the lift force includes a component which is in phase with the cylinder velocity (T).
- Up to a 75% increase in the drag coefficient from the fixed cylinder value is measured at a peak amplitude of one diameter (E).

Like the Hartlen and Currie model, the Skop and Griffin model [98] contradicts several findings by Feng [32]. Feng finds that the maximum lift and maximum cylinder displacement occurred at the same value of flow speed. Feng also finds that the cylinder will continue to oscillate at its natural frequency outside the lock-in range.

Iwan and Blevins [55] arrive at fluid-oscillator equations by considering the fluid mechanics of the vortex street. The model is based on the introduction of a hidden fluid variable z, which captures the fluid dynamics effects of the problem. The equations are

$$\ddot{y} + 2\zeta_T \omega_n \dot{y} + \omega_n^2 y = a_1^{'} \ddot{z} + a_4^{''} \dot{z} \frac{U}{D} \tag{2.6}$$

$$\ddot{z} + K^{'} \frac{u_t}{D} \omega_s z = (a_1^{'} - a_4^{'}) \frac{U}{D} \dot{z} - a_2^{'} \frac{\dot{z}^3}{UD} + a_3^{'} \ddot{y} + a_4^{'} \frac{U}{D} \dot{y}, \tag{2.7}$$

where ζ_T is the total effective damping coefficient, u_t is the translational velocity of the vortex street shed from the cylinder, and $K^{'}$ is a parameter related to the Strouhal number and the ratio u_t/U. The total effective damping coefficient is the sum of the structural viscous damping and the viscous fluid damping. All of the empirical parameters $a_i^{'}$ and $a_i^{''}$ of the model but one are determined from experimental data for fixed and harmonically forced cylinders. The model is then used to predict the response of elastically mounted rigid cylinders.

The response of the cylinder is found to be dependent on the structural viscous damping ζ_s, the ratio of the shedding frequency to the natural frequency of the cylinder ω_s/ω_n, and the ratio of the displaced fluid mass to the cylinder mass. This mass ratio is defined as $\rho D^2/2m$. The peak amplitude of cylinder oscillation for the resonant condition is found to depend on a single variable called the reduced mass-damping parameter, $\delta_r = 4\pi m \zeta_s / \rho D^2$. Note that this parameter is identical to the Scruton number,

$$S_c = \frac{4\pi m \zeta}{\rho D^2}.$$

The model correctly predicts the entrainment effect (or lock-in). The entrainment effect (width of the frequency band over which lock-in persists) is shown to increase with decreased structural damping, and increased ratio of displaced fluid mass to cylinder mass. The amplitude of the peak resonant response is found to be inversely proportional to the reduced damping.

Landl [67] includes a nonlinear aerodynamic damping term of fifth order in his two-equation model for vortex-induced vibrations of a bluff body. The equations are given in dimensionless form by

$$\ddot{x} + \delta \dot{x} + x = a\Omega^2 c_L \tag{2.8}$$

$$\ddot{c}_L + (\alpha - \beta c_L^2 + \gamma c_L^4) \dot{c}_L + \Omega^2 c_L = b\dot{x}, \tag{2.9}$$

where δ is a damping parameter, a is a mass parameter, and $\Omega = \omega_s/\omega_o$ is the ratio of the Strouhal frequency to the natural frequency of the cylinder. The parameters α, β, γ, and b are constants that can be chosen to approximate a given problem.

The author believes that inclusion of the damping term $\gamma c_L^4 \dot{c}_L$ results in a wake-oscillator model better able to capture the hysteresis effect. The hard excitation and soft excitation regimes seen in experimental results can be explained in terms of the three physically possible solutions of Eqs. 2.8 and 2.9: the zero solution and two additional positive solutions. The stability and instability of these solutions are investigated using the method of Lyapunov. Hard excitation regimes of flow velocities (or frequency ratios f_s/f_o) are those where two stable states are possible for a given flow velocity (or frequency ratio): the position of rest and a vibration of finite amplitude. Soft excitation ranges are those where the rest position is unstable so that a finite oscillation is always generated. Sometimes the second state in the hard excitation ranges is not that of rest, but an oscillation with small amplitude at the same frequency as the high amplitude oscillation. This phenomena cannot be explained by the mathematical model.

More recently, Facchinetti et al. [31] present an excellent review of the dynamics of wake-oscillator models for $2D$ vortex-induced vibrations. More specifically, the authors examine three different types of coupling terms for the action f of the structure on the fluid wake oscillator. In general, the action term is the right-hand side of a given fluid-oscillator equation. For instance, $f = b\dot{x}$ for the Landl model as can be easily deduced from Eq. 2.9. Velocity coupling $f = A\dot{x}$, displacement coupling $f = Ax$, and acceleration coupling $f = A\ddot{x}$ are considered. Velocity coupling is used extensively in the literature [47, 55, 67, 98]. With these different forms of coupling, the wake-oscillator models are compared with experimental data from the literature. It is found that the displacement and velocity couplings fail to predict the lift phase seen in experimental results of vortex shedding from cylinders forced to oscillate. Displacement coupling fails to predict the lift magnification at lock-in and almost all prominent features of vortex-induced vibration at low values of the Skop–Griffin parameter S_G, while velocity coupling fails to predict the range of lock-in for low values of S_G. The Skop–Griffin parameter is a single combined mass-damping parameter often used in the literature and is given by $S_G = 8\pi^2 S^2 \mu\zeta$, where μ is the dimensionless mass ratio and $\zeta = r_s/2m\Omega_s$ is the structure reduced damping. r_s is the viscous dissipation in the supports, m is the mass of the structure plus the fluid added mass, and Ω_s is the structure natural frequency. The dimensionless mass ratio is defined by the authors as $\mu = \left(m_f + m_s\right)/\rho D^2$, where $m_f = C_M \rho \pi D^2/4$ is the fluid added mass, and m_s is the mass of the structure. C_M is the added mass coefficient.

The key finding made by the authors is that the acceleration coupling succeeded in qualitatively modeling the features of VIV considered in the paper. Figure 2.9 illustrates the differences between the lock-in domains predicted by the model equations for (a) displacement coupling, (b) velocity coupling, and (c) acceleration coupling for a representative low value of $S_G = 0.01$. Comparison experimental data showing the upper and lower bounds of lock-in is represented by the triangles.

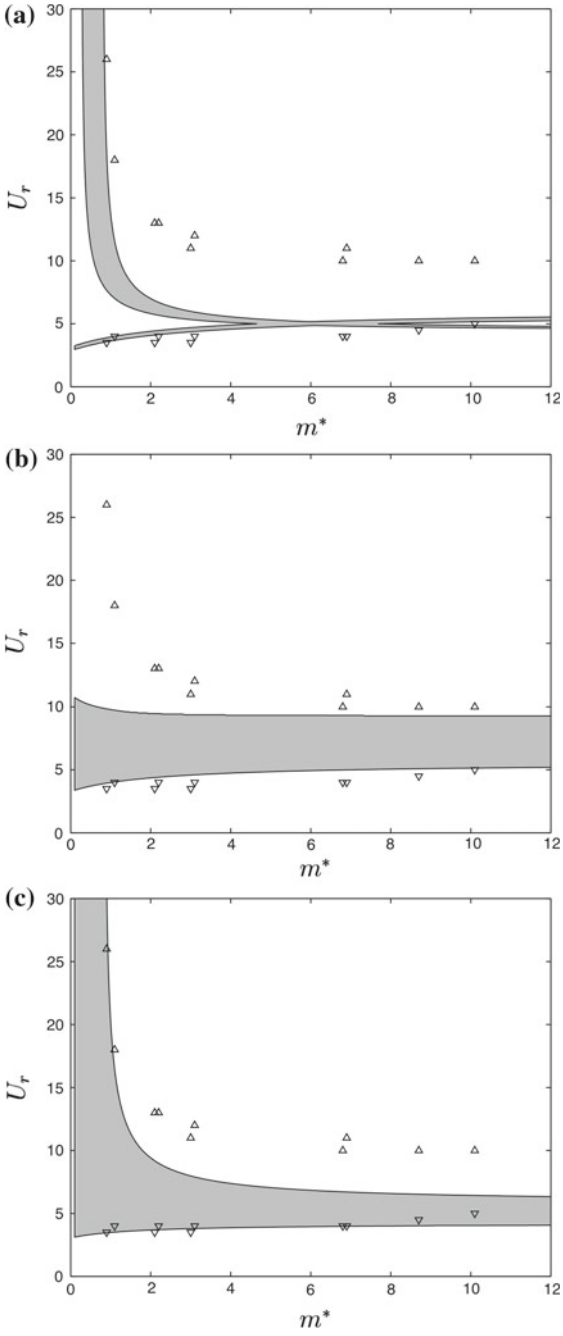

Fig. 2.9 Lock-in domains as a function of the reduced mass m^* for $S_G = 0.01$ and for the three different couplings: **a** displacement coupling, **b** velocity coupling, and **c** acceleration coupling. Comparison experimental data showing the upper and lower bounds of lock-in is represented by Δ [31]. Reprinted with permission

2.3.1.2 Elastic Cylinders

Several attempts have been made to extend the wake-oscillator models to elastic structural elements such as beams and cables. Iwan [53] extended the Iwan–Blevins model to predict the maximum VIV amplitude of taut strings and circular cylindrical beams with different end conditions. It is assumed that a strip theory approach can be applied to extend the equation of motion for the hidden flow variable z to the elastic structure. The strip theory approach assumes that there is no spanwise coupling in the flow, although the theory may fail to be accurate at small amplitudes of structural vibration since at these amplitudes the shedding process tends to be uncorrelated in spanwise composition. The structure is assumed to possess classical normal modes and the analysis is restricted to the cases in which the natural frequency of one of the modes is very near the shedding frequency, while all other modal frequencies are substantially removed from the shedding frequency. The author obtains an equation relating the maximum response amplitude for the structure in the n^{th} mode, $Y_{n_{\max}}$, to various structural parameters:

$$\frac{Y_{n_{\max}}}{D} = \frac{a_4\sqrt{4/3}\gamma_n}{2\pi^3 S^2 \mu_r \zeta_n^T}\left[\frac{(a_1 - a_{4)})}{a_2} + \frac{a_4^2}{\pi^2 a_2 S \mu_r \zeta_n^T}\right]^{\frac{1}{2}}. \tag{2.10}$$

Interestingly enough, the details of the structure enter into Eq. 2.10 only through a dimensionless mode shape parameter γ_n, and the product of the mass ratio $\mu_r = 4m/\rho\pi D^2$ and the modal damping ratio of the structure ζ_n. ζ_n^T is taken to be the sum of ζ_n and damping due to interaction with the fluid. The a_i are dimensionless model parameters.

A comparison is made of a "universal" maximum response amplitude with various experimental results of maximum VIV for three structural elements: cables, pivoted rods, and rigid cylinders. The response amplitude curves $(Y_{n_{\max}}/D)/\ \gamma_n$ are plotted as a function of $\mu_r\zeta_n$ using Eq. 2.10 for each structural element (Figure 2.10). The product $\mu_r\zeta_n$ is often referred to as the reduced damping and is almost identical to the Skop–Griffin parameter and the Scruton number discussed previously. The theoretical results show good agreement with experiments for amplitudes of response greater than 0.1 diameter. The data for the three different structural elements are shown to be consistent when normalized by the mode shape parameter.

Skop and Griffin [99] start with their version of a wake-oscillator model and proceed to extend it to elastic cylinders in an almost identical fashion, as above. They obtain the following equation for the maximum oscillation amplitude in the i^{th} pure mode,

$$\frac{Y_{i,MAX}(x)}{D} = \frac{A_{MAX}\left(S_{G,i}\right)|\psi_i(x)|}{\sqrt{I_{iiii}}},$$

where $\psi_i(x)$ is expression for the normalized mode. For example, $\psi_1(x) = x/L$ with $\psi_{i\neq 1} = 0$ for a pivoted rigid rod, and $\psi_i(x) = \sin(i\pi x/L)$ for a pinned–pinned beam. A_{MAX} is an amplitude parameter that is a function of the modal response parameter

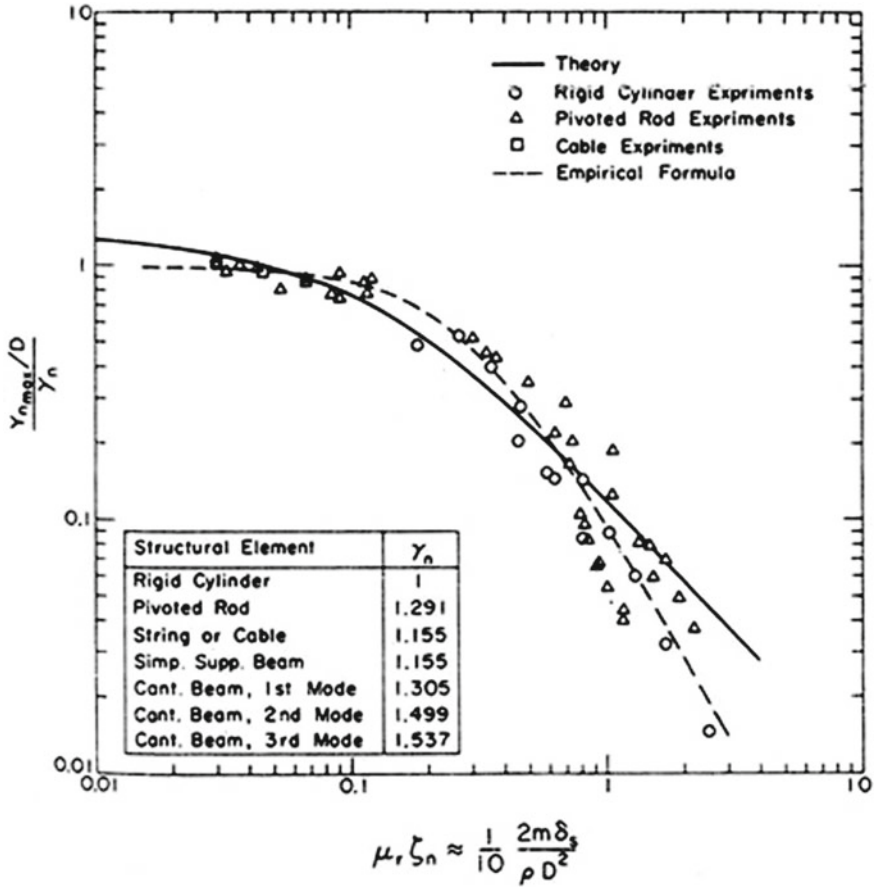

Fig. 2.10 Normalized maximum amplitude of response $Y_{n-max}/D/\gamma_n$ versus mass-damping parameter $\mu_r \zeta_n$ for different structural elements. ◯, rigid cylinder experiments; △, pivoted rod experiments; □, cable experiments; —, theory; – –, empirical formula. $\gamma_n = 1$ (rigid cylinder), $\gamma_n = 1.291$ (pivoted rod) and $\gamma_n = 1.155$ (string or cable) [53]. Reprinted with permission of the author

$S_{G,i} = \zeta_i/\mu_{ii}$, and μ_{ii} is given by

$$\mu_{ii} = \frac{\bar{\rho}\bar{D}}{8\pi S^2 M_i} \int_0^L \rho^*(x) \left[D^*(x)\right]^3 \left[\omega_S^*(x)\right]^2 \left[\psi_i(x)\right]^2 dx, \tag{2.11}$$

where $(\cdot)^*$ denotes a dimensionless variable, $\omega_S^*(x)$ is the dimensionless shedding frequency, $\bar{\rho}$ is the average fluid density over the shedding region, $\bar{D}$ is the average cylinder diameter over the shedding region, and M_i is the effective mass in the i^{th} mode. The integral in Eq. 2.11 is taken only over cylinder sections at which shedding occurs. I_{iiii} is defined by

$$I_{iiii} = \int_0^L [\psi_i(x)]^4 \, dx \Big/ \int_0^L [\psi_i(x)]^2 \, dx \; .$$

For example, $I_{iiii}^{-1/2} = I_{1111}^{-1/2} = 1.2910$ for a pivoted rigid rod. In general, good agreement is obtained with experimental data for flexible structures and cables, especially for $S_G < 0.5$ and $S_G > 2$.

Iwan [54] derives an analytical model for the VIV of nonuniform structures. In particular, he considers elastic systems that could be described by the one-dimensional damped wave equation (e.g., cables). His model also allows for nonuniform flow profiles and accounts for inactive elements. Iwan finds that for a particular pure response mode, the equations describing the system response reduced to those obtained for a rigid cylinder. In particular, for the n^{th} mode,

$$\frac{d^2\bar{y}_n}{dt^2} + 2\zeta_n^T \omega_n \frac{d\bar{y}_n}{dt} + \omega_n^2 \bar{y}_n = \left(\frac{\alpha_4}{\nu_n}\right) \frac{d\bar{z}_n}{dt}, \tag{2.12}$$

where α_4 is a model parameter, ζ_n^T is an effective (including fluid damping) structural damping, $\bar{y}_n(t)$ is the modal coefficient of the transverse displacement of the elastic system, $y(x, t)$, and $z_n(t)$ is the modal coefficient of the flow variable $z(x, y)$. ν_n is a parameter representing the effective system mass, defined as

$$\nu_n = \int_0^L m(x)\xi_n^2(x)dx \Big/ \int_0^L s(x)\xi_n^2(x)dx,$$

where $m(x)$ is the mass per unit length of the cable including the added fluid mass and any point masses, $s(x)$ is a function specifying which portions of the cable are being excited by locked-in vortex shedding, and $\xi_n(x)$ are the mode shapes. Equation 2.12 is essentially the same equation that governs the response of an elastically mounted rigid cylinder, with the presence of the parameter ν_n and the definition of ζ_n^T being the only differences.

The numerical results for various cable systems show that the response amplitude is strongly affected by cable nonuniformity. The reduction of the active region, the region over which vortex shedding occurs, and/or the addition of masses, generally reduces the amplitude of VIV.

Later models have added further refinements to the older models just described. Dowell [24] presents a method of constructing a fluid-oscillator equation for C_L which takes into account known theoretical and experimental behaviors of the fluid. Various self-consistency checks are performed on the model and numerical results are compared with those obtained from the Skop–Griffin model [98]. Several fundamental differences between the results are noted. Dowell's fluid oscillator is given by

$$\begin{aligned} &\ddot{C}_L - \varepsilon \left[1 - 4C_L/C_{L_o})^2\right] \omega_s \dot{C}_L + \omega_s^2 C_L = -B_1 (D/V^2) y \\ &+ \omega_s^2 \left[A_1 \left(\dot{y}/V\right) - A_3 \left(\dot{y}/V\right)^3 + A_5 \left(\dot{y}/V\right)^5 + A_7 \left(\dot{y}/V\right)^7\right], \end{aligned} \tag{2.13}$$

where ω_s is the fluid frequency given by the Strouhal relationship, ε is a parameter to be determined, $\{A_1, A_3, A_5, A_7, B_1\}$ are slowly varying functions of Reynolds number that are held fixed, and C_{L_o} is the peak magnitude of the limit-cycle oscillation obtained from Eq. 2.13 with $y = 0$ (a fixed cylinder). C_{L_o} is assumed to be a weak function of the Reynolds number and is assigned typical values.

Skop and Balasubramanian [97] present a modified form of the Skop–Griffin model [99] for flexible cylinders. The goal of the model is to accurately capture the asymptotic, self-limiting structural response near zero structural damping. The fluctuating lift force C_L is separated into two components: one component satisfying a van der Pol equation driven by the transverse motion of the cylinder, and one component which is linearly proportional to the transverse velocity of the cylinder (the stall term). Mathematically,

$$C_L(x,t) = Q(x,t) - \frac{2\alpha}{\omega_s}\dot{Y}(x,t),$$

where α is the stall parameter, ω_s is the intrinsic vortex-shedding frequency determined from the Strouhal relationship, $Q(x,t)$ is the component of C_L satisfying a van der Pol-type equation, $\dot{Y}$ is the time derivative of the amplitude of structural motion, and x is the length variable along the structure.

Krenk and Nielsen [65] propose a double oscillator model in which the mutual forcing terms are developed based on the premise that energy flows directly between the fluid and structure. This means that the forcing terms correspond to the same flow of energy at all times. In dimensional form, the coupled equations are given by

$$m_o\left(\ddot{x} + 2\zeta_o\omega_o\dot{x} + \omega_o^2 x\right) = \frac{1}{2}\rho U^2 DL\frac{\dot{w}}{U}\gamma \tag{2.14}$$

$$m_f\left[\ddot{w} - 2\zeta_f\omega_s\left(1 - \frac{w^2 + \dot{w}^2/\omega_s^2}{w_o^2}\right)\dot{w} + \omega_s^2 w\right] = -\frac{1}{2}\rho U^2 DL\frac{\dot{x}}{U}\gamma, \tag{2.15}$$

where x is the structural displacement, w is the transverse motion of a representative fluid mass m_f, ζ_f is the fluid damping ratio, ω_s is the undamped angular frequency of the fluid oscillator (determined from the Strouhal relation), γ is a dimensionless coupling parameter taken as a constant, and the parameters m_o, ζ_o, and ω_o have their usual meanings. The parameter w_o controls the amplitude of the self-induced vibration of the fluid oscillator in the case of a stationary cylinder. Note that a quadratic fluid damping term has been included in the formulation. Energy generation over a period begins with the negative damping (provides the self-excitation) term in Eq. 2.15. This energy is extracted by means of the right-hand side of Eq. 2.14. The transfer of energy to the cylinder occurs via the right-hand side of Eq. 2.15. This energy is then dissipated by the structural damping term.

Values for the model parameters are taken from experiments, and the model results display branching from below and above the lock-in region. The solution in the lock-in region is unstable, which the authors claim will lead to transition between the two

modes of oscillation. However, changes in model parameters do not show similar effects to changes in experimental parameters.

2.3.2 SDOF Models

Proponents of this type of modeling include Scanlan and Simiu [96], Basu and Vickery [2], and Goswami et al. [38]. Single degree-of-freedom (SDOF) models use a single ordinary differential equation to describe the behavior of the structural oscillator.

Using the notation of Goswami et al. [38], the general form of such models is given by

$$m(\ddot{x} + 2\zeta\omega_n\dot{x} + \omega_n^2 x) = F(x, \dot{x}, \ddot{x}, \omega_s t), \tag{2.16}$$

where m is the mass of cylinder, x is the transverse (lift direction) displacement, ω_s is the Strouhal frequency, and F is an aeroelastic forcing function. The influence of the wake dynamics is incorporated into Eq. 2.16 via the appropriate choice of the function F. They propose a model for the VIV of a flexibly supported cylinder that is a hybrid of the nonlinear SDOF model of Scanlan and Simiu [96] and the coupled wake-oscillator model of Billah [8]. The general form of this model is given by

$$\begin{aligned} &m(\ddot{x} + 2\zeta\omega_n\dot{x} + \omega_n^2 x) \\ &= \frac{1}{2}\rho U^2 D\left[Y_1(K)\frac{\dot{x}}{D} + Y_2(K)\frac{x^2}{D^2}\frac{\dot{x}}{U} + J_1(K)\frac{x}{D} + J_2(K)\frac{x}{D}\cos(2\omega_s t)\right]. \end{aligned} \tag{2.17}$$

In Eq. 2.17, $K = \omega_n D/U$ is the reduced frequency, $Y_1(K)$ is a linear aeroelastic damping term, $Y_2(K)$ is a nonlinear aeroelastic damping term, $J_1(K)$ is an aeroelastic stiffness term, and $J_2(K)$ is a parametric stiffness term. In essence, $Y_1(K)$ and $Y_2(K)$ represent the self-excitation and self-limitation characteristics of the response. $J_2(K)$ represents the coupling between the wake and the cylinder, and represents the key contribution of the wake oscillator. $J_1(K)$ represents the shift in the mechanical response frequency from the zero-wind frequency f_n. In other words, $J_1(K)$ represents any shift in the cylinder natural frequency from its zero-wind (resting state) value. The parameter values (Y_1, Y_2, J_1, J_2) are estimated through a range of reduced velocities and damping from experimental results [37] and the method of slowly varying parameters.

The results indicate a negligible frequency shift and consequently J_1 can be taken as zero. The remaining parameters (Y_1, Y_2, J_2) are collectively found to influence the peak amplitude of the response at lock-in, the location of the maximum response, and the band of appreciable response. The authors do not compare the performance of their model with experimental results from the literature.

Bearman [4] considers the following equation for a flexibly mounted bluff body (not necessarily a circular cylinder),

$$M\ddot{y} + 4\pi N_o \delta_s M\dot{y} + 4\pi^2 N_o^2 My = C_y \rho U^2 D/2, \tag{2.18}$$

where y is the displacement in the transverse direction, N_o is the undamped natural frequency of the body, M is the mass per unit length of the body, δ_s is the fraction of critical damping, and C_y is the transverse force coefficient for the bluff body due to the shedding vortices. Assuming that for large enough amplitudes the fluid force and the body displacement both oscillate at a certain frequency n_v, and that the fluid force must lead the cylinder motion by some phase angle ϕ, then solutions of the form $y = \bar{y}\sin(2\pi n_v t)$ and $C_y = \bar{C}_y \sin(2\pi n_v t + \phi)$ are sought. The following relationships are obtained by replacing the assumed solutions into Eq. 2.18,

$$\frac{N_o}{n_v} = \left[1 - \frac{\bar{C}_y}{4\pi^2}\cos(\phi)\left(\frac{\rho D^2}{2M}\right)\left(\frac{U}{N_o D}\right)^2\left(\frac{y}{D}\right)^{-1}\right]^{-1/2} \tag{2.19}$$

$$\frac{\bar{y}}{D} = \frac{\bar{C}_y}{4\pi^2}\sin(\phi)\left(\frac{\rho D^2}{2M\delta_s}\right)\left(\frac{U}{N_o D}\right)^2\frac{N_o}{n_v}, \tag{2.20}$$

where $\rho D^2/2M$ is the mass ratio, $\rho D^2/2M\delta_s$ is the mass-damping parameter, and $U/N_o D$ is the reduced velocity. Clearly, the frequency ratio N_o/n_v and the amplitude ratio $\bar{y}/D$ depend on the mass ratio. As seen from Eq. 2.19, a large value of the mass ratio means that the frequency of oscillation of the cylinder is appreciably different from its natural frequency. It is only for small values of the mass ratio that $N_o \approx N_v$. Equation 2.20 shows that it is that part of the fluctuating transverse force coefficient that is in-phase with the cylinder velocity which affects the amplitude ratio.

Chen et al. [20] present an unsteady flow theory for the structural response of a one DOF circular cylinder to vortex shedding. The model correctly pointed out the fluid-elastic instabilities in the lock-in region. For low oscillation amplitudes, as the flow passes through the lock-in region, the modal damping may become negative and the system becomes unstable. The amplitude continues to grow until it becomes large enough so that modal damping values increase and the system is stabilized.

2.3.2.1 Specific Applications of SDOF Models

Cai and Chen [16] studied the wind-induced large-amplitude response of a stack supported by cable guy wires at four levels. An unsteady flow theory developed in Chen et al. [20] is used to model the VIV of the stack. The theory is essentially a single degree-of-freedom model in which the effects of the flowing fluid are characterized as the fluid damping and stiffness, and these parameters are in turn dependent on oscillation amplitude, reduced flow velocity, and Reynolds number. For the stack considered by itself, it is found that the third mode, with natural frequency ≈2.2 Hz, is most vulnerable to vortex-shedding-induced resonance due to a large modal participation factor. The stack vibration can then be said to be due primarily to vortex shedding at the lower portion, which is mostly associated with the third mode. For

the stack-cable system, both the stack and the cables show characteristic peaks in their spectra at the lock-in resonances of the stack modes. Parametric resonances (secondary peaks) in the cables are a result of stack motion at the ends of the cable supports. In general, primary parametric resonances occur in cables with natural frequencies that are approximately half the lock-in frequency (i.e., the shedding frequency) of a given stack mode. Wind speed, cable tension, and damping are found to affect the parametric resonances. The parametric resonances in the cables may be significantly reduced by changing their natural frequencies through careful adjustment of the tensions.

A technique for the extraction of aeroelastic parameters from wind tunnel tests is described in Gupta et al. [46]. These parameters are used in the SDOF mathematical model for the VIV of a structure at lock-in. The authors use Scanlan's model,

$$m(\ddot{z} + 2\zeta\omega_n\dot{z} + \omega_n^2 z) = \frac{1}{2}\rho U^2 D\left[Y_1\left(1 - \epsilon\frac{z^2}{D^2}\right)\frac{\dot{z}}{U} + Y_2\frac{z}{D}\right] = F(z, \dot{z}, U, t). \tag{2.21}$$

The instantaneous fluctuating lift force term, $\frac{1}{2}C_L\sin(\omega t + \phi)$, has been neglected in this formulation since it is generally smaller than the aerodynamic lift caused by the motion of the body (i.e., $F(z, \dot{z}, U, t)$). The unknown parameters in Eq. 2.21 are the linear aeroelastic damping, Y_1, and the nonlinear aeroelastic damping, ϵ. The linear aeroelastic stiffness, Y_2, can be easily determined from oscillation frequency measurements. The technique described in the paper is based on the concepts of invariant embedding and nonlinear filtering theory, and is shown to be effective even for turbulent (noisy) conditions. Furthermore, the method works regardless of the initial conditions of the experiments (decaying method vs. self-excited method) and in situations where the steady state amplitude is very small. The calculated values of the parameters Y_1 and ϵ are presented as a function of the Scruton number, $S_c = 4\pi m\zeta/\rho D^2$, for a variety of section models, including laminar flow over a smooth cylinder and turbulent flow over a smooth cylinder.

2.3.3 Force-Decomposition Models

Sarpkaya [87] is credited with introducing the force decomposition model. In his model, the lift force on an elastically mounted rigid cylinder is decomposed into a fluid inertia force related to the cylinder displacement and a fluid damping force related to the cylinder velocity. The lift coefficient, C_L, is expressed as

$$C_L = C_{ml}\pi^2\frac{U_m T}{D}\left(\frac{D}{\bar{V}T}\right)^2\sin\{\omega t\} - \frac{8}{3\pi}C_{dl}\left(\frac{U_m T}{D}\right)^2\left(\frac{D}{\bar{V}T}\right)^2\cos\{\omega t\}, \tag{2.22}$$

where C_{ml} is the inertia coefficient, C_{dl} is the drag coefficient, T is the period of the transverse motion of the cylinder, $U_m = 2\pi A/D$, and $V_r = \bar{V}T/D$ is the reduced velocity. A is the maximum amplitude of the cylinder motion, and $\bar{V}$ is the velocity

of the ambient flow. Equation 2.22 can then be incorporated into the equation of motion for an elastically mounted, linearly damped, and periodically forced cylinder, yielding

$$\ddot{x}_r + 2\zeta \dot{x}_r + x_r = \rho_r \Omega^2 \left(C_{ml} \sin\{\Omega\tau\} - \frac{16}{3\pi^2} X_r C_{dl} \cos\{\Omega\tau\} \right). \tag{2.23}$$

In Eq. 2.23, $x_r = x/D$, Ω is the ratio of the cylinder oscillation frequency to its natural frequency f_c/f_n, ρ_r is the ratio of the fluid density to the density of the cylinder ρ_f/ρ_c, and $\tau = \omega_n t$. If the values of C_{ml} and C_{dl} corresponding to the V_r value at perfect synchronization can be determined from experiments, then Eq. 2.23 can be solved, and the response of the cylinder in the synchronization region ascertained.

Sarpkaya shows through a parametric study that the maximum response of the cylinder is governed by a single parameter, the stability (mass-damping) parameter S_G, for values of this parameter larger than about unity. This stability parameter is defined as $S_G = \zeta/a_o$, the ratio of the material damping to a mass ratio. For low values of the stability parameter, the mass ratio a_o and damping ζ affect the response separately. It is important to note that S_G, as defined by the author, can also be written as $S_G = 8\pi^2 \zeta S^2 M/\rho D$. In this form, it can be recognized as the Skop–Griffin parameter.

Griffin [42] and Griffin and Koopman [43] split the fluid force into an excitation part and a reaction part that includes all the motion-dependent force components. In nondimensional form, the equation of motion for an elastically mounted rigid cylinder is written as

$$\ddot{y} + 2\omega_n \zeta_s \dot{y} + \omega_n^2 y = \mu \omega_s^2 (C_L - C_R),$$

where C_L is the lift coefficient, C_R is the reaction coefficient, ω_s is the Strouhal frequency, ζ_s is the structural viscous damping, and μ is a mass parameter equal to the inverse Skop–Griffin parameter (i.e., $\mu = 1/S_G$). The fluid dynamic reaction (damping) force in phase opposition with the cylinder velocity is measured as a function of incident flow speeds (Re: 300–1000), including the lock-in speed. Also measured is the lift component in phase with the cylinder velocity. This is the component of the lift coefficient that is associated with energy transfer to the vibrating cylinder.

Wang et al. [103] introduce a nonlinear fluid-force model for the VIV of a single elastically supported rigid cylinder in a uniform crossflow. The vibration of the cylinder in the transverse (y) and streamwise (x) directions are analyzed using a 2-DOF structural model. The equations of motion are obtained from Euler–Bernoulli beam theory and the effects of vibration mode are accounted for through a modal analysis approach. The uncoupled modal equations of motion are given in dimensionless form by

$$\begin{aligned} \ddot{X}_n(z,t) + 2\zeta_{sn}\omega_{n0}\dot{X}_n(z,t) + \omega_{n0}^2 X_n(z,t) &= f_{xn}(z,t)\,/2M_r \\ \ddot{Y}_n(z,t) + 2\zeta_{sn}\omega_{n0}\dot{Y}_n(z,t) + \omega_{n0}^2 Y_n(t) &= f_{yn}(z,t)\,/2M_r\ , \end{aligned}$$

where z is along the axis of the cylinder, ζ_{sn} is the structural damping in the n^{th} mode, M_r is structural mass ratio, ω_{n0} is the natural frequency of a stationary cylinder, $f_{xn}(z,t)$ is the fluid-force coefficient in the streamwise direction in the n^{th} mode, and $f_{yn}(z,t)$ is the fluid-force coefficient in the transverse direction in the n^{th} mode. Note that for an elastically mounted rigid cylinder $(n=1), f_{x1}(t) = c_D(t) - c_L(t)\dot{Y}_1(t)$ and $f_{y1}(t) = c_D(t)\dot{Y}_1(t) - c_L(t)$, where $c_D(t)$ is the drag force coefficient and $c_L(t)$ is the lift force coefficient. It is also worth mentioning that for a stationary rigid cylinder, the transverse and streamwise fluid-force coefficients will coincide with the lift and drag force coefficients, respectively.

A 2-DOF model is used because it has been found that streamwise oscillations have a substantial effect on the transverse vibrations and their characteristics [115]. Higher harmonics representing the nonlinearity in the fluid–structure interaction are accounted for in the form of nonlinear expressions for the fluid forcing terms. The fluid-force components of the model are obtained from amplitude and frequency data for a freely vibrating cylinder in crossflow by carrying out a spectral analysis of the time series of structural vibrations using the autoregressive–moving-average (ARMA) technique. Analysis of the power spectral density of the cylinder response indicates the presence of higher harmonics in both the resonance and off-resonance responses. Specifically, the vortex-shedding frequency and higher harmonics of the shedding frequency are present in the resonance response. The off-resonance response shows the presence of the vortex-shedding frequency and higher normal modes of the structure. The fluid-force components of the model are found to be dependent on structural damping and mass ratio. The model is used to predict the VIV of an elastic cylinder which is fixed at both ends, and the results were compared with experimental results and the SDOF model of Sarpkaya. The experimental results of Goswami et al. [37] verify the presence of both the shedding frequency and the natural frequency of the structure in the spectrum of the cylinder vibration within lock-in and outside lock-in. The structural response thus contains two distinct frequencies and these are manifested in the form of a beat. This has been verified by the Benaroya-Wei [6] model discussed in more detail in Chap. 4.

2.4 Variational Approach

Efforts to model fluid dynamics by using variational principles can be traced back to a work by Millikan in [77]. He tried to obtain the governing equations of steady motion of a viscous, incompressible fluid by using Lagrange's equations. He started from the energy balance equation of a control volume. Then, he imposed the continuity equation on the energy balance equation by means of Lagrangian undetermined multipliers. He concluded that it is impossible to obtain the Navier–Stokes equations for a steady motion of a viscous, incompressible fluid from Lagrange's equations unless certain conditions are met. However, Millikan could not find realistic examples where those conditions are met.

Since Millikan's work, tens of attempts have been made to carry out similar studies. Next, we review a few of these that are believed to be good representative works. In Chaps. 6 and 7, we refer to some of these papers in order to point out some of the difficulties faced in using variational methods for fluid systems. The challenges are extensive.

Another early attempt in applying Hamilton's principle to a system of particles is the work by Eckart [26]. His goal was to obtain the equations governing electrodynamic motions. He used Hamilton's principle and imposed Maxwell's equations in the form of electromagnetic potentials (as constraints) by utilizing Lagrange multipliers. The resulting variational equation can be considered for modeling an irrotational ideal fluid system if the electromagnetic potentials are replaced with velocity potentials.

In 1954, Herivel [48] argued that it is hard to imagine how Hamilton's principle would follow the same exact rules in the Eulerian description as it follows in the Lagrangian one. Therefore, one must first transform the Lagrangian function to Eulerian form before imposing the variations. He also explained that Hamilton's principle can only be used in the absence of irreversible processes, that is, it can only be applied to an ideal fluid. Therefore, Herivel used a Jacobian matrix and transformed the Lagrangian coordinates into the Eulerian frame. Similar to Eckart's work, he used Lagrangian multipliers to impose the continuity and the entropy transport equations. Then, he utilized a specific form of Clebsch's transformation to obtain the velocity potentials. The resulting variational equation was an extension of Hamilton's principle containing Lagrangian variations and Eulerian functions. Compared to the earlier models, Herivel's method has the advantage that it can also be used for rotational motions.

In a later paper, Eckart [27] discussed the difficulties of deriving a general variational principle in a Eulerian representation, and that, therefore, the Lagrangian approach is preferable. Considering the conservation law in terms of a Lagrangian energy–moment tensor, he used a Jacobian matrix to backtrack the particles to their initial positions while normalizing the coordinates with respect to density. Then, he obtained the Lagrangian equations for the motion of both incompressible and compressible fluids. Also, he discussed the importance of Clebsch's transformation when integrating problems involving vorticity. Eckart's model has the disadvantage that it requires the coordinates of each particle to be specified at least at two different points in time.

Penfield [84] used Hamilton's principle to derive the equation of motion for a simple, inviscid fluid. He makes some interesting points regarding the application of Hamilton's principle. The pertinent variables can be classified as either geometric (e.g., position, velocity, strain) or force (force, pressure, stress). Constitutive laws govern the physical properties of the material or system and relate force and geometric variables. Penfield mentions that geometric laws are usually the most obvious while force laws the least.

Seliger and Whitham [93] present a discussion of variational principles in continuum mechanics, in particular, fluid dynamics, plasma physics and elasticity. The

discussion is in the context of finding a variational principle for a given system of equations. An interesting discussion opens their paper:

> When Lagrangian coordinates are used in continuum mechanics, the similarity with a system of discrete particles is observed. In particular, the equations of motion can be derived from Hamilton's principle that the difference between the kinetic energy and potential energy be stationary. The sum over particles becomes an integral over a volume of material, but no essential change is required. However, when an Eulerian description is adopted, this close similarity with a system of particles is lost; it becomes more difficult to find suitable variational principles and to see the connection between the variational principles that have been found for different specific problems. Perhaps one can argue that the Eulerian description is introduced primarily as a mathematical device and, as a consequence, we get more involved in straight mathematical manipulations; the basic physics is described by Hamilton's principle, but the Eulerian description raises mathematical problems.

Bretherton [14] tried to obtain the Eulerian equations of motion from the Lagrangian formulation of Hamilton's principle. His main aim was to clarify some of the inconsistencies in the literature. He stipulated that there must exist an inverse mapping function of Lagrangian trajectories that can be used to trace particle positions to some earlier configuration. As a result, he assumed that the density at each instant of time is related to the density at some reference time via the Jacobian mapping of Lagrangian trajectories to the inverse mapping function. Having obtained the Eulerian variations as functions of the Lagrangian virtual displacement, he applied the Eulerian variation to the action integral. The results were equations containing the Eulerian functions and the Lagrangian virtual displacements. As an example, Bretherton obtained Kelvin's circulation theorem using his variational approach.

Another effort in applying Hamilton's principle to fluid mechanics problems is the work by Leech [70]. He argued that Hamilton's principle cannot be directly applied to a control volume as it is defined for a system of particles. Also, he discussed that the variational operator does not commute with the control volume. Rather it commutes with mass integrals as the integration limits are invariant. Moreover, he noted that Hamilton's principle expressed in the form $\delta \int L dt = 0$ can only be used for conservative systems. For nonconservative systems, the original statement of the principle must be used. Additionally, he assumed that there must exist a function that maps the instantaneous displacements of fluid particles to a reference state. Then, he used the Jacobian matrix to map the integrals back to a reference frame—in the same manner that is usually used to prove Reynolds transport theorem (RTT). His manipulations resulted in an integral equation containing the variation of the mapping functions. Then, Leech suggested that one may use Hamilton's principle to optimize an assumed solution. Therefore, a class of displacement functions (called *admissible functions*) can be chosen for a problem and their weighting functions can be optimized using his formula. To elaborate on his method, he considered a few problems. One such problem was the interaction between an incompressible inviscid flow and a structure, called d'Alembert's paradox, in which d'Alembert proved that the drag force is zero.

Salmon [85, 86] developed a substantive discussion of the application of Hamilton's principle to problems of fluid mechanics. Of particular interest is his development of Eulerian forms of Hamilton's principle.

McIver [75] formulated an approach to modeling fluid dynamics using an extended form of Hamilton's principle for problems involving fluid–structure interactions. His approach is provided in more detail in Chap. 7. Having considered Hamilton's principle for a system of continuous particles, McIver utilized Reynolds transport theorem to modify the principle for a system of changing mass (control volume, CV). For a moving control volume, it is customary to consider the relative velocities of the fluid particles with respect to the control volume. However, McIver considered the velocity of the control volume with respect to the fluid particles, $\boldsymbol{u}_r$, for which he did not provide any justification. Perhaps McIver's aim was to introduce the backtracking concept that has been used by the previously mentioned authors at this stage of his formulation. Also, he assumed that the virtual work performed on a control volume is purely due to the surface tractions at the control surface. Therefore, using the stress dyadic, $\bar{\boldsymbol{\sigma}}$, he considered the virtual work to be

$$\delta W = \int_{CS} \delta \boldsymbol{r} \cdot \bar{\boldsymbol{\sigma}} \cdot \boldsymbol{n} \, dA, \tag{2.24}$$

where $\delta \boldsymbol{r}$ is the virtual displacement, $\boldsymbol{n}$ is the normal vector to the differential surface element dA, and CS is the control surface. For fluid–structure interaction problems, the control volume can be chosen so that some portions of the control surface match the structural surfaces. Denoting the portions of the CS where the flow cannot pass through by CS_C (closed CS), and representing the rest of the CS by CS_O (open CS), McIver's extension of Hamilton's principle is given by

$$\delta \int_{t_1}^{t_2} (T - \Pi)_{CV} dt + \int_{t_1}^{t_2} \int_{CS_O} \left[\delta \boldsymbol{r} \cdot \bar{\boldsymbol{\sigma}} \cdot \boldsymbol{n} + \rho \left(\boldsymbol{u} \cdot \delta \boldsymbol{r} \right) \left(\boldsymbol{u}_r \cdot \boldsymbol{n} \right) \right] dA dt + \int_{t_1}^{t_2} \int_{CS_C} \delta \boldsymbol{r} \cdot \bar{\boldsymbol{\sigma}} \cdot \boldsymbol{n} dA dt = 0, \tag{2.25}$$

where $\boldsymbol{u}$ is the absolute velocity of the fluid particles, T is the kinetic energy and Π is the potential energy.

Equation 2.25 represents a stationary process if the integrand of the second term always disappears at CS_O, that is,

$$\bar{\boldsymbol{\sigma}} + \rho \boldsymbol{u} \boldsymbol{u}_r = 0, \quad \text{or} \quad (\bar{\boldsymbol{\sigma}} + \rho \boldsymbol{u} \boldsymbol{u}_r) \cdot \boldsymbol{n} = 0 \ \text{ at } CS_O. \tag{2.26}$$

Therefore, the applicability of McIver's equation is restricted to the cases where such a control volume can be distinguished from the physics of the problem, where the fluid is bounded by the structure. McIver considered two simple problems as examples, a rocket problem and a flexible pipe problem.

Along similar lines, Xing and Price [112] modified Hamilton's principle for nonlinear ship–water interactions. They considered that imposing virtual displacements cause the particles to be virtually transported across an assumed control volume. They defined a general integral function of interest, say H, as

$$H[\phi] = \int_{t_1}^{t_2} \int_{CV} F\left(\phi, \frac{\partial \phi}{\partial t}\right) dV dt, \tag{2.27}$$

where ϕ is a continuously differentiable function of displacement, $\boldsymbol{x}$, and time, t. Denoting the local variation (Eulerian) by $\bar{\delta}$ and the material variation (Lagrangian) by δ, they obtained the local variation of H to be

$$\bar{\delta} H = \int_{t_1}^{t_2} \left\{ \int_{CV} \bar{\delta} F dV + \int_{CS} F\left(\phi, \frac{\partial \phi}{\partial t}\right) (\delta \boldsymbol{x} \cdot \boldsymbol{n})\, dA \right\} dt. \tag{2.28}$$

Therefore, the variation of H is twofold: the Eulerian variation inside the control volume and the flux of H due to Lagrangian virtual displacements. Then, their model was applied to a rigid ship traveling in calm water and in waves. Xing and Price's method requires further simplifications and assumptions as it contained both Lagrangian and Eulerian variations.

Benaroya and Wei [6] considered a more general type of FSI problem than McIver, where the fluid contains the structure. They showed that Hamilton's principle becomes a statement of the first law of thermodynamics, or conservation of energy, when the configuration is not known at any time. Similar to McIver's approach, they used the RTT to relate Hamilton's principle to a control volume. However, unlike the McIver's use of RTT, they chose the conventional form of RTT where the relative velocities, $\boldsymbol{u}_r$, are the relative fluid particle velocities with respect to the control volume. They presented their governing equation as

$$\begin{aligned} \frac{d}{dt} \left(T_{\text{structure}} + \Pi_{\text{structure}}\right)_{CV} = & \int_{CS} \frac{1}{2} \rho u^2 \left(\boldsymbol{u}_r \cdot \boldsymbol{n}\right) dA \\ & + \int_{CS} \left(-p\boldsymbol{n} + \boldsymbol{\tau}\right) \cdot \boldsymbol{u} dA - \left(m_{\text{fluid}} u \dot{u}\right)_{CV}, \end{aligned} \tag{2.29}$$

where m_{fluid} is the mass of fluid contained by the CV, p is the pressure, and $\boldsymbol{\tau}$ is the shearing force. They explained that the terms on left-hand side of Eq. 2.29 are the structural dynamic terms, and the right-hand side terms can be evaluated experimentally. The result is the acceleration of the structure that can be integrated twice to obtain the structure's displacement.

In parallel with their theoretical development, Benaroya and Wei conducted a series of experiments [23] on the VIV of a circular cylinder in uniform flow. The cylinder was free to vibrate transversely to the flow direction. Having input the experimental data to Eq. 2.29, they showed that their model is successful in predicting the frequencies of the structural oscillation as well as in capturing the beating behavior that is usually observed in VIV. However, the predicted response amplitudes were roughly half of the experimental values. Their results are shown in Fig. 2.11. They concluded that these differences are most likely due to the choice of control volume. Having obtained a CV for which the predictions of the model matched the experimental values (shown in Fig. 2.12), they concluded that the control volume must contain both upstream and downstream sections of the flow where the downstream

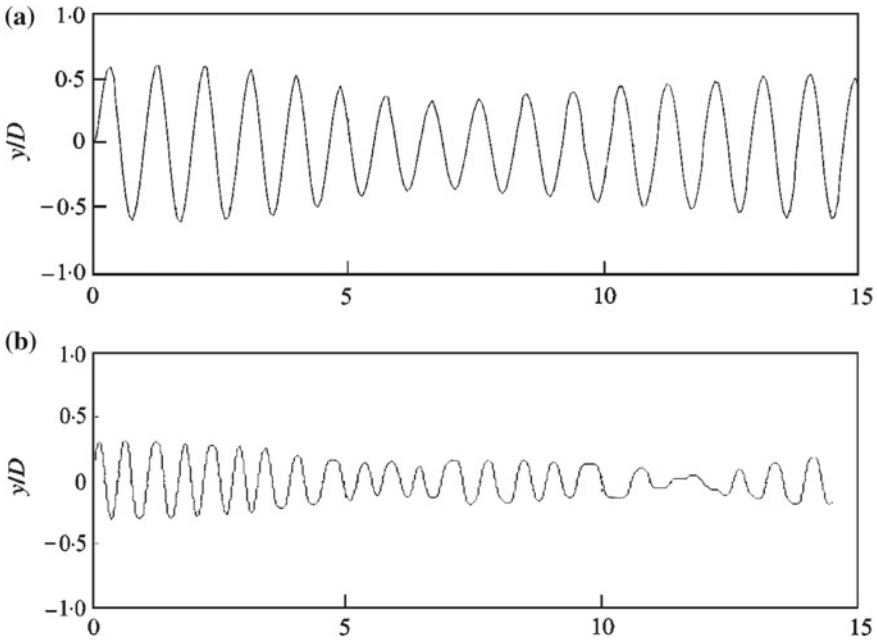

Fig. 2.11 Predicted (bottom) versus experimental (top) amplitudes. Both plots are in seconds [6]. Reprinted with permission

control surface is far enough from the structure as to not pass through the vortex formation region, yet not too far as it will not capture the true kinetic energy flux due to the dissipation of energy. Benaroya and Wei showed that when the configuration is unknown, which is the case for the majority of fluid and fluid–structure interaction problems, the result of Hamilton's principle is not a variational principle. This approach is detailed in Chap. 4.

However, the satisfactory results of their studies motivated the research work by Gabbai and Benaroya to modify the same approach as to obtain a variational method [35]. The experiments show the existence of a *formation region* (cavity) in the vicinity of a cylinder that is immersed in a flow. They assumed that the energy is evenly exchanged between the cylinder and the wake in the formation region. Denoting the displacement of this cavity by w, they obtained their variational equation as

$$\int_{t_1}^{t_2} am_{\text{cavity}}\dot{w}\delta\dot{w}dt + \delta\int_{t_1}^{t_2}\frac{1}{2}m\dot{x}^2dt - \delta\int_{t_1}^{t_2}\frac{1}{2}kx^2dt - \int_{t_1}^{t_2}c\dot{x}\delta xdt - \int_{t_1}^{t_2}\delta W\left(\dot{w},\ddot{w},x,\dot{x},\ddot{x},t\right)dt - \delta\int_{t_1}^{t_2}F(w,t)\delta wdt = 0, \quad (2.30)$$

where the overdot denotes d/dt, m denotes the mass, x is the displacement of the cylinder, k is the structural stiffness, c is the structural damping, δ is the variational operator, t is time, F is the fluid stiffness, and W represents instantaneous total work

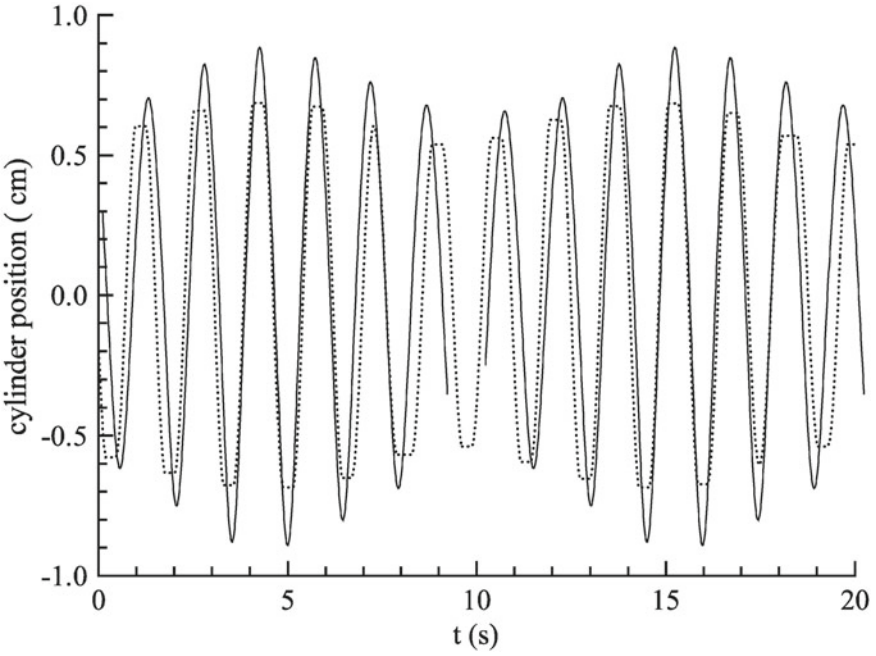

Fig. 2.12 Comparison of phase-averaged cylinder position versus time measurements (solid line) with reduced-order model response (dotted line). Reprinted with permission

done by the transverse hydrodynamic force acting on the cylinder, $F_{fl/st}$, and by the viscous and pressure forces inside the cavity, $F_{\mu/p}$. Therefore,

$$\delta W\left(\dot{w}, \ddot{w}, x, \dot{x}, \ddot{x}, t\right) = -F_{fl/st}\left(\dot{w}, \ddot{w}, \dot{x}, \ddot{x}, t\right)\delta x + F_{\mu/p}\left(\dot{w}, \ddot{w}, \dot{x}, \ddot{x}, t\right)\delta w. \quad (2.31)$$

Then, based on the literature, the authors proposed some general functions for $\dot{w}$, $\ddot{w}$, $\dot{x}$, $\ddot{x}$, t, and lift coefficient for $F_{fl/st}$ and $F_{\mu/p}$. They showed that three of the existing wake-oscillator models are each a specific case of their more general model. This approach is discussed in Chap. 5.

As evident from the literature, the efforts to apply Hamilton's principle and Lagrange's equations to the problems of fluid dynamics have had relative success in certain cases, mainly ideal fluids. There exist no general variational approaches for fluid–structure interactions, nor for fluid dynamics problems. One main challenge arises from relating the variational principles in the Lagrangian frame to the Eulerian frame, and the relations between dynamic properties described in these reference frames. A recent development along these lines has been put forth by Mottaghi and Benaroya [79, 80], and is discussed in Chaps. 6 and 7.

2.5 Numerical Methods

Numerical methods are an alternative way to solve the fully coupled problem of VIV of bluff bodies. Among the major methods used are time-marching schemes (for example, Jadic et al. [56]) and direct numerical simulation (for example, Evangelinos [28]), the discrete vortex method, and the vortex-in-cell method. These numerical simulations are usually restricted to the lower end of the Reynolds number spectrum.

Zhou et al. [115] use the vortex-in-cell method to solve the problem of two-dimensional incompressible flow past an elastic circular cylinder. The detailed numerical formulation of the vortex-in-cell method is quite complex and beyond the scope of this review. Details can be found in Meneghini and Bearman [76] and Sarpkaya [89, 90]. The structure is modeled as a spring–damper–mass system with two translational degrees-of-freedom. A constant Reynolds number of 200 is chosen for all simulations, based on the fact that at this Reynolds number the shedding vortices are still two-dimensional and the wake is laminar. A finite-difference scheme is implemented to solve the vorticity transport equation. The forcing terms on the right-hand side of the cylinder equations of motion at each time step are obtained from the flow-field calculations through the integration of the pressure and wall shear stress around the cylinder surface. The reference frame is fixed on the cylinder and consequently, after the cylinder motion is determined at each time step, a flow equal and opposite to the cylinder motion must be superimposed to the flow field. The frequency characteristics of the force, displacement, and velocity fields are obtained using an ARMA technique. The fluid motion is then solved in the next time step accounting for these effects. The process is repeated in an iterative way.

The results of the numerical simulations indicate that the cylinder response is not only strongly dependent on the Skop–Griffin parameter (reduced damping), but also on the mass ratio. It is the natural frequency of the fluid–structure system f_n^* and not the structural natural frequency f_n that is very close to the natural shedding frequency f_s^* when the peak structural response occurs. The importance of the fluid damping, through the Skop–Griffin parameter, is illustrated by noting that even when the natural frequency of the fluid–structure system is near the natural shedding frequency, a limit-cycle oscillation (i.e., a self-limited oscillation) results. The amplitude of the limit-cycle oscillation decreases as the Skop–Griffin parameter increases. In general, the 1-DOF (transverse motion only) model is only able to qualitatively reproduce some of the results obtained with the 2-DOF model. This suggests that the streamwise motion does indeed influence the motion in the transverse direction.

2.5.1 Direct Numerical Simulation

Evangelinos et al. [29] use direct numerical simulations (DNS) based on spectral elements to simulate the flow past rigid and flexible cylinders. The simulations are conducted at a Reynolds number of 1000, where the flow exhibits a turbulent wake,

Table 2.1 Summary of time- and span-averaged amplitude, lift and drag coefficients at lock-in [29]. Reprinted with permission

Cylinder type	$y_{\max}/d$	y_{rms}/d	$(C_l)_{rms}$	C_d	$(C_d)_{rms}$
Stationary	0	0	0.12	1.04	0.02
Rigid	0.75	0.51	1.53	2.11	0.65
Short beam—free	0.93	0.51	0.83	1.86	0.48
Short beam—fixed	1.09	0.43	0.86	1.81	0.43
Long beam—free	0.61	0.36	0.93	1.75	0.51
Long beam—fixed	0.85	0.25	1.16	1.62	0.44

and the cylinder is allowed only vertical motions in the crossflow direction. The main assumptions are that there is no structural damping and that the structural eigenfrequency is "locked-in" to the Strouhal number of the corresponding stationary cylinder flow. Simulations are conducted for a rigid cylinder of normalized spanwise length $L_z = 4\pi$, where the cylinder diameter d is used as the scaling factor. Simulations for flexible cylinders are conducted for the following cases: (1) a short cylinder of spanwise length $L_z = 4\pi$ with free ends, (2) a long cylinder of spanwise length $L_z = 378$ with free ends, (3) a short cylinder of spanwise length $L_z = 4\pi$ with pinned ends, and (4) a long cylinder of spanwise length $L_z = 378$ with pinned ends.

Table 2.1 presents a summary of the results of the simulations. It is stated that the errors in the given values are less than 10%. Note that the RMS lift coefficient $(C_l)_{rms}$ for the freely oscillating rigid cylinder is much larger than it is for the other cases, while the stationary cylinder has the smallest value. The same can be said for the mean and RMS values of the drag coefficients, C_d and $(C_d)_{rms}$, respectively.

Guilmineau and Quetey [45] consider vortex shedding from the forced oscillation of a circular cylinder in two distinct cases: the flow induced by the harmonic in-line oscillation of a cylinder in a quiescent body of water, and the flow induced by a transversely oscillating cylinder in a uniform flow of Reynolds number 185. In both cases, the two-dimensional unsteady Navier–Stokes equations are solved using a control volume approach with an algorithm (consistent physical interpolation, CPI) implemented to reconstruct the velocity fluxes. For the in-line oscillation study, the Reynolds number is fixed at 100 and the Keulegan–Carpenter (KC) number is fixed at 5. The Reynolds number is defined by $Re = U_m D/\nu$ and the Keulegan–Carpenter number is defined by $KC = U_m/f_e D$, where U_m is the maximum oscillatory velocity, ν is the kinematic viscosity, and f_e is the frequency of the oscillatory flow.

At the KC number used in the study, a periodic vortex formation is observed, consisting of vortices with symmetrical locations with respect to the line of motion of the cylinder. The in-line force time history acting is computed and the results compared with that predicted by the Morison equation. Agreement is generally good, except for the extremes of the time history. For the transverse oscillation study, the mechanisms of vortex switching are examined as functions of the ratio of the vortex shedding or excitation frequency (f_e) to the natural shedding frequency from

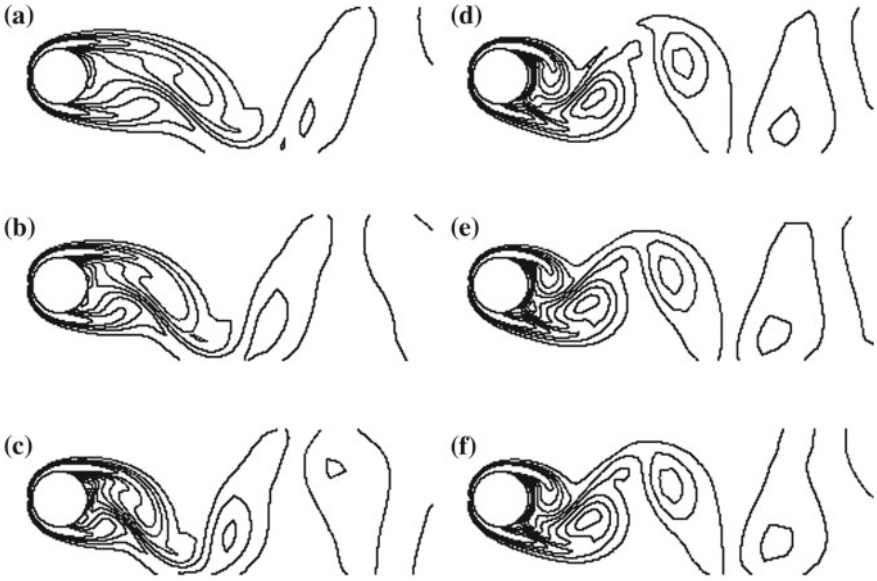

Fig. 2.13 Instantaneous vorticity contours for $Re = 185$ and $A/D = 0.2$. In all frames, the location of the cylinder is at its extreme upper position. Values of $f_e = f_0$ equal to: **a** 0.80, **b** 0.90, **c** 1.00, **d** 1.10, **e** 1.12, **f** 1.20 [45]. Reprinted with permission

a stationary cylinder (f_o), f_e/f_o. As f_e/f_o increased, the concentration of vorticity in the wake of the cylinder moves closer to the cylinder, resulting in a tighter vortex structure (Fig. 2.13). A limiting position is reached and the vorticity concentration abruptly switches to the opposite side of the cylinder.

Willden and Graham [104] use a quasi-three-dimensional extension of strip theory to simulate the low Reynolds number VIV of a long flexible circular cylinder with a low mass ratio and zero damping. The reduced velocity is defined as $V_r = U/f_n D$, where f_n is the natural frequency of the cylinder. The mass ratio is defined as $m^* = 2m/\rho D^2$, where m is the mass per unit length of the cylinder. The simulations for free transverse vibration of the flexibly mounted cylinder indicate that for very low mass ratios, the fluid (through the added mass) is dominant over the structure in controlling the oscillatory frequency throughout lock-in. In other words, the oscillatory and vortex-shedding frequencies remain locked-in to one another throughout the reduced velocity range simulated, $V_r = 2.5$–16. This phenomenon does not occur in systems with high mass ratios. For such systems, the vortex-shedding frequency is entrained by the structural frequency, $f_v \approx f_n$. It is also seen that the body oscillates at approximately the natural frequency of the combined fluid and structure system throughout lock-in. By decomposing the component of lift coefficient in-phase with the cylinder motion into contributions from pressure and shear forces, it is found that the shear force component in-phase with the cylinder velocity effectively acts as hydrodynamic damping, balancing the positive excitation force provided by the pressure force in-phase with the cylinder velocity. These shear and

pressure forces are found to be quite large in magnitude. Shear flow simulations past the $3D$ cylinder are also performed and cellular shedding in the wake is observed. Despite the presence of the shear flow, the vortex shedding remained correlated over a substantial length of the cylinder.

Blackburn et al. [11] present a complementary numerical and experimental study of the VIV of a rigid cylinder at low Reynolds number flow. The fluid and mechanical (mass ratio, mass-damping) dynamic parameters are matched in both the simulations and the experiments. Two-dimensional flow simulations were unable to predict the nature of the multi-branched plot of amplitude A^* versus SV_r. The Strouhal number S for a fixed cylinder is used to normalize the reduced velocity V_r, thus leading to the product SV_r. The reasoning behind this normalization is that the $2D$ and $3D$ simulations actually have different Strouhal numbers for the same Reynolds numbers, 0.225 and 0.205, respectively. Three-dimensional flow simulations generate results similar to the experimental results, in spite of the fact that the cylinder end boundary conditions are not exactly the same as in the experiments and the axial resolution and extent of the simulations are less than desirable. The $3D$ simulations coincide with the experimental results in the prediction of a $2P$ type vortex-shedding mode for a representative SV_r value of 1.27 along the lower branch of the response curve. The $2P$ type vortex-shedding mode is first reported in Williamson and Roshko [110] and corresponds to two pairs of counterrotating vortices per shedding cycle.

Blackburn and Henderson [10] conduct a detailed numerical study of the phase change of vortex shedding with respect to cylinder motion commonly observed in experimental studies of flows past stationary and oscillating cylinders. In this context, phase change means the change in the phase angle ϕ between the cylinder crossflow displacement $y(t)$ and the fundamental harmonic of the lift force F_L. The Reynolds number is fixed at 500 and the oscillation amplitude of the cylinder is fixed at $y_{\max}/D = 0.25$. Experimental studies have indicated that the timing of vortex formation switches phase by approximately 180° over a narrow band of structural oscillation frequencies in the primary lock-in regime. In other words, there exists a certain frequency range such that for a fixed point in the cylinder motion cycle, the side of the cylinder where the first vortex is formed will change abruptly. The switch is found to affect the sign of the mechanical energy transfer between the cylinder and the surrounding fluid, as well as the phase of the vortex-induced forces on the cylinder. Furthermore, the timing of this phase shift is strongly affected by the frequency ratio $F = f_o/f_v$, where f_o is the cylinder crossflow oscillation frequency and f_v is the natural shedding frequency from a fixed cylinder. The dimensionless form of the mechanical energy transferred from the flowing fluid to an oscillating cylinder per motion cycle is given as

$$E = \frac{1}{2}\oint (C_L d\alpha + \alpha dC_L), \tag{2.32}$$

where C_L is the lift coefficient and α is an instantaneous dimensionless displacement variable $\alpha(t) = y(t)/D$. Positive values of E correspond to work done on the cylinder, while negative values correspond to work done on the surrounding fluid. It can be

shown that E is positive when ϕ is in the range 0–180°. The sign of E is ascertained from the phase plane plot of $y(t)$ versus C_L, which is in the form of a limit cycle during frequency entrainment (lock-in). The sign of E is positive if the direction of traverse in the limit cycle is clockwise. By considering the range $0.75 < F < 1.05$ and calculating E for each increment (or decrement) ΔF from two initial points $F = 0.875$ and $F = 0.975$, a bifurcation solution with hysteresis effects is found in the transition to these states.

Four solution branches corresponding to periodic shedding states are observed: two branches associated with Kármán street wakes (K_1 and K_2), a branch characterized as the asymmetric two-cycle mode (A_1), and a branch characterized as the asymmetric synchronized branch (A_2). The K_1 branch has negative values of E at lower frequencies and progresses to positive values at higher frequencies. The A_1 and A_2 branches always have positive values of E. The K_2 branch always has negative values of E. The transitions between the branches is rather complicated and cannot be easily categorized. Of interest is a band of frequencies $0.905 < F < 0.95$, termed the weakly chaotic oscillator range, in which the sign of E changes between the K_1 and K_2 branches. In this band, the sign of E and the phase angle ϕ transition from positive to negative values in a discontinuous fashion. Figure 2.14 shows the different branches in the F–E plane. It is suggested that the relaxation oscillator behavior seen in this range is indicative of different mechanisms vying for control of the wake dynamics. The competing mechanisms are the relative magnitudes of the pressure-gradient and the surface-acceleration vorticity generation. Several tests are performed to test the validity of this hypothesis, and results presented do lend validity to this claim.

2.5.2 The Finite Element Method

Barhoush et al. [1] use an approach based on the finite element method and Scanlan's vortex-shedding empirical model to analyze the VIV response of plane frame ($2D$) structures. The equations of motion for a plane frame element, having two degrees-of-freedom per node, are obtained from Hamilton's principle. The equations motion for the plane frame element are obtained in terms of the displacements and rotations at its nodes. The virtual work of the nonconservative forces acting on the element consists of two components: (1) the mechanical damping, which is represented by a velocity-dependent force; and (2) the aerodynamic damping, which is assumed to have a form similar to that found in Scanlan's model [96]. See Eq. 2.21.

The response of the structure is obtained by adding up the contributions of each element. A good representation of steady-state vortex-induced vibration behavior is obtained. The extension of the approach to space frame elements (elements of a $3D$ structure) is readily made and is discussed in the paper.

A finite element analysis of the VIV of a circular cylinder at Reynolds numbers in the range of 100–140 is performed by Nomura [82]. Similarly, Mittal and Kumar [78] use the finite element method to investigate the VIV of a circular cylinder mounted on lightly damped springs. The cylinder is allowed to vibrate in both the

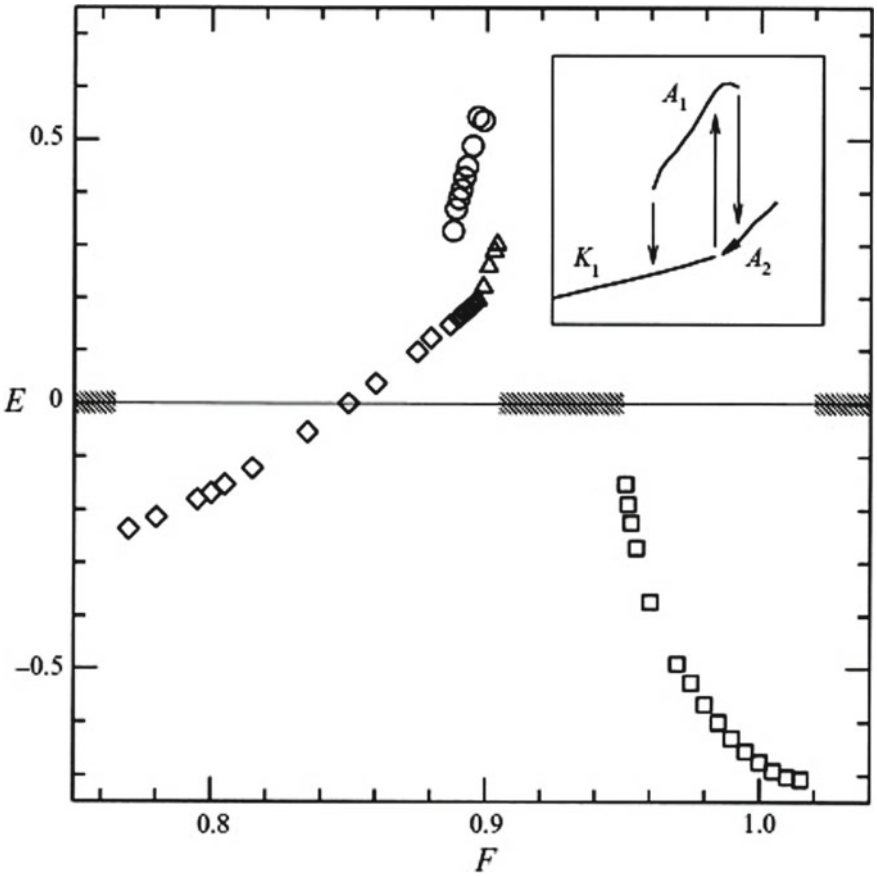

Fig. 2.14 Energy transfer coefficient E as a function of the frequency ratio F for periodic wake flows. ⋄, Kármán street mode, branch K_1; □, Kármán street mode, branch K_2; ◯, asymmetric two-cycle mode, branch A_1; △, asymmetric synchronized mode, branch A_2; frequency ratios for aperiodic regimes are shown hatched. Inset shows paths followed during sweeps of the frequency ratio F. Note the bifurcations between the different wake modes [10]. Reprinted with permission

in-line and in the crossflow directions at Re = 325. The behavior of the oscillator for various values of the structural natural frequency (F_s), including those that are sub and superharmonics of the natural vortex shedding, is investigated. In most cases, the trajectory of the cylinder is found to correspond to a Lissajou figure. For cylinders with effective material density much smaller than that of the surrounding fluid, a region of slight detuning is found to exist in a certain range of F_s values. In this region, the vortex-shedding frequency of the oscillating cylinder does not exactly match the structural frequency. This phenomenon is called "a soft lock-in" by the authors and the detuning is found to vanish if the cylinder density is made much larger than the mass of the surrounding fluid.

2.6 Discussion

A variety of issues concerning the vortex-induced vibration of circular cylinders have been discussed. Selected papers highlighted the influence of vortex-induced unsteady forces on the cylinder, including the phase of the forces relative to the body motion. The phenomenon of lock-in has been discussed and the factors that influence the response of the cylinder (mass and damping) have been listed. The mathematical modeling of vortex-induced oscillations, using nonlinear oscillators and flow-field simulations has been described. The development in the techniques used to attempt to solve the fully coupled problem, based on the fundamental principles of fluid dynamics and the theory of elasticity, has been illustrated with examples from the literature.

In the future, research should be directed toward the better prediction of the dynamic response of structures to VIV, which is an inherently nonlinear, self-regulated, multi degree-of-freedom phenomenon. Vortex shedding gives rise to unpredictable forces. This is only one of a multitude of factors that continues to make VIV prediction in industrial applications substandard. In the words of Sarpkaya [91]: "They [industrial applications] continue to require the input of the in-phase and out-of-phase components of the transverse force, in-line drag, correlation lengths, damping coefficients, relative roughness, shear, waves, and currents, among other governing and influencing parameters, and thus the input of relatively large safety factors."

Better prediction of VIV will hopefully lead to better suppression. This is most important to the structural integrity of our offshore structures and our tall land structures constantly subjected to winds. The payoff will be in longer service lives for these structures.

The following chapters are the focus of this monograph. They represent an effort to couple reduced-order VIV models to first principles in the form of variational laws. Chapter 3 provides a review of basic variational mechanics. Chapter 4 derives a reduced-order model based on Hamilton's principle as an extension of the ideas of McIver. Chapter 5 derives reduced-order models based on Hamilton's principle and virtual displacements with comparisons to key reduced-order models in the literature. Chapters 6 and 7 derive reduced-order models based on Jourdain's principle and virtual velocities. Each chapter also includes highlights of the earlier chapters in order to ease the reader through the complex material.

References

1. Barhoush H, Namini AH, Skop RA (1995) Vortex shedding analysis by finite elements. J Sound Vib 184(1):111–127
2. Basu RI, Vickery BJ (1983) Across-wind vibrations of structures of circular cross-section. Part 2: development of a mathematical model for full-scale application. J Wind Eng Ind Aerodyn 12(1):75–97

3. Baz A, Kim M (1993) Active modal control of vortex-induced vibrations of a flexible cylinder. J Sound Vib 165(1):69–84
4. Bearman PW (1984) Vortex shedding from oscillating bluff bodies. Annu Rev Fluid Mech 16:195–222
5. Bearman PW (2011) Circular cylinder wakes and vortex-induced vibrations. J Fluids Struct 27(1):648–658
6. Benaroya H, Wei T (2000) Hamilton's principle for external viscous fluid structure interactions. J Sound Vib 238(1):113–145
7. Berger E, Wille R (1972) Periodic flow phenomena. Annu Rev Fluid Mech 4:313–340
8. Billah KYR (1989) A study of vortex-induced vibration. PhD thesis, Princeton University
9. Bishop RED, Hassan AY (1963) The lift and drag forces on a circular cylinder in a flowing fluid. Proc R Soc. Ser A Math Phys Sci 277:32–50
10. Blackburn HM, Henderson RD (1999) A study of the two-dimensional flow past an oscillating cylinder. J Fluid Mech 385:255–286
11. Blackburn HM, Govardhan RN, Williamson CHK (2000) A complementary numerical and physical investigation of vortex-induced. J Fluids Struct 15(3–4):481–488
12. Bourdier S, Chaplin JR (2012) Vortex-induced vibrations of a rigid cylinder on elastic supports with end-stops: part 1: experimental results. J Fluids Struct 29:62–78
13. Branković M, Bearman PW (2006) Measurements of transverse forces on circular cylinders undergoing vortex-induced vibration. J Fluids Struct 22(6):829–836
14. Bretherton FP (1970) A note on Hamilton's principle for perfect fluids. J Fluid Mech 44:19–31
15. Cagney N, Balabani S (2013) Wake modes of a cylinder undergoing free streamwise vortex-induced vibrations. J Fluids Struct 38:127–145
16. Cai Y, Chen SS (1996) Dynamic response of a stack-cable system subjected to vortex-induced vibration. J Sound Vib 196(3):337–349
17. Chakrabarti SK (2002) The theory and practice of hydrodynamics and vibration. World Scientific Publishing Co., New Jersey
18. Chang CC, Gu M (1999) Suppression of vortex-excited vibration of tall buildings using tuned liquid dampers. J Wind Eng Ind Aerodyn 83(1–3):225–237
19. Chen SS (1987) Flow-induced vibration of circular cylindrical structures. Hemisphere Publishing Corp., New York
20. Chen SS, Zhu S, Cai Y (1995) An unsteady flow theory for vortex-induced vibration. J Sound Vib 184(1):73–92
21. Christensen C, Roberts J (1998) Parametric identification of vortex-induced vibration of a circular cylinder from measured data. J Sound Vib 211(4):617–636
22. D'Asdia P, Noè S (1998) Vortex induced vibration of reinforced concrete chimneys: in situ experimentation and numerical previsions. J Wind Eng Ind Aerodyn 74–76:765–776
23. Dong P, Benaroya H, Wei T (2004) Integrating experiments into an energy-based reduced-order model for vortex-induced-vibrations of a cylinder mounted as an inverted pendulum. J Sound Vib 276(1–2):45–63
24. Dowell EH (1981) Non-linear oscillator models in bluff body aero-elasticity. J Sound Vib 75(2):251–264
25. Dowling AP (1988) The dynamics of towed flexible cylinders. Part 1: neutrally buoyant elements. J Fluid Mech 187:507–532
26. Eckart C (1938) The electrodynamics of material media. Phys Rev 54:920–923
27. Eckart C (1960) Variational principles of hydrodynamics. Phys Fluids 3(3):421–427
28. Evangelinos C (1999) Parallel simulations of vortex-induced vibrations in turbulent flow: linear and non-linear models. PhD dissertation, Brown University
29. Evangelinos C, Lucor D, Karniadakis GE (2000) DNS-derived force distribution on flexible cylinders subject to vortex-induced vibration. J Fluids Struct 14(3):429–440
30. Facchinetti ML, de Langre E, Biolley F (2001) Vortex-induced waves along cables. Bull Am Phys Soc 46:128
31. Facchinetti ML, de Langre E, Biolley F (2004) Coupling of structure and wake oscillators in vortex-induced vibrations. J Fluids Struct 19(2):123–140

32. Feng CC (1968) The measurement of vortex-induced effects in flow past stationary and oscillating circular and d-section cylinders. Master's thesis, University of British, Columbia
33. Fujarra ALC, Pesce CP, Flemming F, Williamson CHK (2001) Vortex-induced vibration of a flexible cantilever. J Fluids Struct 15(3):651–658
34. Gabbai RD, Benaroya H (2005) An overview of modeling and experiments of vortex-induced vibration of circular cylinders. J Sound Vib 282:575–616
35. Gabbai RD, Benaroya H (2008) A first-principles derivation procedure for wake-body models in vortex-induced vibration: proof-of-concept. J Sound Vib 312:19–38
36. Gopalkrishnan R (1993) Vortex-induced forces on oscillating bluff cylinders. PhD dissertation, MIT and Woods Hole
37. Goswami I, Scanlan RH, Jones NP (1993) Vortex-induced vibration of circular cylinders. Part 1: experimental data. J Eng Mech 119(11):2270–2287
38. Goswami I, Scanlan RH, Jones NP (1993) Vortex-induced vibration of circular cylinders. Part 2: new model. J Eng Mech 119(11):2288–2302
39. Govardhan R, Williamson CHK (2000) Modes of vortex formation and frequency response for a freely-vibrating cylinder. J Fluid Mech 420:85–130
40. Govardhan R, Williamson CHK (2002) Resonance forever: existence of a critical mass and infinite regime of resonance in vortex-induced vibration. J Fluid Mech 473:147–166
41. Govardhan R, Williamson CHK (2003) Frequency response and the existence of a critical mass for an elastically mounted cylinder. In: Proceedings of the IUTAM symposium on integrated modeling of fully coupled fluid-structure interactions using analysis, computations, and experiments (New Brunswick, NJ, USA)
42. Griffin OM (1980) Vortex-excited cross-flow vibrations of a single cylindrical tube. J Press Vessel Technol 102:158–166
43. Griffin OM, Koopman GH (1977) The vortex-excited lift and reaction forces on resonantly vibrating cylinders. J Sound Vib 54(3):435–448
44. Griffin OM, Skop RA, Koopman GH (1973) The vortex-excited resonant vibrations of circular cylinders. J Sound Vib 31(2):235–249
45. Guilmineau E, Quetey P (2002) A numerical simulation of vortex shedding from an oscillating circular cylinder. J Fluids Struct 16(6):773–794
46. Gupta H, Sarkar PP, Mehta KC (1996) Identification of vortex-induced response parameters in time domain. J Eng Mech 122(11):1031–1037
47. Hartlen RT, Currie IG (1970) Lift-oscillator model of vortex induced vibration. J Eng Mech 96(5):577–591
48. Herivel JW (1955) The derivation of the equations of motion of an ideal fluid by Hamilton's principle. Math Proc Camb Philos Soc 51:344–349
49. Hiejima S, Nomura T, Kimura K, Fujino Y (1997) Numerical study on the suppression of the vortex-induced vibration of a circular cylinder by acoustic excitation. J Wind Eng Ind Aerodyn 67–68:325–335
50. Hover F, Miller S, Triantafyllou N (1997) Vortex-induced vibration of marine cables: experiments using force feedback. J Fluids Struct 11(3):307–326
51. Huera-Huarte FJ, Bearman PW (2009) Wake structures and vortex-induced vibrations of a long flexible cylinder. Part 1: dynamic response. J Fluids Struct 25(6):969–990
52. Huera-Huarte FJ, Bearman PW (2009) Wake structures and vortex-induced vibrations of a long flexible cylinder. Part 2: drag coefficients and vortex modes. J Fluids Struct 25(6):991–1006
53. Iwan WD (1975) The vortex induced oscillation of elastic structures. J Eng Ind 97:1378–1382
54. Iwan WD (1981) The vortex-induced oscillation of non-uniform structural systems. J Sound Vib 79(2):291–301
55. Iwan WD, Blevins RD (1974) A model for vortex induced oscillation of structures. J Appl Mech 41:581–586
56. Jadic I, So RMC, Mignolet P (1998) Analysis of fluid-structure interactions using a time-marching technique. J Fluids Struct 12(6):631–654

57. Jauvtis N, Williamson CHK (2003) Vortex-induced vibration of a cylinder with two degrees of freedom. J Fluids Struct 17(7):1035–1042
58. Jeon D, Gharib M (2001) On circular cylinders undergoing two-degree-of-freedom forced motions. J Fluids Struct 15(3):533–541
59. Kawai H (1993) Bending and torsional vibration of tall buildings in strong wind. J Wind Eng Ind Aerodyn 50:281–288
60. Khalak A, Williamson CHK (1996) Dynamics of a hydroelastic cylinder with very low mass and damping. J Fluids Struct 10(5):455–472
61. Khalak A, Williamson CHK (1997) Fluid forces and dynamics of a hydroelastic structure with very low mass and damping. J Fluids Struct 11(8):973–982
62. Khalak A, Williamson CHK (1997) Investigation of relative effects of mass and damping in vortex-induced vibration of a circular cylinder. J Wind Eng Ind Aerodyn 69–71:341–350
63. Khalak A, Williamson CHK (1999) Motions, forces and mode transitions in vortex-induced vibrations at low mass damping. J Fluids Struct 13(7–8):813–851
64. King R (1977) A review of vortex shedding research and its application. Ocean Eng 4(3):141–172
65. Krenk S, Nielsen SRK (1999) Energy balanced double oscillator model for vortex-induced vibrations. J Eng Mech 125:263–271
66. Lam KM, Liu P (2013) A circular cylinder undergoing large-amplitude transverse oscillations in a slow uniform cross flow. J Fluids Struct 39:408–417
67. Landl R (1975) A mathematical model for vortex-excited vibrations of bluff bodies. J Sound Vib 42(2):219–234
68. Laneville A (2006) On vortex-induced vibrations of cylinders describing x–y trajectories. J Fluids Struct 22(6):773–782
69. Larsen A (1995) Generalized model for assessment of vortex-induced vibrations of flexible structures. J Wind Eng Ind Aerodyn 57(2–3):281–294
70. Leech CM (1977) Hamilton's principle applied to fluid mechanics. Q J Mech Appl Math 30:107–130
71. Lin JC, Rockwell D (1999) Horizontal oscillations of a cylinder beneath a free surface: vortex formation and loading. J Fluid Mech 389:1–26
72. Lyons GJ, Vandiver JK, Larsen CM, Ashcombe GT (2003) Vortex-induced vibrations measured in service in the Foinaven dynamic umbilical, and lessons from prediction. J Fluids Struct 17(8):1079–1094
73. Marris A (1964) A review of vortex streets, periodic wakes, and induced vibration phenomena. J Basic Eng 86:185–196
74. Matsumoto M, Yagi T, Shigemura Y, Tsushima D (2001) Vortex-induced cable vibration of cable-stayed bridges at high reduced wind velocity. J Wind Eng Ind Aerodyn 89(7–8):633–647
75. McIver DB (1973) Hamilton's principle for systems of changing mass. J Eng Mech 7(3):249–261
76. Meneghini JR, Bearman PW (1995) Numerical simulation of high amplitude oscillatory flow about a circular cylinder. J Fluids Struct 9(4):435–455
77. Millikan CB (1929) On the steady motion of viscous, incompressible fluids; with particular reference to a variation principle. Philos Mag Ser 7(44):641–662
78. Mittal S, Kumar V (1999) Finite element study of vortex-induced cross-flow and in-line oscillations of a circular cylinder at low reynolds numbers. Int J Numer Methods Fluids 31(7):1087–1120
79. Mottaghi S (2015) Modeling vortex-induced fluid-structure interaction using an extension of Jourdain's principle. PhD dissertation, Rutgers, the State University of New Jersey, New Brunswick, NJ
80. Mottaghi S, Benaroya H (2016) Reduced-order modeling of fluid-structure interaction and vortex-induced vibration systems using an extension of Jourdain's principle. J Sound Vib 382(1):193–212
81. Ng L, Rand RH, Wei T, Keith WL (2001) An examination of wake oscillator models for vortex-induced vibrations. Technical report, Naval Undersea Warfare Division, Newport, Rhode Island

82. Nomura T (1993) Finite element analysis of vortex-induced vibrations of bluff cylinders. J Wind Eng Ind Aerodyn 46–47:587–594
83. Parkinson G (1989) Phenomena and modelling of flow-induced vibrations of bluff bodies. Prog Aerosp Sci 26(2):169–224
84. Penfield P (1966) Hamilton's principle for fluids. Phys Fluids 9:1184
85. Salmon R (1983) Practical use of Hamilton's principle. J Fluid Mech 132:431–444
86. Salmon R (1988) Hamiltonian fluid mechanics. Annu Rev Fluid Mech 20(1):225–256
87. Sarpkaya T (1978) Fluid forces on oscillating cylinders. J Waterw Port Coast Ocean Eng 104:275–291
88. Sarpkaya T (1979) Vortex induced oscillations: a selective review. J Appl Mech 46(2):241–258
89. Sarpkaya T (1989) Computational methods with vortices. J Fluids Eng 111(1):5–52
90. Sarpkaya T (1994) Vortex element methods for flow simulation. Adv Appl Mech 31:113–247
91. Sarpkaya T (2003) A critical review of the intrinsic nature of vortex induced vibrations. Technical report, Department of Mechanical Engineering, Naval Postgraduate School
92. Sarpkaya T (2004) A critical review of the intrinsic nature of vortex-induced vibrations. J Fluids Struct 19(4):389–447
93. Seliger RL, Whitham GB (1968) Variational principles in continuum mechanics. Proc R Soc Lond A: Math Phys Eng Sci 305:1–25 (The Royal Society)
94. Sheridan J, Lin JC, Rockwell D (1997) Flow over a cylinder close to a free surface. J Fluid Mech 330:1–30
95. Sheridan J Carberry J Rockwell D (2002) Cylinder wake states - the influence of free surfaces. In: Proceedings of the conference on bluff body wakes and vortex induced vibration (Port Douglas, Australia)
96. Simiu E, Scanlan RH (1986) Wind effects on structures. Wiley, New York
97. Skop RA, Balasubramanian S (1997) A new twist on an old model for vortex-excited vibrations. J Fluids Struct 11(4):395–412
98. Skop RA, Griffin OM (1973) A model for the vortex-excited resonant response of bluff cylinders. J Sound Vib 27(2):225–233
99. Skop RA, Griffin OM (1975) On a theory for the vortex-excited oscillations of flexible cylindrical structures. J Sound Vib 41(3):263–274
100. Vandiver JK (1993) Dimensionless parameters important to the prediction of vortex-induced vibration of long, flexible cylinders in ocean currents. J Fluids Struct 7(5):423–455
101. Vikestad K, Vandiver JK, Larsen CM (2000) Added mass and oscillatory frequency for a circular cylinder subjected to vortex-induced vibrations and external disturbance. J Fluids Struct 14(7):1071–1088
102. Voorhees A, Wei T (2002) Three-dimensionality in the wake of a surface piercing cylinder mounted as an inverted pendulum. In: Proceedings of the conference on bluff body wakes and vortex induced vibration (Port Douglas, Australia)
103. Wang XQ, So RMC, Chan KT (2003) A non-linear fluid force model for vortex-induced vibration of an elastic cylinder. J Sound Vib 260(2):287–305
104. Willden RHJ, Graham JMR (2001) Numerical prediction of VIV on long flexible circular cylinders. J Fluids Struct 15(3–4):659–669
105. Willden RHJ, Graham JMR (2002) Multi-modal vortex-induced vibrations of a vertical riser pipe subject to uniform current profile. In: Proceedings of the conference on bluff body wakes and vortex induced vibration (Port Douglas, Australia)
106. Williamson CHK (1988) The existence of two stages in the transition to three-dimensionality of a cylinder wake. Phys Fluids 31(11):3165–3168
107. Williamson CHK (1996) Vortex dynamics in the cylinder wake. Annu Rev Fluid Mech 28:477–539
108. Williamson CHK (1997) Advances in our understanding of vortex dynamics in bluff body wakes. J Wind Eng Ind Aerodyn 69–71:3–32
109. Williamson CHK, Govardhan R (2008) A brief review of recent results in vortex-induced vibrations. J Wind Eng Ind Aerodyn 96(1):713–735

110. Williamson CHK, Roshko A (1988) Vortex formation in the wake of an oscillating cylinder. J Fluids Struct 2(4):355–381
111. Wu X, Ge F, Hong Y (2012) A review of recent studies on vortex-induced vibrations of long slender cylinders. J Fluids Struct 28(1):292–308
112. Xing JT, Price WG (2000) The theory of non-linear elastic ship-water interaction dynamics. J Sound Vib 230(4):877–914
113. Zdravkovich MM (1982) Modification of vortex shedding in the synchronization range. J Fluids Eng 104:513–517
114. Zdravkovich MM (1996) Different modes of vortex shedding: an overview. J Fluids Struct 10(5):427–437
115. Zhou CY, So RM, Lam K (1999) Vortex-induced vibrations of an elastic circular cylinder. J Fluids Struct 13(2):165–189

Chapter 3
Introduction to Analytical Mechanics

Abstract This chapter presents several of the most important concepts from analytical dynamics. We derive *Lagrange's equation* and how it can be used for the derivation of governing equations of motion. It is, especially, useful for the derivation of the equations of motion for systems, discrete or continuous, with more than one degree-of-freedom, where the Newtonian free body diagrams become more difficult to apply. We also derive *Hamilton's principle*, an integral energy formulation, also applicable to both discrete and continuous systems, and see how it is related to Lagrange's equation. Hamilton's principle is, especially, relevant to the work in Chaps. 4 and 5.

3.1 Introduction

The basis of this chapter is the *principle of virtual work*. There are many advantages to the *analytical approach* of Lagrange and Hamilton over Newton's force analysis. This is, especially, true for systems of interacting bodies, where each exerts a force on the other and where constraints, such as boundaries, also exert forces on the system, limiting motion. Such *auxiliary conditions* can be more easily handled using the analytical approach.

The analytical approaches are based on *variational principles*, which are the unifying basis of the equations that follow. The term variational is from the *calculus of variations,* the foundation for such techniques. An important advantage of the analytical method is that the equations of motion are coordinate-independent. Newton's second law of motion is not.

To motivate and explain the procedure, consider the simple function: $y = f(x)$. The variable y can represent a displacement curve of a cable or beam. The variational approach is based on comparing the function $f(x)$ with a slightly modified function $f_\epsilon(x) = f(x) + \epsilon\phi(x)$, where ϵ can be as small as necessary, including zero, and ϕ must be continuous and differentiable. For any value of the independent variable x, the *variation*, or difference is defined as

$$\delta y \equiv f_\epsilon(x) - f(x) = \epsilon\phi(x).$$

S. Mottaghi et al., *An Analytical Mechanics Framework for Flow-Oscillator Modeling of Vortex-Induced Bluff-Body Oscillations*, Solid Mechanics and Its Applications 260,
https://doi.org/10.1007/978-3-030-26133-7_3

There are two fundamental points to be emphasized, here, *(i)* the variation is *arbitrary* or *virtual* and *(ii)* it is an infinitesimal change since ϵ can be made arbitrarily small. Note that while both δy and dy represent infinitesimal changes in the function $f(x)$, dy refers to a change in $f(x)$ caused by an infinitesimal change of the independent variable dx, while δy is an infinitesimal change of y that results in a *new function* $y + \delta y$.

This process of variation is for each fixed value of x. Therefore, x is not varied, meaning that $\delta x = 0$, and the two end points of this function are prescribed and therefore also not varied. The variation is between definite limits. When we work with time as the independent variable, the beginning and ending times are prescribed and therefore not varied.

As we will discover below, in applying the variational procedures to a particular system, in addition to finding the governing the equation of motion, the necessary number of boundary conditions is also derived. *The stationary value conditions imposed by the variational principles result in both the differential equations and the boundary conditions.*

Before proceeding with the details of the analytical techniques, it is useful to summarize the key topics to be examined in this chapter:

- The *principle of virtual work* is introduced along with its relation to the equilibrium of a body.
- The principle of virtual work, in conjunction with *d'Alembert's* principle, is extended to include dynamic systems.
- Lagrange's equation and Hamilton's variational principle are then derived from d'Alembert's principle.

Jourdain's principle, which is related to the topics in this chapter, is introduced and discussed later in this monograph, where it is applied directly.

3.2 Virtual Work

The principle of virtual work is the basis for the remainder of this chapter and also forms the foundation for the variational principles of mechanics. Some of the most powerful computational models are based on a variational approach.

3.2.1 Work and Energy

The concepts of work and energy are reviewed before proceeding to *virtual work*. Consider a particle of mass m moving along a curve C under the action of a force $\mathbf{F}$ as shown in Fig. 3.1. In this chapter, we follow the custom in dynamics of showing vectors as boldface variables.

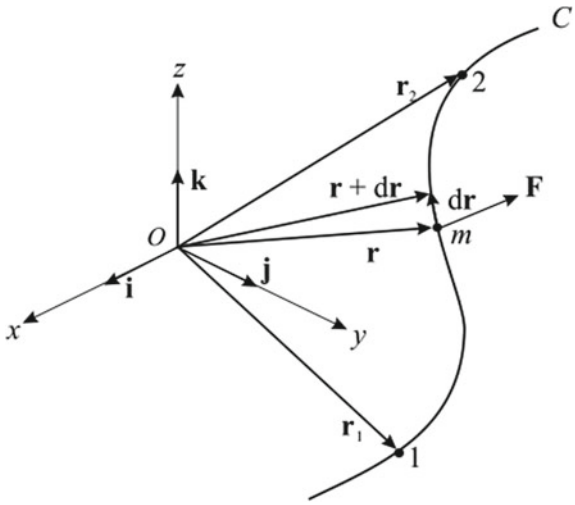

Fig. 3.1 Work done by force **F** in the direction $d\mathbf{r}$

The position of the particle with respect to an origin O is given by the vector $\mathbf{r}$, which is a function of time. The work necessary to move the mass a distance $d\mathbf{r}$ is $dW = \mathbf{F} \cdot d\mathbf{r}$. The *work done* to move the particle from position $\mathbf{r_1}$ to position $\mathbf{r_2}$ is

$$W_{12} = \int_{\mathbf{r}_1}^{\mathbf{r}_2} \mathbf{F} \cdot d\mathbf{r}.$$

Assuming the mass of the particle to be constant, Newton's second law of motion can be written as

$$\mathbf{F} = m\frac{d\dot{\mathbf{r}}}{dt} = m\frac{d}{dt}\left(\frac{d\mathbf{r}}{dt}\right).$$

The goal here is to connect force, work, and energy. Using $d\mathbf{r} = \dot{\mathbf{r}}dt$, and the above equations,

$$\begin{aligned} W_{12} &= \int_{t_1}^{t_2} m\frac{d\dot{\mathbf{r}}}{dt} \cdot \dot{\mathbf{r}}dt \\ &= \frac{1}{2}\int_{t_1}^{t_2} m\frac{d}{dt}\left(\dot{\mathbf{r}} \cdot \dot{\mathbf{r}}\right)dt \\ &= \frac{1}{2}m[(\dot{\mathbf{r}}_2 \cdot \dot{\mathbf{r}}_2) - (\dot{\mathbf{r}}_1 \cdot \dot{\mathbf{r}}_1)] \\ &= \frac{1}{2}m(\dot{r}_2^2 - \dot{r}_1^2) \\ &= T_2 - T_1, \end{aligned}$$

where the limits of integration have been transformed from $\mathbf{r}$ to t, and T is the kinetic energy of the mass, $T = \frac{1}{2}m\dot{\mathbf{r}} \cdot \dot{\mathbf{r}}$. As expected, we started with a scalar, the work,

Fig. 3.2 Path dependence

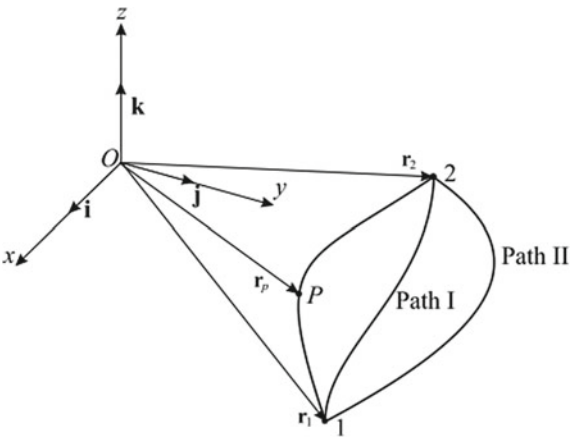

and ended with a scalar, the change in kinetic energy. The kinetic energy of a body is defined as the total work that must be done on the body to bring it from a state of rest to a velocity $\dot{\mathbf{r}}$. Thus, for $v = |\dot{\mathbf{r}}|$,

$$\begin{aligned} T &= \int_0^v mv\,dv \\ &= \frac{1}{2}mv^2. \end{aligned}$$

Next, the work done by the force is related to the respective change in position of the mass. To do this, define a *conservative force field* as one where the work done depends only on the *initial* and the *final* positions of the particle and is *independent* of the path connecting these positions. An example of a conservative force field is gravity. Nonconservative forces, such as friction and external forces, are *energy-dissipating*, and for these the work done is path-dependent.

From Fig. 3.2, any path within the conservative force field which connects points 1 and 2 can be selected, and the work done bringing the particle from 1 to 2 will be the same, and is denoted by

$$W_{12c} = \underbrace{\int_{\mathbf{r}_1}^{\mathbf{r}_2} \mathbf{F}\cdot d\mathbf{r}}_{\text{Path I}} = \underbrace{\int_{\mathbf{r}_1}^{\mathbf{r}_2} \mathbf{F}\cdot d\mathbf{r}}_{\text{Path II}}.$$

The *potential energy* $V(\mathbf{r}_1)$ is associated with position $\mathbf{r}_1$ and is defined as the work done[1] by a conservative force moving a particle from position $\mathbf{r}_1$ to a *reference position* $\mathbf{r}_p$,

[1] Had the limits been interchanged, subsequent equations would be of opposite signs.

$$V(\mathbf{r}_1) = \int_{\mathbf{r}_1}^{\mathbf{r}_p} \mathbf{F} \cdot d\mathbf{r}.$$

Relate the work done moving a particle in a conservative force field to the potential energy of the particle. To do this, consider again W_{12c} but choose the arbitrary path through reference position $\mathbf{r}_p$, then

$$\begin{aligned} W_{12c} &= \int_{\mathbf{r}_1}^{\mathbf{r}_p} \mathbf{F} \cdot d\mathbf{r} + \int_{\mathbf{r}_p}^{\mathbf{r}_2} \mathbf{F} \cdot d\mathbf{r} \\ &= \int_{\mathbf{r}_1}^{\mathbf{r}_p} \mathbf{F} \cdot d\mathbf{r} - \int_{\mathbf{r}_2}^{\mathbf{r}_p} \mathbf{F} \cdot d\mathbf{r} \\ &= -[V(\mathbf{r}_2) - V(\mathbf{r}_1)] \\ &= -(V_2 - V_1). \end{aligned}$$

By this equation, *the work done in a conservative force field is the negative of the change in potential energy*. From vector calculus, a conservative force equals the negative of the gradient of the potential energy function.

Finally, if we denote W_{12nc} as the nonconservative work, then

$$\begin{aligned} W_{12nc} &= W_{12} - W_{12c} \\ &= (T_2 - T_1) + (V_2 - V_1) \\ &= (T_2 + V_2) - (T_1 + V_1) \\ &= E_2 - E_1, \end{aligned}$$

where E_i denotes the total energy in state i. Therefore, W_{12nc} is a measure of the change in particle energy due to dissipation, and if $W_{12nc} = 0$ then $E_2 = E_1$. That is, the energy of the particle is constant and there is conservation of energy.

Gravitational potential energy is defined as the work (mgh) done against the gravitational field to elevate a body of mass m a distance h above an arbitrary reference plane (datum).

3.2.2 Virtual Work

The *Principle of Virtual Work* states that *the virtual work performed by the applied forces undergoing infinitesimal virtual displacements compatible with the system constraints is zero,*

$$\delta W = \sum_{i=1}^{N} \mathbf{F}_i \cdot \delta \mathbf{r}_i = 0. \tag{3.1}$$

A *constraint* is a physical barrier to free motion, for example, a wall, a string connecting two bodies, or a magnetic field. Equation 3.1 applies to static systems, or quasi-static systems where inertia effects can be ignored. The dynamic version of the principle of virtual work, known as *d'Alembert's principle*, is developed in the next section. These principles form the basis for the variational principles that follow.

Our formulation is for a system of N particles moving in three dimensions. The results are applicable for discrete as well as continuous systems. *Virtual displacements* are defined in each of the three dimensions for each particle,

$$\delta x_i,\ \delta y_i,\ \delta z_i,$$

where $1 \leq i \leq N$. *Virtual displacements may be interpreted as possible alternate configurations of the system of particles.* These alternate configurations must be consistent with the system constraints. We consider the system at its initial configuration and at its alternate configuration due to the virtual displacement. Time is not a variable here since we are only examining the system in two possible configurations. Time will be soon considered with d'Alembert's principle.

Consider the initial configuration of the N masses along with the constraints on them via a *constraint equation*,

$$g(x_1, y_1, z_1, x_2, y_2, z_2, \ldots, x_N, y_N, z_N, t) = c, \tag{3.2}$$

and the alternate configuration resulting from a virtual displacement,

$$g(x_1 + \delta x_1, y_1 + \delta y_1, z_1 + \delta z_1, \ldots, z_N + \delta z_N, t) = c, \tag{3.3}$$

where parameter t is included to demonstrate that it is not varied. The system constraints are within the constant c.

A goal is to examine in detail the rules that govern the variations in Eq. 3.3. When completed, we will be able to relate the virtual work done by forces undergoing a virtual displacement. This is interpreted as a statement of static equilibrium.

Proceed by expanding Eq. 3.3 about the *unvaried* path via a Taylor series representation. Only first-order terms are retained,

$$g(x_1, y_1, z_1, \ldots, x_N, y_N, z_N, t) + \sum_{i=1}^{N} \left(\frac{\partial g}{\partial x_i}\delta x_i + \frac{\partial g}{\partial y_i}\delta y_i + \frac{\partial g}{\partial z_i}\delta z_i \right) = c. \tag{3.4}$$

We know from Eq. 3.2 that $g() = c$, and upon substitution, Eq. 3.4 yields the relations that must be satisfied so that the virtual displacements are compatible with system constraints,

$$\sum_{i=1}^{N} \left(\frac{\partial g}{\partial x_i}\delta x_i + \frac{\partial g}{\partial y_i}\delta y_i + \frac{\partial g}{\partial z_i}\delta z_i \right) = 0. \tag{3.5}$$

Each of the N masses can move in three possible coordinate directions. Therefore, in general, Eq. 3.5 relates $3N$ unknowns, but with one equation. Since one variable may be written in terms of the remainder, there are $3N - 1$ variables.

Next, assume that the N particles are subject to resultant force $\mathcal{F}_i = \mathbf{F}_i + \mathbf{f}_i$, where $\mathbf{F}_i$ is an applied force, and $\mathbf{f}_i$ is a constraint force. For the system to be in static equilibrium, every particle is at rest, and $\mathcal{F}_i = 0$ in any possible configuration. For the virtual displacement configuration, static equilibrium requires that

$$\mathcal{F}_i \cdot \delta \mathbf{r}_i = 0,$$

or

$$\mathcal{F}_i \cdot (\delta x_i \cdot \mathbf{i} + \delta y_i \cdot \mathbf{j} + \delta z_i \cdot \mathbf{k}) = 0,$$

where $\mathbf{i}$, $\mathbf{j}$, and $\mathbf{k}$ are the unit vectors in three-dimensional space.

Given virtual displacements, one can proceed to define *virtual work* as the product of a force and its corresponding virtual displacement. For the system in equilibrium, the virtual work for the entire system vanishes according to the relation

$$\begin{aligned} \delta W &= \sum_{i=1}^{N} \mathcal{F}_i \cdot \delta \mathbf{r}_i = 0 \\ &= \sum_{i=1}^{N} \mathbf{F}_i \cdot \delta \mathbf{r}_i + \sum_{i=1}^{N} \mathbf{f}_i \cdot \delta \mathbf{r}_i = 0. \end{aligned}$$

Before proceeding, consider the types of constraints to which a structure may be exposed. Likely examples include physical boundaries, in which case the boundary force is perpendicular to the motion of the body and there is no work performed. It is possible that contact friction will do work in resisting a motion. Dissipative forces such as friction will be introduced later in this chapter when dynamic motion is added. Therefore, $\sum_{i=1}^{N} \mathbf{f}_i \cdot \delta \mathbf{r}_i = 0$. The remaining equation is given the name *principle of virtual work* for a static system,

$$\delta W = \sum_{i=1}^{N} \mathbf{F}_i \cdot \delta \mathbf{r}_i = 0,$$

where $\mathbf{F}_i$ represents the external forces on the system.

For the special but useful case of a conservative system,

$$\begin{aligned} \delta W &= \sum_{i=1}^{N} \mathbf{F}_i \cdot \delta \mathbf{r}_i \\ &= -\delta V \end{aligned}$$

$$
\begin{aligned}
&= -\sum_{i=1}^{N}\left(\frac{\partial V}{\partial x_i}\delta x_i + \frac{\partial V}{\partial y_i}\delta y_i + \frac{\partial V}{\partial z_i}\delta z_i\right)\\
&= 0,
\end{aligned}
$$

where V is the potential energy of the system. Since the variations are independent and arbitrary, the coefficients of the variations must equal zero,

$$
\begin{aligned}
F_{x_i} &= \frac{\partial V}{\partial x_i} = 0\\
F_{y_i} &= \frac{\partial V}{\partial y_i} = 0\\
F_{z_i} &= \frac{\partial V}{\partial z_i} = 0.
\end{aligned}
$$

These three equations can be used to define the static equilibrium configuration for the system. We proceed next with d'Alembert's principle, which extends the principle of virtual work to time-dependent problems.

3.2.3 D'Alembert's Principle

D'Alembert extended the applicability of the principle of virtual work to dynamic problems. Newton's law of motion can be rewritten as d'Alembert's principle in the following form for N particles:

$$
\mathbf{F}_i + \mathbf{f}_i - m_i\ddot{\mathbf{r}}_i = 0, \quad i = 1, 2, \ldots, N. \tag{3.6}
$$

The term $-m_i\ddot{\mathbf{r}}_i$ is considered an *inertia force*. Each force in Eq. 3.6 may be a constant or a function of time. The virtual work performed by the ith particle is

$$
(\mathbf{F}_i + \mathbf{f}_i - m_i\ddot{\mathbf{r}}_i)\cdot\delta\mathbf{r}_i = 0,
$$

where the virtual displacements $\delta\mathbf{r}_i$ are compatible with the constraints. Assuming virtual work due to constraint forces equals zero, the virtual work for the system is

$$
\sum_{i=1}^{N}(\mathbf{F}_i - m_i\ddot{\mathbf{r}}_i)\cdot\delta\mathbf{r}_i = 0, \tag{3.7}
$$

where this is called the *generalized principle of d'Alembert*. $(\mathbf{F}_i - m_i\ddot{\mathbf{r}}_i)$ is sometimes called the *effective force*. d'Alembert's principle will be used in the next section to derive Lagrange's equation.

> The importance of d'Alembert's principle lies in the fact that it is *more* than a reformulation of Newton's equation. It is the expression of a *principle*. We know that the vanishing of a force in Newtonian mechanics means equilibrium. Hence, [Eq. 3.6] says that the addition of the force of inertia to the other forces produces equilibrium. But this means that if we have any criterion for the equilibrium of a mechanical system, we can immediately extend that criterion to a system which is in motion. All we have to do is add the new "force of inertia" to the previous forces. By this device *dynamics is reduced to statics.* [1, p. 89].

The linking of Newton's second law of motion with the principle of virtual work clarifies that the principle is equally applicable to masses at rest and to masses in motion. The virtual displacement involves a possible but purely mathematical experiment that can be applied at any specific time. At that instant, the actual motion of the body does not enter into account and the dynamic problem is reduced to a static one.

3.3 Lagrange's Equation

Lagrange's equation is an energy-based expression that provides a general formulation for the equations of motion of a dynamical system. The behavior of the system may be linear or nonlinear, and the advantage of the method becomes evident for multi-degree-of-freedom systems. In addition, this approach is based on the energies of the system, the kinetic, potential, and strain energies. Therefore, it is not necessary to invoke the vectorial approach in applying Lagrange's equation as one must with Newton's second law of motion.

The equations derived below are written in terms of the *generalized coordinates* q_k. The physical coordinates, $\mathbf{r}_i$, of an n degree-of-freedom system for N particles can be related to the generalized coordinates by an appropriate set of equations,

$$\mathbf{r}_i = \mathbf{r}_i(q_1, q_2, \ldots, q_n), \quad i = 1, 2, \ldots, N. \tag{3.8}$$

The purpose of these transformations from physical coordinates, which are vectorial, to generalized coordinates, which are not, is to recast the vectorial d'Alembert's principle into the scalar Lagrange's equation.

In the following derivations, d'Alembert's generalized principle is expanded and rewritten in terms of potential and kinetic energies, all functions of the generalized coordinates. First, derive the relations between physical and generalized coordinates.

The total derivative of Eq. 3.8 is

$$\begin{aligned}\dot{\mathbf{r}}_i &= \frac{\partial \mathbf{r}_i}{\partial q_1}\frac{dq_1}{dt} + \frac{\partial \mathbf{r}_i}{\partial q_2}\frac{dq_2}{dt} + \cdots + \frac{\partial \mathbf{r}_i}{\partial q_n}\frac{dq_n}{dt} \\ &= \frac{\partial \mathbf{r}_i}{\partial q_1}\dot{q}_1 + \frac{\partial \mathbf{r}_i}{\partial q_2}\dot{q}_2 + \cdots + \frac{\partial \mathbf{r}_i}{\partial q_n}\dot{q}_n\end{aligned}$$

$$= \sum_{k=1}^{n} \frac{\partial \mathbf{r}_i}{\partial q_k} \dot{q}_k, \; i = 1, 2, \ldots, N.$$

Then differentiate these equations with respect to $\dot{q}_k$,

$$\frac{\partial \dot{\mathbf{r}}_i}{\partial \dot{q}_k} = \frac{\partial \mathbf{r}_i}{\partial q_k}, \quad i = 1, 2, \ldots, N, \quad k = 1, 2, \ldots, n.$$

Since variations $\delta \mathbf{r}_i$ follow the same rules as differentials $d\mathbf{r}_i$, the variations of $\mathbf{r}_i$ and $\dot{\mathbf{r}}_i$ are

$$\begin{aligned}
\delta \mathbf{r}_i &= \frac{\partial \mathbf{r}_i}{\partial q_1} \delta q_1 + \frac{\partial \mathbf{r}_i}{\partial q_2} \delta q_2 + \cdots + \frac{\partial \mathbf{r}_i}{\partial q_n} \delta q_n \\
&= \sum_{k=1}^{n} \frac{\partial \mathbf{r}_i}{\partial q_k} \delta q_k, \quad i = 1, 2, \ldots, N \\
\delta \dot{\mathbf{r}}_i &= \frac{\partial \mathbf{r}_i}{\partial q_1} \delta \dot{q}_1 + \frac{\partial \mathbf{r}_i}{\partial q_2} \delta \dot{q}_2 + \cdots + \frac{\partial \mathbf{r}_i}{\partial q_n} \delta \dot{q}_n \\
&= \sum_{k=1}^{n} \frac{\partial \mathbf{r}_i}{\partial q_k} \delta \dot{q}_k, \quad i = 1, 2, \ldots, N.
\end{aligned}$$

Now consider the second term of d'Alembert's principle, Eq. 3.7, written in terms of the generalized coordinates,

$$\begin{aligned}
\sum_{i=1}^{N} m_i \ddot{\mathbf{r}}_i \cdot \delta \mathbf{r}_i &= \sum_{i=1}^{N} \left(m_i \ddot{\mathbf{r}}_i \cdot \sum_{k=1}^{n} \frac{\partial \mathbf{r}_i}{\partial q_k} \delta q_k \right) \\
&= \sum_{k=1}^{n} \left(\sum_{i=1}^{N} m_i \ddot{\mathbf{r}}_i \cdot \frac{\partial \mathbf{r}_i}{\partial q_k} \right) \delta q_k. \qquad (3.9)
\end{aligned}$$

Examine Eq. 3.9 more closely in order to recast it in an energy form. For a particular term within the interior sum, we can perform the following algebra:

$$\begin{aligned}
m_i \ddot{\mathbf{r}}_i \cdot \frac{\partial \mathbf{r}_i}{\partial q_k} &= \frac{d}{dt} \left(m_i \dot{\mathbf{r}}_i \cdot \frac{\partial \mathbf{r}_i}{\partial q_k} \right) - m_i \dot{\mathbf{r}}_i \cdot \frac{d}{dt} \left(\frac{\partial \mathbf{r}_i}{\partial q_k} \right) \\
&= \frac{d}{dt} \left(m_i \dot{\mathbf{r}}_i \cdot \frac{\partial \mathbf{r}_i}{\partial q_k} \right) - m_i \dot{\mathbf{r}}_i \cdot \frac{\partial \dot{\mathbf{r}}_i}{\partial q_k} \\
&= \left[\frac{d}{dt} \left(\frac{\partial}{\partial \dot{q}_k} \right) - \frac{\partial}{\partial q_k} \right] \left(\frac{1}{2} m_i \dot{\mathbf{r}}_i \cdot \dot{\mathbf{r}}_i \right). \qquad (3.10)
\end{aligned}$$

Then Eq. 3.9 becomes

$$\sum_{i=1}^{N} m_i \ddot{\mathbf{r}}_i \cdot \delta \mathbf{r}_i = \sum_{k=1}^{n} \left[\frac{d}{dt} \left(\frac{\partial T}{\partial \dot{q}_k} \right) - \frac{\partial T}{\partial q_k} \right] \delta q_k,$$

where the kinetic energy T is defined as

$$T = \frac{1}{2} \sum_{i=1}^{N} m_i \dot{\mathbf{r}}_i \cdot \dot{\mathbf{r}}_i = T(q_1, \ldots, q_n, \dot{q}_1, \ldots, \dot{q}_n).$$

The other term in d'Alembert's principle is the virtual work $\delta W = \sum_{i=1}^{N} \mathbf{F}_i \cdot \delta \mathbf{r}_i$, and so d'Alembert's equation can be written as

$$\sum_{k=1}^{n} \left[\frac{d}{dt} \left(\frac{\partial T}{\partial \dot{q}_k} \right) - \frac{\partial T}{\partial q_k} \right] \delta q_k = \delta W. \tag{3.11}$$

To explicitly show the virtual work in terms of forces $\mathbf{F}_i$, write them in terms of the generalized coordinates. Consider the virtual work done by these forces,

$$\begin{aligned} \delta W &= \sum_{i=1}^{N} \mathbf{F}_i \cdot \delta \mathbf{r}_i \\ &= \sum_{i=1}^{N} \mathbf{F}_i \cdot \sum_{k=1}^{n} \frac{\partial \mathbf{r}_i}{\partial q_k} \delta q_k \\ &= \sum_{k=1}^{n} \left(\sum_{i=1}^{N} \mathbf{F}_i \cdot \frac{\partial \mathbf{r}_i}{\partial q_k} \right) \delta q_k \\ &= \sum_{k=1}^{n} Q_k \, \delta q_k, \end{aligned} \tag{3.12}$$

where Q_k are called the *generalized forces*. The generalized force also may be a torque, and will likely be a complicated expression. Before further specializing the generalized force, look at an example that shows how the generalized force can be identified.

D'Alembert's equation can be further specialized on the way to Lagrange's equation by separately considering the *conservative* (derivable from potential energy V) and *nonconservative* forces acting on the system. From Eq. 3.12,

$$\sum_{i=1}^{N} \mathbf{F}_i \cdot \delta \mathbf{r}_i = \delta W = \delta W_c + \delta W_{nc}.$$

Work in a conservative vector field equals the negative of the change in potential, $-\delta V$. The virtual work of nonconservative generalized forces $Q_{k_{nc}}$ undergoing virtual

displacements δq_k is given by $\sum_{k=1}^{n} Q_{k_{nc}}\,\delta q_k$. Therefore,

$$\begin{aligned}\delta W &= -\left(\frac{\partial V}{\partial q_1}\delta q_1 + \ldots + \frac{\partial V}{\partial q_n}\delta q_n\right) + \sum_{k=1}^{n} Q_{k_{nc}}\,\delta q_k \\ &= -\sum_{k=1}^{n}\left(\frac{\partial V}{\partial q_k} - Q_{k_{nc}}\right)\delta q_k.\end{aligned}$$

D'Alembert's generalized principle, Eq. 3.11, becomes

$$\sum_{k=1}^{n}\left[\frac{d}{dt}\left(\frac{\partial T}{\partial \dot{q}_k}\right) - \frac{\partial T}{\partial q_k} + \frac{\partial V}{\partial q_k} - Q_{k_{nc}}\right]\delta q_k = 0.$$

Since the virtual displacements δq_k are arbitrary, the expression in the square brackets must equal zero for each k. Therefore,

$$\frac{d}{dt}\left(\frac{\partial T}{\partial \dot{q}_k}\right) - \frac{\partial T}{\partial q_k} + \frac{\partial V}{\partial q_k} = Q_k, \quad k = 1, 2, \ldots, n, \tag{3.13}$$

where $Q_k \equiv Q_{k_{nc}}$ includes dissipative forces such as damping and nonconservative external forces. These are *Lagrange's equations of motion*, one equation for each of the n degrees of freedom. It is customary to define the *Lagrangian* function as

$$L = T - V.$$

Since potential energy V is a function of position only, it cannot vary with velocity, and therefore,

$$\frac{\partial T}{\partial \dot{q}_k} = \frac{\partial (T - V)}{\partial \dot{q}_k} = \frac{\partial L}{\partial \dot{q}_k},$$

and Eq. 3.13 becomes

$$\frac{d}{dt}\left(\frac{\partial L}{\partial \dot{q}_k}\right) - \frac{\partial L}{\partial q_k} = Q_k, \quad k = 1, 2, \ldots, n. \tag{3.14}$$

There are several key advantages to Lagrange's equation:

- Lagrange's equation contains only scalar quantities, eliminating the force and acceleration vectors inherent in Newton's second law of motion.
- There is one Lagrange equation for each degree-of-freedom, whereas the use of free body diagrams in Newton's formulation leads to extraneous equations resulting from the internal forces between bodies that are attached to each other. Via Newton's approach, such internal forces have to be eliminated after the equations of motion are derived. Of course, in some applications, these internal forces are needed.

- Lagrange's equation is independent of the coordinate system since the energy functions T and V are scalar.

3.3.1 Lagrange's Equation for Small Oscillations

We have learned that Lagrange's equation can be utilized to derive the fully nonlinear equations of motion for a dynamic system. But in many applications, vibration is essentially linear. Therefore, it is of interest to examine how Lagrange's equation simplifies for small amplitude oscillations about equilibrium.

Expand the expression for the potential energy $V(q_1, q_2, \ldots, q_n)$ in an n-variable Taylor series[2] about an arbitrary equilibrium reference position $V(0, 0, \ldots, 0)$,

$$V(q_1, q_2, \ldots, q_n) = \frac{1}{2}\left(\frac{\partial^2 V}{\partial q_1^2}q_1^2 + \frac{\partial^2 V}{\partial q_2^2}q_2^2 + \cdots + 2\frac{\partial^2 V}{\partial q_1 \partial q_2}q_1 q_2 + \cdots\right) + \cdots .$$

Use is made that $V(0, 0, \ldots, 0) = 0$ and $\partial V/\partial q_i = 0$ in the equilibrium position. For small amplitudes, q_i to powers two and higher can be ignored, leaving the approximation

$$V \approx \frac{1}{2}\sum_{i=1}^{n}\sum_{j=1}^{n}\frac{\partial^2 V}{\partial q_i \partial q_j}q_i q_j = \frac{1}{2}\sum_{i=1}^{n}\sum_{j=1}^{n}k_{ij}q_i q_j,$$

where k_{ij} are known as the *stiffness coefficients*. The kinetic energy is given by

$$T = \frac{1}{2}\sum_{i=1}^{n}\sum_{j=1}^{n}m_{ij}\dot{q}_i\dot{q}_j.$$

Substituting the above expressions into Lagrange's equation leads to the following *n coupled* equations of motion:

$$[m]\{\ddot{q}\} + [k]\{q\} = \{0\}. \tag{3.15}$$

2

$$f(x, y, z) = f(0, 0, 0) + f_x(0, 0, 0)\cdot(x - x(0)) + f_y(0, 0, 0)\cdot(y - y(0))$$
$$+ f_z(0, 0, 0)\cdot(z - z(0)) + \frac{1}{2}(f_{xx}(0, 0, 0)\cdot(x - x(0))^2 + \cdots$$
$$+ 2f_{xy}(0, 0, 0)\cdot(x - x(0))(y - y(0)) + \cdots) + \cdots .$$

3.3.2 *Lagrange's Equation with Damping*

Prior to this section, damping was not formally considered in the variational formulation. Here, the inclusion of damping is examined. Rather than proceeding with a full derivation, as we have for Lagrange's equation and Hamilton's principle, it is preferable to state a final result, and refer the reader to an excellent reference, Wells [2], that includes many examples.

There are many types of damping, and the particular application will determine which is most suitable. For example, when damping has been included, it has been exclusively viscous damping, which is proportional to the first power of the speed and opposite in direction to its motion. This form of damping is adequate if the speed is "not too great." At higher speed, the damping may be proportional to the speed taken to a power greater than one.

For viscous damping, there is a special form for the generalized force,

$$Q_D = -\frac{\partial R}{\partial \dot{q}}$$

for each generalized coordinate, where R is known as the *Rayleigh dissipation function* and is given by

$$R = \frac{1}{2}\sum_k \sum_l c_{kl}\dot{q}_k\dot{q}_l,$$

where the c_{kl} are damping coefficients. For the kth generalized coordinate then,

$$Q_{D_k} = -\frac{\partial R}{\partial \dot{q}_k} = -\sum_l c_{kl}\dot{q}_l,$$

with the resulting Lagrange's equation,

$$\frac{d}{dt}\left(\frac{\partial T}{\partial \dot{q}_k}\right) - \frac{\partial T}{\partial q_k} + \frac{\partial V}{\partial q_k} + \frac{\partial R}{\partial \dot{q}_k} = Q_k, \quad k = 1, 2, \ldots, n.$$

3.4 Hamilton's Principle

We now offer an alternate approach to the derivation of Lagrange's equation. Along the way we derive *Hamilton's principle*, a very powerful integral variational statement. Begin with Eq. 3.9, and continue along a new path by rewriting the left-hand side of that equation as follows:

$$\sum_{i=1}^{N} m_i \ddot{\mathbf{r}}_i \cdot \delta\mathbf{r}_i = \sum_{i=1}^{N} m_i \frac{d}{dt}\left(\dot{\mathbf{r}}_i \cdot \delta\mathbf{r}_i\right) - \delta \sum_{i=1}^{N} \frac{1}{2} m_i (\dot{\mathbf{r}}_i \cdot \dot{\mathbf{r}}_i)$$

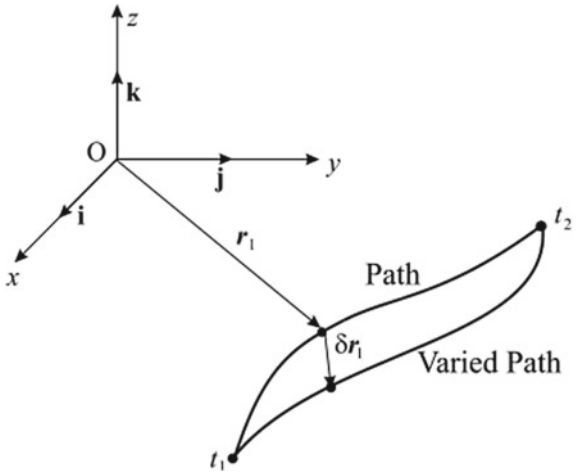

Fig. 3.3 A varied path between two fixed endpoints

$$= \sum_{i=1}^{N} m_i \frac{d}{dt} (\dot{\mathbf{r}}_i \cdot \delta \mathbf{r}_i) - \delta T. \tag{3.16}$$

Use has been made of the relation

$$\frac{d}{dt} (\dot{\mathbf{r}}_i \cdot \delta \mathbf{r}_i) = \ddot{\mathbf{r}}_i \cdot \delta \mathbf{r}_i + \dot{\mathbf{r}}_i \cdot \delta \dot{\mathbf{r}}_i = \ddot{\mathbf{r}}_i \cdot \delta \mathbf{r}_i + \delta (\frac{1}{2} \dot{\mathbf{r}}_i \cdot \dot{\mathbf{r}}_i).$$

Substitute Eq. 3.16, and $\sum_{i=1}^{N} \mathbf{F}_i \cdot \delta \mathbf{r}_i = \delta W$ into d'Alembert's principle, and find

$$\delta T + \delta W = \sum_{i=1}^{N} m_i \frac{d}{dt} (\dot{\mathbf{r}}_i \cdot \delta \mathbf{r}_i).$$

Consider a *varied path*, as shown in Fig. 3.3, where the paths coincide at the initial and final times, and integrate between t_1 and t_2,

$$\begin{aligned} \int_{t_1}^{t_2} (\delta T + \delta W) dt &= \int_{t_1}^{t_2} \sum_{i=1}^{N} m_i \frac{d}{dt} (\dot{\mathbf{r}}_i \cdot \delta \mathbf{r}_i) dt \\ &= \sum_{i=1}^{N} \int_{t_1}^{t_2} m_i \frac{d}{dt} (\dot{\mathbf{r}}_i \cdot \delta \mathbf{r}_i) dt \\ &= \sum_{i=1}^{N} m_i \dot{\mathbf{r}}_i \cdot \delta \mathbf{r}_i \Big|_{t_1}^{t_2} \\ &= 0, \end{aligned}$$

where based on previous discussion, $\delta r_i = 0$ at t_1 and t_2. Therefore,

$$\int_{t_1}^{t_2} (\delta T + \delta W) dt = 0. \tag{3.17}$$

This is called *the extended Hamilton's principle*. δW includes both conservative and nonconservative work. If the forces are only conservative, then $\delta W = -\delta V$, and

$$\delta \int_{t_1}^{t_2} (T - V) dt = 0,$$

where the *Lagrangian* $L = T - V$. This equation may be physically interpreted as nature trying to equalize the kinetic and potential energies of a system, in absence of dissipation.

Lagrange's equation can be derived from Hamilton's principle. To do this, in Eq. 3.17, vary $T(q_i, \dot{q}_i)$ for each generalized coordinate,

$$\delta T = \sum_{i=1}^{N} \frac{\partial T}{\partial q_i} \delta q_i + \sum_{i=1}^{N} \frac{\partial T}{\partial \dot{q}_i} \delta \dot{q}_i. \tag{3.18}$$

Let

$$\delta \dot{q}_i = \frac{d(\delta q_i)}{dt},$$

and integrate by parts the ith component of the second term in Eq. 3.18:

$$\int_{t_1}^{t_2} \frac{\partial T}{\partial \dot{q}_i} \frac{d(\delta q_i)}{dt} dt = \frac{\partial T}{\partial \dot{q}_i} \delta q_i \Big|_{t_1}^{t_2} - \int_{t_1}^{t_2} \delta q_i \frac{d}{dt} \left(\frac{\partial T}{\partial \dot{q}_i} \right) dt,$$

where

$$\frac{\partial T}{\partial \dot{q}_i} \delta q_i \Big|_{t_1}^{t_2} = 0$$

at the end times. Equation 3.17 then becomes

$$\int_{t_1}^{t_2} \sum_{i=1}^{N} \left[\left(\frac{\partial T}{\partial q_i} - \frac{d}{dt} \left(\frac{\partial T}{\partial \dot{q}_i} \right) + Q_i \right) \delta q_i \right] dt = 0, \tag{3.19}$$

where $\delta W = -\sum_i (\partial V / \partial q_i - Q_{i_{nc}}) \delta q_i \equiv \sum_i Q_i \delta q_i$.

Since all δq_i are arbitrary except at the end times, for each i in Eq. 3.19, the expression within the parentheses equals zero. This is again Lagrange's equation, one for each generalized coordinate, as in Eq. 3.13.

3.5 Discussion

Variational methods are powerful and beautiful formulations that relate system energies to their dynamical behavior. They are worthy of study and application to fields across the spectrum of the physical and biological sciences.

In the following chapter, we examine the use of variational mechanics concepts to fluid mechanics, along with an introduction to the work of McIver, as well as our extension of his work.

References

1. Lanczos C (1986) The variational principles of mechanics. Dover Publications Inc, New York
2. Wells DA (1967) Lagrangian dynamics. Schaum's Outlines, New York, NY

Chapter 4
Variational Models in Fluid Mechanics

Abstract This chapter introduces a novel approach to the use of variational mechanics in the modeling of fluid mechanics. That is, Hamilton's principle is used in conjunction with Reynolds transport theorem by McIver in a control volume framework for structures containing fluid. We continue by extending McIver's ideas to structures that are surrounded by an incompressible fluid. Simple problems are given as example applications.

4.1 Introduction

One of the great challenges in engineering science also happens to be one of engineering design. This is the modeling, analysis, and design of vibrating structures driven by fluid motion. Our particular concern here is the vortex-induced oscillations of a bluff body. While the importance of the subject has long been known, it is only during the past almost 50 years that there have been concerted efforts to analytically model the general behavior of the coupling between vortex shedding and structural vibration. One may view the efforts of Hartlen and Currie [1] as initiating the flow-oscillator phase of modern research in this discipline.

In parallel, and over a longer period of time, experimentalists have been gathering data of such interactions in order to help define the various regimes of behavior as a function, for example, of flow velocity. There are numerous review papers and journals devoted to this subject. The literature in fluid–structure interaction is vast, and it can be said to comprise a large fraction of all papers published in the mechanical sciences. The review of Chap. 2 provides the reader with a critical sample of the various studies.

Hamilton's principle in analytical dynamics is certainly among the great intellectual achievements since the work of Newton. This variational principle, while developed as part of the evolution of our understanding of elastic body dynamics, has been applied in many disciplines, including optics and quantum mechanics. In Sect. 4.2, for completeness and to establish the notation used here, we will derive the principle, and then in Sect. 4.3 show how it has been extended in the fundamental

S. Mottaghi et al., *An Analytical Mechanics Framework for Flow-Oscillator Modeling of Vortex-Induced Bluff-Body Oscillations*, Solid Mechanics and Its Applications 260,
https://doi.org/10.1007/978-3-030-26133-7_4

work of McIver [2] for systems of changing mass. In particular, the development by McIver was a successful attempt to model structures with internal moving fluid. We will build on this idea to extend Hamilton's principle for structures vibrating in a fluid. Our purpose, in addition to being fascinated by the variational principles of mechanics, is to use such an approach to semi-analytically model vortex-induced vibration. The "semi" implies that part of the model may depend on experimental data. As the resulting equations will show, there is no way that such a modeling effort can be accomplished without a close linkage to data derived in physical experiments and the input of the experimentalist. Experimental data not only helps us verify the model predictions but also allows us to develop the most advantageous model framework from the variational mechanics perspective, as we will begin to discuss in Sect. 4.4.

The basic theory of Sect. 4.4 is applied to simple examples in Sect. 4.5. Section 4.6 suggests an extension of the theory for more general formulations. These ideas are extended in Chaps. 5–7.

4.2 Hamilton's Principle

4.2.1 The Classical Theory

From d'Alembert's principle for a system of n particles,

$$\sum_{i=1}^{n}\left(m_i\frac{d^2\mathbf{r}_i}{dt^2}+\frac{\partial\Pi}{\partial\mathbf{r}_i}-\mathbf{F}_i\right)\cdot\delta\mathbf{r}_i=0, \tag{4.1}$$

where $\Pi=\Pi(\mathbf{r}_1,\mathbf{r}_2,...,\mathbf{r}_n)$ is the potential energy of the particles, $\mathbf{F}_i$ denotes forces without potentials acting on the i^{th} particle, $\mathbf{r}_i$ is the position vector of the particle of mass m_i, and $\delta\mathbf{r}_i$ is a virtual displacement. The notation δ implies a variation of a function. It is a possible alternate configuration that complies with the system constraints. The variation equals zero where the system is prescribed. For example, at a fixed boundary or support, the variation is zero since there are no alternative possible configurations and there cannot be any work done in this case. Considering each term in Eq. 4.1, we note that

$$\delta\Pi=\sum_{i=1}^{n}\left(\frac{\partial\Pi}{\partial\mathbf{r}_i}\right)\cdot\delta\mathbf{r}_i \tag{4.2}$$

$$\delta W=\sum_{i=1}^{n}(\mathbf{F}_i)\cdot\delta\mathbf{r}_i \tag{4.3}$$

and (by the product rule of differentiation)

$$\sum_{i=1}^{n}\left(m_i\frac{d^2\mathbf{r}_i}{dt^2}\right)\cdot\delta\mathbf{r}_i=\frac{d}{dt}\left[\sum_{i=1}^{n}\left(m_i\frac{d\mathbf{r}_i}{dt}\right)\cdot\delta\mathbf{r}_i\right]$$
$$-\sum_{i=1}^{n}\left(m_i\frac{d\mathbf{r}_i}{dt}\right)\cdot\delta\frac{d\mathbf{r}_i}{dt} \tag{4.4}$$
$$=\frac{d}{dt}\left[\sum_{i=1}^{n}\left(m_i\frac{d\mathbf{r}_i}{dt}\right)\cdot\delta\mathbf{r}_i\right]-\delta T, \tag{4.5}$$

where T is called the kinetic energy of the particles. Substitute Eqs. 4.2, 4.3 and 4.5 into Eq. 4.1, and d'Alembert's principle becomes

$$\delta\mathcal{L}+\delta W-\frac{d}{dt}\left[\sum_{i=1}^{n}\left(m_i\frac{d\mathbf{r}_i}{dt}\right)\cdot\delta\mathbf{r}_i\right]=0, \tag{4.6}$$

where $\mathcal{L}=T-\Pi$ is known as the Lagrangian of the system. Equation 4.6 for a discrete system may be written for a continuous system as

$$\delta\mathcal{L}+\delta W-\frac{d}{dt}\left[\int_v(\rho\mathbf{U})\cdot\delta\mathbf{r}\,dv\right]=0, \tag{4.7}$$

where ρ denotes the density, $\mathbf{U}=d\mathbf{r}/dt$, the velocity field of the system at time t, $\mathcal{L}$ is the Lagrangian of the continuous system, and δW is the virtual work performed on the system by the generalized (nonconservative) forces undergoing virtual displacements. v denotes a fixed material system enclosed in a volume, over which the integration is performed.

Hamilton's principle is obtained by integrating Eq. 4.7 (or Eq. 4.6) with respect to time over an interval t_1 to t_2, yielding

$$\delta\int_{t_1}^{t_2}\mathcal{L}dt+\int_{t_1}^{t_2}\delta W dt-\left[\int_v(\rho\mathbf{U})\cdot\delta\mathbf{r}\,dv\right]_{t_1}^{t_2}=0. \tag{4.8}$$

If one imposes the requirement that at times t_1 and t_2 the configuration be prescribed, then it must be that $\delta\mathbf{r}=0$, and then the last term in the above equation drops out, leaving only

$$\delta\int_{t_1}^{t_2}\mathcal{L}dt+\int_{t_1}^{t_2}\delta W dt=0. \tag{4.9}$$

The equations of motion and their respective boundary conditions are a result of performing the stated variations.

In this case, where the configuration is prescribed at the end times, Hamilton's principle states that there is an optimal (minimum) path in time for the configuration

of the system. This is not generally the case where the end times are not prescribed, as we will examine in our subsequent discussion. It is important to emphasize the physical meaning of prescribing the configuration and how this leads to a variational principle to which there is an optimal configuration in dynamic space. Prescribing the variation $\delta\mathbf{r}$ at the end times implies that the system configuration is known at those times, thus leading to $\delta\mathbf{r} = \mathbf{0}$, and then it is therefore possible to meaningfully speak of an optimal path between the end times.

4.2.2 A Generalization

If we cannot state that the variation is between definite limits t_1 and t_2, then there may be a variation as well at the ends of the time interval. The implication is that the system is not prescribed at these end times. Equation 4.9 was obtained assuming no such variation. Begin with Eq. 4.6 and integrate between t_1 and t_2. Then,

$$\delta\int_{t_1}^{t_2}\mathcal{L}\,dt + \int_{t_1}^{t_2}\delta W\,dt - \int_{t_1}^{t_2}\frac{d}{dt}\left[\sum_{i=1}^{n}\left(m_i\frac{d\mathbf{r}_i}{dt}\right)\cdot\delta\mathbf{r}_i\right]dt = 0$$

$$\delta\int_{t_1}^{t_2}\mathcal{L}\,dt + \int_{t_1}^{t_2}\delta W\,dt = \left[\sum_{i=1}^{n}\left(m_i\frac{d\mathbf{r}_i}{dt}\right)\cdot\delta\mathbf{r}_i\right]_{t_1}^{t_2}. \tag{4.10}$$

Following Lanczos,[1] let the virtual displacement $\delta\mathbf{r}_i$ at each instant of time coincide with the actual displacement $d\mathbf{r}_i$ which takes place during an infinitesimal time $dt \equiv \epsilon$. Then $\delta\mathbf{r}_i = d\mathbf{r}_i = \epsilon\mathbf{r}_i$ and

$$\left[\sum_{i=1}^{n}\left(m_i\frac{d\mathbf{r}_i}{dt}\right)\cdot\delta\mathbf{r}_i\right]_{t_1}^{t_2} = \left[\sum_{i=1}^{n}(m_i\mathbf{r}_i)\cdot\epsilon\mathbf{r}_i\right]_{t_1}^{t_2}$$

$$= \left[\sum_{i=1}^{n}\epsilon m_i\dot{r}_i^2\right]_{t_1}^{t_2},$$

where, as an aside, it is noted that $m_i\dot{r}_i^2 \equiv p_i\dot{r}_i$ and p_i is the momentum of particle i. Furthermore,

$$\delta\int_{t_1}^{t_2}\mathcal{L}\,dt = \int_{t_1}^{t_2}d\mathcal{L}\,dt = \int_{t_1}^{t_2}\epsilon\dot{\mathcal{L}}\,dt = [\epsilon\mathcal{L}]_{t_1}^{t_2}$$

$$\int_{t_1}^{t_2}\delta W\,dt = \int_{t_1}^{t_2}dW\,dt = \int_{t_1}^{t_2}\epsilon\,\dot{W}dt = [\epsilon W]_{t_1}^{t_2}.$$

[1] See: **The Variational Principles of Mechanics** by C. Lanczos, Dover, Fourth Edition, 1970, pp. 119–124.

Eq. 4.10 can now be written as

$$[\epsilon \mathcal{L}]_{t_1}^{t_2} + [\epsilon W]_{t_1}^{t_2} = \left[\sum_{i=1}^{n} \epsilon m_i \dot{r}_i^2 \right]_{t_1}^{t_2},$$

or, substituting the expression for p_i and eliminating ϵ,

$$\left[\sum_{i=1}^{n} p_i \dot{r}_i - \mathcal{L} \right]_{t_1}^{t_2} = [W]_{t_1}^{t_2}. \tag{4.11}$$

In Eq. 4.11, the right-hand side represents the nonconservative work done on the system and the left-hand side represents the total energy in the system. We know that $\mathcal{L} = T - \Pi$, where T is a quadratic in the velocities $\dot{r}_i$,

$$T = \frac{1}{2} \sum_{i,k=1}^{n} a_{ik} \dot{r}_i \dot{r}_k,$$

where a_{ik} are not functions of $\dot{r}_i$, and Π is ordinarily independent of velocity. Therefore,

$$p_i = \frac{\partial T}{\partial \dot{r}_i} = \sum_{k=1}^{n} a_{ik} \dot{r}_k,$$

and

$$\sum_{i=1}^{n} p_i \dot{r}_i = \sum_{i,k=1}^{n} a_{ik} \dot{r}_i \dot{r}_k = 2T.$$

Therefore, Eq. 4.11 can be written as

$$[2T - (T - \Pi)]_{t_1}^{t_2} = [W]_{t_1}^{t_2}.$$

If there is no nonconservative work done on the system, then $[W]_{t_1}^{t_2} = 0$, and we have $T + \Pi = constant$, which is a statement of the principle of conservation of energy. In general, however, $\Delta (T + \Pi) = \Delta W$. Divide both sides by Δt and take the limit as $\Delta t \to 0$, then over the time span t_1 to t_2,

$$\frac{d (T + \Pi)}{dt} = \dot{W}; \tag{4.12}$$

that is, the total change in system energy is equal to the rate at which (nonconservative) work is done on the system. These developments can be extended to an open system, as shown in the following section, where we summarize some of the key results due to McIver.

4.3 McIver's Extension of Hamilton's Principle

In 1973, McIver published a work with broad implications for modeling complex fluid–structure interactions. The central feature of his work was the broadening of Hamilton's principle to include integral control volume concepts from fluid mechanics. In this section, we summarize the key developments by McIver, however, adopting a notation that is consistent with our own developments that begin in Sect. 4.4.

4.3.1 A Brief Review of Reynolds Transport Theorem

Before proceeding with a discussion of McIver's extension, it would perhaps be instructive to briefly review Reynolds transport theorem. We first define a *system* as a collection of fluid particles comprising part of a flow of interest. The system boundaries are such that the same fluid elements are always contained therein. Necessarily, the mass of a system is constant, and it is in principle possible to write equations of motion for the system. For many flows, however, such a formulation would be intractable or inconvenient at best. For this reason, we define a *control volume* as a clearly defined, albeit imaginary, space through which fluid may pass. The external boundary of the control volume is referred to as the *control surface*. The advantage of this approach is that the boundaries of the control volume are prescribed at all times. Typically, one dictates that the control volume coincides with some physically meaningful boundary in the flow, e.g., the internal passageways of a jet aircraft engine. In this context, it may be expedient to allow the control volume to move or change shape depending on the flow of interest.

Now suppose that at some time, t_0, a collection of fluid particles comprising a system occupies the same space as a control volume. It is possible to write the rate of change of any property of that system in terms of control volume parameters. This is the classic Reynolds transport theorem which may be written as

$$\frac{d}{dt}\int_{system}(\mathcal{A}\rho)\,dv = \int_{\substack{control\\vol}}\frac{\partial}{\partial t}(\mathcal{A}\rho)\,dv - \int_{\substack{control\\surface}}(\mathcal{A}\rho)\,\mathbf{U}\cdot\mathbf{n}\,ds. \tag{4.13}$$

In this form, $\mathcal{A}$ represents the property of interest per unit mass (intensive property), ρ is the fluid density, dv and ds are differential volumes and control surface area elements, respectively, and $\mathbf{U} = \mathbf{U}(\mathbf{x}, t)$ is the fluid velocity at any point on the control surface. Observing that $\rho\,(\mathbf{U}\cdot\mathbf{n})$ is the mass flow rate of fluid across a differential area element of the control surface, Eq. 4.13 may therefore be physically interpreted as a balance equation for the property $\mathcal{A}$. Specifically, the rate of change of $\mathcal{A}$ contained within the system (i.e., the left-hand side of Eq. 4.13) is equal to the rate of change of $\mathcal{A}$ within the control volume plus the net flux of $\mathcal{A}$ across the boundaries of the control volume. The unit normal $\mathbf{n}$ is defined as positive when pointing outward from a control surface. Therefore, for a flow into the control volume the sign of $\mathbf{U}\cdot\mathbf{n}$

is negative and for a flow out of the control volume the sign of $\mathbf{U} \cdot \mathbf{n}$ is positive. The control surface integral above is given a negative sign so that an increase in the system property $\mathcal{A}\rho$ with time occurs with a flow into the control volume.

Finally, it is important to note that $\mathbf{U}$ represents the fluid velocity relative to an inertial reference frame. Thus, if any part of the control surface is moving relative to that inertial frame, it becomes necessary to subtract the control surface velocity from the fluid velocity, $\mathbf{U} - \mathbf{V}_{control}$, to obtain the flow rate across the control volume boundaries. All quantities are defined or measured with respect to an observer at a fixed, or inertial control volume.

4.3.2 McIver's Extension

The strength of McIver's work was in identifying an approach for analyzing complex interactions where the system boundaries are not necessarily well defined or where the system configuration at two distinct times may not be readily prescribed. In the classical Hamilton's principle approach, the system contains one or more solid objects whose positions may be prescribed at specific times. That is, the system is of fixed mass containing the same material elements at all times. By introducing Reynolds transport theorem, McIver generalized the analysis to include control volumes where the material is permitted to cross the boundaries. Specifically, by applying Reynolds transport theorem, Eq. 4.13, to the last term in Eq. 4.7, we obtain

$$\delta \mathcal{L}_{system} + \delta W - \int_{\substack{control \\ vol}} \frac{\partial}{\partial t} (\rho \mathbf{U}) \cdot \delta \mathbf{r} \, dv + \int_{\substack{control \\ surface}} (\rho \mathbf{U}) \cdot \delta \mathbf{r} \, (\mathbf{U} - \mathbf{V}_{control}) \cdot \mathbf{n} \, ds = 0, \tag{4.14}$$

where, in the Lagrangian of the open control volume, $\mathcal{L}_{system}$, the mass is not fixed. We have retained the possibility of a moving control surface by including $\mathbf{V}_{control}$, which may have a different value in different regions of the control surface. The control surface here implies an open region since at closed portions flow velocity $\mathbf{U} = \mathbf{V}_{structure}$. Equation 4.14 is a statement of the principle of virtual work.

Now integrate with respect to time over the interval t_1 to t_2, and, *again requiring the system configurations at t_1 and t_2 to be prescribed*, the extended form of Hamilton's principle for a system of changing mass can be expressed as

$$\delta \int_{t_1}^{t_2} \mathcal{L}_{system} dt + \int_{t_1}^{t_2} \delta W \, dt + \int_{t_1}^{t_2} dt \int_{\substack{control \\ surface}} (\rho \mathbf{U}) \cdot \delta \mathbf{r} \, (\mathbf{U} - \mathbf{V}_{control}) \cdot \mathbf{n} \, ds = 0, \tag{4.15}$$

where δW is the virtual work performed by the non-potential forces acting on the same system. If the control surface (CS) does not move, then $\mathbf{V}_{control} = 0$. If only a portion of the control surface moves then the integral will be split into parts that follow the moving control surface and parts that are static. For the case where the virtual work arises from the surface tractions over the closed and open boundaries of the system, we have

$$\begin{aligned}\delta W &= \delta W_{closed\,CS} + \delta W_{open\,CS} \\ &= \int_{closed\,CS} (\sigma \cdot \mathbf{n}) \cdot \delta \mathbf{r}\, ds + \int_{open\,CS} (\sigma \cdot \mathbf{n}) \cdot \delta \mathbf{r}\, ds, \end{aligned} \tag{4.16}$$

where σ is the general stress tensor. Equation 4.15 then becomes

$$\begin{aligned}\delta \int_{t_1}^{t_2} \mathcal{L}_{system} dt + \int_{t_1}^{t_2} dt \int_{open\,CS} [(\sigma \cdot \mathbf{n}) \cdot \delta \mathbf{r} + \rho \mathbf{U} \cdot \delta \mathbf{r}\, (\mathbf{U} - \mathbf{V}_{control}) \cdot \mathbf{n}\,]\, ds \\ + \int_{t_1}^{t_2} dt \int_{closed\,CS} (\sigma \cdot \mathbf{n}) \cdot \delta \mathbf{r}\, ds = 0. \end{aligned} \tag{4.17}$$

For a system that is comprised of a structure and a fluid, the above terms must account for both. Term $\mathcal{L}_{system}$ includes both structure and fluid, $\delta W_{open\,CS}$ represents open portions of the control surface through which fluid flows, and $\delta W_{closed\,CS}$ represents boundaries through which there is no flow, such as a solid boundary or a streamline.

McIver's system is composed of one control volume, of which part is open and the rest is closed. Therefore, both are treated simultaneously, as shown in the two examples developed in his paper. The first is the derivation of the equation of motion of a rocket where the open part of the control surface coincides with the exhaust for combusted fuel. The second example discusses an early controversy regarding the modeling of the dynamics of a moving beam.

4.3.3 *System Configuration Not Prescribed at t_1 and t_2*

If the system configuration is not prescribed at the end times, we must proceed differently after Eq. 4.14. If *the system is not prescribed at* t_1 and t_2, the variation of the displacement $\delta \mathbf{r} \neq 0$, rather, we have the following[2] relation $\delta \mathbf{r} = \mathbf{U} dt$. From this, we can see that the variational operator is related to the time differential operator by $\delta(\cdot) = dt\, d(\cdot)/dt$. Begin with Eq. 4.14, repeated here,

$$\delta \mathcal{L}_{system} + \delta W - \int_{\substack{control \\ vol}} \frac{\partial}{\partial t} (\rho \mathbf{U}) \cdot \delta \mathbf{r}\, dv + \int_{\substack{control \\ surface}} (\rho \mathbf{U}) \cdot \delta \mathbf{r}\, (\mathbf{U} - \mathbf{V}_{control}) \cdot \mathbf{n}\, ds = 0,$$

interchange the partial derivative with the integration over the control volume, and replace the variation as noted above,

$$\begin{aligned} dt \frac{d \mathcal{L}_{system}}{dt} + dt \frac{dW}{dt} - \int_{\substack{control \\ vol}} \frac{\partial}{\partial t} (\rho \mathbf{U}) \cdot \mathbf{U} dt\, dv \\ + \int_{\substack{control \\ surface}} (\rho \mathbf{U}) \cdot \mathbf{U} dt\, (\mathbf{U} - \mathbf{V}_{control}) \cdot \mathbf{n}\, ds = 0. \end{aligned}$$

[2] As before, we replace the *arbitrary* variation $\delta \mathbf{r}$ by the actual $d\mathbf{r} = \mathbf{r} dt$.

Eliminate the common dt factor to find

$$\frac{d\mathcal{L}_{system}}{dt} + \frac{dW}{dt} - \int_{\substack{control\\vol}} \frac{\partial}{\partial t}\rho U^2 dv + \int_{\substack{control\\surface}} \rho U^2 \left(\mathbf{U} - \mathbf{V}_{control}\right) \cdot \mathbf{n}\, ds = 0. \tag{4.18}$$

For this system, we have

$$\begin{aligned}\mathcal{L}_{system} &= \int_{system} \left(\frac{1}{2}\rho U^2\right) dv - \int_{system} (\rho e)\, dv \\ &= \int_{system} \left(\frac{1}{2}\rho U^2 - \rho e\right) dv,\end{aligned}$$

where e is the potential energy per unit mass. Now apply Reynolds transport theorem, Eq. 4.13, to $\mathcal{L}_{system}$,

$$\begin{aligned}\frac{d}{dt}\mathcal{L}_{system} &= \frac{d}{dt}\int_{system} \left(\frac{1}{2}\rho U^2 - \rho e\right) dv \\ &= \int_{\substack{control\\vol}} \frac{\partial}{\partial t}\left(\frac{1}{2}\rho U^2 - \rho e\right) dv \\ &\quad - \int_{\substack{control\\surface}} \left(\frac{1}{2}\rho U^2 - \rho e\right) \left(\mathbf{U} - \mathbf{V}_{control}\right) \cdot \mathbf{n}\, ds.\end{aligned}$$

Substitute this expression into Eq. 4.18 to find

$$\begin{aligned}&\int_{\substack{control\\vol}} \frac{\partial}{\partial t}\left(\frac{1}{2}\rho U^2 - \rho e\right) dv + \dot{W} - \frac{d}{dt}(2T) \\ &+ \int_{\substack{control\\surface}} \rho \left[U^2 - \frac{1}{2}U^2 + e\right] \left(\mathbf{U} - \mathbf{V}_{control}\right) \cdot \mathbf{n}\, ds = 0,\end{aligned}$$

where

$$\int_{\substack{control\\vol}} \rho U^2 dv = 2T,$$

and T represents the kinetic energy of all the fluid within the control volume. Then,

$$\frac{d\left(-T - \Pi\right)}{dt} + \dot{W} + \int_{\substack{control\\surface}} \left[\frac{1}{2}\rho U^2 + \rho e\right] \left(\mathbf{U} - \mathbf{V}_{control}\right) \cdot \mathbf{n}\, ds = 0.$$

Finally,

$$\frac{d\left(T + \Pi\right)_{\substack{control\\vol}}}{dt} = \dot{W} + \int_{\substack{control\\surface}} \rho \left[\frac{1}{2}U^2 + e\right] \left(\mathbf{U} - \mathbf{V}_{control}\right) \cdot \mathbf{n}\, ds. \tag{4.19}$$

This equation states that the change in energy of a system equals the rate at which nonconservative work is done on the system plus the rate of gain of energy by virtue of the fluid flowing through the control surface and the advancing control surface engulfing particles. With the exception of the integral on the right-hand side, this equation is identical to Eq. 4.12.

4.4 The Extension for External Viscous Flows

McIver derived his extension for applications where the fluid is encased in the structure. The equations derived above assume a steady frictionless flow. Examples he studied include the rocket, and flow in a pipe. The application of interest here has the structure within the fluid. In particular, we are interested in generalizing the McIver extension of Hamilton's principle so that we can model the vortex-induced oscillations of a structure. This is a viscous external fluid–structure interaction. McIver's extension utilizes the control volume concept to account for fluid mass that enters and leaves the structure. This same idea can be applied to a control volume around a fluid that has a structure internally.

Modeling of the internal flow problem has the advantage that, assuming no cavitation, the fluid is bound by the structure. With external flows, the fluid is unbounded and the modeling becomes more challenging, requiring additional physical and mathematical considerations.

In this development, it is useful to think of the system, comprising a structure surrounded by a moving fluid, as one that is defined using *two* control surfaces. The first control surface is at the structure surface. It is a closed control volume. The second control surface is at some distance from the structure. This control surface may be partially closed and partially open, or all open, depending on the application. It is important to keep track of the various portions of the control surface so that the parameters are appropriately prescribed.

For such a control volume,

- there is a time rate change of momentum within the control volume due to the unsteady character of the flow,
- there is a net momentum flux across the boundaries of the control surface,
- there is an instantaneous pressure p acting on the control surface,
- there is an instantaneous shear stress τ acting on the control surface.

Begin with Eq. 4.14, repeated here,

$$\delta \mathcal{L}_{system} + \delta W - \int_{\substack{control \\ vol}} \frac{\partial}{\partial t} (\rho \mathbf{U}) \cdot \delta \mathbf{r} \, dv + \int_{\substack{control \\ surface}} (\rho \mathbf{U}) \cdot \delta \mathbf{r} \, (\mathbf{U} - \mathbf{V}_{control}) \cdot \mathbf{n} \, ds = 0.$$

The integral over the control volume needs to be interpreted to include the inner (structural) as well as outer (fluid) control volumes.

Replace δW as follows:

$$\delta W = \int_{\substack{closed \\ CS}} (\sigma \cdot \mathbf{n}) \cdot \delta \mathbf{r}\, ds + \int_{\substack{open \\ CS}} (\sigma \cdot \mathbf{n}) \cdot \delta \mathbf{r}\, ds, \tag{4.20}$$

where $\mathbf{n}$ is an outward normal in the positive sense.

The integral over the closed surface represents the virtual work done by shear forces at the boundaries of the control volume where there is no flow across the control surface, for example, at the structural boundary, possibly other solid boundaries, or at streamlines. The integral over the open surface represents the virtual work done by normal and shear forces at the boundaries of the control volume where there is a flow across the control surface, for example, at the upstream and downstream surfaces, which may be perpendicular to the flow direction. The integrals above can be written more specifically as

$$\int_{\substack{closed \\ CS}} (\sigma \cdot \mathbf{n}) \cdot \delta \mathbf{r}\, ds = \int_{\substack{closed \\ CS}} (-p\mathbf{n} + \tau_c) \cdot \delta \mathbf{r}\, ds \tag{4.21}$$

$$\int_{\substack{open \\ CS}} (\sigma \cdot \mathbf{n}) \cdot \delta \mathbf{r}\, ds = \int_{\substack{open \\ CS}} (-p\mathbf{n} + \tau_o) \cdot \delta \mathbf{r}\, ds, \tag{4.22}$$

where $-p\mathbf{n}$ is the normal pressure (inward) and τ_c and τ_o are the shear forces on the closed (structural) and open (fluid) surfaces of the control volume.

There are two ways to proceed. One can prescribe the configuration, or not prescribe the configuration, at the end times. We begin by not prescribing the configuration at the end times.

4.4.1 Configuration Not Prescribed at t_1 and t_2

We now follow the procedure of Sect. 4.3 where the configuration is not prescribed at t_1 or t_2. We define $\delta \mathbf{r}$ as before, with the variational operator related to the time differential operator by $\delta(\cdot) = dt\ d(\cdot)/dt$. Then,

$$\delta W = \int_{\substack{closed \\ CS}} (-p\mathbf{n} + \tau_c) \cdot \delta \mathbf{r}\, ds + \int_{\substack{open \\ CS}} (-p\mathbf{n} + \tau_o) \cdot \delta \mathbf{r}\, ds$$

$$dt \frac{dW}{dt} = dt \int_{\substack{closed \\ CS}} (-p\mathbf{n} + \tau_c) \cdot \mathbf{U}\, ds + dt \int_{\substack{open \\ CS}} (-p\mathbf{n} + \tau_o) \cdot \mathbf{U}\, ds,$$

where it is noted that the work done at the structural surface is independent of the control surface.

The integral over the control volume must be considered in the following way. For the inner control volume $\delta \mathbf{r} = \mathbf{U}_{structure} dt$ and for the outer control volume (annulus) $\delta \mathbf{r} = \mathbf{U} dt$, where $\mathbf{U}_{fluid} \equiv \mathbf{U}$. Therefore,

$$\frac{\partial}{\partial t}\int_{\substack{control\\vol}}(\rho\mathbf{U})\cdot\delta\mathbf{r}\,dv=\frac{\partial}{\partial t}\int_{\substack{control\\vol}}\left[\rho U^2+\rho_{structure}U^2_{structure}\right]dv\,dt.$$

Then, beginning with Eq. 4.18, repeated here, with $\rho\equiv\rho_{fluid}$,

$$\frac{d\mathcal{L}_{system}}{dt}+\frac{dW}{dt}-\frac{\partial}{\partial t}\int_{\substack{control\\vol}}\left[\rho U^2+\rho_{structure}U^2_{structure}\right]dv+\int_{\substack{control\\surface}}\rho U^2\left(\mathbf{U}-\mathbf{V}_{control}\right)\cdot\mathbf{n}\,ds=0,$$

we find

$$\frac{d}{dt}\mathcal{L}_{system}+\left[\int_{\substack{closed\\CS}}(-p\mathbf{n}+\tau_c)\cdot\mathbf{U}\,ds+\int_{\substack{open\\CS}}(-p\mathbf{n}+\tau_o)\cdot\mathbf{U}\,ds\right]-\frac{\partial}{\partial t}\int_{\substack{control\\vol}}\left[\rho U^2+\rho_{structure}U^2_{structure}\right]dv+\int_{\substack{open\\CS}}\rho U^2\left(\mathbf{U}-\mathbf{V}_{control}\right)\cdot\mathbf{n}\,ds=0. \tag{4.23}$$

We know that the integral over the control volume equals twice the total kinetic energies of the fluid and the structure $2T$, where $T=T_{fluid}+T_{structure}$. Now apply the control volume Eq. 4.13 to the quantity $\mathcal{L}_{system}$,

$$\mathcal{L}_{system}=\int_{system}\left(\hat{T}_{structure}+\hat{T}_{fluid}-\hat{\Pi}_{structure}-\hat{\Pi}_{fluid}\right)dv, \tag{4.24}$$

where the terms under the integral are intensive properties and have units of energy per unit volume, that is,

$$\int_{system}\hat{T}_i dv=T_i$$
$$\int_{system}\hat{\Pi}_i dv=\Pi_i.$$

Then,

$$\frac{d}{dt}\mathcal{L}_{system}=\frac{d}{dt}\int_{system}\left(\hat{T}_{structure}+\hat{T}_{fluid}-\hat{\Pi}_{structure}-\hat{\Pi}_{fluid}\right)dv, \tag{4.25}$$

where

$$\begin{aligned}
&\frac{d}{dt}\int_{system}\left(\hat{T}_{structure}+\hat{T}_{fluid}-\hat{\Pi}_{structure}-\hat{\Pi}_{fluid}\right)dv\\
&=\frac{\partial}{\partial t}\int_{\substack{control\\vol}}\left(\hat{T}_{structure}+\hat{T}_{fluid}-\hat{\Pi}_{structure}-\hat{\Pi}_{fluid}\right)dv\\
&\quad-\int_{\substack{open\\CS}}\frac{1}{2}\rho U^2\left(\mathbf{U}-\mathbf{V}_{control}\right)\cdot\mathbf{n}\,ds. \qquad (4.26)
\end{aligned}$$

The integral over the *open control surface* accounts for the fluid entering the control volume (no incoming structure), and therefore *the term* $\frac{1}{2}\rho U^2$ *represents the fluid kinetic energy flux across the control surface*. There is also a possible change in potential energy of the fluid per unit mass e. If there is no cavitation, an approximation can be made that, on average, for every part of the fluid crossing the control surface with an increase in potential, there is an equivalent loss in potential in another region of the surface. Of course, if the flow as a whole gains or loses potential, this assumption is invalid. Thus, e is not included if the average flow is perpendicular to the gravitational vector.

Substitute this expression into Eq. 4.23 to find,

$$\begin{aligned}
&\frac{d}{dt}\int_{\substack{control\\vol}}\left(\hat{T}_{structure}+\hat{T}_{fluid}-\hat{\Pi}_{structure}-\hat{\Pi}_{fluid}\right)dv-2\frac{d}{dt}\left(T_{fluid}+T_{structure}\right)\\
&\qquad+\int_{\substack{open\\CS}}\left[\rho U^2-\frac{1}{2}\rho U^2\right]\left(\mathbf{U}-\mathbf{V}_{control}\right)\cdot\mathbf{n}\,ds\\
&\quad+\int_{\substack{closed\\CS}}\left(-p\mathbf{n}+\tau_c\right)\cdot\mathbf{U}ds+\int_{\substack{open\\CS}}\left(-p\mathbf{n}+\tau_o\right)\cdot\mathbf{U}ds=0,
\end{aligned}$$

and noting that $d\Pi_{fluid}/dt=0$, and simplifying,

$$\begin{aligned}
&\frac{d\left(-T_{structure}-T_{fluid}-\Pi_{structure}\right)}{dt}+\int_{\substack{open\\CS}}\frac{1}{2}\rho U^2\left(\mathbf{U}-\mathbf{V}_{control}\right)\cdot\mathbf{n}\,ds\\
&\quad+\int_{\substack{closed\\CS}}\left(-p\mathbf{n}+\tau_c\right)\cdot\mathbf{U}\,ds+\int_{\substack{open\\CS}}\left(-p\mathbf{n}+\tau_o\right)\cdot\mathbf{U}ds=0. \qquad (4.27)
\end{aligned}$$

Note that the factor dt in all terms have been eliminated. Also, each term in the equation represents a time rate of change of a work term. That is, $\dot{W}$ or $\dot{T}$, meaning that these are expressions for *power*. Equation 4.27 can be put into the form of Eq. 4.19 as follows:

$$\frac{d\left(T_{structure}+T_{fluid}+\Pi_{structure}\right)_{\substack{control\\vol}}}{dt}=\int_{\substack{open\\CS}}\frac{\rho}{2}U^2\left(\mathbf{U}-\mathbf{V}_{control}\right)\cdot\mathbf{n}\,ds$$
$$+\int_{\substack{closed\\CS}}\left(-p\mathbf{n}+\tau_c\right)\cdot\mathbf{U}ds+\int_{\substack{open\\CS}}\left(-p\mathbf{n}+\tau_o\right)\cdot\mathbf{U}\,ds. \tag{4.28}$$

The questions we address later are *(i)* the possible and optimal control volume configurations that are suitable for the problems at hand and *(ii)* whether we can select a control volume such that the open surfaces are prescribed, thus leading to a variational principle, rather than Eq. 4.28. First, however, we would explore Eq. 4.28 in more detail.

Equation 4.28 is a scalar equation, and therefore its evaluation and simplification will result in a single equation of motion for the oscillating structure where all the fluid energy results in a forcing function on the structure. Such an equation of motion is in the single degree-of-freedom class of models for vortex-induced structural oscillations.

The structural terms on the left-hand side of Eq. 4.28,

$$\frac{d\left(T_{structure}+\Pi_{structure}\right)_{\substack{control\\vol}}}{dt},$$

are found by expressing $T_{structure}+\Pi_{structure}$ in terms of structural displacements and velocities and then differentiating with respect to time. The remaining fluid term is related as follows:

$$\frac{d\left(T_{fluid}\right)_{\substack{control\\vol}}}{dt}=\frac{d}{dt}\left(\frac{1}{2}m_{fluid}U^2\right)_{\substack{control\\vol}}=\left(m_{fluid}U\dot{U}\right)_{\substack{control\\vol}}, \tag{4.29}$$

where m_{fluid} within the (open) control volume is constant. In the above, *control vol* respectively refers to either the closed one that hugs the structure, or the open one that is concentric with the closed one. Because of the matched boundary conditions at the interface, that is, fluid velocity equals structural velocity, the existence of this term includes the added mass effect that is included when a structure oscillates in a relatively dense medium. Since this term is evaluated experimentally and fed into the governing equation, any fluid dynamics that is a result of structural oscillation is implicitly included.

The terms on the right-hand side of Eq. 4.28 are the various components of the kinetic energy flux across the control surface. Equation 4.28 is, furthermore, a statement of the first law of thermodynamics where heat transfer and dissipation has been omitted.

In summary, the linking of Hamilton's principle for an unprescribed system with Reynolds transport theorem results in the first law of thermodynamics. A check of the dimensions of all expressions, including the rectilinear acceleration, shows that all the units are rate of work, or power, that is, for example, *ft-lb/sec* or *watts,* depending on the chosen system of units.

Equation 4.28 can be written as

$$\frac{d\left(T_{structure}+\Pi_{structure}\right)_{\substack{control\\vol}}}{dt}+\left(m_{fluid}U\dot{U}\right)_{\substack{control\\vol}}$$
$$=\int_{\substack{open\\CS}}\frac{\rho}{2}U^2\left(\mathbf{U}-\mathbf{V}_{control}\right)\cdot\mathbf{n}\,ds$$
$$+\int_{\substack{closed\\CS}}\left(-p\mathbf{n}+\tau_c\right)\cdot\mathbf{U}ds+\int_{\substack{open\\CS}}\left(-p\mathbf{n}+\tau_o\right)\cdot\mathbf{U}\,ds. \tag{4.30}$$

We envision the following procedure for working with Eq. 4.30. We will substitute expressions for the kinetic energies on the left-hand side. On the right-hand side, we will have experimentally based analytical expressions for the flow velocities, pressures and stresses. This relation will allow the derivation of an expression for the acceleration of the structure. This will be integrated twice to find the expression for the structural displacement as a function of time and the system parameters. This result will then be compared to the experimentally derived structural displacement as a function of time. The two functions will be compared, permitting an evaluation of the analytical framework and its components.

4.4.1.1 Control Volume Definition

We first describe the control volume of interest here. Consider a top view of a circular cylinder with two control surfaces, one at the surface of the cylinder and the other some concentric distance out in the surrounding water. One question that arises when considering various possible control volumes are whether a particular control volume has significant advantages either for the analytical formulation or for the experimental procedures, the results of which are required as input to the analytical model. This will have to be considered as part of an examination of the proposed methodology.

4.4.2 Coupled Experiments

For the modeling effort in this chapter, there is no possibility of analytically arriving at expressions for each term and each function in Eq. 4.30. Therefore, it is necessary that an experimental program is run in parallel for particular applications. The power of this energy-based approach is twofold. The first is that an analytical framework is created to organize our understanding of a complex nonlinear and interactive phenomenon. But second and equally important is that the experimental program provides us with invaluable information about some of the components of these equations, and this permits us to utilize the variational tools in the derivation of the equations of motion.

We expand and generalize on this model in two ways, first in Chap. 5 with Hamilton's formulation, and then in Chaps. 6 and 7 with Jourdain's formulation.

4.5 Simple Example Problems

Several example problem formulations are presented next. These are, of course, simple cases meant to initiate us to the application of the general equation. It is straightforward to add structural and other damping mechanisms.

4.5.1 Annular Control Volumes Moving in Tandem

Specifically, for an idealized oscillation of a rigid cylinder, there will be one generalized coordinate, say $x(t)$. Then, the kinetic energy of the structure is related to $\dot{x}^2$ and the strain energy in the supporting springs (with net stiffness constant equal to k) will be related to x^2. The speed of the closed and open control volumes are $\dot{x}$, since they are defined to move with the structure. Similarly, the relative rectilinear accelerations of the closed and open control volumes are $\ddot{x}$. The expressions required to evaluate the terms $(-p\mathbf{n}+\tau_c)\cdot\mathbf{U}$, and $(-p\mathbf{n}+\tau_o)\cdot\mathbf{U}$ are determined experimentally. It has been assumed that the cylinder oscillates in the plane perpendicular to the flow direction, and that the acceleration (of the closed control volume) is rectilinear.

For this rigidly translating cylinder, we have

$$\begin{aligned}\frac{d\left(T_{structure}+\Pi_{structure}\right)_{\substack{control\\vol}}}{dt} &= \frac{d}{dt}\left(\frac{1}{2}m_{cylinder}\dot{x}^2+\frac{1}{2}kx^2\right)\\ &= \dot{x}\left(m_{cylinder}\ddot{x}+kx\right).\end{aligned}$$

Equation 4.30 can be written as

$$\begin{aligned}\dot{x}\left(m_{cylinder}\ddot{x}+kx\right)+m_{fluid}U\dot{U} &= \int_{\substack{open\\CS}}\frac{1}{2}\rho U^2\left(\mathbf{U}-\mathbf{x}\right)\cdot\mathbf{n}\,ds\\ &+\int_{\substack{closed\\CS}}\left(-p\mathbf{n}+\tau_c\right)\cdot\mathbf{U}ds+\int_{\substack{open\\CS}}\left(-p\mathbf{n}+\tau_o\right)\cdot\mathbf{U}\,ds,\end{aligned}$$

where, in this simplified problem, $\mathbf{V}_{control}=\mathbf{x}=\dot{x}$, the last equality due to the fact that the structural and outer fluid control volumes are stipulated to travel only in the x direction perpendicular to the flow. The *open* and *closed* control surfaces refer to the outer and inner control surfaces, respectively. The expression $m_{fluid}U\dot{U}$ refers to the fluid between the two concentric control surfaces. $\Pi_{structure}$ includes all the potential stored in the structure. Because the motion of the cylinder is pure translation

perpendicular to the gravitational field, we don't see the net force resulting from the difference between cylinder weight and buoyancy force. This net force acts along the axis of the cylinder.

Combining like terms yields

$$\dot{x}\left(m_{cylinder}\ddot{x} + kx\right) + m_{fluid}U\dot{U} = \int_{\substack{closed\\CS}} (-p\mathbf{n} + \tau_c)\cdot\mathbf{U}\,ds + \int_{\substack{open\\CS}} \left[\frac{1}{2}\rho U^2\,(\mathbf{U}-\mathbf{x})\cdot\mathbf{n} + (-p\mathbf{n}+\tau_o)\cdot\mathbf{U}\right] ds. \tag{4.31}$$

4.5.1.1 Stationary Outer Control Volume: Translating Cylinder

If the open control surface is stationary, while the inner control surface attached to the cylinder is still in motion as before, then $\dot{x} = 0$ in the integral over the open control surface, and we have the simplified equation,

$$\dot{x}\left(m_{cylinder}\ddot{x} + kx\right) + m_{fluid}U\dot{U} = \int_{\substack{closed\\CS}} (-p\mathbf{n} + \tau_c)\cdot\mathbf{U}\,ds + \int_{\substack{open\\CS}} \left[\frac{\rho}{2}U^2\mathbf{U}\cdot\mathbf{n} + (-p\mathbf{n}+\tau_o)\cdot\mathbf{U}\right] ds. \tag{4.32}$$

It is important to note that even in a free vibration in an initially still fluid, the flow velocity $U \neq 0$ since any motion of the structure from nonzero initial conditions will result in fluid motion. Therefore, here the equation of motion does not reduce to $m_{cylinder}\ddot{x} + kx = 0$, even though $U(0) = 0$.

4.5.1.2 Stationary Outer Control Volume: Cylinder Oscillating About Contact at Base

Here we take the cylinder to be connected only at its base via a leaf spring. It behaves like a column supported only at its base. For purposes of this example, we assume that the cylinder is rigid, as above, and that three-dimensional effects can be ignored. The single generalized coordinate that defines the cylinder location is the angle of rotation θ rad. We have an additional term in the potential of the structure due to the difference between the buoyancy force and the weight. We assume that the resultants of these distributed forces act at the center of geometry of the circular cylinder. Then, for some rotation θ, this additional potential results in the moment $(mg - B)\frac{L}{2}\sin\theta$, where mg is the weight of the cylinder, B is the total buoyancy force (which equals the weight of the displaced fluid) and L is the length of the cylinder. Let I_o be the mass moment of inertia for the circular cylinder about its base, k_T be the torsional spring constant at the base, then the governing equation is

$$\dot{\theta}\left(I_o\ddot{\theta}+k_T\theta-(mg-B)\frac{L}{2}\sin\theta\right)+m_{fluid}U\dot{U}=\int_{\substack{closed\\CS}}(-p\mathbf{n}+\tau_c)\cdot\mathbf{U}\,ds$$
$$+\int_{\substack{open\\CS}}\left[\frac{\rho}{2}U^2\mathbf{U}\cdot\mathbf{n}+(-p\mathbf{n}+\tau_o)\cdot\mathbf{U}\right]ds. \tag{4.33}$$

This equation, as well as the other cases above, can also be evaluated numerically if written in the form

$$\frac{1}{2}\frac{d}{dt}\left\{I_o\dot{\theta}^2+k_T\theta^2+(mg-B)L\cos\theta\right\}=F(t), \tag{4.34}$$

where $F(t)$ is the sum of all the remaining terms,

$$F(t)=-m_{fluid}U\dot{U}+\int_{\substack{closed\\CS}}(-p\mathbf{n}+\tau_c)\cdot\mathbf{U}\,ds+\int_{\substack{open\\CS}}\left[\frac{\rho}{2}U^2\mathbf{U}\cdot\mathbf{n}+(-p\mathbf{n}+\tau_o)\cdot\mathbf{U}\right]ds.$$

Then, we solve for θ by integrating both sides of Eq. 4.34, and then integrating again with respect to time. There are numerical issues to be resolved due to the complexities of the functions on both sides of the equal sign.

4.6 A More General Variational Approach

4.6.1 Configuration Prescribed at t_1 and t_2

Suppose we prescribe the system at t_1 and t_2, then a variational formulation becomes possible. Begin with Eq. 4.17, repeated here,

$$\delta\int_{t_1}^{t_2}\mathcal{L}_{system}dt+\int_{t_1}^{t_2}dt\int_{\substack{open\\CS}}\left[(\sigma\cdot\mathbf{n})\cdot\delta\mathbf{r}-\rho(\mathbf{U}-\mathbf{V}_{control})\cdot\delta\mathbf{r}(\mathbf{U}\cdot\mathbf{n})\right]ds$$
$$+\int_{t_1}^{t_2}dt\int_{\substack{closed\\CS}}(\sigma\cdot\mathbf{n})\cdot\delta\mathbf{r}\,ds=0,$$

and substitute Eqs. 4.21 and 4.22 to find

$$\delta\int_{t_1}^{t_2}\mathcal{L}_{system}dt+\int_{t_1}^{t_2}dt\int_{\substack{open\\CS}}\left[(-p\mathbf{n}+\tau_o)\cdot\delta\mathbf{r}-\rho(\mathbf{U}-\mathbf{V}_{control})\cdot\delta\mathbf{r}(\mathbf{U}\cdot\mathbf{n})\right]ds$$
$$+\int_{t_1}^{t_2}dt\int_{\substack{closed\\CS}}(-p\mathbf{n}+\tau_c)\cdot\delta\mathbf{r}\,ds=0. \tag{4.35}$$

The next step here would be to work with each term in order to arrive at an equation of the form

$$\int_{t_1}^{t_2} \left\{ \int_{\substack{physical \\ domain}} [EOM]\, \delta\mathbf{r} + |[...]\delta\mathbf{r}|_{boundaries} \right\} dt = 0, \tag{4.36}$$

from which, using the argument that $\delta\mathbf{r}$ is arbitrary everywhere except at the boundaries at t_1 and t_2 leads to the equations of motion EOM. There will be as many equations of motion as there are generalized coordinates in the system. The conditions $|[...]\delta\mathbf{r}|_{boundaries} = 0$ lead to the possible boundary conditions. $\delta\mathbf{r}$ is a vector with dimension equal to the number of generalized coordinates. Our results using this approach can then be compared with that of the last section. At this time it is not possible to draw any specific conclusions, but we would like to expand a bit on this development.

We know that the Lagrangian of the continuous system, structure, and fluid, is obtainable by standard methods, resulting in one equation of motion for each generalized coordinate. Assume, for a rectangular cross section in the open control volume, that the ordinate is the coordinate y and the abscissa is the coordinate x, then the variation $\delta\mathbf{r}$ will be $\pm\delta y$ or $\pm\delta x$, respectively. Performing the variation of the Lagrangian yields the respective boundary conditions. Formally, we have

$$\delta \int_{t_1}^{t_2} \mathcal{L}_{system}\, dt = \int_{t_1}^{t_2} \left[(S_x + F_x)\, \delta x + \left(S_y + F_y\right) \delta y \right] dt + BCs. \tag{4.37}$$

There remains the need to expand the variations within the open and closed control volumes. Consider first the open control volume. We will find

$$\int_{t_1}^{t_2} dt \int_{\substack{open \\ CS}} [(-p\mathbf{n} + \tau_o) \cdot \delta\mathbf{r} - \rho(\mathbf{U} - \mathbf{V}_{control}) \cdot \delta\mathbf{r}(\mathbf{U} \cdot \mathbf{n})\,]\, ds$$
$$= \int_{t_1}^{t_2} dt \left\{ \left[(O_x)\, \delta x + \left(O_y\right) \delta y \right] \right\}. \tag{4.38}$$

For the inner control volume, the cross section is circular. Therefore, the outward normal $\delta\mathbf{r}$ will be of the form $\delta\mathbf{r} = \pm\cos\delta\mathbf{x} \pm \sin\delta\mathbf{y}$. Then,

$$\int_{t_1}^{t_2} dt \int_{\substack{closed \\ CS}} (-p\mathbf{n} + \tau_c) \cdot \delta\mathbf{r}\, ds = \int_{t_1}^{t_2} dt \left\{ \left[(C_x)\, \delta x + \left(C_y\right) \delta y \right] \right\}. \tag{4.39}$$

Equation 4.35 then becomes

$$\int_{t_1}^{t_2} \left[(S_x + F_x + O_x + C_x)\, \delta x + \left(S_y + F_y + O_y + C_y\right) \delta y \right] dt + BCs = 0. \tag{4.40}$$

Functions S, F, O, and C are those that arise from the surface integration. BCs are the boundary conditions. Using familiar arguments that since the variations are arbitrary and independent, the only way that the integral can be identically zero is if each factor of the variations equals zero, that is

$$S_x + F_x + O_x + C_x = 0 \tag{4.41}$$
$$S_y + F_y + O_y + C_y = 0. \tag{4.42}$$

These two equations are the two, nonlinear coupled partial differential equations that are the reduced-order model for the fluid–structure interaction. It is important to emphasize that we chose two generalized coordinates in order to demonstrate the procedure. There will be as many coupled partial differential equations as there are generalized coordinates. For example, if the structural model can bend in two coordinates as well as extend, then it alone will have three generalized coordinates.

4.7 Discussion

The work of McIver has been extended to model the oscillation of a structure in a fluid flow. Two variational approaches have been developed. The first approach assumes that the system configuration is *not* prescribed at the end times. This led to a single equation governing the motion of the structure as it is coupled to the fluid system. This equation has the units of power, and is therefore a power balance between fluid and structure. The second approach, which is only introduced, will be examined further in the next chapter. As outlined, this approach will result in a series of governing equations, one for each degree- of-freedom. This approach holds promise for more complicated flow patterns and structural behavior.

The above theoretical developments rest heavily in a practical and literal sense upon experimental input. The derived governing equations are semiempirical, requiring experimentally developed functions. However, this is certainly an explicit trademark of all fluid mechanics, and is implicit in all of science and engineering. We view it as a positive aspect of the model, that it is inexorably linked to physical data.

In the following chapter, we consider Hamilton's principle more generally to derive a general flow-oscillator model, and show how several published flow-oscillator models can be extracted from the general model.

References

1. Hartlen RT, Currie IG (1970) Lift-oscillator model of vortex induced vibration. J Eng Mech 96(5):577–591
2. McIver DB (1973) Hamilton's principle for systems of changing mass. J Eng Mech 7(3):249–261

Chapter 5
Lagrangian Flow-Oscillator Models

Abstract This chapter extends the development of the previous chapter by applying Hamilton's extended principle to a fluid surrounding a rigid structure. The energies are derived, and the control volume is examined in detail. Boundary conditions are derived and studied. 2D flows past a circular cylinder that is free to move transversely are formulated, and applied to reduced-order modeling. The derived general governing equations for the structure and the flow oscillator are compared with certain published models: Krenk and Nielsen, Hall, Berger, and Tamura and Matsui. It is concluded that the general formulation of this chapter is a good framework for the development of flow-oscillator models of vortex-induced oscillations.

5.1 Advanced Coupled Models

We again focus on the flow of a viscous incompressible fluid around a rigid circular cylinder. A viscous incompressible fluid can be thought of as a real fluid with an internal constraint manifesting the requirement of incompressibility. In general, real fluids are holonomic and nonconservative [18]. The no-slip condition at a boundary (fluid/solid or fluid/fluid), for example, is a holonomic constraint. By holonomic, it is meant that a constraint on the configuration (position) of the particles in a system of the form $G(\mathbf{x}, t) = 0$ exists. Time may (rheonomic) or may not (scleronomic) enter into this constraint equation explicitly.

We begin next by considering the extended Hamilton's principle and derive the energies of the system.

5.1.1 The Extended Hamilton's Principle

Consider the system of particles inhabiting the open control volume $R_o(\mathbf{x}, t)$ at time t. This system of particles is referred to as the *open system*. Only instantaneously does it coincide with the *closed system* of particles which constitute the material system M. The control volume has a part $B_o(\mathbf{x}, t)$ of its bounding surface $B(\mathbf{x},t)$, which

S. Mottaghi et al., *An Analytical Mechanics Framework for Flow-Oscillator Modeling of Vortex-Induced Bluff-Body Oscillations*, Solid Mechanics and Its Applications 260,
https://doi.org/10.1007/978-3-030-26133-7_5

is open to the flow particles. The closed part of the bounding surface is $B_c(\mathbf{x}, t)$, and includes any solid boundaries and portions of the surface in which the local streamline is normal to the surface. The kinetic energy of the open system is denoted $(\mathcal{K})_o$. The sum of the gravitational potential energy $\left(\mathcal{E}^{(g)}\right)_o$, the potential energy due to buoyancy $\left(\mathcal{E}^{(b)}\right)_o$, the strain energy $\left(\mathcal{E}^{(s)}\right)_o$, and the internal energy $\left(\mathcal{E}^{(i)}\right)_o$ of the open system is denoted $(\mathcal{E})_o$. $\mathbf{u}_{\text{rel}}(\mathbf{x}, t) = \mathbf{u}(\mathbf{x}, t) - \mathbf{u}_B$ is the fluid velocity relative to the velocity of control surface.

The extended form of Hamilton's principle for a system of changing mass (e.g., the exhaust jet of a rocket) or a system of constant mass which does not always consist of the same set of particles (e.g., a pipe of constant diameter conveying fluid) can be written as [3]

$$\delta \int_{t_1}^{t_2} (\mathcal{L})_o dt + \int_{t_1}^{t_2} (\delta W)_o \, dt + \int_{t_1}^{t_2} \iint_{B_o(t)} \rho \, (\mathbf{u}_{\text{rel}} \cdot \delta \mathbf{r}) \, (\mathbf{u} \cdot \mathbf{n}) \, ds dt = 0, \tag{5.1}$$

where $(\mathcal{L})_o = (\mathcal{K} - \mathcal{E})_o$ is the Lagrangian of the open system, and $(\delta W)_o$ is the virtual work performed by non-potential forces on the same system. Note that $ds = ds(\mathbf{x}, t)$ is used here to represent a differential surface element. At position $\mathbf{x}$ and time t, the density is ρ and the velocity is $\mathbf{u}$.

Note that Eq. 5.1 is related to the Reynolds transport theorem, which allows one to calculate the time rate of change of any extensive property of system M from Eulerian measurements made inside a spatial volume which instantaneously coincides with that occupied by the mass system at time t. Designating the volume occupied by system M by $R_M(\mathbf{x},t)$, the open control volume instantaneously coinciding with $R_M(\mathbf{x},t)$ by $R_o(\mathbf{x},t)$, and the bounding surface of $R_o(\mathbf{x},t)$ by $B(\mathbf{x},t)$, the Reynolds transport theorem is given by [19]

$$\frac{D}{Dt} \iiint_{R_M(\mathbf{x},t)} \rho \mathcal{A} dv = - \iint_{B(\mathbf{x},t)} \rho \mathcal{A} \, (\mathbf{u}_{\text{rel}} \cdot d\mathbf{A}) \, ds + \iiint_{R_o(\mathbf{x},t)} \frac{\partial}{\partial t} (\rho \mathcal{A}) \, dv. \tag{5.2}$$

In Eq. 5.2, $\mathcal{A}$ is an arbitrary intensive property of the system reckoned per unit mass, $\rho = \rho(\mathbf{x}, t)$ is the spatial density field, and $d\mathbf{A} = \mathbf{n} ds$ with $\mathbf{n}$ a positive *outward* normal. In the surface integral, $\mathbf{u}_{\text{rel}}(\mathbf{x}, t) = \mathbf{u}(\mathbf{x}, t) - \mathbf{u}_B$ is the fluid velocity relative to the velocity of the control surface, assumed constant in time and spatially independent if nonzero. $\mathbf{u}_{\text{rel}}(\mathbf{x}, t) = \mathbf{0}$ on any solid boundaries, so $B(\mathbf{x},t)$ in Eq. 5.2 is understood to exclude any such boundaries. Also excluded are any portions of the surface in which the instantaneous local streamline is normal to the surface, since in that case $\mathbf{u}_{\text{rel}} \cdot d\mathbf{A} = 0$.

In Eq. 5.1, the virtual displacements δr_i must preserve the mass balance law. This is in addition to the requirements imposed by any geometric constraints, the balance laws of internal energy and entropy, and any constitutive relations.

Suppose the *open system* is inhabited instantaneously by fluid particles moving along with the flow and a single solid body in the path of the fluid. The boundary of this solid body constitutes part of the closed boundary $B_c(\mathbf{x}, t)$. The following assumptions are made:

1. The open part of the control surface is stationary, i.e., $\mathbf{u}_{B_o} = \mathbf{0}$. As a result, $\mathbf{u}_{\text{rel}} = \mathbf{u}$.
2. The flow is considered to be two-dimensional. That is, all flow quantities are independent of z and $u_3(\mathbf{x}, t) = 0$. The vorticity is then perpendicular to the plane of motion.
3. The length and time scales are such that the fluid is in local thermodynamic equilibrium (LTE), even when the fluid is in motion. All macroscopic length and time scales are considerably larger than the largest molecular length and time scales.
4. An inertial rectangular Cartesian coordinate system is used, with basis vectors $\mathbf{e}_1$, $\mathbf{e}_2$, and $\mathbf{e}_3$ in the x, y, and z-directions, respectively.
5. The resultant of all body forces, both conservative and nonconservative, in the open control volume is assumed small. As a consequence of this assumption the gravitational and buoyancy effects are neglected, and $\left(\mathcal{E}^{(g)}\right)_o = \left(\mathcal{E}^{(b)}\right)_o = 0$.
6. Changes in the internal energy $D\left(\mathcal{E}^{(i)}\right)_o / Dt$, which are due entirely to the motion of the fluid, are neglected. As a consequence of the commutative property of the operators $\delta(\cdot)$ and $D(\cdot)/Dt$, this is equivalent to

$$\delta\left(\mathcal{E}^{(i)}\right)_o = \delta\left(\mathcal{E}^{(i)}_{\text{fluid}}\right)_o = \delta \iiint_{R_o(\mathbf{x},t)} \rho e(\rho, T) dv = 0, \tag{5.3}$$

where e is the specific internal energy and $T(\mathbf{x}, t)$ is the thermodynamic temperature field. Note that $e(\rho, T)$ is the so-called caloric equation of state [19].

While the fluid is initially allowed to be compressible, potentially rendering this last assumption invalid, subsequent application of the incompressibility approximation vindicates said assumption.

Finally, the dependence of R_o, B_o, and B_c on $\mathbf{x}$ is omitted from here on since it is understood that these variables refer to the spatial description. The dependencies of ρ and $\mathbf{u}$ on $\mathbf{x}$ and t are also dropped.

5.1.2 Uniform Viscous Flow Past a Stationary Cylinder

Let the control volume be defined as the rectangular volume of unit depth surrounding the stationary cylinder. The origin of the coordinate system is at the center of the cylinder. The part of the control surface that is pervious represents a significant portion of the outer surface defined by the perimeter of the rectangle shown in Fig. 5.1 multiplied by a unit projection out of the plane of said figure. This part is the *open*

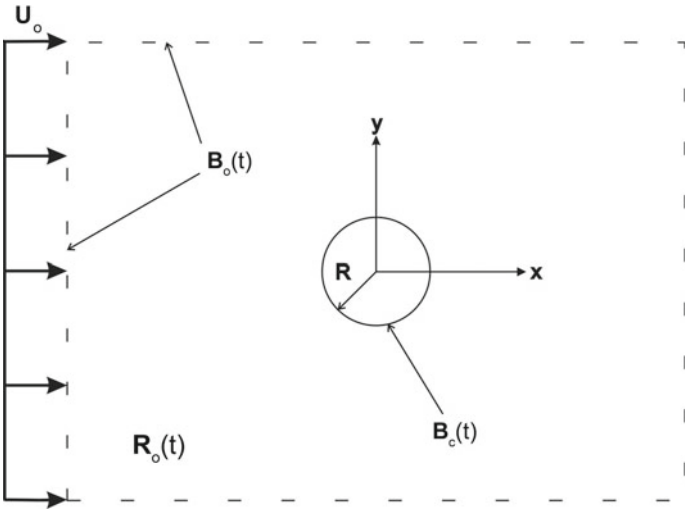

Fig. 5.1 The open control surface $B_o(t)$, the closed control surface $B_c(t)$, and the open control volume $R_o(t)$. Reference is made to the case of uniform flow U_o past a stationary circular cylinder of radius R

control surface $B_o(t)$. The *closed control surface* $B_c(t)$, includes the circumference of the cylinder $x^2 + y^2 = R^2$, and any portions of the outer surface that are closed to fluid motion (i.e., those portions where $\mathbf{u}(\mathbf{x}, t) \parallel \mathbf{n}$).

Note that in this particular problem, the surfaces $B_o(t)$ and $B_c(t)$ are neither functions of time nor space. This obviously means that the open control volume $R_o(t)$ is also independent of time and space. The CV and CS definitions are illustrated in Fig. 5.1. The open control volume, $R_o(t)$, is clearly of constant mass, yet it does not consist of the same set of particles at any two instances. The uniform, steady free stream velocity is $\mathbf{u}_o = U_o \mathbf{e}_1$.

The kinetic energy of the open system is given by

$$(\mathcal{K})_o = (\mathcal{K}_{\text{fluid}})_o = \iiint_{R_o(t)} \frac{1}{2} \rho \, (\mathbf{u} \cdot \mathbf{u}) \, dv, \tag{5.4}$$

where $dv = dv(\mathbf{x}, t)$ is the differential volume element. For the sake of brevity, the functional dependencies of dv and ds are dropped. Clearly, $\left(\mathcal{K}_{\text{cyl}}\right)_o = 0$. Also, $\left(\mathcal{E}^{(s)}\right)_o = 0$ since the cylinder is rigid. From Eq. 5.3, and the additional relations $\left(\mathcal{E}^{(g)}\right)_o = \left(\mathcal{E}^{(b)}\right)_o = 0$, $\delta \left(\mathcal{E}\right)_o = 0$, it follows that

$$\delta \int_{t_1}^{t_2} (\mathcal{L})_o dt = \delta \int_{t_1}^{t_2} (\mathcal{K})_o dt = \delta \int_{t_1}^{t_2} \iiint_{R_o(t)} \frac{1}{2} \rho \, (\mathbf{u} \cdot \mathbf{u}) \, dv dt. \tag{5.5}$$

The virtual work done by the normal and tangential stresses in the fluid during a virtual displacement is given by [9]

$$(\delta W)_o = (\delta W_{\text{fluid}})_o = -\iiint_{R_o(t)} \sigma_{ij}\delta\varepsilon_{ij}dv, \tag{5.6}$$

where σ_{ij} is the natural or Eulerian stress tensor and

$$\delta\varepsilon_{ij} = \frac{1}{2}\left[\frac{\partial\left(\delta r_j\right)}{\partial x_i} + \frac{\partial\left(\delta r_i\right)}{\partial x_j}\right]. \tag{5.7}$$

It is tempting to regard $\delta\varepsilon_{ij}$ as the Lagrangian variation of Cauchy's infinitesimal (linear) strain tensor,

$$\varepsilon_{ij} = \frac{1}{2}\left[\frac{\partial r_i}{\partial x_j} + \frac{\partial r_j}{\partial x_i}\right].$$

However,

$$\delta\varepsilon_{ij} = \frac{1}{2}\left[\delta\left(\frac{\partial r_i}{\partial x_j}\right) + \delta\left(\frac{\partial r_j}{\partial x_i}\right)\right] \neq \frac{1}{2}\left[\frac{\partial\left(\delta r_i\right)}{\partial x_j} + \frac{\partial\left(\delta r_j\right)}{\partial x_i}\right].$$

The balance of angular momentum applied to a differential fluid volume element $dv = dxdy(dz = 1)$ leads to the conclusion that the stress tensor is symmetric, $\sigma_{ij} = \sigma_{ji}$. Using this symmetry property, it can be easily shown that

$$\frac{1}{2}\sigma_{ij}\left[\frac{\partial\left(\delta r_j\right)}{\partial x_i} + \frac{\partial\left(\delta r_i\right)}{\partial x_j}\right] = \sigma_{ij}\left[\frac{\partial\left(\delta r_i\right)}{\partial x_j}\right].$$

As a consequence, Eq. 5.6 becomes

$$(\delta W)_o = -\iiint_{R_o(t)} \sigma_{ij}\left[\frac{\partial\left(\delta r_i\right)}{\partial x_j}\right]dv. \tag{5.8}$$

Using Eqs. 5.5, 5.8 and 5.1 can be written as

$$\delta\int_{t_1}^{t_2}\iiint_{R_o(t)}\frac{1}{2}\rho\left(\mathbf{u}\cdot\mathbf{u}\right)dvdt - \int_{t_1}^{t_2}\iiint_{R_o(t)}\sigma_{ij}\left[\frac{\partial\left(\delta r_i\right)}{\partial x_j}\right]dvdt + \int_{t_1}^{t_2}\iint_{B_o(t)}\rho\left(\mathbf{u}\cdot\delta\mathbf{r}\right)\left(\mathbf{u}\cdot\mathbf{n}\right)dsdt = 0. \tag{5.9}$$

Before proceeding with the development of Eq. 5.9, the components σ_{ij} of the stress tensor $\underline{\sigma}$ that appear in Eq. 5.9, are defined.

5.1.3 The Stress Tensor

It can be shown that the constitutive relation relating the stress tensor $\underline{\sigma}$ to the density field $\rho(\mathbf{x}, t)$, the thermodynamic pressure field $p(\mathbf{x}, t)$, and the velocity gradient tensor $\underline{\mathbf{L}} = [\nabla \mathbf{u}(\mathbf{x}, t)]^{\mathrm{T}}$ in a Newtonian fluid is given by [8]

$$\underline{\sigma} = [-p + \lambda (\nabla \cdot \mathbf{u})] \underline{\mathbf{I}} + \mu \left[(\nabla \mathbf{u}) + (\nabla \mathbf{u})^{\mathrm{T}} \right], \tag{5.10}$$

where $\underline{\mathbf{I}}$ is the identity tensor. The operator ∇ is understood to be a spatial operator. That is $\nabla \equiv \nabla_{\mathbf{x}}$. The thermodynamic pressure field is defined by the equation of state

$$p = p(\rho, T).$$

The Cartesian components of Eq. 5.10 are

$$\sigma_{ij} = -p\delta_{ij} + \lambda \delta_{ij} \frac{\partial u_k}{\partial x_k} + \mu \left(\frac{\partial u_i}{\partial x_j} + \frac{\partial u_j}{\partial x_i} \right). \tag{5.11}$$

The parameters μ and λ are usually referred to as the dynamic viscosity coefficient and the second viscosity coefficient, respectively. From Assumption 3 above, it is possible to make an important simplification: $\mu = \mu(\rho, T)$ and $\lambda = \lambda(\rho, T)$ depend only on the equilibrium properties of ρ and T. Here, the additional simplification is made that μ and λ are effectively constant.

Equation 5.10 follows from the general form

$$\underline{\sigma} = -p\underline{\mathbf{I}} + \mathbf{G}(\nabla \mathbf{u}), \tag{5.12}$$

where $\mathbf{G}$ is a *linear* tensor valued function. $\nabla \mathbf{u}$ can be written as the sum of a symmetric tensor $\underline{\mathbf{D}}$ and a skew-symmetric tensor $\underline{\mathbf{W}}$, which are defined by

$$\underline{\mathbf{D}} = \frac{1}{2} \left[(\nabla \mathbf{u}) + (\nabla \mathbf{u})^{\mathrm{T}} \right]$$
$$\underline{\mathbf{W}} = \frac{1}{2} \left[(\nabla \mathbf{u}) - (\nabla \mathbf{u})^{\mathrm{T}} \right].$$

The tensors $\underline{\mathbf{D}}$ and $\underline{\mathbf{W}}$ are the rate of deformation and spin tensor, respectively.

Using these tensors, Eq. 5.12 can then be written as

$$\underline{\sigma} = -p\underline{\mathbf{I}} + \mathbf{G}\left(\underline{\mathbf{D}} + \underline{\mathbf{W}}\right).$$

In a rigid body rotation of the fluid, there can be no shear stresses since there is no shearing action. The shear stresses are represented entirely by the components of tensor $\underline{\mathbf{W}}$. Since these components are nonzero for a rigid body rotation, it is clear that $\underline{\sigma}$ must be independent of $\underline{\mathbf{W}}$. Assuming the fluid is isotropic, then $\mathbf{G}\left(\underline{\mathbf{D}}\right)$ can be written as [19]

$$\mathbf{G}\left(\underline{\mathbf{D}}\right) = \lambda\left(\mathrm{tr}\underline{\mathbf{D}}\right)\underline{\mathbf{I}} + 2\mu\underline{\mathbf{D}},$$

where tr$\underline{\mathbf{D}}$ is the trace of $\underline{\mathbf{D}}$.

The stress tensor can now be expressed as

$$\underline{\sigma} = -p\underline{\mathbf{I}} + \lambda\left(\mathrm{tr}\underline{\mathbf{D}}\right)\underline{\mathbf{I}} + 2\mu\underline{\mathbf{D}}. \tag{5.13}$$

The variation of the first term of Eq. 5.9, representing the variation of the total fluid kinetic energy in the open control volume, is intimately related to variational form of the integral or global mass balance law, discussed next.

5.1.4 The Global Mass Balance Law

Regarding the mass balance law, McIver [20] states that the necessary condition in integral form becomes

$$\delta \iiint_{R_o(t)} \rho\,(\cdot)\,dv = \iiint_{R_o(t)} \rho\delta\,(\cdot)\,dv, \tag{5.14}$$

where $(\cdot)$ is an arbitrary function of $\mathbf{x}$ and t. The origin of Eq. 5.14 lies in the statement of global mass balance for mass system M, which occupies the volume $R_M(t)$ at time t. In variational form, this is given by [28]:

$$\delta \iiint_{R_M(t)} \rho\,(\cdot)\,dv = \iiint_{R_M(t)} \rho\delta\,(\cdot)\,dv. \tag{5.15}$$

Recall that system M is closed. That is, it consists always of the same collection of particles and there is no mass transport through its surface. Its bounding surface, $B_M(t)$ moves with translational velocity $N = u_i n_i$, which is the same as the local fluid velocity.

McIver [20] argues that as far as the operator δ is concerned, Eqs. 5.14 and 5.15 are equivalent at the instant when $R_M(t)$ and $R_o(t)$ coincide. He describes this correspondence:

> The control volume, open or closed, is always a closed system as far as the variation is concerned regardless of whether or not material is transported across its boundaries in the real motion: there is no virtual material transport out of the system.

The continuity equation

$$\frac{D\rho}{Dt} + \rho\left(\frac{\partial u_k}{\partial x_k}\right) = \frac{\partial \rho}{\partial t} + \frac{\partial\left(\rho u_k\right)}{\partial x_k} = 0, \tag{5.16}$$

representing the local mass conservation law, is in fact a necessary condition for Eq. 5.15.

5.1.5 The Kinetic Energy

The third term in Eq. 5.5 can be written as

$$\delta \int_{t_1}^{t_2} \iiint_{R_o(t)} \rho \left(\mathbf{u} \cdot \mathbf{u}\right) dvdt = \int_{t_1}^{t_2} \iiint_{R_o(t)} \rho \left(\mathbf{u} \cdot \delta\mathbf{u}\right) dvdt$$
$$= \int_{t_1}^{t_2} \iiint_{R_o(t)} \rho \left[\mathbf{u} \cdot \delta\left(\frac{D\mathbf{r}}{Dt}\right)\right] dvdt. \tag{5.17}$$

Using the fact that the variation denoted by the operator $\delta(\cdot)$ and the rate of change denoted by $D(\cdot)/Dt$ are both material variations and are consequently interchangeable, Eq. 5.17 can be written as

$$\int_{t_1}^{t_2} \iiint_{R_o(t)} \rho \left[\mathbf{u} \cdot \delta\left(\frac{D\mathbf{r}}{Dt}\right)\right] dvdt = \int_{t_1}^{t_2} \iiint_{R_o(t)} \rho \left[\mathbf{u} \cdot \frac{D\left(\delta\mathbf{r}\right)}{Dt}\right] dvdt. \tag{5.18}$$

Consider next the following result from Dost and Tabarrok [9]

$$\int_{t_1}^{t_2} \frac{D}{Dt}\left[\iiint_{R_o(t)} \rho \left(\mathbf{u} \cdot \delta\mathbf{r}\right) dv\right] dt = \int_{t_1}^{t_2} \iiint_{R_o(t)} \rho \left[\mathbf{u} \cdot \frac{D\left(\delta\mathbf{r}\right)}{Dt}\right] dvdt$$
$$+ \int_{t_1}^{t_2} \iiint_{R_o(t)} \left(\frac{D\rho}{Dt} + \rho\nabla \cdot \mathbf{u}\right) dvdt$$
$$+ \int_{t_1}^{t_2} \iiint_{R_o(t)} \rho \left(\frac{D\mathbf{u}}{Dt} \cdot \delta\mathbf{r}\right) dvdt.$$

On account of the continuity equation, Eq. 5.16, the second integral on the right-hand side vanishes, and then

$$\int_{t_1}^{t_2} \frac{D}{Dt}\left[\iiint_{R_o(t)} \rho \left(\mathbf{u} \cdot \delta\mathbf{r}\right) dv\right] dt = \int_{t_1}^{t_2} \iiint_{R_o(t)} \rho \left[\mathbf{u} \cdot \frac{D\left(\delta\mathbf{r}\right)}{Dt}\right] dvdt$$
$$+ \int_{t_1}^{t_2} \iiint_{R_o(t)} \rho \left(\frac{D\mathbf{u}}{Dt} \cdot \delta\mathbf{r}\right) dvdt.$$

Substituting

$$\int_{t_1}^{t_2} \iiint_{R_o(t)} \rho \left[\mathbf{u} \cdot \frac{D\left(\delta\mathbf{r}\right)}{Dt}\right] dvdt = \int_{t_1}^{t_2} \frac{D}{Dt}\left[\iiint_{R_o(t)} \rho \left(\mathbf{u} \cdot \delta\mathbf{r}\right) dv\right] dt$$
$$- \int_{t_1}^{t_2} \iiint_{R_o(t)} \rho \left(\frac{D\mathbf{u}}{Dt} \cdot \delta\mathbf{r}\right) dvdt$$

in Eq. 5.17 leads to

$$\int_{t_1}^{t_2} \iiint_{R_o(t)} \rho \left[\mathbf{u} \cdot \delta \left(\frac{D\mathbf{r}}{Dt} \right) \right] dvdt = \int_{t_1}^{t_2} \frac{D}{Dt} \left[\iiint_{R_o(t)} \rho \left(\mathbf{u} \cdot \delta \mathbf{r} \right) dv \right] dt - \int_{t_1}^{t_2} \iiint_{R_o(t)} \rho \left(\frac{D\mathbf{u}}{Dt} \cdot \delta \mathbf{r} \right) dvdt. \tag{5.19}$$

Integrating the first term of Eq. 5.19 gives

$$\left[\iiint_{R_o(t)} \rho \left(\mathbf{u} \cdot \delta \mathbf{r} \right) dv \right]_{t_1}^{t_2},$$

which vanishes on account of the constraint $\delta \mathbf{r}(t_1) = \delta \mathbf{r}(t_2) = \mathbf{0}$. Equation 5.19 is then simply

$$\delta \int_{t_1}^{t_2} \iiint_{R_o(t)} \rho \left(\mathbf{u} \cdot \mathbf{u} \right) dvdt = \int_{t_1}^{t_2} \iiint_{R_o(t)} \rho \left[\mathbf{u} \cdot \delta \left(\frac{D\mathbf{r}}{Dt} \right) \right] dvdt = - \int_{t_1}^{t_2} \iiint_{R_o(t)} \rho \left(\frac{D\mathbf{u}}{Dt} \cdot \delta \mathbf{r} \right) dvdt. \tag{5.20}$$

Substituting Eq. 5.20 in Eq. 5.9 yields

$$- \int_{t_1}^{t_2} \iiint_{R_o(t)} \rho \left(\frac{D\mathbf{u}}{Dt} \cdot \delta \mathbf{r} \right) dvdt - \int_{t_1}^{t_2} \iiint_{R_o(t)} \sigma_{ij} \left[\frac{\partial \left(\delta r_i \right)}{\partial x_j} \right] dvdt + \int_{t_1}^{t_2} \iint_{B_o(t)} \rho \left(\mathbf{u} \cdot \delta \mathbf{r} \right) \left(\mathbf{u} \cdot \mathbf{n} \right) dsdt = 0. \tag{5.21}$$

5.1.6 Virtual Work

Having obtained the variation of the kinetic energy of the fluid, which in the present case represents the Lagrangian of the open system, attention is now focused on the virtual work. The second term of Eq. 5.21 can be expressed in the equivalent form

$$\int_{t_1}^{t_2} \iiint_{R_o(t)} \sigma_{ij} \left[\frac{\partial \left(\delta r_i \right)}{\partial x_j} \right] dvdt = \int_{t_1}^{t_2} \iiint_{R_o(t)} \left[\frac{\partial \left(\sigma_{ij} \delta r_i \right)}{\partial x_j} - \frac{\partial \sigma_{ij}}{\partial x_j} \delta r_i \right] dvdt. \tag{5.22}$$

The divergence theorem is used to transform the first term inside the integral.

The divergence theorem for a (sufficiently well-behaved) vector field $\mathbf{w}$ is given in Cartesian form by

$$\iint_{B(t)} w_i n_i ds = \iiint_{R_o(t)} \frac{\partial w_i}{\partial x_i} dv, \tag{5.23}$$

where $B(t)$ is the bounding surface of region $R_o(t)$.

Applying Eq. 5.23 with $\mathbf{w} = \underline{\sigma}^T \delta\mathbf{r}$, i.e., $w_i = \sigma_{ij}\delta r_i$, the following form of Eq. 5.22 is obtained:

$$\begin{aligned} &\int_{t_1}^{t_2} \iiint_{R_o(t)} \left[\frac{\partial \left(\sigma_{ij}\delta r_i\right)}{\partial x_j} - \frac{\partial \sigma_{ij}}{\partial x_j}\delta r_i \right] dvdt \\ &= \int_{t_1}^{t_2} \iint_{B(t)} \sigma_{ij} n_j \delta r_i ds dt - \int_{t_1}^{t_2} \iiint_{R_o(t)} \left[\frac{\partial \sigma_{ij}}{\partial x_j}\delta r_i \right] dvdt. \end{aligned} \tag{5.24}$$

Using Eqs. 5.24 and 5.21 becomes

$$\begin{aligned} &-\int_{t_1}^{t_2} \iiint_{R_o(t)} \rho \left(\frac{D\mathbf{u}}{Dt} \cdot \delta\mathbf{r} \right) dvdt \\ &+\int_{t_1}^{t_2} \iiint_{R_o(t)} \left[\frac{\partial \sigma_{ij}}{\partial x_j}\delta r_i \right] dvdt \\ &-\int_{t_1}^{t_2} \iint_{B(t)} \sigma_{ij} n_j \delta r_i ds dt \\ &+\int_{t_1}^{t_2} \iint_{B_o(t)} \rho \left(\mathbf{u}\cdot\delta\mathbf{r}\right)\left(\mathbf{u}\cdot\mathbf{n}\right) ds dt = 0, \end{aligned} \tag{5.25}$$

where $B(t) = B_o(t) \cup B_c(t)$ and $\mathbf{n}$ is the outward normal. Note that $\mathbf{n}$ points *into* the cylinder on surface $B_c(t)$. It must be emphasized that in using the divergence theorem to convert Eq. 5.22 to Eq. 5.24, a subtlety arises. The domain $R_o(t)$ is actually doubly connected.

5.1.6.1 The Doubly Connected Domain

In fact, the region occupied by the fluid in a 2D flow field due to *any* moving body is necessarily doubly connected [2]. A problem arises in the direct application of the divergence theorem. However, this problem is easily dealt with by defining the bounding surface of $R_o(t)$ to be $B^*(t) = B_o(t) \cup B_c(t) \cup B_u(t)$, where $B_u(t)$ is the surface of the umbilicus (branch cut) which joins the exterior surface $B_o(t)$ to the body surface $B_c(t)$. This is illustrated in Fig. 5.2. It can be shown that integration of $\underline{\sigma}\mathbf{n}$ over the umbilicus does not contribute to the total surface integral [21]. Thus, $B^*(t)$ may be effectively taken as equal to $B(t)$.

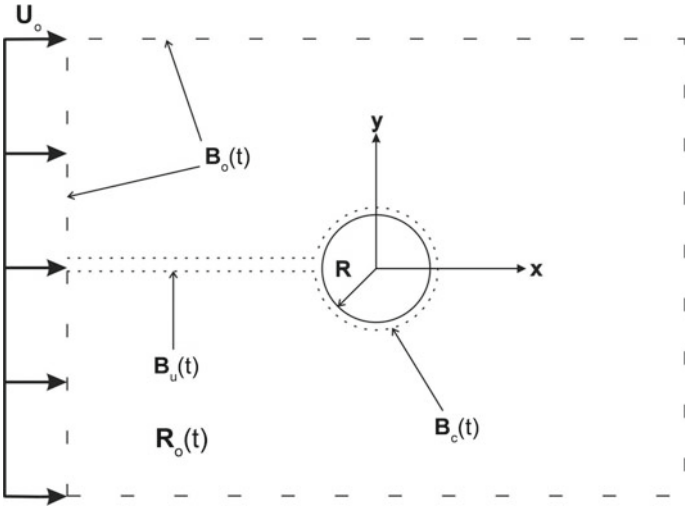

Fig. 5.2 The open control surface $B_o(t)$, closed control surface $B_c(t)$, the umbilicus $B_u(t)$, and the open control volume $R_o(t)$. Reference is made to the case of uniform flow U_o past a stationary circular cylinder of radius R

5.1.7 The Euler–Lagrange Equations and the Natural Boundary Conditions

Collecting like terms in Eq. 5.25 gives

$$\int_{t_1}^{t_2} \iiint_{R_o(t)} \left[-\rho \frac{Du_i}{Dt} + \frac{\partial \sigma_{ij}}{\partial x_j} \right] \delta r_i dv dt - \int_{t_1}^{t_2} \iint_{B_c(t)} \sigma_{ij} n_j \delta r_i ds dt - \int_{t_1}^{t_2} \iint_{B_o(t)} \left[\sigma_{ij} n_j - \rho u_i u_j n_j \right] \delta r_i dv dt = 0.$$

Arguing in the usual way that the variations δr_i are arbitrary in $R_o(t) \times [t_1, t_2]$ leads to the Euler–Lagrange (EL) equation

$$\rho \frac{Du_i}{Dt} = \frac{\partial \left(\sigma_{ij} \right)}{\partial x_j} \text{ in } R_o(t). \tag{5.26}$$

A similar argument regarding the variations δr_i on $B_o(t) \times [t_1, t_2]$ and $B_c(t) \times [t_1, t_2]$ leads to the natural boundary conditions

$$\sigma_{ij} n_j \delta r_i = 0 \text{ on } B_c(t) \tag{5.27}$$

$$\left[\sigma_{ij}n_j - \rho u_i u_j n_j\right]\delta r_i = 0 \text{ on } B_o(t). \tag{5.28}$$

Substituting Eq. 5.11 into Eq. 5.26 yields the components of the balance of linear momentum equation for a Newtonian viscous compressible fluid with constant viscosity coefficients:

$$\rho\frac{Du_i}{Dt} = -\frac{\partial p}{\partial x_i} + \lambda\left(\frac{\partial^2 u_j}{\partial x_i \partial x_j}\right) + \mu\left[\frac{\partial}{\partial x_j}\left(\frac{\partial u_i}{\partial x_j} + \frac{\partial u_j}{\partial x_i}\right)\right] \text{ in } R_o(t). \tag{5.29}$$

The next step is to use Stokes' condition, $\lambda = -2\mu/3$. Stokes' condition is equivalent to the assumption that the thermodynamic pressure and the mechanical pressure are the same for a compressible fluid.

To see this, consider the difference between the thermodynamic pressure p and the mean mechanical pressure $\bar{p}_m$ [19],

$$p - \bar{p}_m = -\left(\lambda + \frac{2}{3}\mu\right)\frac{\partial u_k}{\partial x_k} = -\left(\lambda + \frac{2}{3}\mu\right)\frac{1}{\rho}\frac{D\rho}{Dt}, \tag{5.30}$$

where the last equality follows from the continuity equation, Eq. 5.16. In Eq. 5.29, the mean mechanical pressure is defined as

$$\bar{p}_m = -\frac{1}{3}\sigma_{ii}.$$

In a fluid at rest the stress is purely hydrostatic, $\sigma_{ij} = -\bar{p}_m\delta_{ij}$, and consequently $\bar{p}_m = p$.

Since $D\rho/Dt \neq 0$ for a compressible fluid, the thermodynamic and mechanical pressures can only be the same if the coefficient is equal to zero, $\left(\lambda + \frac{2}{3}\mu\right) = 0$. The quantity $\left(\lambda + \frac{2}{3}\mu\right) = \mu_B$ is usually referred to as the bulk viscosity. The vanishing of the bulk viscosity has an interesting interpretation: The dissipation power per unit volume is due entirely to shape-change rate of deformation. The volume change or dilatational dissipation is zero [19]. It can be shown that in order to satisfy the Clausius–Duhem entropy inequality, $\mu \geq 0$ and $(\lambda + 2\mu/3) \geq 0$.

Using Stokes' condition, Eq. 5.29 becomes

$$\rho\frac{Du_i}{Dt} = -\frac{\partial p_m}{\partial x_i} - \frac{2\mu}{3}\left(\frac{\partial^2 u_j}{\partial x_i \partial x_j}\right) + \mu\left[\frac{\partial}{\partial x_j}\left(\frac{\partial u_i}{\partial x_j} + \frac{\partial u_j}{\partial x_i}\right)\right] \text{ in } R_o(t). \tag{5.31}$$

Expanding the last term of Eq. 5.31 and combining with the second gives

$$\rho\frac{Du_i}{Dt} = -\frac{\partial p_m}{\partial x_i} + \mu\left(\frac{\partial^2 u_k}{\partial x_k^2}\right) + \frac{1}{3}\mu\left[\frac{\partial}{\partial x_i}\left(\frac{\partial u_k}{\partial x_k}\right)\right] \text{ in } R_o(t). \tag{5.32}$$

In summary, Eq. 5.32 gives the components of the Navier–Stokes (N-S) equation for a compressible fluid with zero bulk viscosity. Similarly, Eq. 5.31 gives the components of the generalized N-S equation for a compressible fluid with nonzero bulk viscosity.

5.1.8 The Application to an Incompressible Fluid

An incompressible fluid is one in which the density of each material element is unaffected by changes in pressure. This definition holds provided that density changes in the fluid as a result of molecular conduction of heat are negligible [2]. In an incompressible fluid, the mean mechanical pressure is equal to the thermodynamic pressure at all times. This result follows directly from Eq. 5.30, since the rate of change of ρ following a material element is zero, $D\rho/Dt = 0$. The simplified continuity equation,

$$\frac{\partial u_k}{\partial x_k} = 0, \tag{5.33}$$

when used to simplify Eq. 5.32, leads to

$$\rho\left(\frac{\partial u_i}{\partial t} + u_j\frac{\partial u_i}{\partial x_j}\right) = -\frac{\partial p}{\partial x_i} + \mu\frac{\partial^2 u_i}{\partial x_j^2} \text{ in } R_o(t). \tag{5.34}$$

Note that in Eq. 5.34, the material derivative Du_i/Dt has been expanded. Equation 5.34 represents the components of the Navier–Stokes equation for viscous incompressible flows.

For convenience, let the stress tensor for an incompressible Newtonian fluid be denoted $\underline{\hat{\sigma}}$. Using the continuity equation, Eq. 5.33, to simplify the constitutive relation, Eq. 5.11, the components of $\underline{\hat{\sigma}}$ are given by

$$\hat{\sigma}_{ij} = -p\delta_{ij} + \mu\left(\frac{\partial u_i}{\partial x_j} + \frac{\partial u_j}{\partial x_i}\right). \tag{5.35}$$

The natural boundary condition manifested in Eq. 5.27 is interpreted as $\delta r_i = 0$ on $B_c(t)$ since the displacement $r_i = 0$ is prescribed on the cylinder surface. However, there is no local equilibrium on the cylinder surface $\hat{\sigma}_{ij}n_j \neq 0$. The natural boundary condition manifested in Eq. 5.28 is interpreted as $\left[\hat{\sigma}_{ij}n_j - \rho u_i u_j n_j\right] = 0$ on $B_o(t)$ since the displacement δr_i is not prescribed anywhere on this surface. Physically, this last boundary condition states that convective flux of momentum (per unit area as ds shrinks to a point) $\rho u_i u_j n_j$ at any point on $B_o(t)$ is equal to the resultant contact force $t_i = \hat{\sigma}_{ij}n_j$ exerted at that boundary point by the surrounding matter.

5.1.9 An Examination of the Boundary Condition Manifested by Eq. 5.28

To better understand the meaning of this last boundary condition, consider the balance of momentum in integral form for an incompressible fluid:

$$\iiint_{R_o(t)} \frac{\partial(\rho u_i)}{\partial t} dv = -\iint_{B(t)} \rho u_i u_j n_j ds + \iint_{B(t)} \hat{\sigma}_{ij} n_j ds. \tag{5.36}$$

Equation 5.28 implies that

$$\iint_{B_o(t)} \left[\hat{\sigma}_{ij} n_j - \rho u_i u_j n_j\right] ds = 0.$$

Consequently, Eq. 5.36 becomes

$$\iiint_{R_o(t)} \frac{\partial(\rho u_i)}{\partial t} dv = -\iint_{B_c(t)} \rho u_i u_j n_j ds + \iint_{B_c(t)} \hat{\sigma}_{ij} n_j ds. \tag{5.37}$$

Now for a stationary rigid cylinder, $u_1 = u_2 = 0$ and the first integral on the RHS vanishes. This integral also vanishes for a rigid cylinder in motion since the velocity components u_i on the surface of the cylinder are independent of position along the circumference cylinder (along each point on this path they must equal the velocity components V_i of the body) and

$$\iint_{B_c(t)} \mathbf{n} ds = \mathbf{0}.$$

Equation 5.37 becomes

$$\iiint_{R_o(t)} \frac{\partial(\rho u_i)}{\partial t} dv = \iint_{B_c(t)} \hat{\sigma}_{ij} n_j ds.$$

This result can be interpreted as follows: The rate of change of momentum inside the chosen control volume is due entirely to the resultant force system at the boundary of the cylinder! The validity of this result is in general only for infinite domains $R_\infty(t)$ enclosing all of the vorticity. The surface integrals of the viscous and convective terms must also vanish at infinity.

Under these conditions, it can be shown [21] that the balance of momentum equation, Eq. 5.37, reduces to a form that does not include contributions from the outer boundary at infinity. This is because a boundary term arises upon the conversion of the left-hand-side (LHS) of Eq. 5.36 to a vorticity impulse-type term which cancels out the nonzero pressure term on the distant boundary, $-\iint_{B_\infty(t)} p n_j ds$. Since it is assumed that $B_o(t)$ is sufficiently far away from the cylinder such that the above conditions are satisfied, the boundary condition on $B_o(t)$ obtained above is valid.

This completes the derivation of the relevant field equations and boundary conditions for the flow of a viscous incompressible fluid past a stationary cylinder. The starting point of the derivation was Hamilton's principle for a system of variable mass. In the next section, the cylinder is allowed to move freely in the direction transverse to the flow. The cylinder responds to the vortex-shedding, which

generates unsteady forces on the cylinder. When the frequency of the vortex shedding f_{vs} matches the cylinder oscillation frequency f_{ex}, synchronization takes place and the cylinder can undergo large oscillations. A more detailed discussion on vortex-induced vibration of circular cylinders can be found in various recent review papers, including [12, 22, 27].

5.2 Uniform 2D Viscous Flow Past a Cylinder Free to Move Transversely

Consider an elastically mounted cylinder, with a mechanical restraint preventing motion in the flow direction (x). Since the cylinder is rigid, its motion in the transverse direction (y) can be described by a single generalized coordinate. Let this generalized coordinate be represented by χ. Assuming a perfect correlation of the shedding vortices, the transverse displacement of all points on the cylinder is the same: $\chi = \chi(t)$. The horizontal plane passing through the cylinder's center of mass is chosen as the reference plane and all dynamic variables (i.e., displacement, velocity, acceleration) are thus defined at the center of mass. The total stiffness of the supporting springs is $k_s^{(\chi)}$. The mass of the cylinder is m_c.

The goal here is to obtain the equations of motion for both the cylinder and the fluid in the CV. It is obvious that the equations of motion must be coupled. The motion of the cylinder must have an effect on the fluid flowing around it and vice versa.

Again, let the CV be defined as the rectangular volume surrounding the nonstationary cylinder. The origin of the coordinate system is at the center of the cylinder when the cylinder is at rest. The coordinate system does *not* move with the cylinder and is considered to be at rest relative to the free stream. As in Sect. 5.1.2, the open part of the CS, $B_o(t)$, is the perimeter of the rectangle shown in Fig. 5.3 multiplied by a unit projection out of the plane of the paper.

While $B_o(t)$ is again independent of time, the closed part $B_c(t)$, defined as the circumference of the cylinder $x^2 + (y \pm \chi(t))^2 = R^2$, is clearly a function of time. The open control volume $R_o(t)$ is also a function of time since its shape, though not its volume, is changing as the cylinder moves. The CV and CS definitions are illustrated in Fig. 5.3. The uniform free stream velocity is again denoted U_o. The presentation in this section highlights the derivation of the structural equation of motion and the corresponding boundary conditions on $B_c(t)$. Derivations involving the fluid field, which are identical to those presented of Sect. 5.1.2, are simply presented in final form.

In this problem, $(\mathcal{K})_o = \left(\mathcal{K}_{\text{fluid}} + \mathcal{K}_{\text{cyl}}\right)_o$ and $(\mathcal{E})_o = \left(\mathcal{E}_{\text{cyl}}^{(s)}\right)_o$, with $(\mathcal{K}_{\text{fluid}})_o$ given by Eq. 5.4,

$$\left(\mathcal{K}_{\text{cyl}}\right)_o = \frac{1}{2} m_c \dot{\chi}^2,$$

and

$$\left(\mathcal{E}_{\text{cyl}}^{(s)}\right)_o = \frac{1}{2} k_s^{(\chi)} \chi^2.$$

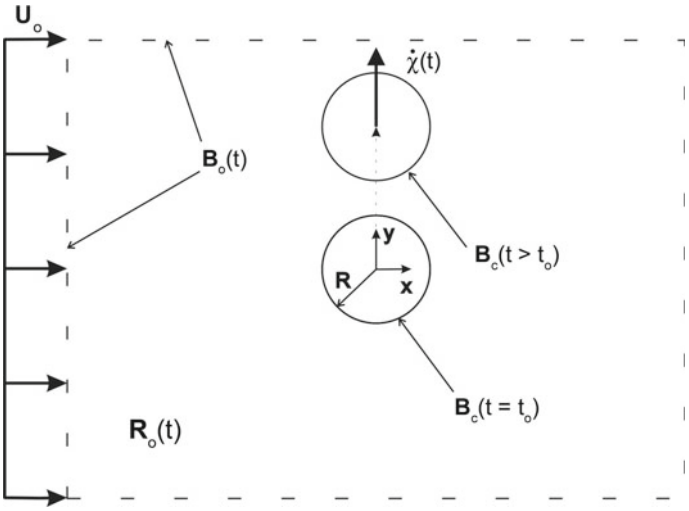

Fig. 5.3 The open control surface $B_o(t)$, closed control surface $B_c(t)$ (at two different instances), and the open control volume $R_o(t)$ for the case of a rigid circular cylinder of radius R with 1 DOF. The cylinder is free to move transversely to the uniform incoming flow of velocity U_o. The transverse generalized coordinate is $\chi(t)$. The restraining springs are not shown

It follows that

$$(\mathcal{L})_o = \iiint_{R_o(t)} \frac{1}{2}\rho\,(\mathbf{u}\cdot\mathbf{u})\,dv + \frac{1}{2}m_c\dot{\chi}^2 - \frac{1}{2}k_s^{(\chi)}\chi^2. \tag{5.38}$$

Using Eqs. 5.38, 5.1 becomes

$$\begin{aligned}&\delta\int_{t_1}^{t_2}\iiint_{R_o(t)}\frac{1}{2}\rho\,(\mathbf{u}\cdot\mathbf{u})\,dvdt + \delta\int_{t_1}^{t_2}\frac{1}{2}m_c\dot{\chi}^2dt - \delta\int_{t_1}^{t_2}\frac{1}{2}k_s^{(y)}\chi^2dt\\ &-\int_{t_1}^{t_2}\iiint_{R_o(t)}\sigma_{ij}\delta\varepsilon_{ij}dvdt + \int_{t_1}^{t_2}\iint_{B_o(t)}\rho\,(\mathbf{u}\cdot\delta\mathbf{r})\,(\mathbf{u}\cdot\mathbf{n})\,dsdt = 0.\end{aligned} \tag{5.39}$$

The variation of the first term of Eq. 5.39 is obtained directly from Eq. 5.20. The variation of the second and third terms are

$$\begin{aligned}\delta\left(\mathcal{K}_{\text{cyl}}\right)_o &= m_c\dot{\chi}\delta\dot{\chi}\\ \delta\left(\mathcal{E}_{\text{cyl}}^{(s)}\right)_o &= k_s^{(\chi)}\chi\delta\chi,\end{aligned}$$

respectively. Integration by parts, with $\delta\mathbf{r}(t_1) = \delta\mathbf{r}(t_2) = \mathbf{0}$ and $\delta\chi(t_1) = \delta\chi(t_2) = 0$, yields

$$
\begin{aligned}
&- \int_{t_1}^{t_2} \iiint_{R_o(t)} \rho \left(\frac{Du_i}{Dt} \delta r_i \right) dv dt - \int_{t_1}^{t_2} m_c \ddot{\chi} \delta \chi dt \\
&- \int_{t_1}^{t_2} k_s^{(y)} \chi \delta \chi dt + \int_{t_1}^{t_2} \iiint_{R_o(t)} \left[\frac{\partial \sigma_{ij}}{\partial x_j} \delta r_i \right] dv dt \\
&- \int_{t_1}^{t_2} \iint_{B_o(t)} \sigma_{ij} n_j \delta r_i ds dt - \int_{t_1}^{t_2} \iint_{B_c(t)} \sigma_{ij} n_j \delta r_i ds dt \\
&\qquad + \int_{t_1}^{t_2} \iint_{B_o(t)} \rho u_i \delta r_i u_j n_j ds dt = 0. \qquad (5.40)
\end{aligned}
$$

In arriving at Eqs. 5.40, 5.20 and 5.24 are used.

Collecting like terms yields

$$
\begin{aligned}
&- \int_{t_1}^{t_2} \iiint_{R_o(t)} \left[\rho \frac{Du_i}{Dt} - \frac{\partial \sigma_{ij}}{\partial x_j} \right] \delta r_i dv dt - \int_{t_1}^{t_2} \left(m_c \ddot{\chi} + k_s^{(\chi)} \chi \right) \delta \chi dt \\
&+ \int_{t_1}^{t_2} \iint_{B_o(t)} \left[\rho u_i u_j n_j - \sigma_{ij} n_j \right] \delta r_i ds dt - \int_{t_1}^{t_2} \iint_{B_c(t)} \sigma_{ij} n_j \delta r_i ds dt = 0. \qquad (5.41)
\end{aligned}
$$

The no-slip condition on the surface of the cylinder, together with the kinematic boundary condition ensuring that the normal components of the velocity are conserved across the fluid–structure interface, which is the no-through flow condition in the case of a solid boundary, require that $\mathbf{u} = \mathbf{V} \cdot \mathbf{V} = (0, \dot{\chi})$ is the velocity vector of the cylinder. This condition implies that $\delta r_1 = 0$ and $\delta r_2 = \chi$ on $B_c(t)$ at all times t. Furthermore, these virtual displacements hold on all points on the cylinder. The last term in Eq. 5.41 can then be written as

$$
\int_{t_1}^{t_2} \iint_{B_c(t)} \sigma_{ij} n_j \delta r_i ds dt = \int_{t_1}^{t_2} \delta \chi \left(\iint_{B_c(t)} \sigma_{2j} n_j ds \right) dt.
$$

It follows that Eq. 5.41 can be rewritten as

$$
\begin{aligned}
&- \int_{t_1}^{t_2} \iiint_{R_o(t)} \left[\rho \frac{Du_i}{Dt} - \frac{\partial \sigma_{ij}}{\partial x_j} \right] \delta r_i dv dt \\
&- \int_{t_1}^{t_2} \left(m_c \ddot{\chi} + k_s^{(y)} \chi + \iint_{B_c(t)} \sigma_{2j} n_j ds \right) \delta \chi dt \\
&+ \int_{t_1}^{t_2} \iint_{B_o(t)} \left[\rho u_i u_j n_j - \sigma_{ij} n_j \right] \delta r_i ds dt = 0.
\end{aligned}
$$

The arbitrariness of the variations δr_i in $R_o(t) \times [t_1, t_2]$ leads to the Euler–Lagrange equations for the fluid,

$$
\rho \frac{Du_i}{Dt} = \frac{\partial \sigma_{ij}}{\partial x_j} \text{ in } R_o(t). \qquad (5.42)
$$

Likewise, the variations $\delta\chi$ are arbitrary $\forall\, \mathbf{x} \in x^2 + (y \pm \chi)^2 \leq R^2$ and for all times $[t_1, t_2]$, and this argument leads to the equation of motion of the cylinder,

$$m_c\ddot{\chi} + k_s^{(\chi)}\chi = -\iint_{B_c(t)} \sigma_{2j} n_j ds. \tag{5.43}$$

A similar argument regarding the variations δr_i on $B_o(t) \times [t_1, t_2]$ leads to the natural boundary condition

$$\left[\sigma_{ij} n_j - \rho u_i u_j n_j\right] \delta r_i = 0 \text{ on } B_o(t). \tag{5.44}$$

The assumption of incompressibility and the corresponding constitutive relation, Eq. 5.35, lead to the following form of Eq. 5.42:

$$\rho\left(\frac{\partial u_i}{\partial t} + u_j \frac{\partial u_i}{\partial x_j}\right) = -\frac{\partial p}{\partial x_i} + \mu \frac{\partial^2 u_i}{\partial x_j x_j} \text{ in } R_o(t). \tag{5.45}$$

Equation 5.45 must be solved in conjunction with Eq. 5.43, the continuity equation, and the boundary condition manifested in Eq. 5.44 (with $\sigma_{ij} \rightarrow \hat{\sigma}_{ij}$). This boundary condition is interpreted as $\left[\hat{\sigma}_{ij} n_j - \rho u_i u_j n_j\right] = 0$ since the fluid displacements are not prescribed on $B_o(t)$. The fluid drives the cylinder with a force

$$F_2(t) = -\iint_{B_c(t)} \hat{\sigma}_{2j} n_j ds.$$

5.3 Applications to Reduced-Order Modeling

Consider Eq. 5.39 with an additional term representing the work done by the structural damping force (i.e., that which changes vibrational energy into heat):

$$\overbrace{\delta \int_{t_1}^{t_2} \iiint_{R_o(t)} \frac{1}{2}\rho\,(\mathbf{u}\cdot\mathbf{u})\, dvdt}^{\mathbf{1}} + \delta \int_{t_1}^{t_2} \frac{1}{2} m_c \dot{\chi}^2 dt - \delta \int_{t_1}^{t_2} \frac{1}{2} k_s^{(y)} \chi^2 dt - \int_{t_1}^{t_2} c^{(vac)} \dot{\chi}\delta\chi dt$$
$$- \overbrace{\int_{t_1}^{t_2} \iiint_{R_o(t)} \hat{\sigma}_{ij} \left[\frac{\partial\,(\delta r_i)}{\partial x_j}\right] dvdt}^{\mathbf{2}} + \overbrace{\int_{t_1}^{t_2} \iint_{B_o(t)} \rho\,(\mathbf{u}\cdot\delta\mathbf{r})\,(\mathbf{u}\cdot\mathbf{n})\, dsdt}^{\mathbf{3}} = 0. \tag{5.46}$$

$c^{(vac)} > 0$ is the linear material damping coefficient measured in vacuo. The structural damping force is always opposed to the velocity, such that the nonconservative virtual work, $\left(\delta W_{\text{cyl}}\right)_o = c^{(vac)}\dot{\chi}\delta\chi$, is always negative for positive $\dot{\chi}$.

In order to reduce the complexity of Eq. 5.46, the control volume $R_o(t)$ is first reduced to a small rectangular region R^{**} incorporating the formation region. The negative damping condition initiating the cylinder motion, as well as the periodic

wake feeding the growing amplitudes of the cylinder, are generated in the formation region. The existence of a temporal global wake instability in the formation region allows a second, more crucial simplification to be made: The flow in R^{**} is assumed to be represented by the representative mass m_{fl} whose transverse displacement is $w(t)$. All spatial dependencies are lost.

It emphasized that while $\dot{w}(t)$ and $\dot{\chi}(t)$ ($\ddot{w}(t)$ and $\ddot{\chi}(t)$) are both transverse velocities (accelerations), they need not always have the same sign at any one instant. It is therefore important to address *relative* velocities (accelerations).

Term "1" of Eq. 5.46 is reduced to

$$\delta \int_{t_1}^{t_2} \iiint_{R_o(t)} \frac{1}{2}\rho\,(\mathbf{u}\cdot\mathbf{u})\,dvdt \Longrightarrow \int_{t_1}^{t_2} \hat{a}_0 m_{fl}\dot{w}\delta\dot{w}dt, \tag{5.47}$$

where $\hat{a}_0$ is a dimensionless constant. Term "2" can likewise be reduced. Term "3" is eliminated because the energy fed through the vertical face fore (upstream) of the cylinder only *indirectly* contributes to near-wake dynamics by providing the energy for the development of the wake flow. The face aft (downstream) of the cylinder is no longer involved in the near-wake mechanics.

Suppose the following separation is made:

$$-\int_{t_1}^{t_2} \hat{\sigma}_{ij}\left[\frac{\partial\,(\delta r_i)}{\partial x_j}\right]dvdt \;\Longrightarrow\; -\int_{t_1}^{t_2} \delta W(w,\dot{w},\ddot{w},\chi,\dot{\chi},\ddot{\chi},t)dt - \int_{t_1}^{t_2} F(w,t)\delta w dt. \tag{5.48}$$

The functional $F(w,t) = \hat{a}_1 m_{fl} f_{st} U_o w(t)/D$ represents the "fluid stiffness" term, where $\hat{a}_1$ is a dimensionless constant and $f_{st} = SU/D$ is the vortex shedding or Strouhal frequency of the cylinder when it is stationary ($S \sim 0.2$ is the Strouhal number). The coefficient $\hat{a}_1 m_{fl} f_{st} U_o/D$ represents the natural frequency of the undamped wake-oscillator for small $w(t)$ (no motion of the cylinder), and is consistent with the observation that the damped (and hence the undamped) natural frequency of the wake-oscillator must change as the flow velocity U_o changes [6].

The fundamental character of a wake-oscillator model is that when it is uncoupled from the cylinder motion, it has a definite natural frequency,

$$\left(\hat{a}_1 m_{fl} f_{st} U_o/D\right)^{0.5},$$

which changes when U_o changes.

Using Eqs. 5.47, 5.48 and 5.46 becomes

$$\int_{t_1}^{t_2} \hat{a}_0 m_{fl}\dot{w}\delta\dot{w}dt + \delta\int_{t_1}^{t_2} \frac{1}{2}m_c\dot{\chi}^2 dt - \delta\int_{t_1}^{t_2} \frac{1}{2}k_s^{(y)}\chi^2 dt - \int_{t_1}^{t_2} c^{(vac)}\dot{\chi}\delta\chi dt$$
$$-\int_{t_1}^{t_2} \delta W(w,\dot{w},\ddot{w},\chi,\dot{\chi},\ddot{\chi},t)dt - \int_{t_1}^{t_2} F(w,t)\delta w dt = 0. \tag{5.49}$$

Next, consider dividing the functional $\delta W(w, \dot{w}, \ddot{w}, \chi, \dot{\chi}, \ddot{\chi}, t)$ as follows:

$$\delta W(w, \dot{w}, \ddot{w}, \chi, \dot{\chi}, \ddot{\chi}, t) = -F^{(y)}_{fl/st}(w, \dot{w}, \ddot{w}, \chi, \dot{\chi}, \ddot{\chi}, t)\delta\chi + F^{(y)}_{\mu/p}(w, \dot{w}, \ddot{w}, \chi, \dot{\chi}, \ddot{\chi}, t)\delta w. \quad (5.50)$$

$F^{(y)}_{fl/st}(w, \dot{w}, \ddot{w}, \chi, \dot{\chi}, \ddot{\chi}, t)\delta\chi$ is the instantaneous virtual work done by total transverse hydrodynamic force acting on the cylinder, while $F^{(y)}_{\mu/p}(w, \dot{w}, \ddot{w}, \chi, \dot{\chi}, \ddot{\chi}, t)\delta w$ represents virtual work done by the vertical components of the viscous and pressure forces within R^{**}, excluding the boundary of the cylinder. The negative sign on the $F^{(y)}_{fl/st}(w, \dot{w}, \ddot{w}, \chi, \dot{\chi}, \ddot{\chi}, t)\delta\chi$ term is due to the fact that on the surface of the cylinder $\delta\chi = -\delta w$ because of the no-slip condition.

Suppose the following form is assumed for $F^{(y)}_{fl/st}$:

$$F^{(y)}_{fl/st}(w, \dot{w}, \ddot{w}, \chi, \dot{\chi}, \ddot{\chi}, t) = -\frac{1}{4}\rho\pi D^2 L C_a \ddot{\chi}(t)$$
$$+\frac{1}{2}\rho D L C_d\,[\dot{w}(t) - \dot{\chi}(t)]\,|\dot{w}(t) - \dot{\chi}(t)| + \frac{1}{4}\pi\rho D^2 L(1 + C_a)\ddot{w}(t). \quad (5.51)$$

C_a represents the time-dependent-added mass coefficient for a moving cylinder in a crossflow. It is not the same as the potential flow-added mass $C_A = 1$. C_d represents the component of the instantaneous vortex lift coefficient $C_L(t)$ that is out of phase with the cylinder displacement.

Note that the form of Eq. 5.51 is equivalent to the Morison–O'Brien–Johnson–Schaff (MOJS) equation for the fluid force on a cylinder moving parallel to a time-dependent fluid stream [22]. In principle, geometric considerations require that the MOJS equation be modified when the cylinder is moving transversely to the free stream. Here, however, Eq. 5.51 is retained unaltered with the understanding that said equation can then be only referred to as "MOJS-like" .

The following form is assumed for $F_{\mu/p}(\dot{w}, \ddot{w}, \chi, \dot{\chi}, \ddot{\chi}, t)$:

$$F_{\mu/p}(\dot{w}, \ddot{w}, \chi, \dot{\chi}, \ddot{\chi}, t) = \hat{a}_2 m_{fl} f_{st}\,[\dot{w}(t) - \dot{\chi}(t)] + \frac{\hat{a}_3 m_{fl} f_{st}}{U_o^2}\,[\dot{w}(t) - \dot{\chi}(t)]^3\,. \quad (5.52)$$

The $\hat{a}_i$'s are again dimensionless constants.

The functional $F_{\mu/p}(w, \dot{w}, \ddot{w}, \chi, \dot{\chi}, \ddot{\chi}, t)$ has two distinct roles. In the first place, it is intended to capture the nonlinear damping effects in the wake-oscillator, much like the $\varepsilon f_{st}(\dot{q}^2(t) - 1)\dot{q}(t)$ term in the Rayleigh equation, or the $\varepsilon f_{st}(q^2(t) - 1)\dot{q}(t)$ term in the van der Pol equation. This damping term must be such that the wake-oscillator is self-excited and self-limiting.

Self-excitation of the wake is due to amplification by the shear layers of initial instabilities generated at the separation points, and an upstream influence caused by a region of absolute instability in the near wake. This region of absolute instability, whose downstream boundary is the point in the wake where traveling waves can be reflected, is associated with causing the propagation of an upstream traveling wave disturbance which amounts to a "feedback" to the separation points.

In addition, $F_{\mu/p}(\dot{w}, \ddot{w}, \chi, \dot{\chi}, \ddot{\chi}, t)$ must represent the nonlinear interaction (i.e., the right-hand-side) between the wake-oscillator and the motion of the cylinder.

First, Eqs. 5.51 and 5.52 are substituted into Eq. 5.50. The result is then substituted into Eq. 5.49, and the indicated variations performed. The conditions $\delta w|_{t_1}^{t_2} = \delta\chi|_{t_1}^{t_2} = 0$ are imposed and similar terms collected. The independence of the variations $\delta\chi$ and δw leads to the following set of coupled differential equations:

$$\left(m_c + \frac{1}{4}\pi\rho D^2 L C_a\right)\ddot{\chi}(t) + c^{(vac)}\dot{\chi}(t) + k_s^{(\chi)}\chi(t)$$
$$= \frac{1}{2}\rho D L C_d\,|\dot{w}(t) - \dot{\chi}(t)|\,[\dot{w}(t) - \dot{\chi}(t)] + \frac{1}{4}\pi\rho D^2 L(C_a + 1)\ddot{w}(t), \tag{5.53}$$

and

$$\hat{a}_0 m_{fl}\ddot{w}(t) + \hat{a}_1 m_{fl}\frac{U_o f_{st}}{D}w(t) + \frac{m_{fl} f_{st}}{U_o^2}\left[\hat{a}_3\dot{w}^2(t) + \hat{a}_2 U_o^2\right]\dot{w}(t)$$
$$= \hat{a}_2 m_{fl} f_{st}\dot{\chi}(t) + \frac{\hat{a}_3 m_{fl} f_{st}}{U_o^2}\dot{\chi}^3(t) + \frac{3\hat{a}_3 m_{fl} f_{st}}{U_o^2}\left[\dot{w}^2(t)\dot{\chi}(t) - \dot{w}(t)\dot{\chi}^2(t)\right]. \tag{5.54}$$

5.4 Comparison with Other Wake-Oscillator Models

Equations 5.53 and 5.54 are obtained as a reduced-order model for the self-excited transverse motion of an elastically mounted rigid circular cylinder in a smooth flow. The displacement of the cylinder from equilibrium, $\chi(t)$, is governed by Eq. 5.53. The fluctuating lift force resulting from vortex shedding acts as the primary driving force. Again, the fluctuating lift force is assumed to be correlated along the entire span.

The forcing function on RHS of Eq. 5.53 is a function of both the relative transverse velocity and the acceleration of the representative fluid mass m_{fl}. Recall that the transverse displacement of this fluid mass from the cylinder's horizontal (x) line of symmetry is denoted $w(t)$. For a stationary cylinder, the displacement is denoted $w_o(t)$. The fluid DOF $w(t)$ represents the mean transverse displacement of the collection of fluid particles having a total mass m_{fl} at each time t.

First, define the dimensionless displacement variables

$$\Xi(t) = \frac{\chi(t)}{D},$$
$$W(t) = \frac{w(t)}{D},$$

and the dimensionless time variable

$$T = t\omega_{st},$$

where $\omega_{st} = 2\pi f_{st}$ is the circular Strouhal frequency.

5.4.1 The Structural Oscillator

Using the above transformed variables, Eq. 5.53 becomes

$$\begin{aligned}&\left(m_c + m_d C_a\right)\Xi''(T) + \frac{c^{(vac)}}{\omega_{st}}\Xi'(T) + \frac{k_s^{(y)}}{\omega_{st}^2}\Xi(T)\\ &= \frac{1}{2}\rho D^2 L C_d \left|W'(T) - \Xi'(T)\right|\left[W'(T) - \Xi'(T)\right] + m_d\left(1 + C_a\right)W''(T),\end{aligned} \tag{5.55}$$

where $m_d = \rho\pi D^2 L/4$.

Next, define the in vacuo natural frequency,

$$\omega_n^{(vac)} = \sqrt{\frac{k_s^{(y)}}{m_c}} \simeq \omega_n^{(\text{air})}, \tag{5.56}$$

and the in situ [24] or *true* [26] natural frequency of the cylinder in crossflow,

$$\omega_n^{(\text{true})} = \sqrt{\frac{k_s^{(y)}}{\left(m_c + m_d C_a\right)}}, \tag{5.57}$$

where $m_d C_a = \rho\pi D^2 L C_a/4 \equiv \Delta m$ is the added mass.

The identity

$$\Delta m = m_d C_a = m_c\left[\left(\frac{\omega_n^{(vac)}}{\omega_n^{(\text{true})}}\right)^2 - 1\right] \tag{5.58}$$

is readily verified via Eqs. 5.56 and 5.57. Using this identity, the virtual mass can be expressed as

$$\left(m_c + \Delta m\right) = \left(m_c + m_d C_a\right) = m_c\left(\frac{\omega_n^{(vac)}}{\omega_n^{(\text{true})}}\right)^2. \tag{5.59}$$

Substituting Eq. 5.59 in Eq. 5.55 yields

$$\Xi''(T)+\frac{1}{\omega_{st}}\left(\frac{\omega_n^{(\text{true})}}{\omega_n^{(vac)}}\right)^2\frac{c^{(vac)}}{m_c}\Xi'(T)+\frac{1}{\omega_{st}^2}\left(\frac{\omega_n^{(\text{true})}}{\omega_n^{(vac)}}\right)^2\frac{k_s^{(y)}}{m_c}\Xi(T)$$
$$=\frac{1}{2m_c}\left(\frac{\omega_n^{(\text{true})}}{\omega_n^{(vac)}}\right)^2\rho D^2LC_d\left|W'(T)-\Xi'(T)\right|\left[W'(T)-\Xi'(T)\right]$$
$$+\frac{m_d}{m_c}\left(\frac{\omega_n^{(\text{true})}}{\omega_n^{(vac)}}\right)^2(1+C_a)\,W''(T)\,. \tag{5.60}$$

Introducing the reduced mass,

$$\hat{m}^*=\frac{\rho\pi D^2L}{4m_c}=\frac{m_d}{m_c}, \tag{5.61}$$

and the in vacuo structural damping ratio,

$$\zeta^{(vac)}=\frac{c^{(vac)}}{2m_c\omega_n^{(vac)}}, \tag{5.62}$$

into Eq. 5.60, and using Eq. 5.56, yields

$$\Xi''(T)+\frac{2}{\omega_{st}}\left(\frac{\omega_n^{(\text{true})}}{\omega_n^{(vac)}}\right)^2\zeta^{(vac)}\omega_n^{(vac)}\Xi'(T)+\frac{1}{\omega_{st}^2}\left(\frac{\omega_n^{(\text{true})}}{\omega_n^{(vac)}}\right)^2\omega_n^{(vac)^2}\Xi(T)$$
$$=\frac{2}{\pi}\left(\frac{\omega_n^{(\text{true})}}{\omega_n^{(vac)}}\right)^2\hat{m}^*C_d\left|W'(T)-\Xi'(T)\right|\left[W'(T)-\Xi'(T)\right]$$
$$+\hat{m}^*\left(\frac{\omega_n^{(\text{true})}}{\omega_n^{(vac)}}\right)^2(1+C_a)\,W''(T)\,. \tag{5.63}$$

By rearranging Eq. 5.58, and using Eq. 5.61, the useful identity

$$\left(\frac{\omega_n^{(\text{true})}}{\omega_n^{(vac)}}\right)^2=\frac{1}{\left(1+\hat{m}^*C_a\right)}, \tag{5.64}$$

is obtained.

Suppose the mass ratio

$$\mu=\frac{\rho\pi D^2L}{4\left(m_c+\Delta m\right)}=\frac{\rho\pi D^2L}{4\left(m_c+m_dC_a\right)}$$
$$=\frac{m_d}{\left(m_c+m_dC_a\right)} \tag{5.65}$$

is now introduced. Note that there exists the following relationship between $\hat{m}^*$, defined by Eq. 5.61, and μ:

$$\mu = \frac{m_d}{(m_c + m_d C_a)} = \frac{m_d}{m_c}\left[\frac{1}{\left(1 + \hat{m}^* C_a\right)}\right] = \frac{\hat{m}^*}{\left(1 + \hat{m}^* C_a\right)}. \tag{5.66}$$

The *corrected* structural damping [24] is defined as

$$\zeta^{(\text{true})} = \zeta^{(vac)} \sqrt{\frac{1}{\left(1 + \hat{m}^* C_a\right)}}. \tag{5.67}$$

See [11] for additional possibilities and alternatives for the structural oscillator. From Eqs. 5.64 and 5.67, the identity

$$\begin{aligned}\left(\frac{\omega_n^{(\text{true})}}{\omega_n^{(vac)}}\right)^2 \zeta^{(vac)} &= \left(\frac{\omega_n^{(\text{true})}}{\omega_n^{(vac)}}\right)\left(\frac{\omega_n^{(\text{true})}}{\omega_n^{(vac)}}\right)\zeta^{(vac)} \\ &= \left(\sqrt{\frac{1}{1 + \hat{m}^* C_a}}\,\zeta^{(vac)}\right)\left(\frac{\omega_n^{(\text{true})}}{\omega_n^{(vac)}}\right) \\ &= \left(\frac{\omega_n^{(\text{true})}}{\omega_n^{(vac)}}\right)\zeta^{(\text{true})}\end{aligned} \tag{5.68}$$

is established.

Using Eqs. 5.67 and 5.68 in Eq. 5.63 leads to

$$\begin{aligned}&\Xi''(T) + 2\zeta^{(\text{true})}\left(\frac{\omega_n^{(\text{true})}}{\omega_{st}}\right)\Xi'(T) + \left(\frac{\omega_n^{(\text{true})}}{\omega_{st}}\right)^2 \Xi(T) \\ =&\frac{2}{\pi}\frac{\hat{m}^*}{\left(1 + \hat{m}^* C_a\right)} C_d \left|W'(T) - \Xi'(T)\right|\left[W'(T) - \Xi'(T)\right] \\ &+ \frac{\hat{m}^*}{\left(1 + \hat{m}^* C_a\right)}(1 + C_a) W''(T).\end{aligned} \tag{5.69}$$

Finally, using Eqs. 5.66 and 5.69 can be rewritten as

$$\begin{aligned}&\Xi''(T) + 2\zeta^{(\text{true})}\left(\frac{\omega_n^{(\text{true})}}{\omega_{st}}\right)\Xi'(T) + \left(\frac{\omega_n^{(\text{true})}}{\omega_{st}}\right)^2 \Xi(T) \\ =&\frac{2}{\pi}\mu C_d \left|W'(T) - \Xi'(T)\right|\left[W'(T) - \Xi'(T)\right] + \mu(1 + C_a) W''(T).\end{aligned} \tag{5.70}$$

5.4.2 The Wake Oscillator

Introducing the dimensionless variables $\left(\Xi, \Xi', \Xi'', W, W', W'', T\right)$ into Eq. 5.54 and rearranging gives

$$\begin{aligned}\hat{a}_0\omega_{st}^2 D W''(T) + \frac{\omega_{st}}{U_o^2}\left[\hat{a}_3 D^2\omega_{st}^2 W'^2(T) + \hat{a}_2 U_o^2\right] D\omega_{st} W'(T) + \frac{\hat{a}_1\omega_{st}U_o}{D} D W(T)\\ = -\frac{3\hat{a}_4\omega_{st}}{U_o^2} D^3\omega_{st}^3\left[W'(t)\,\Xi'^2(T) - \Xi'(T)\,W'^2(T)\right]\\ + \frac{\hat{a}_3\omega_{st}^4 D^3}{U_o^2}\Xi'^3(T) + \hat{a}_2 D\omega_{st}^2\Xi'(T).\end{aligned} \tag{5.71}$$

Dividing both sides of Eq. 5.71 by $\hat{a}_0\omega_{st}^2 D$ yields[1]

$$\begin{aligned}W''(T) + \frac{\omega_{st}}{U_o^2}\left[D^2\omega_{st}\frac{\hat{a}_3}{\hat{a}_0}W'^2(T) + \frac{U_o^2}{\omega_{st}}\frac{\hat{a}_2}{\hat{a}_0}\right] W'(T) + \frac{U_o}{D\omega_{st}}\frac{\hat{a}_1}{\hat{a}_0}W(T)\\ = -\frac{3D^2\omega_{st}^2}{U_o^2}\frac{\hat{a}_4}{\hat{a}_0}\left[W'(t)\,\Xi'^2(T) - \Xi'(T)\,W'^2(T)\right]\\ + \frac{D^2\omega_{st}^2}{U_o^2}\frac{\hat{a}_3}{\hat{a}_0}\Xi'^3(T) + \frac{\hat{a}_2}{\hat{a}_0}\Xi'(T).\end{aligned} \tag{5.72}$$

Noting that from the definition of the Strouhal frequency,

$$\frac{U_o}{D\omega_{st}} = \frac{U_o}{D\left(\frac{2\pi S U_o}{D}\right)} = \frac{1}{(2\pi S)},$$

Equation 5.72 can be rewritten as

$$\begin{aligned}W''(T) + \left[(2\pi S)^2\frac{\hat{a}_3}{\hat{a}_0}W'^2(T) + \frac{\hat{a}_2}{\hat{a}_0}\right] W'(T) + \frac{1}{(2\pi S)}\frac{\hat{a}_1}{\hat{a}_0}W(T)\\ = -3(2\pi S)^2\frac{\hat{a}_4}{\hat{a}_0}\left[W'(T)\,\Xi'^2(T) - \Xi'(T)\,W'^2(T)\right]\\ + (2\pi S)^2\frac{\hat{a}_3}{\hat{a}_0}\Xi'^3(T) + \frac{\hat{a}_2}{\hat{a}_0}\Xi'(T).\end{aligned} \tag{5.73}$$

Consider for the moment the case of a stationary cylinder. In this case, $\Xi(T)$ and its derivatives are all identically zero, and Eq. 5.73 reduces to

$$W_o''(T) + \left[(2\pi S)^2\frac{\hat{a}_3}{\hat{a}_0}W_o'^2(T) + \frac{\hat{a}_2}{\hat{a}_0}\right] W_o'(T) + \frac{1}{(2\pi S)}\frac{\hat{a}_1}{\hat{a}_0}W_o(T) = 0, \tag{5.74}$$

[1] The model constant $\hat{a}_0$ is assumed to be nonzero at all times.

where

$$W_o(T) = \frac{w_o(T)}{D}.$$

The van der Pol and Rayleigh equations are the nonlinear oscillators most commonly used to model the fluctuating nature of the vortex shedding. For a stationary cylinder, they adequately model the self-sustained, quasi-harmonic oscillations seen experimentally in the lift coefficient, for example. The reader is referred to Facchinetti et al. [10] for a more comprehensive discussion. Here, the focus is on constructing a Rayleigh-type equation from Eq. 5.74.

The dimensionless Rayleigh equation,

$$Q''(T) + \varepsilon \left(Q'^2(T) - 1\right) Q'(T) + Q(T) = 0,$$

with $0 < \varepsilon \ll 1$, is known to provide a stable quasi-harmonic oscillation of finite amplitude at the frequency

$$\Omega = 1.$$

Equation 5.74 is then of the Rayleigh type provided that the conditions

$$\begin{aligned} \frac{1}{(2\pi S)}\frac{\hat{a}_1}{\hat{a}_0} &= 1 \\ \frac{\hat{a}_2}{\hat{a}_0} &< 0 \\ \left|\frac{\hat{a}_2}{\hat{a}_0}\right| &\ll 1 \\ \frac{\hat{a}_3}{\hat{a}_0} &< 0, \end{aligned}$$

and

$$(2\pi S)^2 \left|\frac{\hat{a}_3}{\hat{a}_0}\right| \ll 1$$

are satisfied. It is evident from the above conditions that if $\hat{a}_0 < 0$, then $\hat{a}_2 > 0$ and $\hat{a}_{1,3} < 0$. On the other hand, if $\hat{a}_0 > 0$, then $\hat{a}_2 < 0$ and $\hat{a}_{1,3} > 0$.

Next, define

$$\hat{b}_i = \left|\frac{\hat{a}_i}{\hat{a}_0}\right|,$$

where $i = 2, 3$. The sign of the model constant $\hat{a}_4$ is not known a priori, and, therefore, there are no constraints to determine the sign of the ratio $\hat{a}_4/\hat{a}_0$. As a result, said ratio is represented as b_4, where $b_4 \gtreqless 0$.

Equation 5.73 can now be written as

$$\begin{aligned} &W''(T) + \left[(2\pi S)^2 \hat{b}_3 W'^2(T) - \hat{b}_2\right] W'(T) + W(T) \\ &= -3(2\pi S)^2 b_4 \left[W'(T)\,\Xi'^2(T) - \Xi'(T)\,W'^2(T)\right] \\ &\quad + (2\pi S)^2 \hat{b}_3 \Xi'^3(T) - \hat{b}_2 \Xi'(T)\,. \end{aligned} \tag{5.75}$$

Upon examining Eqs. 5.70 and 5.75, it is apparent that there are five model parameters, $\left(\hat{b}_2, \hat{b}_3, b_4, C_a, C_d\right)$. However, since $\hat{b}_2$, $\hat{b}_3$, and b_4 are not all independent, the true number of independent model parameters is actually six, $\left(\hat{a}_0, \hat{a}_2, \hat{a}_3, \hat{a}_4, C_a, C_d\right)$.

5.4.3 Comparison with the Model of Krenk and Nielsen (1999)

In dimensionless form, the model equations derived by Krenk and Nielsen (KN) [17] are given by

$$\ddot{\Xi}(t) + \zeta^{(\text{true})}\omega_n^{(\text{true})}\dot{\Xi}(t) + \left[\omega_n^{(\text{true})}\right]^2 \Xi(t) = \mu_f c_o \omega_{st} \dot{P}(t)\,, \tag{5.76}$$

and

$$\ddot{P}(t) + 2\zeta_f \omega_{st}\left[P^2(t) + \left(\frac{\dot{P}(t)}{\omega_{st}}\right)^2 - 1\right]\dot{P}(t) + \omega_{st}^2 P(t) = -\frac{1}{v_o^2} c_o \omega_{st} \dot{\Xi}(t)\,, \tag{5.77}$$

where

$$\mu_f = \frac{\rho D^2 L}{(m_c + \Delta m)}, \tag{5.78}$$

and $\zeta_f \equiv$ equivalent fluid damping ratio.

It is not clear from Ref. [17] how the added fluid mass, Δm in Eq. 5.78, is defined. Since KN test the validity of their model using data from experiments conducted in air, the added fluid mass is small. That is, for $\hat{m}^* \ll 1$, $\Delta m_{\text{potential}} = C_A \hat{m}^* m_c \simeq \Delta m = C_a \hat{m}^* m_c \simeq 0$. Thus, the distinction between $\Delta m_{\text{potential}}$ and Δm matters little in this case. This is not the case if the fluid medium is water.

The physical meaning of fluid variable[2] $W^*(t)$ in the KN model is also not clearly defined. It is conjectured here that this fluid variable represents the *relative* transverse displacement of the fluid mass m_{fl}. Designating this conjectured KN wake variable as $W^*_{conj.}(t)$, it follows that

$$W^*_{conj.}(t) = w(t) - \chi(t)\,.$$

[2]The *actual* fluid variable that is used in the formulation of their model.

Krenk and Nielsen nondimensionalize their fluid variable as follows:

$$P(t) = \frac{W^*(t)}{w_o}.$$

As before, the scale w_o is a parameter that "...controls the amplitude of self-induced vibrations of the wake oscillator in the case of a stationary cylinder..." [17].

The parameters c_o and v_o of Eqs. 5.76 and 5.77 are defined as

$$c_o = \frac{w_o \gamma}{4\pi SD}, \tag{5.79}$$

and

$$v_o = \frac{w_o}{D}, \tag{5.80}$$

where γ is a dimensionless coupling parameter.

The dimensionless time variable $T = \omega_{st} t$ is now introduced. Effecting the change of variables $t \to T$ in Eqs. 5.76 and 5.77 results in

$$\Xi''(T) + \zeta^{(\text{true})} \left(\frac{\omega_n^{(\text{true})}}{\omega_{st}} \right) \Xi'(T) + \left(\frac{\omega_n^{(\text{true})}}{\omega_{st}} \right)^2 \Xi(T) = \mu_f c_o P'(T), \tag{5.81}$$

and

$$P''(T) + 2\zeta_f \left[P^2(T) + P'^2(T) - 1 \right] + P(T) = -\frac{1}{v_o^2} c_o \Xi'(T), \tag{5.82}$$

respectively.

Comparing Eqs. 5.65 and 5.78, it is seen that

$$\mu_f = \frac{\rho D^2 L}{(m_c + \Delta m)} = \frac{4}{\pi} \mu.$$

Using this result and Eqs. 5.79, 5.80, 5.81 and 5.82 can then be rewritten, respectively, as

$$\Xi''(T) + \zeta^{(\text{true})} \left(\frac{\omega_n^{(\text{true})}}{\omega_{st}} \right) \Xi'(T) + \left(\frac{\omega_n^{(\text{true})}}{\omega_{st}} \right)^2 \Xi(T) = \frac{4 w_o \gamma}{\pi^2 SD} \mu P'(T), \tag{5.83}$$

and

$$P''(T) + 2\zeta_f \left[P^2(T) + P'^2(T) - 1 \right] P'(T) + P(T) = -\frac{D\gamma}{4\pi S w_o} \Xi'(T). \tag{5.84}$$

Using the definition of $W^*_{conj.}(t)$, it is possible to define the new dimensionless variable

$$P_{conj.}(T) = \frac{W^*_{conj.}(T)}{w_o}.$$

Its derivative is

$$\begin{aligned} P'_{conj.}(T) &= \frac{W^{*\prime}_{conj.}(T)}{v_o D} \\ &= \frac{1}{v_o}\left(\frac{DW'(T) - D\Xi'(T)}{D}\right) \\ &= \frac{1}{v_o}\left[W'(T) - \Xi'(T)\right]. \end{aligned}$$

Making the substitution $P'(T) \to P'_{conj.}(T)$ on the RHS of Eq. 5.83 yields

$$\begin{aligned} \Xi''(T) + \zeta^{(\text{true})}\left(\frac{\omega_n^{(\text{true})}}{\omega_{st}}\right)\Xi'(T) + \left(\frac{\omega_n^{(\text{true})}}{\omega_{st}}\right)^2 \Xi(T) &= \frac{4w_o\gamma}{\pi^2 SD}\mu P'_{conj.}(T) \\ &= \frac{4w_o\gamma}{\pi^2 SD}\mu\left[W'(T) - \Xi'(T)\right]. \end{aligned} \tag{5.85}$$

Comparing Eqs. 5.70 and 5.85, it is clear that the LHS of each equation is the same. The RHS, on the other hand, differs. Equation 5.85 has a RHS that represents a linearized form of the drag term in Eq. 5.70. Also absent from the RHS of Eq. 5.85 is a term proportional to the acceleration of the representative fluid mass, $P''(T)$.

Now, suppose that $W^*_{conj.}(t) = W^*(t)$. This implies that there is no distinction between $P_{conj.}(T) = P(T)$. In this case, Eq. 5.81 reveals that in this case there is no *per se* fluid-added damping. The structural oscillator is fed energy directly from the wake oscillator via the $\mu_f c_o P'(T)$ term on the RHS, but it is not possible to explicitly express the dependence of this energy transfer on the cylinder velocity $\Xi'(T)$.

Prima facie, Eqs. 5.75 and 5.84 seem nothing alike. In the first place, Eq. 5.75 lacks a term of the form $W^2(T)W'(T)$, which is present in Eq. 5.84. Also, the RHS of Eq. 5.84 is linearly proportional to cylinder velocity $\Xi'(T)$, while Eq. 5.75 possesses an additional nonlinear forcing function.

However, if $P_{conj.}(T)$ and its derivatives,

$$\begin{aligned} P_{conj.}(T) &= \frac{1}{v_o}\left[W(T) - \Xi(T)\right] \\ P'_{conj.}(T) &= \frac{1}{v_o}\left[W'(T) - \Xi'(T)\right], \end{aligned}$$

and

$$P''_{conj.}(T) = \frac{1}{v_o}\left[W''(T) - \Xi''(T)\right],$$

are substituted into Eq. 5.84 in place of $P(T)$ and its derivatives, a complex forcing function is obtained. In fact, this expression will include all the terms on the RHS of Eq. 5.75 plus additional nonlinear terms originating from the product

$$2\zeta_f\left[\left\{\frac{1}{v_o}\left[W(T) - \Xi(T)\right]\right\}^2\right]\left[W'(T) - \Xi'(T)\right].$$

Note that the forcing function will also involve terms that are linear in the cylinder displacement $\Xi(T)$, velocity $\Xi'(T)$, and acceleration $\Xi''(T)$. The $\Xi(T)$ and $\Xi''(T)$ terms are absent from Eq. 5.75.

It is fair to say that comparison with the KN model is complicated by uncertainty with respect to the definition of the fluid variable $W^*(t)$; very different conclusions are reached depending on how $W^*(t)$ is interpreted.

5.4.4 *Hall (1981)*

As part of his doctoral dissertation, Hall [14] considers a modified Blevins model for the transverse VIV of a spring-mounted rigid cylinder in uniform fluid flow. When said fluid is water, the model equations are given in dimensionless form[3]

$$\begin{aligned}\Xi''(T) + \frac{1}{(1+\eta a_3)}\left[2\zeta^{(\text{st. water})}\frac{\omega_n^{(\text{st. water})}}{\omega_{st}} + \frac{a_4\eta}{2\pi S}\right]\Xi'(T) \\ + \left(\frac{1}{\sqrt{(1+\eta a_3)}}\frac{\omega_n^{(\text{st. water})}}{\omega_{st}}\right)^2\Xi(T) \\ = \left[\frac{a_4\eta}{2\pi S(1+\eta a_3)}\right]Z'(T) + \left[\frac{(a_3+a_5)\eta}{(1+\eta a_3)}\right]Z''(T),\end{aligned} \tag{5.86}$$

and

$$\begin{aligned}Z''(T) - \left[\frac{(a_1-a_4)}{2\pi S(a_0+a_3+a_5)}\right]Z'(T) + \left[\frac{2\pi S a_2}{(a_0+a_3+a_5)}\right]Z'^3(T) + Z(T) \\ = \left[\frac{a_4}{2\pi S(a_0+a_3+a_5)}\right]\Xi'(T) + \left[\frac{a_3}{(a_0+a_3+a_5)}\right]\Xi''(T).\end{aligned} \tag{5.87}$$

[3] Hall defines his mechanical parameters per unit length. The necessary invariance of the equations to scaling, however, means they can simply be rewritten using the relevant parameters in Table 5.2 of [12] without compromising their validity.

In the above equations, the a_i's are independent model constants and

$$\eta = \frac{\rho D^2 L}{(m_c + m_d)}$$

is a mass ratio based on the potential flow-added mass.[4]

Note that there exists the following relationship between η and $\hat{m}^*$:

$$\eta = \frac{\rho D^2 L}{(m_c + m_d)} = \frac{\rho D^2 L}{m_c \left(1 + \hat{m}^*\right)} = \frac{4}{\pi} \frac{\hat{m}^*}{\left(1 + \hat{m}^*\right)}. \tag{5.88}$$

Equation 5.86 can now be written as

$$\begin{aligned} \Xi'' (T) + \frac{1}{(1 + \eta a_3)} \left[2\zeta^{(\text{st. water})} \frac{\omega_n^{(\text{st. water})}}{\omega_{st}} + \frac{a_4 \eta}{2\pi S} \right] \Xi' (T) \\ + \left(\frac{1}{\sqrt{(1 + \eta a_3)}} \frac{\omega_n^{(\text{st. water})}}{\omega_{st}} \right)^2 \Xi (T) \\ = \left[\frac{a_4 \eta}{2\pi S (1 + \eta a_3)} \right] Z' (T) + \left[\frac{(a_3 + a_5)\, \eta}{(1 + \eta a_3)} \right] Z'' (T) . \end{aligned} \tag{5.89}$$

T and Ξ have the same meaning in Eqs. 5.87 and 5.89 as they do in Eqs. 5.55 and 5.75. In principle, however, $Z(T)$ has a slightly different interpretation than does $W(T)$. $Z'(T)$ is in fact related to the dimensionless form of the Blevins' [7] "hidden fluid variable," $\dot{z}(t)$.

It is crucial to point out that Hall derives his model for a horizontal cylinder. The "Hall hidden fluid variable" is then defined as

$$\dot{z}_{\text{Hall}}(t) = D\omega_{st} Z' (T) = \frac{1}{a_0 \rho D^2} \iint_{A_o} \rho u_2(y, z, t) dy dz,$$

where A_o is the cross-sectional area of the rectangular control volume of unit axial (x) dimension that surrounds the cylinder.

The distinction between Hall's $\dot{z}_{\text{Hall}}(t)$ and Blevins' $\dot{z}(t)$ vanishes when Hall's model is formulated for a *vertical* cylinder. This is accomplished by rotating Hall's coordinate system about the y-axis by an angle $\alpha = -\pi/2$ radians (i.e., counterclockwise), and then setting a_5 equal to zero. The order of these operations is immaterial.

Is $Z'(T)$ related to $W'(T)$? To find the answer to this question, suppose $u_2(y, z, t)$ is approximately constant over some subset A_o^* of A_o. As a result,

[4] Hall does not directly define his mass in this way. He merely refers to the "mass per unit length." The same ambiguity exists in the Blevins model: In [16] reference is also made to the "mass per unit length m," while in [7] the same mass m includes "the entrained mass of fluid."

$$\dot{z}(t) \simeq \frac{1}{a_0 \rho D^2} u_2(t) \iint_{A_o^*} \rho dx_2 dx_3 = \frac{1}{a_0 \rho D^2} u_2(t) \beta,$$

where β is simply a constant as ρ is assumed constant (the flow is incompressible). From the assumption of fully correlated shedding in the synchronization regime, A_o^* is the same at each axial station. As a result,

$$\beta L = \tilde{m}_{fl},$$

where $\tilde{m}_{fl}$ is the total mass of fluid contained in the volume $A_o^* L$. It is then possible to write

$$\dot{z}(t) \simeq \frac{1}{a_0 \rho D^2 L} u_2(t) \tilde{m}_{fl}.$$

If A_o^* coincides with the x-y projection of the region R^{**}, then $\tilde{m}_{fl} = m_{fl}$ and $u_2(t)$ coincides with the wake degree-of-freedom $\dot{w}(t)$. It follows that

$$\dot{z}(t) \simeq \frac{1}{a_0 \rho D^2 L} \dot{w}(t) m_{fl}.$$

In addition, if $m_{fl} = \rho D^2 L$, as in Ref. [17], then

$$\dot{z}(t) \simeq \frac{1}{a_0} \dot{w}(t).$$

It is clear that $Z'(T)$ is indeed related to $W'(T)$, at least in a limiting sense. This supports the notion that the model represented by Eqs. 5.53 and 5.75 can be meaningfully compared with Hall's model equations.

To that end, consider first rewriting Eq. 5.75 as

$$\begin{aligned} &\Xi''(T) + \frac{2}{\lambda} \zeta^{(\text{st. water})} \frac{\omega_n^{(\text{st. water})}}{\omega_{st}} \Xi'(T) + \left(\frac{1}{\sqrt{\lambda}} \frac{\omega_n^{(\text{st. water})}}{\omega_{st}} \right)^2 \Xi(T) \\ &\quad = \frac{2}{\pi} \frac{\hat{m}^*}{\lambda \left(1 + \hat{m}^*\right)} C_d \left| W'(T) - \Xi'(T) \right| \left[W'(T) - \Xi'(T) \right] \\ &\qquad + \frac{\hat{m}^*}{\lambda \left(1 + \hat{m}^*\right)} \left(C_a^* + 2 \right) W''(T), \end{aligned} \tag{5.90}$$

where the parameters $\omega_n^{(\text{st. water})}$ and $\zeta^{(\text{st. water})}$ are defined in Table 5.1, and $\lambda = \left[1 + \frac{\hat{m}^*}{(1+\hat{m}^*)} C_a^* \right]$. C_a^* represents the deviation of the added mass coefficient from its potential flow value of $C_A = 1$.

Table 5.1 A list of key parameters

Parameter	Defined by	Description
S	$\simeq 0.2$	Strouhal number
m_c	$\cdots$	Cylinder dry mass
L	$\cdots$	Cylinder length
D	$\cdots$	Cylinder diameter
m_{fl}	$\cdots$	Mass of near-wake fluid oscillator
$c^{(vac)}$	$\cdots$	In vacuo material damping of the cylinder + supports
$k_s^{(y)}$	$\cdots$	Total stiffness of the supporting springs
U_o	$\cdots$	Magnitude of the uniform free stream velocity
ρ	$\cdots$	Fluid density
C_A	1.0	Potential flow-added mass coefficient
C_a	$\cdots$	Added mass coefficient for a cylinder in crossflow
m_d	$\frac{\rho\pi L D^2}{4}$	Mass of fluid displaced by the cylinder
$\chi(t)$	$\cdots$	Transverse displacement of the cylinder from equilibrium
$\hat{m}^*$	$\frac{m_d}{m_c}$	Reduced mass
ω_{st}	$\frac{2\pi S U_o}{D}$	Circular Strouhal vortex shedding frequency

Setting $a_5 = 0$ in Eq. 5.89 gives

$$\Xi''(T) + \frac{1}{(1+\eta a_3)}\left[2\zeta^{(\text{st. water})}\frac{\omega_n^{(\text{st. water})}}{\omega_{st}} + \frac{a_4\eta}{2\pi S}\right]\Xi'(T) + \left(\frac{1}{\sqrt{(1+\eta a_3)}}\frac{\omega_n^{(\text{st. water})}}{\omega_{st}}\right)^2 \Xi(T) = \left(\frac{a_4\eta}{2\pi S(1+\eta a_3)}\right)Z'(T) + \left[\frac{a_3\eta}{(1+\eta a_3)}\right]Z''(T). \tag{5.91}$$

Suppose now that the model parameters a_3 and a_4 are related to C_a and C_d, respectively, in the following way:

$$a_3 = \frac{\pi}{4}\frac{\left(\hat{m}^* C_a - \hat{m}^*\right)}{\hat{m}^*} = \frac{\pi}{4}(C_a - 1) = \frac{\pi}{4}C_a^*,$$

and

$$a_4 = \frac{\pi}{4}C_d.$$

Using Eq. 5.88, the following additional relations are obtained:

$$a_3\eta = \frac{\hat{m}^*}{\left(1+\hat{m}^*\right)}C_a^*,$$

and

$$a_4\eta = \frac{\hat{m}^*}{\left(1+\hat{m}^*\right)}C_d.$$

Defining

$$1 + a_3\eta = \left[1 + \frac{\hat{m}^*}{\left(1+\hat{m}^*\right)}C_a^*\right] = \lambda,$$

it follows that

$$\frac{a_3\eta}{(1+a_3\eta)} = \frac{\hat{m}^*}{\lambda\left(1+\hat{m}^*\right)}C_a^*$$
$$\frac{a_4\eta}{(1+a_3\eta)} = \frac{\hat{m}^*}{\lambda\left(1+\hat{m}^*\right)}C_d.$$

Substituting the above relations into Eq. 5.91 yields

$$\Xi''(T) + \frac{1}{\lambda}\left[2\zeta^{(\text{st. water})}\frac{\omega_n^{(\text{st. water})}}{\omega_{st}} + \frac{1}{2\pi S}\frac{\hat{m}^*}{\left(1+\hat{m}^*\right)}C_d\right]\Xi'(T)$$
$$+\left(\frac{1}{\sqrt{\lambda}}\frac{\omega_n^{(\text{st. water})}}{\omega_{st}}\right)^2\Xi(T) = \frac{1}{2\pi S}\frac{\hat{m}^*}{\lambda\left(1+\hat{m}^*\right)}C_d Z'(T)$$
$$+\frac{\hat{m}^*}{\lambda\left(1+\hat{m}^*\right)}C_a^* Z''(T). \tag{5.92}$$

When Eq. 5.90 is rewritten as

$$\Xi''(T) + \frac{2}{\lambda}\zeta^{(\text{st. water})}\frac{\omega_n^{(\text{st. water})}}{\omega_{st}}\Xi'(T) + \left(\frac{1}{\sqrt{\lambda}}\frac{\omega_n^{(\text{st. water})}}{\omega_{st}}\right)^2\Xi(T)$$
$$= \frac{2}{\pi}\frac{\hat{m}^*}{\lambda\left(1+\hat{m}^*\right)}C_d\left|W'(T) - \Xi'(T)\right|\left[W'(T) - \Xi'(T)\right]$$
$$+\frac{\hat{m}^*}{\lambda\left(1+\hat{m}^*\right)}C_a^* W''(T) + \frac{2\hat{m}^*}{\lambda\left(1+\hat{m}^*\right)}W''(T), \tag{5.93}$$

its similarity with Eq. 5.92 becomes apparent.

Equations 5.92 and 5.93 differ primarily with respect to the drag term. This difference is attributable to the fact that Hall's formulation is based on a linear drag term, proportional to $C_d\left[Z'(T) - \Xi'(T)\right]$. The presence of this linear drag term is manifested in both the fluid-added damping term on the left-hand side (LHS) of Eq. 5.92,

$$\frac{1}{2\pi S}\frac{\hat{m}^*}{\lambda\left(1+\hat{m}^*\right)}C_d\Xi'(T),$$

and in the forcing term proportional to $Z'(T)$ on the right-hand-side (RHS) of said equation. Such a separation is not possible in Eq. 5.93.

In addition to the aforementioned difference, Eq. 5.93 possesses the additional term

$$\frac{2\hat{m}^*}{\lambda\left(1+\hat{m}^*\right)}W''(T) = \frac{2\hat{m}^*}{\left[1+\frac{\hat{m}^*}{(1+\hat{m}^*)}C_a^*\right]\left(1+\hat{m}^*\right)}W''(T) = \frac{2\hat{m}^*}{\left(1+\hat{m}^*C_a\right)}W''(T). \tag{5.94}$$

The absence of this term in Eq. 5.92 can be attributed to the fact that the $Z''(T)$ and the $\Xi''(T)$ terms have the same coefficient, $a_3\eta = \hat{m}^*C_a^*/\left(1+\hat{m}^*\right)$, in the forcing function[5] Hall assumes for his structural oscillator. On the other hand, the coefficients of the $W''(T)$ and $\Xi''(T)$ terms in Eq. 5.90 differ, the difference between them being precisely equal to this extra term.

It is of interest to point out that Iwan and Blevins [16] set $a_3 = 0$. They argue that doing so "... does not imply that there is no added mass effect since the flow forward of the separation point remains attached to the cylinder, effectively increasing the oscillating mass of the cylinder." Furthermore, " ... the best agreement between model predictions and experimental response data ... is obtained when $a_3 = 0$." If the added mass effect is not represented by the a_3 term, then this suggests that it is already captured in the effective mass which is computed using the potential flow-added mass.

The assumption $a_3 = 0$ is suitable when the fluid medium is air, in which case $\hat{m}^*$ is small. The additional term of Eq. 5.93 can then be neglected. In a water medium, for which $\hat{m}^*$ may no longer be small, added mass effects are important. Indeed, the potential flow-added mass becomes an increasingly inexact representation of the actual added mass as $\hat{m}^*$ decreases. Under these circumstances, the assumption $a_3 = 0$ no longer seems reasonable, and the term represented by Eq. 5.94 cannot be neglected.

It is difficult to make a comparison between Eqs. 5.75 and 5.87 without reinterpreting the model constants a_i $(i = 1, ..., 5)$. This is because in Hall's model, the a_i's appear directly in both equations. This is not a feature of the present model. With $a_5 = 0$, Eq. 5.87 becomes

$$Z''(T) + \frac{2\pi S}{(a_0+a_3)}\left[a_2 Z'^2(T) - \frac{(a_1-a_4)}{(2\pi S)^2}\right]Z'(T) + Z(T) = \frac{a_4}{2\pi S(a_0+a_3)}\Xi'(T) + \frac{a_3}{(a_0+a_3)}\Xi''(T). \tag{5.95}$$

[5] See Eqs. 2.2.7 and 3.2.16 of Ref. [14].

Noting that a $\Xi''(T)$ term is absent from the RHS of Eq. 5.75, one can also set

$$a_3 = 0.$$

Next, suppose

$$\frac{a_2}{(a_0 + a_3)} = \frac{a_2}{a_0} = 2\pi S\hat{b}_3,$$

and

$$\left(\frac{a_1 - a_4}{a_0 + a_3}\right) = \frac{(a_1 - a_4)}{a_0} = 2\pi S\hat{b}_2. \tag{5.96}$$

Equation 5.95 then becomes

$$Z''(T) + \left[(2\pi S)^2 \hat{b}_3 Z'^2(T) - \hat{b}_2\right] Z'(T) + Z(T) = \frac{a_4}{2\pi S a_0}\Xi'(T).$$

Solving for a_4 from Eq. 5.96 and then substituting the result in the above equation yields

$$Z''(T) + \left[(2\pi S)^2 \hat{b}_3 Z'^2(T) - \hat{b}_2\right] Z'(T) + Z(T) = \frac{1}{2\pi S}\left[\frac{a_1}{a_0} - (2\pi S)\hat{b}_2\right]\Xi'(T). \tag{5.97}$$

A comparison of Eqs. 5.75 and 5.97 reveals that the main difference lies in the forcing function on the RHS of each equation. The forcing function in Eq. 5.75 is the sum of the nonlinear function,

$$f_{NL}\left(W'(T), \Xi'(T)\right) = (2\pi S)^2 \sum_{i=0}^{2} \alpha_i \Xi'^{3-i}(T) W'^{i}(T) \quad (\alpha_0 = \hat{b}_3, \alpha_1 = \alpha_2 = \hat{b}_4), \tag{5.98}$$

and the linear function

$$f_L\left(\Xi'(T)\right) = -\hat{b}_2\Xi'(T).$$

The nonlinear function $f_{NL}\left(W'(T), \Xi'(T)\right)$ represents the autoparametric excitation.

In contrast, the forcing function in Eq. 5.97 is purely a linear function of the cylinder velocity, and $f_{NL}\left(W'(T), \Xi'(T)\right) = 0$. This type of forcing has been extensively used in wake oscillator models (e.g., [17, 24]).

In summary, it is apparent that the model represented by Eqs. 5.90 and 5.75 compares well with the model equations derived by Hall [14]. The major discrepancy between each of the model equations and their counterparts in Hall's formulation is in the form of the forcing function. Hall's forcing functions are in each case linear; the forcing functions in the model derived here include additional nonlinear terms.

5.4.5 Berger (1988)

Berger's [4] model represents a departure from the previous comparison model in that it uses the lift coefficient as the fluid internal degree-of-freedom. Nonetheless, Berger's model serves a useful comparison because it is generally believed to be one of the most successful improvements on the original Hartlen–Currie model [15]. Its touted success lies primarily in its ability to correctly predict, both quantitatively and qualitatively, oscillation hysteresis for certain values of $\zeta^{(vac)}$.

Berger derives the following pair of dimensionless coupled equations as a model for the transverse VIV of an elastically mounted rigid circular cylinder lying in a uniform stream of air:

$$\Xi''(\tau) + \delta\left(\Xi'(\tau)\right)\Xi'(\tau) + \Xi(\tau) = \frac{1}{2\pi^3 L}\hat{m}^* V_r^{(vac)^2} C_y(\tau) = a\Omega^2 C_y(\tau), \tag{5.99}$$

and

$$C_y''(\tau) + f^*\left(C_y'(\tau)\right)C_y'(\tau) + \Omega^2 C_y(\tau) = b\left(\Xi'(\tau)\right)\Xi'(\tau). \tag{5.100}$$

$C_y(\tau)$ is the lift coefficient,[6] $\delta\left(\Xi'(\tau)\right)$ is the nonlinear structural damping function, a is a coupling constant, $f^*\left(C_y'(\tau)\right)$ is the nonlinear damping function for the wake oscillator, and $b\left(\Xi'(\tau)\right)$ is a nonlinear feedback parameter. According to Berger, the $\delta\left(\Xi'(\tau)\right)$ term is used to model the effects of viscous forces. The reduced velocity $V_r^{(vac)}$ is defined in Table 5.2.

The model parameters are defined as

$$\delta\left(\Xi'(\tau)\right) = \sum_{k=0}^{m} \delta_{2k} \Xi'^{2k}(\tau),$$

$$f^*\left(C_y'(\tau)\right) = \sum_{k=0}^{m} \alpha_{2k} C_y'^{2k}(\tau), \text{ with } \alpha_0 < 0 \text{ and } \alpha_{2m} > 0,$$

$$b\left(\Xi'(\tau)\right) = \sum_{k=0}^{m} b_{2k} \Xi'^{2k}(\tau),$$

and

$$\Omega = \frac{f_{st}}{f_n^{(vac)}} = 2\pi S V_r^{(vac)}. \tag{5.101}$$

The coefficient set $(\delta_{2k}, \alpha_{2k}, b_{2k})$ represents the model constants that are to be determined from experimental data. Note that the expansions for $\delta\left(\Xi'(\tau)\right)$, $f^*\left(C_y'(\tau)\right)$ and $b\left(\Xi'(\tau)\right)$ are all necessarily symmetric with respect to the neutral position of

[6] The fluid force term $C_y(\tau)$ implicitly contains the added mass effects.

Table 5.2 A number of possible characterizations of the cylinder natural frequency, and damping and mass ratios

Parameter	Value	Description
$\omega_n^{(vac)}$	$\sqrt{\frac{k_s^{(y)}}{m_c}}$	Cylinder natural frequency in vacuo
$\omega_n^{(\text{true})}$	$\sqrt{\frac{k_s^{(y)}}{(m_c + C_a m_d)}}$	Cylinder true (or in-situ) natural frequency
$\omega_n^{(\text{st. water})}$	$\sqrt{\frac{k_s^{(y)}}{(m_c + C_A m_d)}}$	Cylinder natural frequency in still water
$\zeta^{(vac)}$	$\frac{c^{(vac)}}{2\omega_n^{(vac)} m_c}$	Damping ratio (material/critical) in vacuo
$\zeta^{(\text{true})}$	$\zeta^{(vac)}\sqrt{\frac{1}{\hat{m}^* C_a}}$	True (or in-situ) damping ratio
$\zeta^{(\text{st. water})}$	$\zeta^{(vac)}\sqrt{\frac{1}{\hat{m}^* C_A}}$	Damping ratio in still water
μ	$\frac{m^*}{1 + m^* C_a}$	Mass ratio including added mass
$V_r^{(vac)}$	$\frac{2\pi U_o}{\omega_n^{(vac)} D}$	Reduced velocity defined using the in vacuo natural frequency

the cylinder, $\Xi(\tau) = 0$. This guarantees a system of equations, Eqs. 5.99 and 5.100, that is invariant to the sign changes $y := -y$ and $C_y := -C_y$.

Berger defines the dimensionless cylinder displacement as $\Xi(t) = y(t)/D$ and the dimensionless time as $\tau = \omega_n^{(vac)} t$. His equations are now modified so that they are in terms of the dimensionless time T.

To that end, the following relationship between the time derivatives is used:

$$\frac{d^n(\cdot)}{d\tau^n} = \left(\frac{\omega_{st}}{\omega_n^{(vac)}}\right)^n \frac{d^n(\cdot)}{dT^n}.$$

In order to distinguish the parenthesis indicating a functional relationship, $f^*\left(C_y'(\tau)\right)$ for example, from those used solely for grouping purposes, it is convenient to introduce the variable

$$\varkappa = \frac{\omega_n^{(vac)}}{\omega_{st}}. \tag{5.102}$$

Using the above relationships and the definition of $\varkappa$, the dimensionless structural equation of motion, Eq. 5.99, can be written as

$$\Xi''(T) + \varkappa\delta\left(\varkappa^{-1}\Xi'(T)\right)\Xi'(T) + \varkappa^2\Xi(T) = a\Omega^2\varkappa^2 C_y(T). \tag{5.103}$$

Effecting the change of variables $\tau \to T$ in the wake oscillator, Eq. 5.100, and again using the definition of $\varkappa$ yields

$$C_y''(T) + \varkappa f^*\left(\varkappa^{-1} C_y'(T)\right) C_y'(T) + \Omega^2 \varkappa^2 C_y(T) = \varkappa b\left(\varkappa^{-1}\Xi'(T)\right)\Xi'(T). \tag{5.104}$$

Following Berger and Plaschko [5], only the first two terms are retained in each of the power series representations for $\delta\left(\Xi'(\tau)\right)$, $f^*\left(C_y'(\tau)\right)$, and $b\left(\Xi'(\tau)\right)$. Accordingly,

$$\begin{aligned}
\delta\left(\Xi'(\tau)\right) &= \delta_0 + \delta_2 \Xi'^2(\tau), \\
f^*\left(C_y'(\tau)\right) &= \alpha_0 + \alpha_2 C_y'^2(\tau), \text{ with } \alpha_0 < 0 \text{ and } \alpha_2 > 0, \\
b\left(\Xi'(\tau)\right) &= b_0 + b_2 \Xi'^2(\tau).
\end{aligned}$$

In terms of T, these become

$$\begin{aligned}
\delta\left(\varkappa^{-1}\Xi'(T)\right) &= \delta_0 + \delta_2 \varkappa^{-2} \Xi'^2(T), \\
f^*\left(\varkappa^{-1} C_y'(T)\right) &= \alpha_0 + \alpha_2 \varkappa^{-2} C_y'^2(T), \text{ with } \alpha_0 < 0 \text{ and } \alpha_2 > 0,
\end{aligned}$$

and

$$b\left(\varkappa^{-1}\Xi'(T)\right) = b_0 + b_2 \varkappa^{-2} \Xi'^2(T).$$

Substitution of the truncated expansions into Eqs. 5.103 and 5.104 yields

$$\Xi''(T) + \varkappa\left[\delta_0 + \delta_2 \varkappa^{-2} \Xi'^2(T)\right]\Xi'(T) + \varkappa^2 \Xi(T) = a\Omega^2 \varkappa^2 C_y(T)$$

and

$$\begin{aligned}
C_y''(T) + \varkappa\left[\alpha_0 + \alpha_2 \varkappa^{-2} C_y'^2(T)\right] C_y'(T) + \Omega^2 \varkappa^2 C_y(T) \\
= \varkappa\left[b_0 + b_2 \varkappa^{-2} \Xi'^2(T)\right]\Xi'(T),
\end{aligned}$$

respectively. After rearrangement, one finds

$$\Xi''(T) + \left[\delta_0 \varkappa + \delta_2 \varkappa^{-1} \Xi'^2(T)\right]\Xi'(T) + \varkappa^2 \Xi(T) = a\Omega^2 \varkappa^2 C_y(T), \tag{5.105}$$

and

$$\begin{aligned}
C_y''(T) + \left[\alpha_0 \varkappa + \alpha_2 \varkappa^{-1} C_y'^2(T)\right] C_y'(T) + \Omega^2 \varkappa^2 C_y(T) \\
= b_0 \varkappa \Xi'(T) + b_2 \varkappa^{-1} \Xi'^3(T),
\end{aligned} \tag{5.106}$$

respectively.

Noting that

$$a\Omega^2\varkappa^2 = a\left(\frac{f_{st}}{f_n^{(vac)}}\right)^2\left(\frac{2\pi f_n^{(vac)}}{2\pi f_{st}}\right)^2 = a, \tag{5.107}$$

Equation 5.105 can be rewritten as

$$\Xi''(T) + \delta_0\varkappa\Xi'(T) + \varkappa^2\Xi(T) + \delta_2\varkappa^{-1}\Xi'^3(T) = aC_y(T). \tag{5.108}$$

Returning to Eq. 5.55, consider rewriting it in the form

$$\begin{aligned} &m_c\ddot{\chi}(t) + c^{(vac)}\dot{\chi}(t) + k_s^{(y)}\chi(t) \\ &= \frac{1}{2}\rho DLC_d\left|\dot{w}(t) - \dot{\chi}(t)\right|\left[\dot{w}(t) - \dot{\chi}(t)\right] + m_d(1 + C_a)\ddot{w}(t) - m_d C_a\ddot{\chi}(t). \end{aligned} \tag{5.109}$$

The RHS of Eq. 5.109 simply manifests the assumed form for

$$F_{fl/st}^{(y)}(t) = \frac{1}{2}\rho U_o^2 DLC_y(t)$$

(see Eq. 5.51). Thus, Eq. 5.109 is equivalent to

$$m_c\ddot{\chi}(t) + c^{(vac)}\dot{\chi}(t) + k_s^{(y)}\chi(t) = \frac{1}{2}\rho U_o^2 DLC_y(t).$$

Nondimensionalization of this equation yields

$$\Xi''(T) + 2\zeta^{(vac)}\left(\frac{\omega_n^{(vac)}}{\omega_{st}}\right)\Xi'(T) + \left(\frac{\omega_n^{(vac)}}{\omega_{st}}\right)^2\Xi(T) = \frac{1}{2}\frac{\rho U_o^2 L}{m_c\omega_{st}^2}C_y(T). \tag{5.110}$$

Upon using the definitions of $\hat{m}^*$ and $V_r^{(vac)}$, Eq. 5.110 can be written as

$$\Xi''(T) + 2\zeta^{(vac)}\left(\frac{\omega_n^{(vac)}}{\omega_{st}}\right)\Xi'(T) + \left(\frac{\omega_n^{(vac)}}{\omega_{st}}\right)^2\Xi(T) = \frac{1}{2\pi^3}\hat{m}^* V_r^{(vac)^2}\left(\frac{\omega_n^{(vac)}}{\omega_{st}}\right)^2 C_y(T). \tag{5.111}$$

Finally, upon introducing Ω from Eq. 5.101 and $\varkappa$ from Eq. 5.102 into Eq. 5.111, one obtains

$$\Xi''(T) + 2\zeta^{(vac)}\varkappa\Xi'(T) + \varkappa^2\Xi(T) = a\Omega^2\varkappa^2 C_y(T) = aC_y(T), \tag{5.112}$$

where the final equality follows from Eq. 5.107.

Comparing Eqs. 5.108 and 5.112, it is evident that the right-hand sides are the same. That the RHS of each equation lacks terms proportional to $C_y''(T)$ and/or $C_y'(T)$ is of little surprise. The lift coefficient is, after all, a dimensionless force. If its time derivatives were included, then the LHS of Eq. 5.109 would necessarily involve

terms proportional to $\Xi^{iv}(T)$ and/or $\Xi'''(T)$ when nondimensionalized. These terms are not physically reasonable.

The cubic damping term of Eq. 5.108 is not reproduced in Eq. 5.109. As was previously mentioned, the form of the drag term in Eq. 5.109 must be such that it guarantees the invariance of said equation to a rotation of the coordinate system about the axis of symmetry x. Acceptable modifications to the current form of the drag term are then: (i) a linearization of the drag term, resulting in a term proportional to $\left[W'(T) - \Xi'(T)\right]$, (ii) a representation in higher order odd powers of $\left[W'(T) - \Xi'(T)\right]$, and (iii) a superposition of (i) and (ii).

Additionally, a term consisting of the superposition of the existing drag term and (i) or (ii), or the existing drag term and both (i) and (ii), can be constructed. The addition of a term that is proportional to $\Xi'^{3}(T)$ would therefore constitute an acceptable modification to the RHS of Eq. 5.109. This term might be introduced by assuming that the lift coefficient is represented by $\hat{C}_y(t) = C_y(t) - \kappa\,\Xi'^{3}(T)$, where $C_y(t)$ is determined from Eq. 5.51. The $\kappa\,\Xi'^{3}(T)$ term would then appear in Eq. 5.112, thus cementing its correspondence with Eq. 5.108. Given the complexity of the existing drag term in Eq. 5.109, such a modification is not carried out here.

Turning to the wake oscillators, a comparison of Eq. 5.75,

$$\begin{aligned} &W''(T) + \left[(2\pi S)^2 \hat{b}_3 W'^2(T) - \hat{b}_2\right] W'(T) + W(T) \\ &= -3(2\pi S)^2 b_4 \left[W'(T)\,\Xi'^2(T) - \Xi'(T)\,W'^2(T)\right] \\ &\qquad + (2\pi S)^2 \hat{b}_3 \Xi'^3(T) - \hat{b}_2 \Xi'(T), \end{aligned} \tag{5.113}$$

and Eq. 5.106 reveals many similarities. Noting again that

$$\Omega^2 \left(\frac{\omega_n^{(vac)}}{\omega_{st}}\right)^2 = \Omega^2 \varkappa^2 = \left(\frac{2\pi\omega_{st}}{2\pi\omega_n^{(vac)}}\right)^2 \left(\frac{\omega_n^{(vac)}}{\omega_{st}}\right)^2 = 1,$$

Equation 5.106 can be rewritten as

$$\begin{aligned} &C_y''(T) + \left[\alpha_0 \varkappa + \alpha_2 \varkappa^{-1} C_y'^2(T)\right] C_y'(T) + C_y(T) \\ &\qquad = b_0 \varkappa \Xi'(T) + b_2 \varkappa^{-1} \Xi'^3(T). \end{aligned} \tag{5.114}$$

Suppose that

$$\alpha_0 \frac{\omega_n^{(vac)}}{\omega_{st}} = \alpha_0 \varkappa = -B_0,$$

and

$$\alpha_2 \frac{\omega_{st}}{\omega_n^{(vac)}} = \alpha_2 \varkappa^{-1} = (2\pi S)^2 B_2,$$

where B_0, $B_2 > 0$. Note that the signs are preserved since $\alpha_0 < 0$ and $\alpha_2 > 0$. Upon substituting these definitions into Eq. 5.114, one obtains

$$C_y''(T) + \left[(2\pi S)^2 B_2 C_y'^2(T) - B_0\right] C_y'(T) + C_y(T) = b_0 \varkappa \Xi'(T) + b_2 \varkappa^{-1} \Xi'^3(T). \tag{5.115}$$

The LHS of this equation now has the same form as the LHS of Eq. 5.113.

Consider the case in which

$$\alpha_0 = b_0,$$

and

$$\alpha_2 = b_2.$$

It follows, then, that

$$\alpha_0 \varkappa = b_0 \varkappa = -B_0,$$

and

$$\alpha_2 \varkappa^{-1} = b_2 \varkappa^{-1} = (2\pi S)^2 B_2.$$

Under this special set of conditions, Eq. 5.115 becomes

$$C_y''(T) + \left[(2\pi S)^2 B_2 C_y'^2(T) - B_0\right] C_y'(T) + C_y(T) = -B_0 \Xi'(T) + (2\pi S)^2 B_2 \Xi'^3(T).$$

This equation is identical in form to Eq. 5.113 when $f_{NL}\left(W'(T), \Xi'(T)\right) = 0$.

Thus, the general form of Berger's equations can be obtained as a special case of the model equations presented here. It is again found, however, that $f_{NL}\left(W'(T), \Xi'(T)\right)$ must equal zero for the best agreement.

5.4.6 *Tamura and Matsui (1979)*

In Ref. [25], Tamura and Matsui present a modified Birkhoff wake-oscillator and the equation of motion for an elastically mounted cylinder as a system of simultaneous equations. The length $L_{w.o.}$ of the wake-oscillator is variable[7] and this translates into the presence of a parametric damping term in the fluid-oscillator equation.

Letting α denote the angular displacement of the fluid-oscillator (see Fig. 5.4), the time evolution equation in α is given by

[7] However, the time rate of change of the length, $\dot{L}_{w.o.}$, is neglected for simplicity.

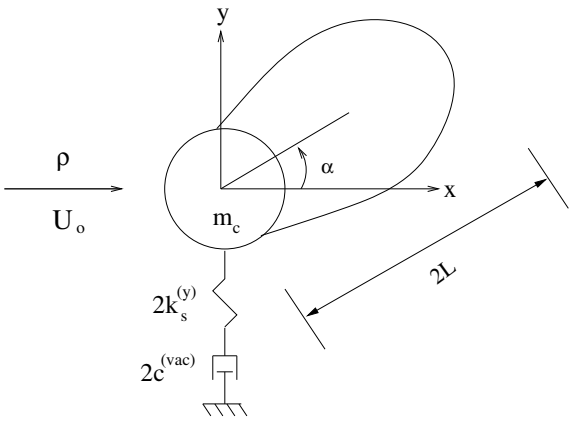

Fig. 5.4 The relevant physical parameters of the Tamura–Matsui model

$$\bar{I}\ddot{\alpha} - \bar{C}\left(1 - P\alpha^2\right)\dot{\alpha} + \bar{K}\left(\alpha + \frac{\dot{\chi}}{U_o}\right) = -\frac{\bar{I}}{\left(0.5D + \bar{L}_{w.o.}\right)}\ddot{\chi}. \tag{5.116}$$

$\bar{I}$ is the mean moment of inertia of the wake-oscillator about the center of the cylinder, $\bar{C}$ is the mean damping coefficient representing the effects of discharged vortices, $\bar{K}$ is the mean coefficient of the fluid dynamic restoring force, P is the coefficient of the nonlinear damping mechanism, and $\bar{L}_{w.o.}$ is the mean length of the wake-oscillator. The rationale behind the $\bar{K}\left(\alpha + \frac{\dot{\chi}}{U_o}\right)$ term is that horizontal motion of the cylinder changes the relative angle over which the fluid dynamic restoring force must act.

The equation of motion for the elastically mounted cylinder is given as

$$m_c\ddot{\chi} + c^{(vac)}\dot{\chi} + k_s^{(y)}\chi\,(t) = -\frac{1}{2}f\rho U_o^2 DL\left(\alpha + \frac{\dot{\chi}}{U_o}\right) - \frac{1}{2}\rho\sqrt{U_o^2 + \dot{\chi}^2}DLC_d\dot{\chi}, \tag{5.117}$$

where $f \simeq 1.16$ is a proportionality constant related to the experimentally observed relationship[8] between the Magnus effect lift and wake angular displacement for a rotating cylinder, and $C_d = 1.2$ is the drag coefficient. For a stationary cylinder, the lift coefficient C_y is assumed to be $C_y = -f\alpha$, while for the self-excited cylinder $C_y = -f(\alpha + \frac{\dot{\chi}}{U_o})$.

Physically, the first term on the RHS of Eq. 5.117 represents the lift force, while the second term represents the transverse (y) component of the drag force.

Tamura and Matsui apply the simplification

$$-\frac{1}{2}\rho\sqrt{U_o^2 + \dot{\chi}^2}DLC_d\dot{\chi} \simeq -\frac{1}{2}\rho U_o DLC_d\dot{\chi},$$

[8]The reader may wish to peruse Ref. [13]. Curiously, the authors find that $f = 1.15$ (C_s in their notation) for the case of a spinning football whose trajectory is tracked in three dimensions.

which is based on the assumption $U_o \gg \dot{\chi}$. Implementing this approximation in Eq. 5.117 yields

$$m_c\ddot{\chi} + c^{(vac)}\dot{\chi} + k_s^{(y)}\chi\,(t) = -\frac{1}{2}f\rho U_o^2 DL\left(\alpha + \frac{\dot{\chi}}{U_o}\right) - \frac{1}{2}\rho U_o DLC_d\dot{\chi}. \quad (5.118)$$

Nondimensionalizing Eqs. 5.116 and 5.118 yields

$$\bar{I}\omega_{st}^2\alpha''\,(T) - \bar{C}\left[1 - P\alpha^2\,(T)\right]\omega_{st}\alpha'\,(T) + \bar{K}\left[\alpha\,(T) + \frac{D\omega_{st}\Xi'\,(T)}{U_o}\right] = -\frac{\bar{I}}{\left(0.5D + \bar{L}_{w.o.}\right)}D\omega_{st}^2\Xi''\,(T),$$

and

$$m_c D\omega_{st}^2\Xi''\,(T) + c^{(vac)}D\omega_{st}\Xi'\,(T) + k_s^{(y)}D\Xi\,(T) = -\frac{1}{2}f\rho U_o^2 DL\left(\alpha + \frac{D\omega_{st}\Xi'\,(T)}{U_o}\right) - \frac{1}{2}\rho U_o DLC_d D\omega_{st}\Xi'\,(T),$$

respectively. Upon simplifying the above equations, one obtains

$$\alpha''\,(T) - \frac{\bar{C}}{\omega_{st}\bar{I}}\left[1 - P\alpha^2\,(T)\right]\alpha'\,(T) + \frac{\bar{K}}{\omega_{st}^2\bar{I}}\alpha\,(T) = -\frac{\bar{K}D}{U_o\omega_{st}\bar{I}}\Xi'\,(T) - \frac{1}{\left(0.5D + \bar{L}_{w.o.}\right)}D\Xi''\,(T), \quad (5.119)$$

and

$$\Xi''\,(T) + \left[2\zeta^{(vac)}\frac{\omega_n^{(vac)}}{\omega_{st}} + 2\hat{m}^*\,(f + C_d)\frac{U_o}{D\pi\omega_{st}}\right]\Xi'\,(T) + \frac{\omega_n^{(vac)^2}}{\omega_{st}^2}\Xi\,(T) = -\frac{1}{2}\frac{f\rho U_o^2 L}{\omega_{st}^2 m_c}\alpha, \quad (5.120)$$

respectively.

Defining

$$\omega_{st} = \sqrt{\frac{\bar{K}}{\bar{I}}}$$

$$\zeta_{w.o.} = \frac{\bar{C}}{2\omega_{st}\bar{I}}$$

and

$$\upsilon = \frac{1}{\left(0.5D + \bar{L}_{w.o.}\right)} D,$$

Equation 5.119 can be rewritten as

$$\alpha''(T) - 2\zeta_{w.o.}\left[1 - P\alpha^2(T)\right]\alpha'(T) + \alpha(T) = -\frac{D\omega_{st}}{U_o}\Xi'(T) - \upsilon\Xi''(T). \tag{5.121}$$

However,

$$-\frac{D\omega_{st}}{U_o} = -2\pi S,$$

and Eq. 5.121 can also be written as

$$\alpha''(T) - 2\zeta_{w.o.}\left[1 - P\alpha^2(T)\right]\alpha'(T) + \alpha(T) = -2\pi S\Xi'(T) - \upsilon\Xi''(T). \tag{5.122}$$

Turning to Eq. 5.118, one finds that it can be expressed in the form

$$\Xi''(T) + \left[2\zeta^{(vac)}\varkappa + 4\hat{m}^*(f + C_d)S\right]\Xi'(T) + \varkappa^2\Xi(T) = -\frac{f\hat{m}^*}{2\pi^2 S^2}\alpha, \tag{5.123}$$

where $\varkappa$ of Eq. 5.102 has been used.

In order to compare Eqs. 5.123 and 5.55, the latter is first rewritten in the following way by using the corresponding parameters from Table 5.2[9]

$$\begin{aligned}\Xi''(T) + \frac{2\zeta^{(vac)}}{\left(1 + \hat{m}^* C_a\right)}\left(\frac{\omega_n^{(vac)}}{\omega_{st}}\right)\Xi'(T) + \left(\sqrt{\frac{1}{\left(1 + \hat{m}^* C_a\right)}}\frac{\omega_n^{(vac)}}{\omega_{st}}\right)^2\Xi(T) \\ = \frac{2}{\pi}\frac{\hat{m}^*}{\left(1 + \hat{m}^* C_a\right)} C_d\left|W'(T) - \Xi'(T)\right|\left[W'(T) - \Xi'(T)\right] \\ + \frac{\hat{m}^*}{\left(1 + \hat{m}^* C_a\right)}(1 + C_a)W''(T).\end{aligned} \tag{5.124}$$

Next, let $\hat{m}^* C_a \simeq 0$ (i.e., assume the experiments are conducted in air). In this case, Eq. 5.124 reduces to

$$\begin{aligned}\Xi''(T) + 2\zeta^{(vac)}\varkappa\Xi'(T) + \varkappa^2\Xi(T) \\ = \frac{2}{\pi}\hat{m}^* C_d\left|W'(T) - \Xi'(T)\right|\left[W'(T) - \Xi'(T)\right] + \hat{m}^* W''(T).\end{aligned} \tag{5.125}$$

It is apparent that (i) a linearization of the drag term in Eq. 5.125 would lead to a LHS that closely resembles the LHS of Eq. 5.123, (ii) the displacement coupling

[9] Use the relation $\frac{\omega_n^{(true)}}{\omega_n^{(vac)}} = \sqrt{\frac{1}{1+\hat{m}^* C_a}}$, which can be easily derived.

present in Eq. 5.123 is not a feature of Eq. 5.125, and the acceleration coupling present in Eq. 5.125 is not a feature of Eq. 5.123.

Comparing Eqs. 5.122 and 5.75, it is evident that if only the linear term on the RHS of the latter is retained, the expressions are rendered quite similar. Indeed,

$$W''(T) + \left[(2\pi S)^2 \hat{b}_3 W'^2(T) - \hat{b}_2\right] W'(T) + W(T) = -\hat{b}_2 \Xi'(T), \quad (5.126)$$

is qualitatively similar to Eq. 5.122. However, that acceleration coupling of Eq. 5.123 is not a feature that is reproduced by Eq. 5.126.

5.5 Discussion

Nonlinear wake-oscillator models have been shown to be leading order approximations for the vortex shedding instability from a fixed cylinder in uniform flow [1], while wake-body models have been shown to represent the same type of leading order approximation for forced oscillations of circular cylinders in uniform flows [23]. These findings imply that these models have, at least to some degree, fluid dynamical origins. It is precisely because of these fluid dynamical origins that wake-body models have been successful. However, by the very nature of being leading order approximations to a very complex interaction, they have limitations. The methodology presented in this chapter serves to address both of these aspects. The fluid dynamical origins can be accounted for since the starting variational principle is rigorous. The limitations are accounted for because any assumptions made in reducing the variational principle are explicitly stated.

Section 5.1.2 has shown that the wake-body model derived from the proposed methodology shares many qualitative features with the three comparison models chosen from the literature. One can argue that the comparison models are special cases of the derived models. This follows from the fact that the derived model is found to involve terms that do not appear in the comparison models. These additional terms are, for the most part, the autoparametric terms. It is not the aim of this paper to weigh in on the issue of whether or not these terms should be retained. Suffice it to say that many authors have previously addressed the inadequacy of linear coupling terms in wake-body models (e.g., Refs. [6, 17]).

There are terms in the comparison models that are not captured in the *derived model. This is simply a manifestation*of the assumed forms in Eqs. 5.51 and 5.52. Subject to a different set of assumptions, these equations could conceivably be modified such that the "missing" terms appear in the derived model. It cannot be stressed enough that these modifications would need to be justified. This is, in essence, the embodiment of the advantage of the method presented in this chapter, and this book generally: That while the wake-body models still contain arbitrary coefficients, their forms are arrived at by a line of reasoning, rather than a "hit or miss" approach.

The authors believe that this approach can be implemented in other fluid–structure interaction problems. The possibility of applying it to derive wake-body models for elastic structures in uniform and shear flows is something that is possible with much work. The current chapter was based on variational methods where the variation was a virtual displacement. Based on these derivations, a flow-oscillator set of equations was formulated. In the next two chapters, a variational approach based on virtual velocities is formulated, where we first relate Lagrangian variables to Eulerian variables.

References

1. Albarède P, Monkewitz PA (1992) A model for the formation of oblique shedding and "chevron" patterns in cylinder wakes. Phys Fluids A: Fluid Dyn 4(4):744–756
2. Batchelor GK (1967) An Introduction to Fluid Dynamics. Cambridge University Press, New York
3. Benaroya H, Wei T (2000) Hamilton's principle for external viscous fluid structure interactions. J Sound Vib 238(1):113–145
4. Berger E (1988) On a mechanism of vortex excited oscillations of a cylinder. J Wind Eng Ind Aerodyn 28(1–3):301–310
5. Berger E, Plaschko P (1993) Hopf bifurcations and hysteresis in flow-induced vibrations of cylinders. J Fluids Struct 7(8):849–866
6. Billah KYR (1989) A study of vortex-induced vibration. PhD thesis, Princeton University
7. Blevins RD (1977) Flow-Induced vibration. Van Nostrand Reinhold Co, New York
8. Currie IG (2003) Fundam Mech Fluids. Marcel Dekker Inc, New York
9. Dost S, Tabarrok B (1979) Application of Hamilton's principle to large deformation and flow problems. J Appl Mech 46:285–290
10. Facchinetti ML, de Langre E, Biolley F (2004) Coupling of structure and wake oscillators in vortex-induced vibrations. J Fluids truct 19(2):123–140
11. Gabbai RD (2006) Hamilton's principle for fluid-structure interaction and applications to the free-vibration of an elastically-mounted cylinder. PhD dissertation, Rutgers, the State University of New Jersey, New Brunswick, NJ
12. Gabbai RD, Benaroya H (2005) An overview of modeling and experiments of vortex-induced vibration of circular cylinders. J Sound Vib 282:575–616
13. Griffiths I, Evans C, Griffiths N (2005) Tracking the flight of a spinning football in three dimensions. Meas Sci Technol 16(10):2056–2065
14. Hall SA (1981) Vortex-Induced vibrations of structures. PhD dissertation, California Institute of Technology
15. Hartlen RT, Currie IG (1970) Lift-oscillator model of vortex induced vibration. J Eng Mech 96(5):577–591
16. Iwan WD, Blevins RD (1974) A model for vortex induced oscillation of structures. J Appl Mech 41:581–586
17. Krenk S, Nielsen SRK (1999) Energy balanced double oscillator model for vortex-induced vibrations. J Eng Mech 125:263–271
18. Leech CM (1977) Hamilton's principle applied to fluid mechanics. Quart J Mech Appl Math 30:107–130
19. Malvern LE (1969) Introduction to the mechanics of a continuous medium. Prentice Hall, Englewood Cliffs, NJ
20. McIver DB (1973) Hamilton's principle for systems of changing mass. J Eng Mech 7(3):249–261

21. Noca F (1997) On the evaluation of time-dependent fluid-dynamic forces on Bluff Bodies. PhD dissertation, California Institute of Technology
22. Sarpkaya T (2004) A critical review of the intrinsic nature of vortex-induced vibrations. J Fluids Struct 19(4):389–447
23. Skop RA, Balasubramanian S (1995) A nonlinear oscillator model for vortex shedding from a forced cylinder. Part 1: uniform flow and model parameters. Int J Offshore Polar Eng 5(4):251–255
24. Skop RA, Balasubramanian S (1997) A new twist on an old model for vortex-excited vibrations. J Fluids Struct 11(4):395–412
25. Tamura Y, Matsui G (1980) Wake-oscillator model for vortex-induced oscillation of a circular cylinder. In: Cermak JE (ed) Proceedings of the fifth international conference on wind engineering (Fort Collins, CO, USA). Pergamon Press, New York, pp 1085–1094
26. Vikestad K, Vandiver JK, Larsen CM (2000) Added mass and oscillatory frequency for a circular cylinder subjected to vortex-induced vibrations and external disturbance. J Fluids Struct 14(7):1071–1088
27. Williamson CHK, Govardhan R (2004) Vortex-induced vibrations. Ann Rev Fluid Mech 36:413–455
28. Xing JT, Price WG (1997) Variational principles of nonlinear dynamical fluid-solid interaction systems. Philosophical transactions of the royal society of London. Series A: mathematical, physical and engineering sciences, 355(1726):1063–1095

Chapter 6
Eulerian and Lagrangian Descriptions

Abstract This chapter derives the relations between Eulerian and Lagrangian descriptions of displacement and velocity fields, relations between the time derivatives of system properties, variations, and introduces Jourdain's variational principle. Jourdain's principle is then applied to viscous incompressible fluids, and the derivation of the energy rate equation. These equations will be utilized in the subsequent chapter for the derivation of the flow-oscillator model for vortex-induced vibration.

6.1 Introduction

Our goal in this chapter and the next is the same as it was in the last chapter. Except here, we wish to operate in the domain of the fluid. That is, we intend to operate in the Eulerian frame of reference. Given that the flow is more complex than the structural oscillations, an Eulerian framework makes sense, but requires that our Lagrangian variational principles be transformed into the Eulerian frame. This challenge is met in this chapter, and then utilized for VIV in the next chapter.

In classical mechanics, one has two alternative descriptions to observe and analyze dynamic systems: the Lagrangian description and the Eulerian description. The Lagrangian reference frame has long been used in solid mechanics, while the Eulerian reference frame has been preferred in fluid mechanics. The fact that the first principles of mechanics are defined in the Lagrangian reference frame is the main advantage of this description. Then again, it has been shown that the equations of motion (EOM) of fluid systems become less complicated in the Eulerian reference frame.

In the Lagrangian frame, also called the particle description or material coordinate, one observes the trajectories of specific particles during some interval of time. Consequently, a set of coordinates, which are usually the initial positions, are tagged to a set of particles and the resulting EOM are differential equations of the trajectories (paths) of those particles. The Lagrangian trajectories, $\boldsymbol{r}$, can be expressed as

$$\boldsymbol{r} = \boldsymbol{r}\left(\boldsymbol{A}, t\right), \tag{6.1}$$

S. Mottaghi et al., *An Analytical Mechanics Framework for Flow-Oscillator Modeling of Vortex-Induced Bluff-Body Oscillations*, Solid Mechanics and Its Applications 260,
https://doi.org/10.1007/978-3-030-26133-7_6

where $\boldsymbol{A}$ is the vector of initial positions and t is time. The elements of $\boldsymbol{A}$ are constant coordinates and therefore $\boldsymbol{r}$ has coordinates that depend on t.

The Eulerian frame of reference, also called the space-fixed coordinate or configuration frame, describes a system at some fixed points in space. Unlike the Lagrangian coordinates, the Eulerian coordinates are not carried by the particles, and they remain unaltered by the physics of the problem. Therefore, the EOM represent the dynamics of the particles that occupy the spatial frame as functions of time. The Eulerian coordinates, $\boldsymbol{x}$, are independent of time, t.

Generally, the transformation of the first principles of mechanics from the Lagrangian frame to the Eulerian description is based on three conditions [19]:

1. The velocity obtained from both frames must be equal to each other at a given time and a given spatial position. This is very clear since an actual flow particle has a unique velocity at any instant.
2. Similar to velocities, the time derivatives of the fluid properties obtained from either one of the representations must match the other one at a given time and spatial position.
3. The time derivative of an integral of a function over a moving material volume can be related to an integral of that function over an arbitrary control volume using Reynolds transport theorem.

The majority of the challenges in applying the first principles of mechanics to systems of fluids are due to the difficulties in satisfying the above conditions. These difficulties are explored in more detail in the following sections.

6.2 Relating the Displacement Fields

The displacement field in the Lagrangian frame is defined by the particle trajectories, Eq. 6.1. In fluid mechanics, they are referred to as *pathlines*. The trajectories of the particles, as they are treated in the Lagrangian frame of reference, do not have an exact equivalent Eulerian concept, as the Eulerian coordinates are independent of time. The closest concept to pathlines is the existence of a function that maps the current state of the particles to an earlier configuration. For convenience, the earlier state can be chosen to be the initial configuration. Therefore, the Eulerian mapping function can be expressed as

$$\boldsymbol{A} = \boldsymbol{A}(\boldsymbol{x}, t). \tag{6.2}$$

In order to relate this mapping function to particle trajectories, assumptions must be made that the mapping from $\boldsymbol{A}$ to $\boldsymbol{r}$ is continuous and unique such that two adjacent particles will never be separated and neither particle will coexist at the same position at the same time. These assumptions are the basis of continuum mechanics, and they require the field to be a smooth continuum down to an arbitrarily small spatial scale. If these assumptions hold, then the relation between $\boldsymbol{A}$ and $\boldsymbol{r}$ can be expressed by [19]

$$\boldsymbol{r} = \boldsymbol{r}(\boldsymbol{A}, t) \quad \Leftrightarrow \quad \boldsymbol{A} = \boldsymbol{A}(\boldsymbol{r}, t), \tag{6.3}$$

where $\boldsymbol{A}(\boldsymbol{r}, t)$ is the inverse of $\boldsymbol{r}(\boldsymbol{A}, t)$. The importance of Eq. 6.3 will become clearer when considering the velocity transformation example of the next section.

6.3 Relating the Velocity Fields

As mentioned earlier, the velocities obtained by using any observation frame must match the real velocity field. Denoting the velocity field in the Lagrangian frame by

$$\boldsymbol{v}(\boldsymbol{A}, t) = \frac{d\boldsymbol{r}(\boldsymbol{A}, t)}{dt}, \tag{6.4}$$

and in the Eulerian frame by $\boldsymbol{u}(\boldsymbol{x}, t)$, then it must be true that

$$\boldsymbol{v}(\boldsymbol{A}, t) = \boldsymbol{u}(\boldsymbol{x}, t)|_{\boldsymbol{x}=\boldsymbol{r}}, \tag{6.5}$$

or, alternatively that

$$\boldsymbol{u}(\boldsymbol{x}, t) = \boldsymbol{v}[\boldsymbol{A}(\boldsymbol{r}, t), t]|_{\boldsymbol{r}=\boldsymbol{x}}. \tag{6.6}$$

In order to make these relations more clear, we consider the following simple example.

Example 1 We assume that the Eulerian velocity field of a one-dimensional flow is known to be

$$u(x, t) = -\alpha x + \beta t, \tag{6.7}$$

where α and β are known constants, and the equation is expressed by scalar variables since the flow is one dimensional.

We wish to obtain the Lagrangian velocity field. Using Eq. 6.5, we can write

$$v(A, t) = u(r, t) \quad \Rightarrow \quad v(A, t) = -\alpha r + \beta t. \tag{6.8}$$

Lagrangian coordinates $r = r(A, t)$ are functions of only time, since the initial positions are fixed. Therefore, the velocity $v(A, t)$ is obtained by differentiating r with respect to time, resulting in

$$v(A, t) = \frac{dr(A, t)}{dt} = -\alpha r(A, t) + \beta t \tag{6.9a}$$

$$r(A, t = 0) = A, \tag{6.9b}$$

which is an ordinary differential equation (ODE). Solving this ODE for r and differentiating it with respect to time, the Lagrangian velocity field is found to be

$$v(A, t) = -\alpha \left[\frac{\beta}{\alpha^2} + A\right] \exp(-\alpha t) + \frac{\beta}{\alpha}. \tag{6.10}$$

Now, we obtain the Eulerian velocity, Eq. 6.7, from Eq. 6.10. In order to utilize Eq. 6.6, the mapping function, $\boldsymbol{A}$, is required. Considering Eq. 6.3, the particle trajectories must be obtained first. This is done by integrating Eq. 6.10 with respect to time and obtaining the constants of integration by imposing the initial conditions. The result is

$$r\left(A,t\right)=\left(\frac{\beta}{\alpha^2}+A\right)\exp\left(-\alpha t\right)+\frac{\beta}{\alpha^2}\left(\alpha t-1\right). \tag{6.11}$$

The mapping function, A, is the inverse function of Eq. 6.11, found to be

$$A\left(r,t\right)=\left[-\frac{\beta}{\alpha^2}\left(\alpha t-1\right)+r\right]\exp\left(\alpha t\right)-\frac{\beta}{\alpha^2}. \tag{6.12}$$

By substituting the mapping function from Eq. 6.12 into the Lagrangian velocity field Eq. 6.10 and replacing r with x, the Eulerian velocity field Eq. 6.7 is obtained.

In general, for two- or three-dimensional flow, these transformations are not as easy as the one-dimensional example here, as the differential equations are generally coupled. Moreover, the velocity field must be known in, at least, one of these configurations, that is, a problem must be first solved. Additionally, the initial positions are not observable for a fluid system, unlike for solids (for instance in theory of elasticity) [19].

6.4 Relating the Time Derivatives of the System Properties

The following notation for derivatives with respect to time has been adopted: d/dt represents the total derivative of a Lagrangian function, D/Dt denotes the material derivative of an Eulerian function, and $\partial/\partial t$ is the partial derivative with respect to time.

The Lagrangian trajectories, $\boldsymbol{r}\left(\boldsymbol{A},t\right)$, and velocities, $\boldsymbol{v}\left(\boldsymbol{A},t\right)$, are functions of initial positions and time. Therefore, their time derivatives are a simple differentiation with respect to time, holding the initial conditions fixed

$$\boldsymbol{v}\left(\boldsymbol{A},t\right)=\frac{d\boldsymbol{r}\left(\boldsymbol{A},t\right)}{dt},\qquad \boldsymbol{a}_L\left(\boldsymbol{A},t\right)=\frac{d\boldsymbol{v}\left(\boldsymbol{A},t\right)}{dt}=\frac{d^2\boldsymbol{r}\left(\boldsymbol{A},t\right)}{dt^2}, \tag{6.13}$$

where $\boldsymbol{a}_L\left(\boldsymbol{A},t\right)$ are the Lagrangian accelerations.

For the Eulerian description, functions are space-time dependent on the Eulerian velocity field. As these functions are essentially the system properties observed at fixed points in space, the advection of the properties must also be included. Therefore, the total derivative is considered to be the material derivative, defined as

$$\frac{D\left(\quad\right)}{Dt}=\frac{\partial\left(\quad\right)}{\partial t}+\boldsymbol{u}\cdot\nabla\left(\quad\right). \tag{6.14}$$

The term material derivative is used since this derivation is aimed to match the total derivative of a Lagrangian function, that is the material-fixed frame. As an example, the Eulerian acceleration, $\boldsymbol{a}$, can be obtained as

$$\boldsymbol{a}(\boldsymbol{x},t)=\frac{D\boldsymbol{u}(\boldsymbol{x},t)}{Dt}=\frac{\partial\boldsymbol{u}(\boldsymbol{x},t)}{\partial t}+\boldsymbol{u}(\boldsymbol{x},t)\cdot\nabla\boldsymbol{u}(\boldsymbol{x},t). \tag{6.15}$$

Since a fluid property obtained from any observational frame must match the unique real property of the system, the derivatives of a property function, say Φ, is

$$\frac{d\boldsymbol{\Phi}_L(\boldsymbol{A},t)}{dt}=\left.\frac{D\boldsymbol{\Phi}_E(\boldsymbol{x},t)}{Dt}\right|_{\boldsymbol{x}=\boldsymbol{r}}, \tag{6.16}$$

where $\boldsymbol{\Phi}_E(\boldsymbol{x},t)$ is the Eulerian representation of the Lagrangian function $\boldsymbol{\Phi}_L(\boldsymbol{A},t)$.

6.5 Reynolds Transport Theorem

The Reynolds Transport Theorem (RTT) is an effective tool to relate an integral over a system volume (SV), or material volume, to an integral over a control volume (CV). It can be thought of as the three-dimensional form of the Leibniz integral. The RTT can be applied to a scalar-valued spatial function, say $b(\boldsymbol{x},t)$, which is a quantity with units (1/mass). For a fixed control volume, the RTT is expressed as [3]

$$\frac{d}{dt}\int_{SV(t)}\rho b(\boldsymbol{x},t)\,dV(t)=\int_{CV}\left\{\frac{D[\rho b(\boldsymbol{x},t)]}{Dt}+\rho b(\boldsymbol{x},t)[\nabla\cdot\boldsymbol{u}]\right\}dV, \tag{6.17}$$

where ρ is the fluid density.

The RTT can be applied to a general moving and deforming control volume $CV(t)$ that contains a solid as well as a fluid. The general form of the RTT is given by

$$\frac{d}{dt}\int_{SV(t)}\rho b(\boldsymbol{x},t)\,dV(t)=\int_{CV(t)}\frac{\partial[\rho b(\boldsymbol{x},t)]}{\partial t}dV(t)+\int_{CS(t)}\rho b(\boldsymbol{x},t)[\boldsymbol{u}\cdot\boldsymbol{n}]\,dA(t), \tag{6.18}$$

where $CS(t)$ is a moving control surface. When using the RTT, the equations can often be simplified by utilizing the Gauss (divergence) theorem, that is,

$$\int_{CV}\nabla\cdot\boldsymbol{F}dV=\int_{CS}\boldsymbol{F}\cdot\boldsymbol{n}dA, \tag{6.19}$$

where $\boldsymbol{F}$ is a vector-valued spatial function. If including a scalar-valued function, say $h(\boldsymbol{x},t)$, it can be shown that Gauss' theorem will become

$$\int_{CV}(\boldsymbol{F}\cdot\nabla h+h\nabla\cdot\boldsymbol{F})\,dV=\int_{CS}h\boldsymbol{F}\cdot\boldsymbol{n}dA. \tag{6.20}$$

Alternatively, the RTT can be used for evaluating the rate of change of a real-valued spatial function, say $b(\boldsymbol{x}, t)$, of a control volume (not a control system) [3]:

$$\frac{D}{Dt}\int_{CV} b(\boldsymbol{x},t)dV = \int_{CV}\frac{\partial}{\partial t}\left[b(\boldsymbol{x},t)\right]dV + \int_{CS}\left[b(\boldsymbol{x},t)\right](\boldsymbol{v}_{CS}\cdot\boldsymbol{n})\,dA, \quad (6.21)$$

where $\boldsymbol{v}_{CS}$ is the velocity of the control surface element, dA, and where we have simplified the notation by removing the time arguments on the domains of integration.

The RTT can also be expressed in terms of the relative velocity, $\boldsymbol{u}_r$, defined as

$$\boldsymbol{u}_r = \boldsymbol{u} - \boldsymbol{v}_{CS} \;\Rightarrow\; \boldsymbol{v}_{CS} = \boldsymbol{u} - \boldsymbol{u}_r, \quad (6.22)$$

where $\boldsymbol{u}$ is the fluid velocity. Substituting $\boldsymbol{v}_{CS}$ from Eq. 6.22 into Eq. 6.21, we obtain

$$\frac{D}{Dt}\int_{CV} b dV = \int_{CV}\frac{\partial b}{\partial t}dV + \int_{CS} b\left((\boldsymbol{u}-\boldsymbol{u}_r)\cdot\boldsymbol{n}\right)dA, \quad (6.23)$$

which, by applying the divergence theorem, becomes

$$\begin{aligned}\frac{D}{Dt}\int_{CV} b dV &= \int_{CV}\left[\frac{\partial b}{\partial t} + \nabla\cdot(b\boldsymbol{u})\right]dV - \int_{CV} b\,(\boldsymbol{u}_r\cdot\boldsymbol{n})\,dA \\ &= \int_{CV}\left[\frac{\partial b}{\partial t} + \nabla b\cdot\boldsymbol{u} + b(\nabla\cdot\boldsymbol{u})\right]dV - \int_{CS} b\,(\boldsymbol{u}_r\cdot\boldsymbol{n})\,dA. \quad (6.24)\end{aligned}$$

For incompressible fluids, imposing the incompressibility condition, $\nabla\cdot\boldsymbol{u} = 0$, on Eq. 6.24, yields the RTT for a general control volume,

$$\frac{D}{Dt}\int_{CV} b dV = \int_{CV}\frac{\partial b}{\partial t}dV - \int_{CS} b\,(\boldsymbol{u}_r\cdot\boldsymbol{n})\,dA. \quad (6.25)$$

Moreover, if $b(\boldsymbol{x}, t)$ is a function of velocity $\boldsymbol{u}$, the RTT can be expressed in terms of $\boldsymbol{u}_r$ and $\boldsymbol{v}_{CS}$ as well.

Considering our discussions in this section, our goal is the derivation of a well-defined relation between the Lagrangian and Eulerian variational operators. However, relating the Lagrangian variation to the Eulerian variation faces challenges that are discussed next.

6.6 Lagrangian and Eulerian Variations

Gelfand and Fomin [5, p. 168] used a family of surface transformations and utilized an interim surface to obtain the relation between the Lagrangian variational operator, δ, and the Eulerian one, $\bar{\delta}$, as

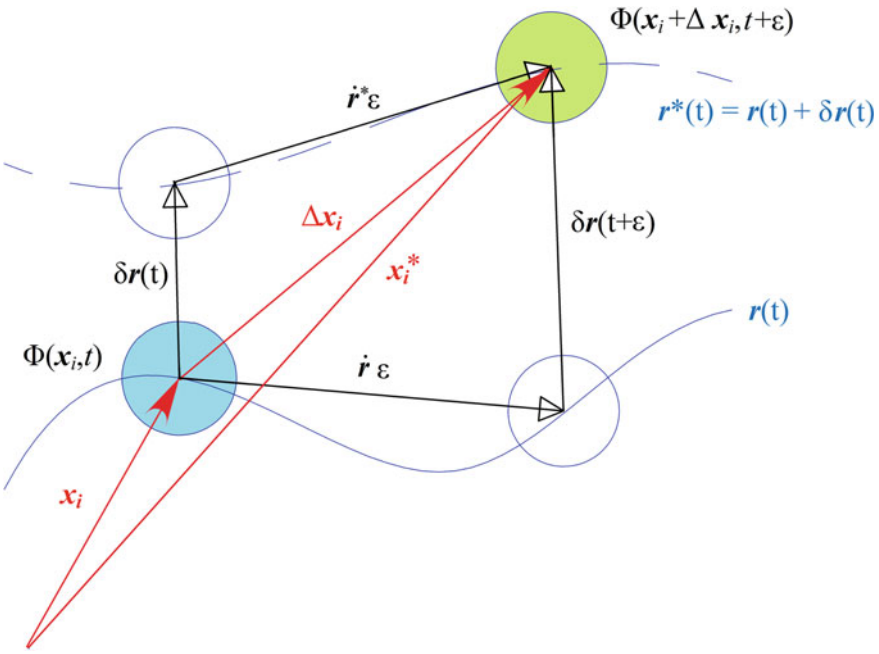

Fig. 6.1 Relating the Lagrangian and the Eulerian variational operators

$$\delta(\quad) = \bar{\delta}(\quad) + \delta x_i \frac{\partial(\quad)}{\partial x_i}. \tag{6.26}$$

While the reader is encouraged to view the mathematically rigorous derivations of Gelfand and Fomin, we will obtain this relation from a graphical point of view so as to clarify the physics of this transformation.

We start by considering a particle i with its known Lagrangian trajectory $\boldsymbol{r} = \boldsymbol{r}(\boldsymbol{A}_i, t)$, where $\boldsymbol{A}_i$ is the initial position of particle i. The Lagrangian path $\boldsymbol{r} = \boldsymbol{r}(\boldsymbol{A}_i, t)$ represents the position of particle i at time t, which was at the position $\boldsymbol{A}_i$ at time $t = 0$. Therefore, $\boldsymbol{r}$ represents the time-varying position of the particle in the same frame in which $\boldsymbol{A}_i$ was originally observed. Consequently, if $\boldsymbol{A}_i$ is Eulerian, $\boldsymbol{r}$ is the Eulerian position at time t.

By applying the virtual displacement $\delta\boldsymbol{r}$, the particle will be transferred to an imaginary path that differs from the actual path by $\delta\boldsymbol{r}$ for all time. Since $\delta\boldsymbol{r}$ are arbitrary infinitesimal vectors that are compliant with system constraints, the resulting new paths can be thought of as an alternative possible trajectories.

As mentioned earlier, the Lagrangian coordinates are time dependent, whereas, the Eulerian ones are time independent. Moreover, even though the virtual displacement, $\delta\boldsymbol{r}$, is imposed by holding time fixed ($\delta t = 0$), it gets carried away by the particle. This is due to the fact that it is imposed in a material frame. Therefore, one must include the advection effect in acquiring the Lagrangian–Eulerian variational relation.

Considering the particle i and its real path $\boldsymbol{r}$, let $\boldsymbol{r}^*$ be a possible alternative path that results by imposing the virtual displacement $\delta\boldsymbol{r}$, as shown in Fig. 6.1. We are interested in obtaining the resulting variation of a spatial function, say $\Phi(\boldsymbol{x}, t)$, due to an imposed $\delta\boldsymbol{r}$. In order to consider advection, we assume that the particle will move on path $\boldsymbol{r}^*$ during an infinitesimal virtual time, say ε. Denoting the difference in value of Φ between the virtual position, $\boldsymbol{r}^*(\boldsymbol{A}_i, t+\varepsilon)$, and actual position, $\boldsymbol{r} = \boldsymbol{r}(\boldsymbol{A}_i, t)$, by $\triangle\Phi$, we have

$$\triangle\Phi = \Phi(\boldsymbol{x}, t)|_{\boldsymbol{r}^*(\boldsymbol{A}_i, t+\varepsilon)} - \Phi(\boldsymbol{x}, t)|_{\boldsymbol{r}=\boldsymbol{r}(\boldsymbol{A}_i, t)}\,. \tag{6.27}$$

Using an Eulerian position vector, $\boldsymbol{x}$, we denote the actual position of the particle by $\boldsymbol{x}_i$, and the virtual position by $\boldsymbol{x}_i^*$. Therefore, the displacement vector, $\triangle\boldsymbol{x}_i$, is

$$\triangle\boldsymbol{x}_i = \boldsymbol{x}_i^* - \boldsymbol{x}_i. \tag{6.28}$$

Consequently, Eq. 6.27 can be modified using Eq. 6.28,

$$\triangle\Phi = \Phi(\boldsymbol{x}_i + \boldsymbol{\Delta x}_i, t+\varepsilon) - \Phi(\boldsymbol{x}_i, t). \tag{6.29}$$

Applying the Taylor expansion about $\boldsymbol{x}_i$ and t to the first term on the right-hand side of Eq. 6.29, we obtain

$$\triangle\Phi = \Phi(\boldsymbol{x}_i, t) + \varepsilon\left[\frac{\partial\Phi(\boldsymbol{x}', t')}{\partial t'}\right]\left\{\begin{matrix}\boldsymbol{x}' = \boldsymbol{x}_i\\ t' = t\end{matrix}\right\} + \boldsymbol{\Delta x}_i\left[\frac{\partial\Phi(\boldsymbol{x}', t')}{\partial \boldsymbol{x}'}\right]\left\{\begin{matrix}\boldsymbol{x}' = \boldsymbol{x}_i\\ t' = t\end{matrix}\right\} - \Phi(\boldsymbol{x}_i, t) + HOT, \tag{6.30}$$

where HOT stands for higher order terms. By definition of the variational operator, we have

$$\delta\Phi = \lim_{\varepsilon\to 0}\frac{\triangle\Phi}{\varepsilon}, \tag{6.31}$$

and therefore,

$$\delta\Phi = \lim_{\varepsilon\to 0}\left\{\frac{\varepsilon}{\varepsilon}\left[\frac{\partial\Phi(\boldsymbol{x}', t')}{\partial t'}\right]\left\{\begin{matrix}\boldsymbol{x}' = \boldsymbol{x}_i\\ t' = t\end{matrix}\right\} + \frac{\boldsymbol{\Delta x}_i}{\varepsilon}\left[\frac{\partial\Phi(\boldsymbol{x}', t')}{\partial \boldsymbol{x}'}\right]\left\{\begin{matrix}\boldsymbol{x}' = \boldsymbol{x}_i\\ t' = t\end{matrix}\right\} + \frac{HOT}{\varepsilon}\right\}. \tag{6.32}$$

By definition

$$\delta\boldsymbol{x}_i = \lim_{\varepsilon\to 0}\frac{\boldsymbol{\Delta x}_i}{\varepsilon}, \tag{6.33}$$

and

$$\bar{\delta}\Phi = \frac{\partial\Phi(\boldsymbol{x}, t)}{\partial t}, \tag{6.34}$$

since $\bar{\delta}\Phi$ is the local variation of function Φ for which $\delta \boldsymbol{x}_i$ acts as if it is a velocity. Therefore, by taking the limit of Eq. 6.32, $\delta\Phi$ is obtained as

$$\delta\Phi(\boldsymbol{x}, t) = \bar{\delta}\Phi(\boldsymbol{x}, t) + \delta \boldsymbol{x}_i \frac{\partial \Phi(\boldsymbol{x}, t)}{\partial \boldsymbol{x}_i}, \tag{6.35}$$

which is the same as Eq. 6.26.

As is apparent in Eq. 6.35, the Lagrangian variation in the Eulerian frame becomes a mixed Lagrangian–Eulerian variation. This is because in the Eulerian description the coordinates are fixed in space, and thus no variation is permitted on the displacement field. Therefore, $\delta \boldsymbol{x}_i$ is an Eulerian representation of a Lagrangian virtual displacement. This introduces major difficulties when modeling fluid systems, as is explained in the next section where some other challenges are also discussed.

6.7 Challenges Faced Using Virtual Displacement

In relating the equations of the solid to the fluid, requiring the relation of the Lagrangian descriptions to the Eulerian ones has its own challenges. Initially, these difficulties manifest themselves in relating the Eulerian and the Lagrangian variational operators, since the Lagrangian concept of virtual displacement does not have an Eulerian counterpart. Some of the main challenges are discussed in this section.

As mentioned in Sect. 6.3, the existence of backtracking steps is required in these types of problems. The reason is clear from the simple velocity transformation example in Sect. 6.3. As evident from our analysis (Eqs. 6.5–6.12), in order to transform the Lagrangian velocity to the Eulerian one, the mapping function (Eq. 6.2) must be known. The mapping function is also required for virtual displacements, which are in many ways similar to velocities. However, the initial conditions are not observable in the Eulerian description, nor are they in most fluid dynamics problems. Therefore, one possibility is to guess an ad hoc mapping function, as explored by Leech [12].

Alternatively, some have chosen to keep the Lagrangian virtual displacements in the variational formulation and obtain the necessary conditions on the control surface by which the action function assumes stationary values inside the control volume. This approach will impose additional constraints on the choice of control volume that generally cannot be made, or at least are not easily distinguished, as was encountered by McIver [13].

Another challenge encountered by keeping the virtual displacement $\delta \boldsymbol{r}$ is when the boundary conditions are expressed in the velocity format, as is generally true for fluid systems. For many problems in solid mechanics, this difficulty has been overcome by utilizing generalized coordinates, q,

$$\delta \boldsymbol{r} = \sum_{i=1}^{n} \frac{\partial \boldsymbol{r}}{\partial q_i} \delta q_i, \tag{6.36}$$

and then, by using the relation

$$\frac{\partial \dot{\boldsymbol{r}}}{\partial \dot{q}_i} = \frac{\partial \boldsymbol{r}}{\partial q_i}. \tag{6.37}$$

While Eq. 6.37 is true for holonomic systems, requiring the velocity field to be integrable, it is not valid for nonholonomic systems [15]. Thus, it cannot be used for *ideal fluids* and it has limited applicability for viscous incompressible fluids. Leech discussed the fact that *ideal fluids* (inviscid and incompressible) are nonholonomic; while viscous incompressible fluids can be considered holonomic, the boundary conditions might not be so [12].

Moreover, the existence of nonconservative forces (that do perform virtual work) can reduce the generality of stationary principles as variational methods. This is due to the fact that generally the contribution of the nonconservative forces in the equations of motion is not a consequence of the variational operations, but rather it is by the appropriate choice of the equations representing nonconservative forces. In order to keep the generality of the variational approach, Bateman [2] proposed that there must exist a secondary system that absorbs the energy dissipated by the original system, resulting in a set of complimentary equations. This secondary set must not add any additional restriction to the system. Thus, the solution of the complimentary equations must be a function of the solutions of the original system. However, he showed that the complimentary equations do not generally meet this requirement for nonlinear systems, that is, the number of variables required in Lagrange's function cannot be reduced. Concluding his paper, Bateman stated:

> The researches of Clark Millikan showed, indeed, that there was no prospect of the discovery of a function L depending only on the quantities occurring in the equations of motion and the equation of continuity.

Although this statement leaves very little promise for using stationary principles for fluid systems, Hamilton's principle of varying action, in the form

$$\int_{t_1}^{t_2} (\delta T + \delta W)\, dt - \sum_{i=1}^{N} \frac{\partial T_i}{\partial \dot{\boldsymbol{r}}} \cdot \delta \boldsymbol{r}_i \Bigg|_{t_1}^{t_2} = 0, \tag{6.38}$$

is not a stationary principle if

$$\sum_{i=1}^{N} \frac{\partial T_i}{\partial \dot{\boldsymbol{r}}} \cdot \delta \boldsymbol{r}_i \Bigg|_{t_1}^{t_2} \neq 0. \tag{6.39}$$

It requires that the configuration be known at two instances of time, that is, $\delta \boldsymbol{r}_i = 0$ at the end times. When modeling fluid systems, the boundary conditions for particle trajectories are generally nonexistent. In the absence of these conditions, Hamilton's principle is not a variational principle, as was shown in Sect. 4.3.3. In this chapter, Jourdain's variational principle, introduced in the next section, is proposed as a possible basis for overcoming some of these difficulties.

6.8 Alternate Variational Perspective—Jourdain's Principle

One of the challenges in using d'Alembert's principle, Lagrange's equations, and Hamilton's principle for fluid mechanics, which is based on an Eulerian frame of reference, is that the virtual displacement used in these methods, which is a Lagrangian concept, does not have a well-defined Eulerian counterpart. In principle, this challenge can be overcome by utilizing Jourdain's variational principle, which assumes the displacement field to be frozen and instead imposes a set of virtual velocities. However, a review of the literature suggests that this principle has not been used in modeling fluid dynamic systems or fluid–structure interaction systems. For the dynamics of solid systems, Jourdain's principle has attracted a very limited number of researchers when compared with other mentioned methods. Mainly, it has been preferred in the modeling of nonholonomic systems because the velocities are not integrable.

For this reason, the following sections introduce Jourdain's principle within the context of analytical mechanics. There is a body of literature on Jourdain's variational principle and its connection to the literature on variational mechanics. Examples include Vujanovic and Atanackovic [22] and Wang and Pao [23]. We do not review this literature and only refer to it as needed for the purposes of this work.

6.8.1 Jourdain's Principle

In 1909, Jourdain published his variational principle to explain the gap between d'Alembert's principle and Gauss' principle of least constraint (Gibbs–Appell equations) and the differences in the variational constraints imposed [7]. He considered the variational constraints to be

$$\delta \boldsymbol{r} = 0 \qquad \delta t = 0. \tag{6.40}$$

The variational principles based on d'Alembert's principle are based on the axiom that the virtual displacement embodies all physically possible displacements and is in this sense arbitrary but not zero.

Analogous to the other mentioned variational methods, Jourdain's principle is based on the *dynamic equilibrium* relation, and for a system of N particles is given by the relation

$$\sum_{i=1}^{N} \left(m_i \ddot{\boldsymbol{r}}_i - \boldsymbol{F}_i \right) \cdot \delta \dot{\boldsymbol{r}}_i \; = 0, \qquad \text{where} \qquad \delta \boldsymbol{r} = 0, \delta t = 0, \tag{6.41}$$

m_i is the mass of particle i, and $\boldsymbol{F}_i$ is the component of the vector force acting on particle i in the direction of $\delta\dot{\boldsymbol{r}}_i$, which is the variation of the velocity of particle i, called virtual velocity.

Jourdain showed that his method demands less derivations for nonholonomic systems when compared with d'Alembert's and Gauss' principles. Jourdain concluded that his constraints lead to a new principle and method. However, he did not explain the physical meaning of his virtual velocities, which do not correspond to any virtual displacements.

Since the terms in Eq. 6.41 are power relations, the equation has also been referred to as the *principle of virtual power* and Kane's equations. We will use the term Jourdain's principle (JP).

6.9 Jourdain's Variational Operator

Jourdain's variational principle assumes an alternative possible velocity field for the system, while time and displacements are considered to be frozen. Therefore, the variation of a real-valued function of vectors is defined as the resulting change in the function value due to the imposed virtual velocities, while neglecting the terms of orders higher than one with respect to the velocity. Thus, Jourdain's variation of a function ψ, say $\delta\psi$, is defined as

$$\delta\psi = \lim_{\varepsilon\to 0}\frac{1}{\varepsilon}[\psi(\boldsymbol{u}+\varepsilon\delta\boldsymbol{u}) - \psi(\boldsymbol{u})], \tag{6.42}$$

where $\boldsymbol{u}$ is the velocity field and $\delta\boldsymbol{u}$ is the variation of the velocity field. From the vector calculus, the derivative ($\partial\psi/\partial\boldsymbol{u}$, also referred to as an abstract derivative) of a real-valued function ψ of vectors $\boldsymbol{u}$ is defined [4] by the relation

$$\left.\frac{\partial\psi(\boldsymbol{u}+\varepsilon\boldsymbol{w})}{\partial\varepsilon}\right|_{\varepsilon=0} \equiv \frac{\partial\psi}{\partial\boldsymbol{u}}\cdot\boldsymbol{w} \tag{6.43}$$

for all $\boldsymbol{w}$. For a specific set of vectors $\boldsymbol{w}$, Eq. 6.43 results in the directional derivative, that is, the derivative of ψ in the direction of $\boldsymbol{w}$. Therefore, by setting $\boldsymbol{w} = \delta\boldsymbol{u}$ on the right-hand side of Eq. 6.43, we have

$$\begin{aligned}\frac{\partial\psi}{\partial\boldsymbol{u}}\cdot\delta\boldsymbol{u} &= \left.\frac{\partial\psi(\boldsymbol{u}+\varepsilon\delta\boldsymbol{u})}{\partial\varepsilon}\right|_{\varepsilon=0}\\ &\equiv \lim_{\varepsilon\to 0}\frac{1}{\varepsilon}[\psi(\boldsymbol{u}+\varepsilon\delta\boldsymbol{u}) - \psi(\boldsymbol{u})].\end{aligned} \tag{6.44}$$

Comparing Eqs. 6.42 and 6.44, we obtain

$$\delta\psi = \frac{\partial\psi}{\partial \boldsymbol{u}} \cdot \delta\boldsymbol{u}. \tag{6.45}$$

Therefore, Jourdain's variation of a function is equal to its derivative with respect to velocity in the direction of the virtual velocity. Since $\delta\boldsymbol{u}$ is a set of arbitrary vectors that are compatible with the system constraints, the existence of any constraint on the velocity field limits the direction of the variational operator. Thus, the kinematic constraints do not necessarily impose limitations on the magnitude of $\delta\boldsymbol{u}$. However, the magnitude of $\delta\boldsymbol{u}$ at a point, say $x^\star$, must be small enough so that the function ψ be smooth in the neighborhood of radius $|\delta\boldsymbol{u}|$ about x.

Next, Jourdain's principle is derived from d'Alembert's principle.

6.10 Deriving Jourdain's Principle from D'Alembert's Principle

Jourdain's principle can be derived from d'Alembert's principle by direct differentiation [18] or by means of a Taylor series expansion [1]. We choose direct differentiation as this approach provides the format required when applying Reynolds Transport Theorem to a fluid system.

D'Alembert's principle can be stated as

$$\sum_{i=1}^{N} \left(m_i\ddot{\boldsymbol{r}}_i - \boldsymbol{F}_i\right) \cdot \delta\boldsymbol{r}_i = 0, \text{ where} \qquad \delta t = 0, \tag{6.46}$$

and the variation $\delta\boldsymbol{r}_i$ is arbitrary. Differentiation of Eq. 6.46 with respect to time yields

$$\sum_{i=1}^{N} \left\{ \frac{d}{dt}\left(m_i\ddot{\boldsymbol{r}}_i - \boldsymbol{F}_i\right) \cdot \delta\boldsymbol{r}_i + \left(m_i\ddot{\boldsymbol{r}}_i - \boldsymbol{F}_i\right) \cdot \frac{d}{dt}\left(\delta\boldsymbol{r}_i\right) \right\} = 0, \text{ where} \qquad \delta t = 0. \tag{6.47}$$

Using the *commutation rule,*

$$\frac{d}{dt}\left(\delta\boldsymbol{r}\right) - \delta\left(\frac{d}{dt}\boldsymbol{r}\right) = 0, \tag{6.48}$$

we have

$$\sum_{i=1}^{N} \left\{ \frac{d}{dt}\left(m_i\ddot{\boldsymbol{r}}_i - \boldsymbol{F}_i\right) \cdot \delta\boldsymbol{r}_i + \left(m_i\ddot{\boldsymbol{r}}_i - \boldsymbol{F}_i\right) \cdot \delta\dot{\boldsymbol{r}}_i \right\} = 0, \text{ where} \qquad \delta t = 0. \tag{6.49}$$

Now, we can impose Jourdain's constraints,

$$\delta t = 0, \qquad \delta \boldsymbol{r}_i = 0, \qquad \text{and} \qquad \delta \dot{\boldsymbol{r}}_i = \frac{d}{dt}\left(\delta \boldsymbol{r}_i\right) \neq 0, \tag{6.50}$$

and obtain Jourdain's principle,

$$\begin{cases} \sum_{i=1}^{N} \left(m_i \ddot{\boldsymbol{r}}_i - \boldsymbol{F}_i\right) \cdot \delta \dot{\boldsymbol{r}}_i = 0 \\ \delta t = 0 \\ \delta \boldsymbol{r}_i = 0 \\ \delta \dot{\boldsymbol{r}}_i = \frac{d}{dt}\left(\delta \boldsymbol{r}_i\right) \neq 0, \end{cases} \tag{6.51}$$

where $\delta \dot{\boldsymbol{r}}_i$ is the virtual velocity. Jourdain's constraints, expressed by Eq. 6.50, assume that a system can have an alternative possible velocity field at a time instant with the same corresponding displacement field.

In order to distinguish between Jourdain's and d'Alembert's variational operators, many authors have used the notation δ_1 to denote Jourdain's variation. We generally prefer to retain the same notation (δ) with Jourdain's constraints in the remainder of this work, except as noted otherwise, where the type of variation will be understood from the context.

Wang and Pao [23] discuss the validity of taking the time derivative of the virtual displacement as was done above and elsewhere in the literature. They state that "one cannot take the time derivative of a quantity that is not a function of time. Therefore, [Jourdain's principle] should be treated as an independent variational equation of motion in mechanics ... and regard it as a mathematical representation of the principle of virtual power because the product of force with virtual velocity is virtual power." They postulate Jourdain's principle as a fundamental principle in mechanics independent of all other principles. A number of questions arise: (i) Since the displacement is a function of time, is the virtual displacement also a function of time? (ii) Is the virtual displacement directly applicable to a fluid as it is to a solid? and (iii) Is the end result—Jourdain's principle—any less a principle in its own right regardless of how we interpret the variations of displacement and velocity? We address these questions as a part of our developments in the following sections.

6.11 Characteristics of Jourdain's Principle

As emphasized by Jourdain, his constraints lead to a different variation principle. Substantively, JP is different than the other virtual principles. These differences are noted next.

Kövecses and Cleghorn [8] investigated Jourdain's principle. They proposed that the position vector, $\boldsymbol{r}$, can be represented by using its trajectories in both Lagrangian and Eulerian frames. Based on their hybrid parameterization, they show that unlike the virtual displacements and velocities utilized in Lagrange's equation, d'Alembert principle, and Hamilton's principle, the virtual velocities in JP are not necessarily

infinitesimal quantities. Also, they pointed out that JP always results in an alternative possible state, whereas this can only be accomplished by the other variational methods for holonomic systems.

While the majority of the limited literature on JP is focused on its application to nonholonomic systems, an important feature of this principle was revealed by Papastavridis [18]. While examining the principle and comparing it with Lagrange's equations, he showed that Jourdain's principle is independent of the commutation rule Eq. 6.48. He showed that, for the case where $\delta^* \boldsymbol{r} \neq 0$ in

$$\delta^* \boldsymbol{r} = \frac{d}{dt}(\delta \boldsymbol{r}) - \delta\left(\frac{d}{dt}\boldsymbol{r}\right), \tag{6.52}$$

the application of Jourdain's principle results in the correct EOM. While the reader is urged to consider the discussion by Papastavridis, we proceed with an interpretation suited for our purposes that results in a simplified proof of this feature.

Let us consider the relation between Lagrangian variations (δ) and Eulerian variations ($\bar{\delta}$) as defined by Eq. 6.35, and impose the Jourdain constraints ($\delta \boldsymbol{x}_i = 0$). The result is

$$\delta\Phi(\boldsymbol{x}, t) = \bar{\delta}\Phi(\boldsymbol{x}, t). \tag{6.53}$$

This is a very important property, as it states that Jourdain's variation of a spatial function is the same in both Lagrangian and Eulerian descriptions. Using this property, some of the problems that have been encountered in extending variational principles for fluid systems can be avoided by using JP.

In order to prove that JP commutes with D/Dt, we apply Jourdain's variational operator to the total derivative of a function. Using Eq. 6.53, except replacing Φ by $D\Phi/Dt$, we can write

$$\delta\left[\frac{D}{Dt}\Phi(\boldsymbol{x}, t)\right] = \bar{\delta}\left[\frac{D}{Dt}\Phi(\boldsymbol{x}, t)\right]. \tag{6.54}$$

It has been shown that the Lagrangian variation commutes with time differentiation while the Eulerian one does not [24]; that is,

$$\delta\left[\frac{D}{Dt}\Phi(\boldsymbol{x}, t)\right] = \frac{D}{Dt}\left[\delta\Phi(\boldsymbol{x}, t)\right] \tag{6.55}$$

$$\bar{\delta}\left[\frac{D}{Dt}\Phi(\boldsymbol{x}, t)\right] \neq \frac{D}{Dt}\left[\bar{\delta}\Phi(\boldsymbol{x}, t)\right]. \tag{6.56}$$

Using Eq. 6.54, then Eq. 6.55, and finally Eq. 6.53, we have

$$\bar{\delta}\left[\frac{D}{Dt}\Phi(\boldsymbol{x}, t)\right] = \delta\left[\frac{D}{Dt}\Phi(\boldsymbol{x}, t)\right]$$

$$= \frac{D}{Dt}\left[\delta\Phi(\boldsymbol{x},t)\right]$$
$$= \frac{D}{Dt}\left[\bar{\delta}\Phi(\boldsymbol{x},t)\right]. \tag{6.57}$$

We arrive at Eq. 6.57 rather than Eq. 6.56, thus proving that for JP, the variation does commute with the time derivative D/Dt.

6.12 Eulerian–Lagrangian Description of Jourdain's Principle

As shown earlier, JP can be obtained by differentiating d'Alembert's principle, and then imposing Jourdain's constraints. Similarly, in the following, we start by manipulating d'Alembert's principle, and then apply Jourdain's constraints. Therefore, Jourdain's constraints are kept beside d'Alembert's principle as shown in Eq. 6.58, where the brace on the left is to remind us that the same mathematical manipulations must be applied to all those terms. As shown in Sect. 6.10, all the terms that are embraced are equivalent to Jourdain's principle.

D'Alembert's principle for a system of N particles can be stated as

$$\sum_{i=1}^{N} \frac{d}{dt}\left(m_i\dot{\boldsymbol{r}}_i\right)\cdot\delta\boldsymbol{r}_i = \sum_{i=1}^{N}\boldsymbol{F}_i\cdot\delta\boldsymbol{r}_i,$$

and by differentiating this with respect to time and imposing Jourdain's constraints, JP can be written as

$$\begin{cases} \frac{d}{dt}\left[\sum_{i=1}^{N}\frac{d}{dt}\left(m_i\dot{\boldsymbol{r}}_i\right)\cdot\delta\boldsymbol{r}_i\right] = \frac{d}{dt}\left[\sum_{i=1}^{N}\boldsymbol{F}_i\cdot\delta\boldsymbol{r}_i\right] \\ \delta t = 0 \\ \delta\boldsymbol{r}_i = 0 \\ \frac{d}{dt}\left(\delta\boldsymbol{r}_i\right) \neq 0. \end{cases} \tag{6.58}$$

In the above, both sides of the equation are differentiated using the product rule and use is made of the $\delta\boldsymbol{r}_i = 0$ constraint.

As discussed in the beginning of this chapter, the velocity and resultant force observed at a point in Eulerian space must be the same as the velocity and forces obtained from the Lagrangian frame for a particle that occupies that Eulerian point, that is,

$$\boldsymbol{v}\left(\boldsymbol{A}_i,t\right) = \boldsymbol{u}\left(\boldsymbol{r}_i,t\right) \tag{6.59}$$

$$\boldsymbol{F}(\boldsymbol{A}_i,t) = \boldsymbol{F}_E(\boldsymbol{r}_i,t), \tag{6.60}$$

where $\boldsymbol{v}\ (=\dot{\boldsymbol{r}})$ is the Lagrangian velocity and $\boldsymbol{u}$ is the Eulerian velocity (the same as before), $\boldsymbol{F}_E$ is the Eulerian representation of the force $\boldsymbol{F}(\boldsymbol{A}_i, t)$. Note that $\boldsymbol{r}_i$ and $\boldsymbol{r}\ (\boldsymbol{A}_i, t)$ are two alternative ways to denote the same parameter.

In continuum mechanics, a set of particles is assumed to be continuous in such a way that two particles do not occupy the same position, and there exist no gaps unless at isolated points. By the assumption that there exists a unique function that maps the Lagrangian reference frame to the Eulerian one, the continuum assumptions are applied to the Eulerian frame. Consequently, the change in the system properties, as viewed from a fixed position in space, is assumed to be smooth, continuous and differentiable, meaning that two consecutive particles occupying a point in space, say $\boldsymbol{x}$, are allowed to possess infinitesimally different properties.

Also, as discussed in Sect. 6.2, for each particle trajectory there exists an inverse mapping function to the initial position of that particle (Eq. 6.3). While the initial position is a fixed variable in the Lagrangian frame, it can be selected to be any position on the path, differing only by the reference times. Let us call any of these points a possible initial position. Alternatively, by mapping these different time references into a specific one, there must exist an instantaneous spatial function whose outcome is the path history of the particle occupying that space. As a result, these possible initial positions can be considered to be a spatial function. Therefore, in the realm of continuum mechanics, we assume that there must exist an Eulerian smooth, continuous, differentiable function $\boldsymbol{\Lambda}\ (\boldsymbol{x}, t)$ where

$$\boldsymbol{r} = \boldsymbol{\Lambda}\ (\boldsymbol{x}, t)\,, \tag{6.61}$$

and

$$\frac{d}{dt}\boldsymbol{r} = \frac{d}{dt}\boldsymbol{\Lambda}\ (\boldsymbol{x}, t) = \left.\frac{D}{Dt}\boldsymbol{\Lambda}\ (\boldsymbol{x}, t)\right|_{\boldsymbol{x}=\boldsymbol{r}}. \tag{6.62}$$

Note that Eq. 6.61 becomes Eq. 6.2 for a fixed initial position, and thus it can then no longer be differentiated. Also, from Eqs. 6.59 and 6.62 we have

$$\boldsymbol{u}\ (\boldsymbol{x}, t) = \frac{D}{Dt}\boldsymbol{\Lambda}\ (\boldsymbol{x}, t)\,, \tag{6.63}$$

since $\boldsymbol{v}\ (\boldsymbol{A}, t) = d\boldsymbol{r}/dt$.

By substituting Eqs. 6.59–6.62 into Eq. 6.58, Jourdain's principle for N particles becomes

$$\begin{cases} \frac{d}{dt}\left\{\sum_{i=1}^{N}\frac{d}{dt}\left[m_i\boldsymbol{u}\ (\boldsymbol{r}_i, t)\right]\cdot\delta\boldsymbol{\Lambda}\ (\boldsymbol{r}_i, t)\right\} = \frac{d}{dt}\left\{\sum_{i=1}^{N}\boldsymbol{F}_E(\boldsymbol{r}_i, t)\cdot\delta\boldsymbol{\Lambda}\ (\boldsymbol{r}_i, t)\right\} \\ \delta t = 0 \\ \delta\boldsymbol{\Lambda}\ (\boldsymbol{r}_i, t) = 0 \\ \frac{d}{dt}\left[\delta\boldsymbol{\Lambda}\ (\boldsymbol{r}_i, t)\right] \neq 0. \end{cases} \tag{6.64}$$

Note that $\boldsymbol{u}$, $\boldsymbol{F}_E$, and $\boldsymbol{\Lambda}$ are all Eulerian functions. However, Eq. 6.64 is a Lagrangian equation due to the presence of $\boldsymbol{r}_i$ (since we are following the particles). Also, the variational operator δ is Lagrangian.

If the set of particles remains continuous for all time, the summation can be replaced with integration over the material domain. In that case, Eq. 6.64 becomes

$$\begin{cases} \frac{d}{dt}\left\{\int_{V_m} \frac{d}{dt}\left[\rho \boldsymbol{u}\left(\boldsymbol{r},t\right)\right]\cdot \delta\boldsymbol{\Lambda}\left(\boldsymbol{r},t\right) dV_m\right\} = \frac{d}{dt}\left\{\int_{V_m} \boldsymbol{f}\left(\boldsymbol{r},t\right)\cdot \delta\boldsymbol{\Lambda}\left(\boldsymbol{r},t\right) dV_m\right\} \\ \delta t = 0 \\ \delta\boldsymbol{\Lambda}\left(\boldsymbol{r},t\right) = 0 \\ \frac{d}{dt}\left(\delta\boldsymbol{\Lambda}\left(\boldsymbol{r},t\right)\right) \neq 0, \end{cases} \tag{6.65}$$

where V_m is the material volume, ρ is the density, and $\boldsymbol{f}$ is the force density. Since all the functions are Eulerian, only the bounds of the integrations are required in order to evaluate those integrals. If the material volume is known in the Eulerian description for all time, then the effects of the Lagrangian paths $\boldsymbol{r}$ inside the domain become irrelevant to the integration and it can be replaced by the Eulerian coordinate $\boldsymbol{x}$.

By mapping the system from the Lagrangian frame of reference to the Eulerian representation, the material volume, V_m, will be mapped to an Eulerian system (material) volume, $V_E\left(t\right)$, so that

$$dV_m\left(\boldsymbol{r},t\right) = \det\left[\frac{\partial \boldsymbol{r}}{\partial \boldsymbol{x}}\right] dV_E\left(\boldsymbol{x},t\right), \tag{6.66}$$

where we used the determinant of the Jacobian for the mapping.

Thus far, the derivations have been kept general, that is, we did not specify the compressibility property of the material. We next limit our derivation to incompressible flows, where the incompressibility condition implies that

$$\det\left[\frac{\partial \boldsymbol{r}}{\partial \boldsymbol{x}}\right] = 1, \tag{6.67}$$

for all time. Therefore, by substituting Eqs. 6.66 and 6.67 into Eq. 6.65, utilizing Eq. 6.16, and then, replacing $\boldsymbol{r}$ for the reason explained after Eq. 6.65, Jourdain's principle for an incompressible set of continuous particles becomes

$$\begin{cases} \frac{d}{dt}\left\{\int_{V_E(t)} \frac{D}{Dt}\left[\rho \boldsymbol{u}\left(\boldsymbol{x},t\right)\right]\cdot \delta\boldsymbol{\Lambda}\left(\boldsymbol{x},t\right) dV_E\left(t\right)\right\} \\ \quad = \frac{d}{dt}\left\{\int_{V_E(t)} \boldsymbol{f}\left(\boldsymbol{x},t\right)\cdot \delta\boldsymbol{\Lambda}\left(\boldsymbol{x},t\right) dV_E\left(t\right)\right\} \\ \delta t = 0 \\ \delta\boldsymbol{\Lambda}\left(\boldsymbol{x},t\right) = 0 \\ \frac{D}{Dt}\left(\delta\boldsymbol{\Lambda}\left(\boldsymbol{x},t\right)\right) \neq 0, \end{cases} \tag{6.68}$$

where by Eq. 6.63, $\boldsymbol{u}(\boldsymbol{x},t) = \frac{D}{Dt}\boldsymbol{\Lambda}(\boldsymbol{x},t)$, where d/dt is used to emphasize that it is a differentiation of a material volume, and D/Dt is used inside the integrand since the associated function is Eulerian.

Equation 6.68 is still mixed Eulerian–Lagrangian. The variations δ are Lagrangian, and the same set of particles is being followed. In the following section, we impose Jourdain's constraints and convert Eq. 6.68 into an equation for a system of changing mass with the Eulerian variational operator.

6.13 Extended JP for General Control Volume

Jourdain's principle for a system of particles was obtained in Eq. 6.68, which must be considered together with Eq. 6.63. In relating the integrals over the system volume to those over a control volume, an effective tool is Reynolds transport theorem (Sect. 6.5). In the following, each side of Eq. 6.68 is considered separately for simplicity, and is manipulated so as to become applicable to the cases where general control volumes are considered. The resulting equation is completely Eulerian.

6.13.1 Left-Hand Side of Eq. 6.68

We start by considering the left-hand side of Eq. 6.68, and apply the RTT for a general control volume as per Eq. 6.18,

$$\begin{aligned}\frac{d}{dt}\left\{\int_{V_E}\frac{D}{Dt}\left[\rho\boldsymbol{u}(\boldsymbol{x},t)\right]\cdot\delta\boldsymbol{\Lambda}(\boldsymbol{x},t)\,dV_E\right\}&\\ =\int_{CV}\frac{\partial}{\partial t}\left\{\frac{D}{Dt}\left[\rho\boldsymbol{u}(\boldsymbol{x},t)\right]\cdot\delta\boldsymbol{\Lambda}(\boldsymbol{x},t)\right\}dV&\\ +\int_{CS}\left\{\frac{D}{Dt}\left[\rho\boldsymbol{u}(\boldsymbol{x},t)\right]\cdot\delta\boldsymbol{\Lambda}(\boldsymbol{x},t)\right\}\left[\boldsymbol{u}(\boldsymbol{x},t)\cdot\boldsymbol{n}\right]dA,&\quad(6.69)\end{aligned}$$

where the time dependence of the domains of integration is implied. Now by applying Gauss' divergence theorem (Eq. 6.20) to the right-hand side of Eq. 6.69, we can combine the two terms on the right-hand side, as follows,

$$\begin{aligned}&\frac{d}{dt}\left\{\int_{V_E}\frac{D(\rho\boldsymbol{u})}{Dt}\cdot\delta\boldsymbol{\Lambda}dV_E\right\}\\ &\quad=\int_{CV}\left[\frac{\partial}{\partial t}\left(\rho\frac{D\boldsymbol{u}}{Dt}\cdot\delta\boldsymbol{\Lambda}\right)+\boldsymbol{u}\cdot\nabla\left(\rho\frac{D\boldsymbol{u}}{Dt}\cdot\delta\boldsymbol{\Lambda}\right)+\left(\rho\frac{D\boldsymbol{u}}{Dt}\cdot\delta\boldsymbol{\Lambda}\right)(\nabla\cdot\boldsymbol{u})\right]dV\end{aligned}$$

$$= \int_{CV} \left[\frac{D}{Dt} \left(\rho \frac{D\boldsymbol{u}}{Dt} \cdot \delta\boldsymbol{\Lambda} \right) + \left(\rho \frac{D\boldsymbol{u}}{Dt} \cdot \delta\boldsymbol{\Lambda} \right) (\nabla \cdot \boldsymbol{u}) \right] dV, \tag{6.70}$$

where the argument $(\boldsymbol{x}, t)$ is omitted since we recognize that all the functions are expressed in the Eulerian frame. Moreover, the density ρ has been pulled out of the differentiation since the density is constant for incompressible flows.

By imposing the incompressibility constraint, $\nabla \cdot \boldsymbol{u} = 0$, and then differentiating the remaining terms, Eq. 6.70 becomes

$$\begin{aligned} \frac{d}{dt} \left\{ \int_{V_E} \frac{D(\rho\boldsymbol{u})}{Dt} \cdot \delta\boldsymbol{\Lambda} dV_E \right\} &= \int_{CV} \frac{D}{Dt} \left(\rho \frac{D\boldsymbol{u}}{Dt} \cdot \delta\boldsymbol{\Lambda} \right) dV \\ &= \int_{CV} \left[\rho \frac{D^2\boldsymbol{u}}{Dt^2} \cdot \delta\boldsymbol{\Lambda} + \rho \frac{D\boldsymbol{u}}{Dt} \cdot \frac{D}{Dt} (\delta\boldsymbol{\Lambda}) \right] dV. \end{aligned} \tag{6.71}$$

In deriving Eq. 6.71, we have not yet imposed Eq. 6.50, Jourdain's constraints. Since δ is the Lagrangian variational operator, the commutation rule still holds,

$$\frac{D[\delta(\boldsymbol{\Lambda})]}{Dt} = \delta \left[\frac{D(\boldsymbol{\Lambda})}{Dt} \right]. \tag{6.72}$$

Substituting Eq. 6.63 in Eq. 6.72, we have

$$\frac{D[\delta(\boldsymbol{\Lambda})]}{Dt} = \delta\boldsymbol{u}. \tag{6.73}$$

Finally, by applying Jourdain's constraints as expressed in Eq. 6.68, in particular $\delta\boldsymbol{\Lambda} = 0$, and using Eq. 6.73, the left-hand side of Eq. 6.68 becomes

$$\frac{d}{dt} \left\{ \int_{V_E} \frac{D(\rho\boldsymbol{u})}{Dt} \cdot \delta\boldsymbol{\Lambda} dV_E \right\} = \int_{CV} \rho \frac{D\boldsymbol{u}}{Dt} \cdot \delta\boldsymbol{u} dV, \tag{6.74}$$

where we realize that $\delta\boldsymbol{u}$ is an Eulerian variation of the Eulerian velocity. This is because Jourdain's variation of a spatial function is the same in both Lagrangian and Eulerian descriptions, as was expressed by Eq. 6.53. We will not use the notation $\bar{\delta}$, suggested earlier, in the remainder of this derivation due to the understanding that the Lagrangian variational operator becomes the Eulerian operator after imposing Jourdain's constraints, $\delta\boldsymbol{\Lambda} = 0$.

6.13.2 *Right-Hand Side of Eq. 6.68*

For the right-hand side of Eq. 6.68, the steps are similar to those above, and result in

$$\frac{d}{dt}\left\{\int_{V_E} \boldsymbol{f}\cdot\delta\boldsymbol{\Lambda}dV_E\right\} = \int_{CV}\left[\frac{\partial}{\partial t}\left(\boldsymbol{f}\cdot\delta\boldsymbol{\Lambda}\right)+\boldsymbol{u}\cdot\nabla\left(\boldsymbol{f}\cdot\delta\boldsymbol{\Lambda}\right)+\left(\boldsymbol{f}\cdot\delta\boldsymbol{\Lambda}\right)\left(\nabla\cdot\boldsymbol{u}\right)\right]dV$$
$$= \int_{CV}\frac{D}{Dt}\left(\boldsymbol{f}\cdot\delta\boldsymbol{\Lambda}\right)dV$$
$$= \int_{CV}\boldsymbol{f}\cdot\delta\boldsymbol{u}dV. \tag{6.75}$$

6.13.3 New Version of Eq. 6.68

By substituting Eqs. 6.74 and 6.75 into Eq. 6.68, and by considering Eq. 6.53, the extended Jourdain's principle for a system of changing mass in a control volume becomes

$$\int_{CV}\rho\frac{D\boldsymbol{u}\left(\boldsymbol{x},t\right)}{Dt}\cdot\delta\boldsymbol{u}\left(\boldsymbol{x},t\right)dV = \int_{CV}\boldsymbol{f}\left(\boldsymbol{x},t\right)\cdot\delta\boldsymbol{u}\left(\boldsymbol{x},t\right)dV, \tag{6.76}$$

where all the variations and functions are represented in the Eulerian frame.

We have derived a variational formulation that is expressed purely in the Eulerian frame. We are not aware of a similar formulation in the literature. In order to verify our mathematical manipulations, we utilize Eq. 6.76 to derive the Navier–Stokes equations in the following section.

6.14 Extended Jourdain's Principle for Viscous Incompressible Fluids

In fluid mechanics, forces acting on a fluid particle are generally divided into three categories: *line forces*, *body forces*, and *surface forces* [9]. *Line forces*, also called *surface tension*, do not appear directly in the EOM as they are considered boundary conditions. Thus, they are not considered in this work. Therefore, the total active force, $\boldsymbol{f}\left(\boldsymbol{x},t\right)$, in a control volume is obtained by integrating the force density over that control volume,

$$\int_{CV}\boldsymbol{f}\left(\boldsymbol{x},t\right)dV = \int_{CV}\boldsymbol{f}_b dV + \int_{CS}\boldsymbol{f}_s dA, \tag{6.77}$$

where $\boldsymbol{f}_b$ denotes the body force per unit volume (body force density) and $\boldsymbol{f}_s$ is the surface force per unit surface area. Considering the definition of the stress tensor, $\bar{\boldsymbol{\sigma}}$, $\boldsymbol{f}_s$ can be obtained as

$$\boldsymbol{f}_s = \boldsymbol{n}^T\cdot\bar{\boldsymbol{\sigma}} = \bar{\boldsymbol{\sigma}}\cdot\boldsymbol{n}, \tag{6.78}$$

where ^{T} denotes transpose and $\boldsymbol{n}$ is the normal vector to the surface of interest. Therefore, the total active force is defined as,

$$\int_{CV} \boldsymbol{f}\,(\boldsymbol{x},t)\,dV = \int_{CV} \left(\boldsymbol{f}_b + \nabla\cdot\bar{\boldsymbol{\sigma}}\right) dV, \tag{6.79}$$

where we have used Gauss' theorem (Eq. 6.19).

Therefore, the extended Jourdain's principle can be modified by substituting Eq. 6.79 into Eq. 6.76, resulting in the equation

$$\int_{CV} \left(\rho\frac{D\boldsymbol{u}\,(\boldsymbol{x},t)}{Dt} - \boldsymbol{f}_b - \nabla\cdot\bar{\boldsymbol{\sigma}}\right)\cdot\delta\boldsymbol{u}\,(\boldsymbol{x},t)\,dV = 0. \tag{6.80}$$

In order to expand Eq. 6.80 further, we consider the constitutive relation for Newtonian incompressible fluids,

$$\bar{\boldsymbol{\sigma}} = -p\bar{\boldsymbol{I}} + 2\mu\bar{\boldsymbol{S}}, \tag{6.81}$$

where p is the thermodynamic pressure, $\bar{\boldsymbol{I}}$ is the identity tensor, μ is the coefficient of dynamic viscosity, and $\bar{\boldsymbol{S}}$ is a symmetric tensor, defined as

$$\bar{\boldsymbol{S}} = \frac{1}{2}\left(\frac{\partial u_i}{\partial x_j} + \frac{\partial u_j}{\partial x_i}\right). \tag{6.82}$$

Therefore, Eq. 6.80 becomes

$$\int_{CV} \left(\rho\frac{D\boldsymbol{u}\,(\boldsymbol{x},t)}{Dt} - \boldsymbol{f}_b\,(\boldsymbol{x},t) + \nabla p\,(\boldsymbol{x},t) - \mu\nabla^2\boldsymbol{u}\,(\boldsymbol{x},t)\right)\cdot\delta\boldsymbol{u}\,(\boldsymbol{x},t)\,dV = 0. \tag{6.83}$$

Since $\delta\boldsymbol{u}$ is an arbitrary nonzero vector, the terms of the integrand inside the parentheses must add to zero. These are the Navier–Stokes equations. Therefore, the governing EOM of an incompressible viscous flow can be obtained from our derived variational formulation.

Next, we explore the derivation of the energy equations utilizing Jourdain's variational principle.

6.15 Energy Equation from the Extended Jourdain's Principle

In this section, we look to derive the energy equation for a fluid via Jourdain's principle. Since Jourdain's principle and the *Lagrangian equations of motion* are related to each other via d'Alembert's principle, we expect that the energy rate equations can be obtained from Jourdain's principle. We begin by deriving the conservation of energy

in the Lagrangian reference frame, and then explore the modifications required in order to obtain this equation in the Eulerian reference frame.

Note that in utilizing d'Alembert's principle we use virtual displacement, whereas for Jourdain's principle we use virtual velocity. It is the Jourdain framework and its stipulation of arbitrary virtual (possible) velocities that appeals to its application to problems that involve fluids.

6.15.1 *Obtaining the Energy Rate Equation in the Lagrangian Reference Frame*

In Sect. 6.10, it was shown that Jourdain's principle can be derived from d'Alembert's principle. Hamilton's principle can be also derived from d'Alembert's principle. For a general system, Hamilton's principle leads to a system of simultaneous differential equations of second order called the *Lagrangian equations of motion* [11, pp.111–119]. In order to demonstrate our methodology for obtaining the energy rate equations from Jourdain's principle, a short review of the derivation of the Lagrangian EOM is provided.

Consider a Lagrangian function L, defined as

$$L = L\left(\dot{\boldsymbol{r}}_i, \boldsymbol{r}_i, t\right), \quad for \quad i = 1, 2, \ldots, N,$$

where N is the number of particles and $\boldsymbol{r}_i$ denote the Lagrangian coordinates of particle i. The function L is defined for a conservative system as

$$L = T - \Pi, \tag{6.84}$$

where T is commonly called the kinetic energy, and Π is the potential energy. The function L defines the entire dynamics of the system. Therefore, the action integral in the absence of nonconservative forces is defined as

$$\int_{t_1}^{t_2} \delta_d L\left(\dot{\boldsymbol{r}}_i, \boldsymbol{r}_i, t\right) dt = 0, \tag{6.85}$$

where $\delta_d L$ is the variation of function L, and the subscript d refers to the d'Alembert variation, in distinction to Jourdain's variation. They are both variations in the same sense, but what is taken to be arbitrary and nonzero is different. That is, d'Alembert's variation assumes that the virtual displacement is arbitrary and nonzero, with the virtual velocity terms integrated so that only virtual displacements remain. Jourdain's variation takes the virtual velocity as arbitrary and nonzero, with the virtual displacement equal to zero. In both instances, the variation on time equals zero, since the respective virtual (possible) displacements and velocities represent alternate states at the same time.

Therefore, in the derivation below, we begin with d'Alembert's variation δ_d since we begin with the function L. Later, when we are working with $\dot{L}$, we eventually use Jourdain's constraint, setting the virtual displacement to zero, resulting in expression Eq. 6.93, which is in terms of Jourdain's variation.

The variation of a Lagrangian function is, by definition, the resulting difference found by imposing d'Alembert's virtual displacements $\delta_d \boldsymbol{r}_i$ on $L\left(\dot{\boldsymbol{r}}_i, \boldsymbol{r}_i, t\right)$ and eliminating the terms with order higher than one with respect to $\delta_d \boldsymbol{r}_i$, while holding time frozen, as follows,

$$\int_{t_1}^{t_2} \delta_d L \, dt = \lim_{\varepsilon \to 0} \frac{1}{\varepsilon} \int_{t_1}^{t_2} \left[L\left(\frac{d}{dt}\left(\boldsymbol{r}_i + \varepsilon \, \delta_d \boldsymbol{r}_i\right), \boldsymbol{r}_i + \varepsilon \, \delta_d \boldsymbol{r}_i, t \right) - L\left(\dot{\boldsymbol{r}}_i, \boldsymbol{r}_i, t\right) \right] dt. \tag{6.86}$$

In the Lagrangian frame of reference, the variational operator and the time differentiation commute. Thus, Eq. 6.86 can be written as

$$\int_{t_1}^{t_2} \delta_d L \, dt = \lim_{\varepsilon \to 0} \frac{1}{\varepsilon} \int_{t_1}^{t_2} \left[L\left(\dot{\boldsymbol{r}}_i + \varepsilon \, \delta_d \dot{\boldsymbol{r}}_i, \boldsymbol{r}_i + \varepsilon \, \delta_d \boldsymbol{r}_i, t\right) - L\left(\dot{\boldsymbol{r}}_i, \boldsymbol{r}_i, t\right) \right] dt. \tag{6.87}$$

Applying the Taylor expansion to $L\left(\dot{\boldsymbol{r}}_i + \varepsilon \, \delta_d \dot{\boldsymbol{r}}_i, \boldsymbol{r}_i + \varepsilon \, \delta_d \boldsymbol{r}_i, t\right)$ and neglecting the terms of order higher than one with respect to $\delta_d \boldsymbol{r}_i$, Eq. 6.87 becomes

$$\begin{aligned} \int_{t_1}^{t_2} \delta_d L \, dt &= \lim_{\varepsilon \to 0} \frac{1}{\varepsilon} \int_{t_1}^{t_2} \left[L\left(\dot{\boldsymbol{r}}_i, \boldsymbol{r}_i, t\right) + \varepsilon \, \delta_d \dot{\boldsymbol{r}}_i \cdot \frac{\partial L}{\partial \dot{\boldsymbol{r}}_i} + \varepsilon \, \delta_d \boldsymbol{r}_i \cdot \frac{\partial L}{\partial \boldsymbol{r}_i} - L\left(\dot{\boldsymbol{r}}_i, \boldsymbol{r}_i, t\right) \right] dt \\ &= \int_{t_1}^{t_2} \left[\delta_d \dot{\boldsymbol{r}}_i \cdot \frac{\partial L}{\partial \dot{\boldsymbol{r}}_i} + \delta_d \boldsymbol{r}_i \cdot \frac{\partial L}{\partial \boldsymbol{r}_i} \right] dt = 0. \end{aligned} \tag{6.88}$$

Since the algebraic relation between $\delta_d \dot{\boldsymbol{r}}_i$ and $\delta_d \boldsymbol{r}_i$ is not known (unless the problem is solved), Eq. 6.88 is not accessible for further analysis. This difficulty can be overcome if the displacements are known at t_1 and t_2. Integrating Eq. 6.88 by parts and, as customary, assume that the virtual displacements equal zero at t_1 and t_2 (since the displacements are assumed to be known at t_1 and t_2), Eq. 6.85 then becomes

$$\int_{t_1}^{t_2} \delta_d L \, dt = \int_{t_1}^{t_2} \delta_d \boldsymbol{r}_i \cdot \left[\frac{\partial L}{\partial \boldsymbol{r}_i} - \frac{d}{dt}\left(\frac{\partial L}{\partial \dot{\boldsymbol{r}}_i} \right) \right] dt = 0. \tag{6.89}$$

Since $\delta_d \boldsymbol{r}_i$ are arbitrary nonzero vectors, the *Lagrangian equations of motion* are obtained by necessarily setting the terms inside square brackets equal to zero [11],

$$\frac{d}{dt}\left(\frac{\partial L}{\partial \dot{\boldsymbol{r}}_i} \right) - \frac{\partial L}{\partial \boldsymbol{r}_i} = 0. \tag{6.90}$$

In Sect. 6.10, Jourdain's principle was obtained by differentiating d'Alembert's principle with respect to time, and then, setting the virtual displacement equal to zero. Similarly, we start by considering the rate of a Lagrangian function,

$$\frac{d}{dt}L = \dot{L}\left(\dot{\boldsymbol{r}}_i, \boldsymbol{r}_i, t\right),$$

and define the respective action integral as

$$\int_{t_1}^{t_2} \delta_d \dot{L}\left(\dot{\boldsymbol{r}}_i, \boldsymbol{r}_i, t\right)\, dt = 0. \tag{6.91}$$

Substituting $\delta_d \dot{L}$ instead of $\delta_d L$ into Eq. 6.86, we obtain

$$\begin{aligned}
\int_{t_1}^{t_2} \delta_d \dot{L}\left(\dot{\boldsymbol{r}}_i, \boldsymbol{r}_i, t\right)\, dt &= \lim_{\varepsilon \to 0} \frac{1}{\varepsilon} \int_{t_1}^{t_2} \left[\dot{L}\left(\frac{d}{dt}\left(\boldsymbol{r}_i + \varepsilon\, \delta_d \boldsymbol{r}_i\right), \boldsymbol{r}_i + \varepsilon\, \delta_d \boldsymbol{r}_i, t \right) \right. \\
&\quad \left. - \dot{L}\left(\dot{\boldsymbol{r}}_i, \boldsymbol{r}_i, t\right) \right] dt \\
&= \lim_{\varepsilon \to 0} \frac{1}{\varepsilon} \int_{t_1}^{t_2} \left[\dot{L}\left(\dot{\boldsymbol{r}}_i, \boldsymbol{r}_i, t\right) + \varepsilon\, \delta_d \dot{\boldsymbol{r}}_i \cdot \frac{\partial \dot{L}}{\partial \dot{\boldsymbol{r}}_i} + \varepsilon\, \delta_d \boldsymbol{r}_i \cdot \frac{\partial \dot{L}}{\partial \boldsymbol{r}_i} \right. \\
&\quad \left. - \dot{L}\left(\dot{\boldsymbol{r}}_i, \boldsymbol{r}_i, t\right) \right] dt \\
&= \int_{t_1}^{t_2} \left[\frac{\partial \dot{L}}{\partial \dot{\boldsymbol{r}}_i} \cdot \delta_d \dot{\boldsymbol{r}}_i + \frac{\partial \dot{L}}{\partial \boldsymbol{r}_i} \cdot \delta_d \boldsymbol{r}_i \right] dt \\
&= 0.
\end{aligned} \tag{6.92}$$

Similar to our approach in Sect. 6.10, Jourdain's variational principle can be obtained in terms of the Lagrangian function L by imposing Jourdain's variational constraint $\delta_d \boldsymbol{r}_i = 0$ to Eq. 6.92, resulting in

$$\int_{t_1}^{t_2} \delta \dot{L}\left(\dot{\boldsymbol{r}}_i, \boldsymbol{r}_i, t\right)\, dt = \int_{t_1}^{t_2} \frac{\partial \dot{L}}{\partial \dot{\boldsymbol{r}}_i} \cdot \delta \dot{\boldsymbol{r}}_i\, dt = 0,$$

or,

$$\delta \dot{L}\left(\dot{\boldsymbol{r}}_i, \boldsymbol{r}_i, t\right) = \frac{\partial \dot{L}}{\partial \dot{\boldsymbol{r}}_i} \cdot \delta \dot{\boldsymbol{r}}_i. \tag{6.93}$$

Therefore, the energy rate equation $\dot{L}\left(\dot{\boldsymbol{r}}_i, \boldsymbol{r}_i, t\right)$ can be obtained from Jourdain's principle using Eq. 6.93. It is important to note that the variation of acceleration is not considered in the derivation of Eq. 6.93 since the acceleration is second order with respect to $\delta_d \boldsymbol{r}_i$. It is emphasized that the only requirement for using Eq. 6.93 is that Jourdain's variational operator must commute with the differential operator d/dt.

Next, we consider two simple examples to clarify the procedure.

Example 2 Consider a single degree of freedom mass–spring system, where $x\,(t)$ is the Lagrangian position of a box of mass m and k is the stiffness of the massless spring. We wish to obtain the energy rate equation by integration and by using Eq. 6.93.

Using Newton's second law, the equation of motion is

$$m\ddot{x}\,(t) + kx\,(t) = 0. \tag{6.94}$$

The acceleration $\ddot{x}\,(t)$ can be rewritten as follows,

$$\begin{aligned}\ddot{x}\,(t) &= \frac{d\dot{x}\,(t)}{dt} \\ &= \frac{d\dot{x}\,(t)}{dx}\frac{dx\,(t)}{dt} \\ &= \frac{d}{dx}\left(\frac{1}{2}\dot{x}^2\,(t)\right).\end{aligned} \tag{6.95}$$

Substituting Eq. 6.95 into Eq. 6.94, we have

$$m\frac{d}{dx}\left(\frac{1}{2}\dot{x}^2\,(t)\right) + kx\,(t) = 0, \tag{6.96}$$

and by integrating this equation with respect to x, the energy equation is obtained,

$$\frac{1}{2}m\dot{x}^2\,(t) + \frac{1}{2}kx^2\,(t) = C, \tag{6.97}$$

where C is a constant. Finally, the energy rate equation is obtained by differentiating Eq. 6.97 with respect to time, to find

$$m\ddot{x}\dot{x} + kx\dot{x} = 0. \tag{6.98}$$

Now, we wish to obtain the energy rate equation using Jourdain's principle. Multiplying Eq. 6.94 by $\delta\dot{x}\,(t)$, Jourdain's principle is expressed by

$$(m\ddot{x} + kx)\,\delta\dot{x} = 0. \tag{6.99}$$

Expanding Eq. 6.99 and using Eq. 6.93, we obtain

$$\begin{aligned}(m\ddot{x} + kx)\,\delta\dot{x} &= m\ddot{x}\delta\dot{x} + kx\delta\dot{x} \\ &= \frac{\partial}{\partial\dot{x}}\,(m\ddot{x}\dot{x})\,\delta\dot{x} + \frac{\partial}{\partial\dot{x}}\,(kx\dot{x})\,\delta\dot{x} \\ &= \frac{\partial}{\partial\dot{x}}\,(m\ddot{x}\dot{x} + kx\dot{x})\,\delta\dot{x} \\ &= \delta\,(m\ddot{x}\dot{x} + kx\dot{x}) \\ &= \delta\dot{L}\,(\dot{x}, x, t)\,.\end{aligned}$$

Therefore, in the absence of nonconservative forces, the energy rate equation is

$$\dot{L}\left(\dot{\boldsymbol{r}}_i, \boldsymbol{r}_i, t\right) = m\ddot{x}\dot{x} + kx\dot{x} = 0, \tag{6.100}$$

which is the same as the energy rate equation obtained by integration.

The next example considers a simple nonlinear problem.

Example 3 Consider a simple pendulum where the mass m is supported by the massless rod of the length L, oscillating with angle θ. The angle of oscillation is large enough that the small angle approximation no longer holds. We wish to obtain the energy rate equation by integrating the EOM as well as by using Jourdain's principle.

The equation of motion is obtained from Newton's second law (Euler's equation) to be

$$mL^2\ddot{\theta} + mgL\sin\theta = 0, \tag{6.101}$$

where g is the gravitational acceleration. Converting the acceleration as follows,

$$\begin{aligned}\ddot{\theta} &= \frac{d\dot{\theta}}{dt}\\ &= \frac{d\dot{\theta}}{d\theta}\frac{d\theta}{dt}\\ &= \frac{d}{d\theta}\left(\frac{1}{2}\dot{\theta}^2\right),\end{aligned} \tag{6.102}$$

and substituting it back into Eq. 6.101, we obtain

$$\frac{d}{d\theta}\left(\frac{1}{2}mL^2\dot{\theta}^2\right) + mgL\sin\theta = 0. \tag{6.103}$$

Integration of this equation with respect to θ yields to the energy equation

$$\frac{1}{2}mL^2\dot{\theta}^2 - mgL\cos\theta = C, \tag{6.104}$$

and by differentiating it with respect to time, the energy rate equation is obtained,

$$mL^2\ddot{\theta}\dot{\theta} + mgL\dot{\theta}\sin\theta = 0. \tag{6.105}$$

Jourdain's variational formulation of the simple pendulum problem is obtained by multiplying the EOM by $\delta\dot{\theta}$ to find,

$$\left(mL^2\ddot{\theta} + mgL\sin\theta\right)\delta\dot{\theta} = 0. \tag{6.106}$$

The energy rate equation is obtained by utilizing Eq. 6.93,

$$\begin{aligned}\left(mL^2\ddot{\theta} + mgL\sin\theta\right)\delta\dot{\theta} &= mL^2\ddot{\theta}\delta\dot{\theta} + mgL\sin\theta\delta\dot{\theta}\\ &= \frac{\partial}{\partial\dot{\theta}}\left(mL^2\ddot{\theta}\dot{\theta}\right)\delta\dot{\theta} + \frac{\partial}{\partial\dot{\theta}}\left(mgL\dot{\theta}\sin\theta\right)\delta\dot{\theta}\end{aligned}$$

$$= \delta\left(mL^2\ddot{\theta}\dot{\theta} + mgL\dot{\theta}\sin\theta\right)$$
$$= \delta\dot{L}\left(\dot{\theta}, \theta, t\right).$$

Therefore,

$$\dot{L}\left(\dot{\boldsymbol{r}}_i, \boldsymbol{r}_i, t\right) = mL^2\ddot{\theta}\dot{\theta} + mgL\dot{\theta}\sin\theta = 0 \tag{6.107}$$

is the same result as that obtained by integrating the EOM.

As evident from the two examples, the energy rate equation can be straightforwardly obtained from Jourdain's principle by using Eq. 6.93. From the variational point of view, the only requirement is that the commutation rule must hold (note that we used the commutation rules in our derivation in Eq. 6.92).

While the commutation rule holds for a system described in the Lagrangian reference frame, it does not hold if it is described in the Eulerian reference frame. This is shown in the following section.

6.15.2 *Obtaining the Energy Rate Equation in the Eulerian Reference Frame*

As mentioned in the previous section, Lagrange's equation is a function of generalized displacements, generalized velocities, and time, as is the rate of Lagrange's equation, which contains acceleration terms as shown in the two prior examples. We saw that the energy rate equations can be obtained from Jourdain's principle by using Eq. 6.93 if the commutation rule holds.

For the rate of Lagrange's equation described in the Eulerian frame of reference, we show next that Jourdain's variational operator δ and the material derivative do not commute, first by considering the acceleration $D\boldsymbol{u}/Dt$ and obtaining $D\left(\delta\boldsymbol{u}\right)/Dt$, and then by finding $\delta\left(D\boldsymbol{u}/Dt\right)$. We then propose a way to separate our function into a commutable part and a non-commutable part as a way to move forward.

We start with $D\left(\delta\boldsymbol{u}\right)/Dt$. Since the variation is imposed prior to differentiation, the velocity is $\boldsymbol{u} + \delta\boldsymbol{u}$, and we have

$$\frac{D\left(\delta\boldsymbol{u}\right)}{Dt} = \frac{\partial\left(\delta\boldsymbol{u}\right)}{\partial t} + \left(\boldsymbol{u} + \delta\boldsymbol{u}\right)\cdot\nabla\left(\delta\boldsymbol{u}\right)$$
$$= \frac{\partial\left(\delta\boldsymbol{u}\right)}{\partial t} + \boldsymbol{u}\cdot\nabla\left(\delta\boldsymbol{u}\right) + \delta\boldsymbol{u}\cdot\nabla\left(\delta\boldsymbol{u}\right). \tag{6.108}$$

The last term on the right of Eq. 6.108 is second-order with respect to $\delta\boldsymbol{u}$, and so it must be neglected according to Jourdain's principle. Therefore, the material derivative of the virtual velocity is found to be

$$\frac{D\left(\delta\boldsymbol{u}\right)}{Dt} = \frac{\partial\left(\delta\boldsymbol{u}\right)}{\partial t} + \boldsymbol{u}\cdot\nabla\left(\delta\boldsymbol{u}\right). \tag{6.109}$$

For the variation of the acceleration $\delta\left(D\boldsymbol{u}/Dt\right)$, for velocity $\boldsymbol{u}$, we consider the definition of Jourdain's variational operator, Eq. 6.42,

$$\begin{aligned}\delta\left(\frac{D\boldsymbol{u}}{Dt}\right) &= \lim_{\varepsilon\to 0}\frac{1}{\varepsilon}\left[\frac{D}{Dt}\left(\boldsymbol{u}+\varepsilon\,\delta\boldsymbol{u}\right)-\frac{D}{Dt}\left(\boldsymbol{u}\right)\right]\\ &= \lim_{\varepsilon\to 0}\frac{1}{\varepsilon}\left[\frac{\partial}{\partial t}\left(\boldsymbol{u}+\varepsilon\,\delta\boldsymbol{u}\right)+\left(\boldsymbol{u}+\varepsilon\,\delta\boldsymbol{u}\right)\cdot\nabla\left(\boldsymbol{u}+\varepsilon\,\delta\boldsymbol{u}\right)-\frac{D}{Dt}\left(\boldsymbol{u}\right)\right]\\ &= \lim_{\varepsilon\to 0}\frac{1}{\varepsilon}\left[\frac{\partial\boldsymbol{u}}{\partial t}+\varepsilon\frac{\partial\left(\delta\boldsymbol{u}\right)}{\partial t}+\boldsymbol{u}\cdot\nabla\boldsymbol{u}+\varepsilon\,\delta\boldsymbol{u}\cdot\nabla\boldsymbol{u}+\boldsymbol{u}\cdot\nabla\left(\varepsilon\,\delta\boldsymbol{u}\right)\right.\\ &\quad\left.+\varepsilon^2\delta\boldsymbol{u}\cdot\nabla\left(\delta\boldsymbol{u}\right)-\frac{D}{Dt}\left(\boldsymbol{u}\right)\right].\end{aligned}\tag{6.110}$$

Taking the limit, the above expression becomes

$$\delta\left(\frac{D\boldsymbol{u}}{Dt}\right)=\frac{\partial\left(\delta\boldsymbol{u}\right)}{\partial t}+\boldsymbol{u}\cdot\nabla\left(\delta\boldsymbol{u}\right)+\delta\boldsymbol{u}\cdot\nabla\boldsymbol{u}.\tag{6.111}$$

Comparing Eqs. 6.109 and 6.111 yields

$$\delta\left(\frac{D\boldsymbol{u}}{Dt}\right)=\frac{D\left(\delta\boldsymbol{u}\right)}{Dt}+\delta\boldsymbol{u}\cdot\nabla\boldsymbol{u},\tag{6.112}$$

where $\delta\boldsymbol{u}\cdot\nabla\boldsymbol{u}$ is the "non-commuting part" of the acceleration in the Eulerian reference frame. That is, Jourdain's variational operator and the material derivative do not generally commute due to the expression $\delta\boldsymbol{u}\cdot\nabla\boldsymbol{u}$ on the right-hand side of Eq. 6.112. If $\delta\boldsymbol{u}\cdot\nabla\boldsymbol{u}=\boldsymbol{0}$, then they do commute in the way d'Alembert's variation does.

Since the commutation rule does not generally hold in the Eulerian reference frame, Eq. 6.93 cannot be used. This difficulty can be overcome if the non-commuting part is extracted from the rate of Lagrange's function $\dot{L}\left(\dot{\boldsymbol{r}}_i,\boldsymbol{r}_i,t\right)$. The following discussion motivates and stipulates a way to separate out the non-commuting part.

In order to demonstrate how the non-commuting part can be separated in the Eulerian reference frame, we consider Newton's second law as described in the Eulerian reference frame,

$$\frac{D\boldsymbol{u}\left(\boldsymbol{x},t\right)}{Dt}=\boldsymbol{f}\left(\boldsymbol{x},t\right),\tag{6.113}$$

where $\boldsymbol{f}$ is the resultant of external loads per unit mass acting at the spatial point $\boldsymbol{x}$. Multiplication of Eq. 6.113 by the virtual velocity, $\delta\boldsymbol{u}$, results in Jourdain's principle,

$$\frac{D\boldsymbol{u}}{Dt}\cdot\delta\boldsymbol{u}=\boldsymbol{f}\cdot\delta\boldsymbol{u}.\tag{6.114}$$

For the acceleration term, $D\boldsymbol{u}/Dt$, the commutation rule does not hold due to the existence of $\delta\boldsymbol{u}\cdot\nabla\boldsymbol{u}$ in Eq. 6.112. However, the acceleration term of a system is reversible (conservative) in the Eulerian reference frame if $\delta\boldsymbol{u}\cdot\nabla\boldsymbol{u}=0$. $D\boldsymbol{u}/Dt$

contains both the conservative (reversible) and nonconservative (irreversible, noncommuting) terms. The question, then, is how to modify Eq. 6.114 so that the commutation rule can be applied. We recall that for the application of variational principles to systems with nonconservative terms, such as damping, we can group these with the external forces, while the conservative terms are grouped together on the left-hand side of the EOM.

In the following derivation, we look to separate out the nonconservative component of the left-hand side of Eq. 6.114 and place it on the right-hand side with the external forces. Therefore, the left-hand side will only contain conservative terms, and we show the material derivative as D^C/Dt to signify this.

Expanding the left-hand side of Eq. 6.114 as

$$\frac{D\boldsymbol{u}}{Dt}\cdot\delta\boldsymbol{u} = \frac{D}{Dt}(\boldsymbol{u}\cdot\delta\boldsymbol{u}) - \frac{D}{Dt}(\delta\boldsymbol{u})\cdot\boldsymbol{u},$$

and applying Eq. 6.112 to the last term on the right, we obtain

$$\begin{aligned}\frac{D\boldsymbol{u}}{Dt}\cdot\delta\boldsymbol{u} &= \frac{D}{Dt}(\boldsymbol{u}\cdot\delta\boldsymbol{u}) - \left[\delta\left(\frac{D\boldsymbol{u}}{Dt}\right) - \delta\boldsymbol{u}\cdot\nabla\boldsymbol{u}\right]\cdot\boldsymbol{u} \\ &= \frac{D}{Dt}(\boldsymbol{u}\cdot\delta\boldsymbol{u}) - \delta\left(\frac{D\boldsymbol{u}}{Dt}\right)\cdot\boldsymbol{u} + \delta\boldsymbol{u}\cdot\nabla\boldsymbol{u}\cdot\boldsymbol{u}.\end{aligned}$$

Substituting back into Eq. 6.114, we obtain

$$\frac{D}{Dt}(\boldsymbol{u}\cdot\delta\boldsymbol{u}) - \delta\left(\frac{D\boldsymbol{u}}{Dt}\right)\cdot\boldsymbol{u} + \delta\boldsymbol{u}\cdot\nabla\boldsymbol{u}\cdot\boldsymbol{u} = \boldsymbol{f}\cdot\delta\boldsymbol{u}. \tag{6.115}$$

Considering Eq. 6.115, if the commutation rule holds, then $\delta\boldsymbol{u}\cdot\nabla\boldsymbol{u}\cdot\boldsymbol{u}$ would not be present ($\delta\boldsymbol{u}\cdot\nabla\boldsymbol{u} = 0$). Thus, the remainder of the terms on the left-hand side are those that are reversible with respect to $\delta\boldsymbol{u}$ (the terms for which the commutation rule holds). Therefore, by moving the term $\delta\boldsymbol{u}\cdot\nabla\boldsymbol{u}\cdot\boldsymbol{u}$ to the right-hand side of the equation, the left-hand side becomes purely conservative,

$$\overbrace{\frac{D^C}{Dt}(\boldsymbol{u}\cdot\delta\boldsymbol{u}) - \delta\left(\frac{D^C\boldsymbol{u}}{Dt}\right)\cdot\boldsymbol{u}}^{\text{conservative terms}} = \overbrace{\boldsymbol{f}\cdot\delta\boldsymbol{u} - \delta\boldsymbol{u}\cdot\nabla\boldsymbol{u}\cdot\boldsymbol{u}}^{\text{nonconservative terms}}, \tag{6.116}$$

where we have added the superscript C on the material derivative in order to emphasize and distinguish that these are reversible, or conservative, operations and, therefore, the commutation rule holds. Using the commutation rule for the conservative terms and rearranging the nonconservative terms, Jourdain's variational principle is obtained alternatively as

$$\frac{D^C\boldsymbol{u}}{Dt}\cdot\delta\boldsymbol{u} = (\boldsymbol{f} - \nabla\boldsymbol{u}\cdot\boldsymbol{u})\cdot\delta\boldsymbol{u}. \tag{6.117}$$

Therefore, the energy rate can be obtained for the left-hand side of Eq. 6.117 by using Eq. 6.93, having considered the non-commuting part as a nonconservative force.

The nonconservative terms reduce the generality of variational methods. A commonly used tool to overcome this challenge is Rayleigh's dissipation function (RDF), which is reviewed in the following section. RDF together with the discussion presented in this section will be used in our manipulations, in Sects. 6.16 and 6.17, of the extended Jourdain's principle obtained in Sect. 6.14.

6.15.3 Rayleigh's Dissipation Function

Generally, variational methods are powerful tools for reversible processes (conservative systems). For nonconservative systems, especially frictional dissipative systems (viscous fluids), variational methods lose their generality. Frictional (viscous) forces originate from a transfer of macroscopic into microscopic motions. Therefore, the number of degrees of freedom needed to describe the motion must be increased to include the dissipation process in variational formulations requiring statistical principles [11, p. 359].

Alternatively, the effects of nonconservative forces can be added to a variational formulation in the same manner that external forces are considered, as we did in the last section. This approach, which is justified by the law of conservation of energy, reduces the generality of the variational methods depending on the dynamics and properties of the system. Having added the terms representing the irreversible processes, we choose dissipation functions the variations of which represent dissipative forces.

Rayleigh's dissipation function is widely utilized in the literature. It has been applied to important types of forces, for instance, forces due to linear dampers and electromagnetic forces. While our discussion in this section is focused on Rayleigh's dissipation function, it is worth noting that there have been many attempts to develop variational methods for nonconservative systems. A good representative work is the paper by Riewe [20], where he proposed the use of fractional derivatives for Lagrangian and Hamiltonian mechanics.

Considering the viscous terms of the Navier–Stokes equations (Eq. 6.83), the symmetric part of $\nabla \boldsymbol{u}$ is only included (Eq. 6.82) assuming that the rotating flow has no effect on the shear stress (assuming rigid body rotation). Since the virtual velocities must be compatible with the system's constraints, the directions of the virtual velocities are constrained to be the same as those of the actual velocities, otherwise, the rotation caused by $\delta \boldsymbol{u}$ will perform work on the system. This is the assumption upon which Rayleigh's dissipation function is based. In vector notation, Rayleigh's dissipation function can be expressed in relation to the generalized force $\boldsymbol{F}_R$,

$$\boldsymbol{F}_R = \nabla_{\boldsymbol{u}} \phi_R,$$

where $\nabla_{\boldsymbol{u}}\phi_R$ denotes the differentiation of Rayleigh's dissipation function, ϕ_R, with respect to $\boldsymbol{u}$ in direction of $\boldsymbol{u}$ [6, pp. 22–24], that is,

$$\nabla_{\boldsymbol{u}}\phi_R = \left.\frac{\partial \phi_R}{\partial \boldsymbol{u}}\right|_{\boldsymbol{u}\text{-direction}}.$$

The directional differential of any function ϕ can be obtained using Eq. 6.43 by setting $\boldsymbol{w} = \boldsymbol{u}$,

$$\nabla_{\boldsymbol{u}}\phi_R \cdot \boldsymbol{u} = \left.\frac{\partial \phi\,(\boldsymbol{u} + \varepsilon \boldsymbol{u})}{\partial \varepsilon}\right|_{\varepsilon=0}. \tag{6.118}$$

Therefore, defining ϕ_R such that $\nabla_{\boldsymbol{u}}\phi_R = \boldsymbol{F}_R$, the term $\boldsymbol{F}_R \cdot \delta\boldsymbol{u}$ in the variational formulation can be replaced by $\delta\phi_R$ since

$$\delta\phi_R = \nabla_{\boldsymbol{u}}\phi_R \cdot \delta\boldsymbol{u}, \tag{6.119}$$

where this is Rayleigh's dissipation function in vector notation for a system.

Comparing Eqs. 6.119 with 6.45, Rayleigh's dissipation function constrains $\delta\boldsymbol{u}$ to be in the same direction as $\boldsymbol{u}$ for the nonconservative terms at any point in the domain. However, this constraint was already imposed by the assumptions that were made in obtaining the constitutive relation for Newtonian fluids (*see* Sect. 6.14 and [9, pp. 100–103]). The reason is that the proportionality of the viscous force and $\nabla\boldsymbol{u}$ was the result of observing laminar flows in the first place.

An important note regarding Rayleigh's dissipation function is that the work (power) of Rayleigh's dissipation function in the variational energy (power) formulation is half of that in the corresponding energy (power) equation [14, Eqs. 5 and 6]. In one dimension, the viscous damping force is given by $F_R = -cu$, where c is the viscous damping constant. Rayleigh's dissipation function is then given by $\phi_R = cu^2/2$. The power is then cu^2 or $2\phi_R$.

In general, we consider the variational energy formulation of a system with frictional dissipative forces as

$$\delta_d\,(T + \Pi - \phi_R - W_{ext}) = 0, \tag{6.120}$$

where δ_d is d'Alembert's variational operator, T is the kinetic energy, Π denotes the potential energy, and W_{ext} is the work due to external loads. Assuming that Eq. 6.120 is obtained from the variational manipulation, the corresponding energy equation is obtained by multiplying Rayleigh's dissipation function by a factor of two,

$$T + \Pi - 2\phi_R - W_{ext} = 0.$$

The reason is that the frictional dissipation only depends on the velocity and is unaffected by the displacement. Using Jourdain's variational operator, we have

$$\delta\left(\dot{T} + \dot{\Pi} - \dot{\phi}_R - \dot{W}_{ext}\right) = 0, \tag{6.121}$$

where the overdot denotes that the terms have dimensions of power and not work. Here, the frictional dissipation remains unaffected by the acceleration and the power equation becomes

$$\dot{T} + \dot{\Pi} - 2\dot{\phi}_R - \dot{W}_{ext} = 0. \tag{6.122}$$

Next, based on the discussions so far, we modify the previously derived extended Jourdain's principle. Both Eqs. 6.121 and 6.122 will be referred to as the energy rate equation, where the reader can distinguish them by the presence of Jourdain's variation δ.

6.16 Energy Rate Equation for Incompressible Viscous Fluids

In Sect. 6.13, the extended Jourdain's principle was expressed in Eq. 6.76. If we substitute the forces from the constitutive relations for a Newtonian incompressible viscid fluid (Eqs. 6.78–6.82), the extended JP for a general control volume becomes

$$\int_{CV} \rho \frac{D\boldsymbol{u}}{Dt} \cdot \delta\boldsymbol{u}\, dV = \int_{CV} \left\{\nabla \cdot \left[-p\bar{\boldsymbol{I}} + \mu\left(\nabla\boldsymbol{u} + \nabla^T\boldsymbol{u}\right)\right]\right\} \cdot \delta\boldsymbol{u}\, dV, \tag{6.123}$$

where $\nabla^T\boldsymbol{u} = (\nabla\boldsymbol{u})^T$ and body forces are neglected. If the only body force present is due to gravity, its potential function can easily be obtained, since gravitational forces are conservative and independent of the fluid velocity field.

In Sect. 6.15.1, it was shown that the energy rate equation can be obtained using Eq. 6.93 for systems described in the Lagrangian reference frame. In Sect. 6.15.2, it was shown that the commutation rule does not hold in the Eulerian reference frame. However, this difficulty was overcome by extracting the non-commuting term from the acceleration as explained in deriving Eq. 6.117. Using the same procedure, Eq. 6.123 becomes

$$\int_{CV} \rho \frac{D^C\boldsymbol{u}}{Dt} \cdot \delta\boldsymbol{u}\, dV = \int_{CV} \left\{\nabla \cdot \left[-p\bar{\boldsymbol{I}} + \mu\left(\nabla\boldsymbol{u} + \nabla^T\boldsymbol{u}\right)\right]\right\} \cdot \delta\boldsymbol{u}\, dV - \int_{CV} \rho\left(\nabla\boldsymbol{u} \cdot \boldsymbol{u}\right) \cdot \delta\boldsymbol{u}\, dV, \tag{6.124}$$

where the left-hand side of the equation now represents only the conservative terms and the right-hand side represents the nonconservative terms. Therefore, we continue our derivation by considering each side of Eq. 6.124 separately, using Eq. 6.93 for the conservative terms, and Eq. 6.119 for the dissipative terms, to obtain the energy rate equation, as follows.

6.16.1 The Left-Hand Side of Eq. 6.124

The term on the left-hand side of Eq. 6.124 is reversible and conservative and therefore Jourdain's variation δ and D/Dt commute. In the following derivation we use the same steps as we did in the derivation of Eq. 6.93, and as in Examples 2 and 3. Begin with the left- hand side,

$$\begin{aligned}\int_{CV} \rho \frac{D^C \boldsymbol{u}}{Dt} \cdot \delta \boldsymbol{u}\, dV &= \int_{CV} \delta \left(\rho \frac{D^C \boldsymbol{u}}{Dt} \cdot \boldsymbol{u} \right) dV \\ &= \delta \int_{CV} \left(\rho \frac{D^C \boldsymbol{u}}{Dt} \cdot \boldsymbol{u} \right) dV \\ &= \delta \int_{CV} \frac{D^C}{Dt} \left(\frac{1}{2} \rho \boldsymbol{u} \cdot \boldsymbol{u} \right) dV, \end{aligned} \tag{6.125}$$

where Jourdain's variational operator commutes with integration over the volume since it assumes zero virtual displacements. That is, the same particles occupy a control volume before and after imposing the virtual velocities. Note that the same statement is not true for d'Alembert's variational operator since the virtual displacements result in a virtual flux across the control surfaces.

Equation 6.125 can be modified further as follows. The total kinetic energy of a control volume, T, is defined as

$$T = \int_{CV} \frac{1}{2} \rho\, \boldsymbol{u} \cdot \boldsymbol{u}\, dV. \tag{6.126}$$

The rate of kinetic energy of a control volume can be obtained by using the Reynolds transport theorem in the form of Eq. 6.25,

$$\begin{aligned}\frac{DT}{Dt} &= \frac{D}{Dt} \int_{CV} \frac{1}{2} \rho\, \boldsymbol{u} \cdot \boldsymbol{u}\, dV \\ &= \int_{CV} \frac{D}{Dt} \left(\frac{1}{2} \rho\, \boldsymbol{u} \cdot \boldsymbol{u} \right) dV - \int_{CS} \left(\frac{1}{2} \rho\, \boldsymbol{u} \cdot \boldsymbol{u} \right) (\boldsymbol{u} - \boldsymbol{v}_{CS}) \cdot \boldsymbol{n}\, dA. \end{aligned} \tag{6.127}$$

Rearranging Eq. 6.127 yields

$$\int_{CV} \frac{D}{Dt} \left(\frac{1}{2} \rho\, \boldsymbol{u} \cdot \boldsymbol{u} \right) dV = \frac{D}{Dt} \int_{CV} \frac{1}{2} \rho\, \boldsymbol{u} \cdot \boldsymbol{u}\, dV + \int_{CS} \left(\frac{1}{2} \rho\, \boldsymbol{u} \cdot \boldsymbol{u} \right) (\boldsymbol{u} - \boldsymbol{v}_{CS}) \cdot \boldsymbol{n}\, dA. \tag{6.128}$$

Finally, by substituting Eq. 6.128 into Eq. 6.125, the left-hand side of Eq. 6.124 becomes

$$\int_{CV} \rho \frac{D^C \boldsymbol{u}}{Dt} \cdot \delta \boldsymbol{u} \, dV = \delta \left[\frac{D^C}{Dt} \int_{CV} \frac{1}{2} \rho \, \boldsymbol{u} \cdot \boldsymbol{u} \, dV + \int_{CS} \left(\frac{1}{2} \rho \, \boldsymbol{u} \cdot \boldsymbol{u} \right) (\boldsymbol{u} - \boldsymbol{v}_{CS}) \cdot \boldsymbol{n} \, dA \right], \tag{6.129}$$

where we have introduced D^C/Dt in the last step. Equation 6.129 represents the energy rate of the conservative terms of the extended Jourdain's principle. The variations are Jourdain's variation since we used the property that the virtual displacement equals zero above.

The energy rate of the nonconservative terms are obtained in the following section.

6.16.2 The Right-Hand Side of Eq. 6.124

In this section, we wish to obtain a function ϕ so that its variation equals the right-hand side of Eq. 6.124, that is,

$$\delta\phi = \int_{CV} \left\{ \nabla \cdot \left[-p\bar{\boldsymbol{I}} + \mu \left(\nabla \boldsymbol{u} + \nabla^T \boldsymbol{u} \right) \right] \right\} \cdot \delta \boldsymbol{u} \, dV - \int_{CV} \rho \left(\nabla \boldsymbol{u} \cdot \boldsymbol{u} \right) \cdot \delta \boldsymbol{u} \, dV, \tag{6.130}$$

where ϕ is a scalar-valued potential function, the variation of which yields the terms on the right-hand side of the energy rate equation.

For simplicity, since the manipulations are lengthy, we separate the terms on the right-hand side of Eq. 6.130 according to their physical meanings and manipulate each of them separately, as follows.

6.16.2.1 Power Due to Pressure

Considering the term containing pressure, p, since ∇p is assumed to be independent of $\boldsymbol{u}$, it does not vary due to $\delta \boldsymbol{u}$, that is, $\delta (\nabla p) = 0$. Therefore, for an incompressible fluid, we have

$$\int_{CV} \left[\nabla \cdot \left(-p\bar{\boldsymbol{I}} \right) \right] \cdot \delta \boldsymbol{u} \, dV = \int_{CV} -\nabla p \cdot \delta \boldsymbol{u} \, dV. \tag{6.131}$$

Using the divergence theorem, the right-hand side becomes

$$-\delta \int_{CS} p \boldsymbol{u} \cdot \boldsymbol{n} \, dA.$$

6.16.2.2 Power Lost Due to Viscous Dissipation

The function $\left[\nabla \cdot \left(\nabla \boldsymbol{u} + \nabla^T \boldsymbol{u} \right) \right] \cdot \delta \boldsymbol{u}$ contains both the virtual power due to the viscous forces acting as an external shear load on the control surface, and the virtual

power due to viscous dissipative forces inside the control volume, that is,

$$\left[\nabla\cdot\left(\nabla\boldsymbol{u}+\nabla^T\boldsymbol{u}\right)\right]\cdot\delta\boldsymbol{u}=\overbrace{\nabla\cdot\left[\left(\nabla\boldsymbol{u}+\nabla^T\boldsymbol{u}\right)\cdot\delta\boldsymbol{u}\right]}^{\text{due to the external shear stresses}}-\overbrace{tr\left[\left(\nabla\boldsymbol{u}+\nabla^T\boldsymbol{u}\right)\cdot\nabla\left(\delta\boldsymbol{u}\right)\right]}^{\text{viscous dissipation}},\quad(6.132)$$

where tr denotes the trace of a tensor.

We wish to utilize Rayleigh's dissipation function for nonconservative (viscous, dissipative) terms. However, applying Eq. 6.119 to the last term of Eq. 6.132 requires extensive mathematical manipulation due to the term $\nabla\left(\delta\boldsymbol{u}\right)$.

Alternatively, the derivations can be simplified by obtaining the scalar potential function of $\left[\nabla\cdot\left(\nabla\boldsymbol{u}+\nabla^T\boldsymbol{u}\right)\right]\cdot\delta\boldsymbol{u}$ in direction of $\boldsymbol{u}$ using Eq. 6.119, and then subtracting the scalar potential function of the external loads obtained similarly. The remaining terms will be Rayleigh's dissipation function,

$$\mu\ tr\left[\left(\nabla\boldsymbol{u}+\nabla^T\boldsymbol{u}\right)\cdot\nabla\left(\delta\boldsymbol{u}\right)\right]=\delta\left\{\frac{1}{2}\mu\ tr\left[\left(\nabla\boldsymbol{u}+\nabla^T\boldsymbol{u}\right)\cdot\nabla\boldsymbol{u}\right]\right\}.\quad(6.133)$$

Details can be found in Mottaghi ([16], pages 75–78).

The scalar potentials associated with the external viscous loads are considered next.

6.16.2.3 Power Due to Shear Forces Acting on the Control Surfaces

From Eq. 6.132, for the external viscous shear loads, we have

$$\begin{aligned}&\int_{CV}\mu\nabla\cdot\left[\left(\nabla\boldsymbol{u}+\nabla^T\boldsymbol{u}\right)\cdot\ \delta\boldsymbol{u}\right]dV\\&=\delta\int_{CV}\mu\nabla\cdot\left[\left(\nabla\boldsymbol{u}+\nabla^T\boldsymbol{u}\right)\cdot\ \boldsymbol{u}\right]\ dV-\int_{CV}\mu\nabla\cdot\left[\delta\left(\nabla\boldsymbol{u}+\nabla^T\boldsymbol{u}\right)\cdot\ \boldsymbol{u}\right]\ dV.\end{aligned}\quad(6.134)$$

The external loads must remain unchanged with respect to $\delta\boldsymbol{u}$ since they are the known parameters of the system, that is, the velocity of the flow is known at the control surfaces. Therefore, the second integral on the right-hand side of Eq. 6.134 equals zero, resulting in

$$\int_{CV}\mu\nabla\cdot\left[\left(\nabla\boldsymbol{u}+\nabla^T\boldsymbol{u}\right)\cdot\ \delta\boldsymbol{u}\right]\ dV=\delta\int_{CV}\mu\nabla\cdot\left[\left(\nabla\boldsymbol{u}+\nabla^T\boldsymbol{u}\right)\cdot\ \boldsymbol{u}\right]\ dV.\quad(6.135)$$

6.16.2.4 The Non-commuting Term

The only term left on the right-hand side of Eq. 6.124 is the non-commuting part of the rate of the kinetic energy due to variation of the acceleration, $\rho\,(\nabla \boldsymbol{u}\cdot\boldsymbol{u})\cdot\delta\boldsymbol{u}$. In order to obtain the scalar potential function corresponding to the non-commuting part, we start by considering the vector identity,

$$\frac{1}{2}\nabla\,(\boldsymbol{u}\cdot\boldsymbol{u}) = \nabla\boldsymbol{u}\cdot\boldsymbol{u}.$$

Therefore,

$$\int_{CV}\rho\,(\nabla\boldsymbol{u}\cdot\boldsymbol{u})\cdot\delta\boldsymbol{u}\,dV = \int_{CV}\frac{1}{2}\rho\nabla\,(\boldsymbol{u}\cdot\boldsymbol{u})\cdot\delta\boldsymbol{u}\,dV. \tag{6.136}$$

For an incompressible fluid, we have $\nabla\cdot\boldsymbol{u}=0$. Since the virtual velocities must be compatible with the system constraints, for an incompressible fluid the virtual velocities must be divergence free (solenoidal) as well, $\nabla\cdot\delta\boldsymbol{u}=0$. Therefore,

$$\nabla\,(\boldsymbol{u}\cdot\boldsymbol{u})\cdot\delta\boldsymbol{u} = \nabla\cdot[(\boldsymbol{u}\cdot\boldsymbol{u})\;\delta\boldsymbol{u}],$$

and using Gauss' theorem,

$$\int_{CV}\rho\,(\nabla\boldsymbol{u}\cdot\boldsymbol{u})\cdot\delta\boldsymbol{u}\,dV = \int_{CS}\frac{1}{2}\rho\,(\boldsymbol{u}\cdot\boldsymbol{u})\,(\delta\boldsymbol{u}\cdot\boldsymbol{n})\;dA. \tag{6.137}$$

Since the velocity of the flow at the control surfaces are assumed to be known, the forcing function at the control surfaces was considered to be invariant with respect to virtual velocity. Similarly, the non-commuting part of the rate of the kinetic energy, shown above, only exists on the control surfaces. Thus, the term $\frac{1}{2}\rho\,(\boldsymbol{u}\cdot\boldsymbol{u})$ in the integrand of Eq. 6.137 is invariant with respect to $\delta\boldsymbol{u}$. Therefore,

$$\int_{CV}\rho\,(\nabla\boldsymbol{u}\cdot\boldsymbol{u})\cdot\delta\boldsymbol{u}\,dV = \delta\int_{CS}\frac{1}{2}\rho\,(\boldsymbol{u}\cdot\boldsymbol{u})\,(\boldsymbol{u}\cdot\boldsymbol{n})\;dA. \tag{6.138}$$

When using Jourdain's variational principle, it is important to recall that Jourdain's virtual velocity does not correspond to any displacement field. Therefore, when the velocity is known, the virtual velocity becomes the actual velocity and not zero.

Having obtained the scalar potential functions associated with both right-hand and left-hand sides of Eq. 6.124, we combine them and obtain the energy rate equation in the following section.

6.16.3 Extended JP in Terms of Energy

Using Eqs. 6.124 and 6.130, substituting all the components derived above, the variational energy rate equation for a general control volume of a Newtonian incompressible viscous fluid is obtained,

$$\delta\left[\frac{D^C}{Dt}\int\limits_{CV}\frac{1}{2}\rho\,\boldsymbol{u}\cdot\boldsymbol{u}dV+\int\limits_{CS}\left(\frac{1}{2}\rho\,\boldsymbol{u}\cdot\boldsymbol{u}\right)(\boldsymbol{u}-\boldsymbol{v}_{CS})\cdot\boldsymbol{n}dA\right]$$
$$=\overbrace{\delta\int\limits_{CS}-p\,\boldsymbol{u}\cdot\boldsymbol{n}dA+\delta\int\limits_{CV}\mu\nabla\cdot\left[\left(\nabla\boldsymbol{u}+\nabla^T\boldsymbol{u}\right)\cdot\boldsymbol{u}\right]dV}^{\text{power due to external loads}}$$
$$-\overbrace{\delta\int\limits_{CV}\frac{1}{2}\mu\,tr\left[\left(\nabla\boldsymbol{u}+\nabla^T\boldsymbol{u}\right)\cdot\nabla\boldsymbol{u}\right]dV}^{\text{power loss due to viscous dissipation}}-\overbrace{\delta\int\limits_{CS}\frac{1}{2}\rho\,(\boldsymbol{u}\cdot\boldsymbol{u})\,(\boldsymbol{u}\cdot\boldsymbol{n})\,dA}^{\text{non-commuting term}}. \tag{6.139}$$

Equation 6.139 can be used in modeling fluid dynamic systems and fluid–structure interactions (FSI).

As mentioned earlier, in order to obtain the energy rate equation corresponding to a variational energy rate equation, Rayleigh's dissipation function must be multiplied by a factor of two. Therefore, the energy rate equation corresponding to Eq. 6.139 is

$$\frac{D^C}{Dt}\int\limits_{CV}\frac{1}{2}\rho\boldsymbol{u}\cdot\boldsymbol{u}dV+\int\limits_{CS}\left(\frac{1}{2}\rho\boldsymbol{u}\cdot\boldsymbol{u}\right)(\boldsymbol{u}-\boldsymbol{v}_{CS})\cdot\boldsymbol{n}dA$$
$$=\overbrace{\int\limits_{CS}-p\boldsymbol{u}\cdot\boldsymbol{n}dA+\int\limits_{CV}\mu\nabla\cdot\left[\left(\nabla\boldsymbol{u}+\nabla^T\boldsymbol{u}\right)\cdot\boldsymbol{u}\right]dV}^{\text{power due to external loads}}$$
$$-\overbrace{\int\limits_{CV}\mu\,tr\left[\left(\nabla\boldsymbol{u}+\nabla^T\boldsymbol{u}\right)\cdot\nabla\boldsymbol{u}\right]dV}^{\text{power loss due to viscous dissipation}}-\overbrace{\int\limits_{CS}\frac{1}{2}\rho\,(\boldsymbol{u}\cdot\boldsymbol{u})\,(\boldsymbol{u}\cdot\boldsymbol{n})\,dA}^{\text{non-commuting term}}. \tag{6.140}$$

For FSI systems, the boundary conditions on the solid surfaces cannot be easily applied to these equations. The following section will show that the viscous terms can be modified further to become more applicable to FSI and VIV. We consider FSI and VIV in detail in Chap. 7.

6.17 An Expanded Form of the Energy Rate Equation

Our ultimate goal is the reduced-order modeling of FSI systems, but the energy rate equation obtained in the previous section (Eq. 6.139) is not easily accessible, mainly, due to two reasons. First, it is not clear how the boundary conditions at the solid surface can be included. Second, the tensor term $\nabla^T \boldsymbol{u}$ provides some challenges, as discussed further below. Therefore, we continue with our derivation by modifying the viscous dissipation and external load terms in order to have them in a more meaningful form.

Following the procedure by Lamb for an incompressible viscous fluid [10], the viscous dissipation function can also be expressed as

$$\int_{CV} \frac{1}{2}\mu \, tr\left[\left(\nabla \boldsymbol{u} + \nabla^T \boldsymbol{u}\right) \cdot \nabla \boldsymbol{u}\right] dV = \delta \int_{CV} \frac{1}{2}\mu \left\{(\nabla \times \boldsymbol{u}) \cdot (\nabla \times \boldsymbol{u}) + \nabla^2 (\boldsymbol{u} \cdot \boldsymbol{u}) - 2\,\nabla \cdot [\boldsymbol{u} \times (\nabla \times \boldsymbol{u})]\right\} dV. \tag{6.141}$$

The power due to the viscous forces external to the control volume can also be expressed as

$$\delta \int_{CV} \mu \nabla \cdot \left[\left(\nabla \boldsymbol{u} + \nabla^T \boldsymbol{u}\right) \cdot \boldsymbol{u}\right] dV = \delta \int_{CV} \mu \nabla \cdot [\nabla (\boldsymbol{u} \cdot \boldsymbol{u}) - \boldsymbol{u} \times (\nabla \times \boldsymbol{u})] \, dV. \tag{6.142}$$

Using Eqs. 6.141 and 6.142, we can obtain the variational energy rate equation as derived from the extended Jourdain's principle,

$$\delta \int_{CV} \frac{D^C}{Dt}\left(\frac{1}{2}\rho \boldsymbol{u} \cdot \boldsymbol{u}\right) dV = \overbrace{\delta \int_{CS} -p\, \boldsymbol{u} \cdot \boldsymbol{n} dA + \delta \int_{CV} \{\mu \nabla \cdot [\nabla (\boldsymbol{u} \cdot \boldsymbol{u}) - \boldsymbol{u} \times (\nabla \times \boldsymbol{u})]}^{\text{external loading}} \overbrace{-\frac{1}{2}\mu \left\{(\nabla \times \boldsymbol{u}) \cdot (\nabla \times \boldsymbol{u}) + \nabla^2 (\boldsymbol{u} \cdot \boldsymbol{u}) - 2\,\nabla \cdot [\boldsymbol{u} \times (\nabla \times \boldsymbol{u})]\right\}\Big\} dV}^{\text{viscous dissipation}} \overbrace{- \delta \int_{CS} \frac{1}{2}\rho \, (\boldsymbol{u} \cdot \boldsymbol{u}) (\boldsymbol{u} \cdot \boldsymbol{n}) \, dA}^{\text{non-commuting term}}, \tag{6.143}$$

where terms of the form $\nabla \cdot [\boldsymbol{u} \times (\nabla \times \boldsymbol{u})]$ will cancel each other out, and the terms $\nabla \cdot [\nabla (\boldsymbol{u} \cdot \boldsymbol{u})]$ and $\nabla^2 (\boldsymbol{u} \cdot \boldsymbol{u})$, which are identical, can be combined. However, since these terms represent different concepts, they are kept separate. The left-hand side

of Eq. 6.143 is the summation of the rate of change of kinetic energy ($\sum \frac{DT}{Dt}$) for all points in the domain. For reduced-order modeling, the rate of change of kinetic energy of the control volume ($\frac{d}{dt}\sum T$) might be of more interest. Also, for a control volume, in the absence of body forces, the external loads can only be applied at the control surfaces. Therefore, by replacing the left-hand side integral in Eq. 6.143 by its equivalent Eq. 6.128 and applying Gauss' divergence theorem (Eq. 6.19) to the control volume integral on the right-hand side, Eq. 6.143 becomes

$$\delta\left\{\overbrace{\frac{D^C}{Dt}\int_{CV}\frac{1}{2}\rho\boldsymbol{u}\cdot\boldsymbol{u}dV}^{\text{kinetic energy}}+\overbrace{\int_{CS}\left(\frac{1}{2}\rho\boldsymbol{u}\cdot\boldsymbol{u}\right)(\boldsymbol{u}-\boldsymbol{v}_{CS})\cdot\boldsymbol{n}dA}^{\text{flux of kinetic energy}}\right\}$$
$$=\delta\left\{\int_{CS}\overbrace{\{-p\,\boldsymbol{u}\cdot\boldsymbol{n}+\mu\left[\nabla(\boldsymbol{u}\cdot\boldsymbol{u})-\boldsymbol{u}\times(\nabla\times\boldsymbol{u})\right]\cdot\boldsymbol{n}}^{\text{external loads}}\right.$$
$$\overbrace{-\frac{1}{2}\mu\left[\nabla(\boldsymbol{u}\cdot\boldsymbol{u})-2\,\boldsymbol{u}\times(\nabla\times\boldsymbol{u})\right]\cdot\boldsymbol{n}}^{\text{viscous dissipation}}\Big\}dA-\frac{1}{2}\int_{CV}\mu(\nabla\times\boldsymbol{u})\cdot(\nabla\times\boldsymbol{u})\,dV$$
$$\left.-\overbrace{\int_{CS}\frac{1}{2}\rho(\boldsymbol{u}\cdot\boldsymbol{u})(\boldsymbol{u}\cdot\boldsymbol{n})\,dA}^{\text{non-commuting term}}\right\}. \tag{6.144}$$

Similar to the previous section, it is important to have in mind that the energy rate equation corresponding to Eq. 6.144 is obtained by multiplying Rayleigh's dissipation function by a factor of two, with the result

$$\overbrace{\frac{D^C}{Dt}\int_{CV}\frac{1}{2}\rho\boldsymbol{u}\cdot\boldsymbol{u}dV}^{\text{kinetic energy}}+\overbrace{\int_{CS}\left(\frac{1}{2}\rho\boldsymbol{u}\cdot\boldsymbol{u}\right)(\boldsymbol{u}-\boldsymbol{v}_{CS})\cdot\boldsymbol{n}dA}^{\text{flux of kinetic energy}}$$
$$=\int_{CS}\overbrace{\{-p\,\boldsymbol{u}\cdot\boldsymbol{n}+\mu\left[\nabla(\boldsymbol{u}\cdot\boldsymbol{u})-\boldsymbol{u}\times(\nabla\times\boldsymbol{u})\right]\cdot\boldsymbol{n}}^{\text{external loads}}$$
$$\overbrace{-\mu\left[\nabla(\boldsymbol{u}\cdot\boldsymbol{u})-2\,\boldsymbol{u}\times(\nabla\times\boldsymbol{u})\right]\cdot\boldsymbol{n}\}dA-\int_{CV}\mu(\nabla\times\boldsymbol{u})\cdot(\nabla\times\boldsymbol{u})\,dV}^{\text{viscous dissipation}}$$

$$\overbrace{-\int_{CS} \frac{1}{2}\rho\,(\boldsymbol{u}\cdot\boldsymbol{u})\,(\boldsymbol{u}\cdot\boldsymbol{n})\,dA}^{\text{non-commuting term}}. \tag{6.145}$$

In [17] and Chap. 7, Eqs. 6.143, 6.144 and 6.145 are used for FSI problems. Having obtained the rate of energy equation from the extended Jourdain's principle, the classical *energy equation in integral form* is derived next using Hamilton's principle. In all the above, we have used CV to represent $CV(t)$, CS for $CS(t)$, dA for $dA(t)$, and dV for $dV(t)$.

6.18 Comparison with the Classical Energy Equation in Integral Form

The classical energy equation in integral form, for a control volume of Newtonian incompressible viscous flow, and in the absence of body forces, is expressed by [16]

$$\frac{d}{dt}\int_{CV}\left(\frac{1}{2}\rho u^2\right)dV = -\int_{CS}\left(\frac{1}{2}\rho u^2\right)(\boldsymbol{u}_r\cdot\boldsymbol{n})\,dA - \int_{CS} p\boldsymbol{u}\cdot\boldsymbol{n}\,dA$$
$$+\int_{CS}\mu\left[\left(\nabla\boldsymbol{u}+\nabla^T\boldsymbol{u}\right)\cdot\boldsymbol{u}\right]\cdot\boldsymbol{n}dA - \int_{CV}\mu\,tr\left[\left(\nabla\boldsymbol{u}+\nabla^T\boldsymbol{u}\right)\cdot\nabla\boldsymbol{u}\right]dV. \tag{6.146}$$

Comparing Eq. 6.146 with our energy rate equation, Eq. 6.140, one difference is the existence of the non-commuting acceleration term. Examining the irreversibility of the Eulerian acceleration with respect to Jourdain's variational operator in Sect. 6.15.2, the non-commuting term was a result of obtaining the acceleration from the first-order velocities, as per the definition of Jourdain's variational operator. Instead, if we choose the zeroth order velocities, the non-commuting term disappears and the conservative terms of our energy rate equation would match the classical ones.

Therefore, our energy rate equation essentially assumes that the particle accelerations can be obtained from first-order approximations of the velocities. On the other hand, the classical energy equation obtains the Eulerian acceleration of the fluid particles by a zeroth order approximation of the velocity field. This may be an important difference beyond the considerations discussed here, and may have significance more generally in fluid mechanics.

Both energy rate equations, ours and the classical one, first integrate the kinetic energy of the control volume and then differentiate it to obtain the rate of kinetic energy. Therefore, both methods obtain the rate of average kinetic energy in the Eulerian reference frame. Conservation laws, however, are defined in the Lagrangian

reference frame. Stokes [21] calculated the first-order velocities and showed that the time average of the Eulerian velocities lags the average of the Lagrangian velocities for oscillatory waves. Similarly, our energy rate equation calculates the rate of change of kinetic energy of a control volume via first-order velocities.

In the following section, the chapter is concluded with a summary and a few additional remarks.

6.19 Discussion

The literature to this point states that a purely Eulerian variational method does not exist, and that the Navier–Stokes equations have not been obtained using a variational method. We have shown that Jourdain's principle can be modified to obtain a purely Eulerian variational formulation. Also, it was shown that the Navier–Stokes equations can be obtained from the extended JP as derived here. In our derivations, we did not make any assumptions, but used Jourdain's principle, continuum mechanics, and constitutive relations for Newtonian incompressible viscous fluids. The key stipulation was the separation of conservative terms and nonconservative terms in Eqs. 6.116 and 6.117, something that is normally done in variational mechanics.

Considering the derivations presented here, the main reason for the difficulties encountered in the literature can be traced to the Lagrangian–Eulerian relations. An essential component in relating a Lagrangian function to an Eulerian one is a mapping function of Lagrangian trajectories. In order to show this dependency, using Eqs. 6.71 and 6.75, we can write

$$\int_{CV}\left[\rho\frac{D^2\boldsymbol{u}}{Dt^2}\cdot\delta\boldsymbol{\Lambda}+\rho\frac{D\boldsymbol{u}}{Dt}\cdot\frac{D}{Dt}(\delta\boldsymbol{\Lambda})\right]dV=\int_{CV}\left[\frac{D}{Dt}\boldsymbol{f}\cdot\delta\boldsymbol{\Lambda}+\boldsymbol{f}\cdot\frac{D}{Dt}(\delta\boldsymbol{\Lambda})\right]dV,$$

that is, our extension of d'Alembert principle before imposing the Jourdain's constraints. As is evident in this equation, the mapping function $\boldsymbol{\Lambda}$ is required. In general, it is not possible to obtain function $\boldsymbol{\Lambda}$ from the information available for a control volume, because Lagrangian trajectories are defined by initial conditions that are not observable in an Eulerian frame. However, they are required in d'Alembert's principle and consequently in Lagrange's equations and Hamilton's principle. This difficulty was avoided by using JP and utilizing Jourdain's constraints ($\delta\boldsymbol{\Lambda}=\boldsymbol{0}$).

The absence of virtual displacements in our variational formulation might lead to a more advantageous approach for modeling viscous fluids. A variational function obtained by imposing virtual displacements is stationary inside an assumed control volume only if the first variation vanishes without any restriction on the second variation. The works of Millikan [14] and Bateman [2], discussed earlier, confirm that a Lagrangian function cannot be found for which this condition holds. Therefore, the existence of extrema must be investigated. If the conditions required to vanish the first variation results in restrictions on the second variation, the function can have an extremum. In general, it is challenging to find an extremum inside the control

volume. Therefore, investigating the control surface is preferable. However, the virtual displacements are not reversible on the control surface. Thus, the conditions imposed to vanish the first variation no longer hold inside the control volume [11, pp. 42–43], forcing one to try to obtain a function that is stationary, again. Since Jourdain's principle does not use the virtual displacement, it does not have the restriction on the boundary surfaces, as is evident from our derivations.

One of the main objectives of this chapter is to lay a theoretical foundation that can be utilized in reduced-order modeling of FSI and VIV. In reduced-order modeling, one tries to reduce the number of degrees of freedom in such a way that the few resulting EOM can capture the main characteristics of the nonlinear problem. In a sense, reduced-order modeling can be thought of as averaging over the material domain over some time span(s).

An interesting yet challenging problem that might arise is the *Stokes drift* type phenomena. Stokes considered the dynamics of oscillatory waves and showed that the time average of the Eulerian velocities lags the average of the Lagrangian velocities [21]. The term *Stokes drift* was later adopted for these differences in velocities. It is interesting that the information required to obtain Stokes drift is readily available from the Eulerian velocities [19], that is, such challenges can be avoided by solving the problem in either Eulerian or Lagrangian descriptions. Therefore, since the variational approach proposed here is purely Eulerian, unlike the methods available in the literature, it may have some additional advantages regarding *Stokes drift* type phenomena. However, it is too early to make such a conclusion and further investigation is required.

Hamilton's principle, Lagrange's equation, and Jourdain's principle are all derivable from d'Alembert's principle. We used this common feature and showed that the energy rate equation can be obtained from Jourdain's principle when the system is described in the Lagrangian frame of reference. However, for a system described in the Eulerian reference frame, it was shown that the commutation rule does not hold. This difficulty was overcome by extracting the non-commuting terms from the acceleration. This result was applied to our extension of Jourdain's principle, with an energy rate equation obtained for Newtonian incompressible viscous fluids. The results of our analytical derivation suggest that an extra term must be added to the classical energy equation in integral form to account for the non-commuting terms from the acceleration in the Eulerian reference frame. Further study is warranted.

We kept the viscous dissipative terms separate from the viscous forces external to the control volume during our derivations in this chapter. However, an interesting result is obtained if we combined those terms in the variational energy rate equation and the energy rate equation, as follows.

Considering Eq. 6.144, summation of the viscous terms results in

$$\delta\left\{\frac{D^C}{Dt}\int\limits_{CV}\frac{1}{2}\rho\boldsymbol{u}\cdot\boldsymbol{u}dV+\int\limits_{CS}\left(\frac{1}{2}\rho\boldsymbol{u}\cdot\boldsymbol{u}\right)(\boldsymbol{u}-\boldsymbol{v}_{CS})\cdot\boldsymbol{n}dA\right\}$$

$$= \delta \left\{ \int_{CS} \left[-p\,\boldsymbol{u}\cdot\boldsymbol{n} + \frac{1}{2}\mu\nabla(\boldsymbol{u}\cdot\boldsymbol{u})\cdot\boldsymbol{n} \right] dA \right.$$

$$\left. -\frac{1}{2}\int_{CV} \mu(\nabla\times\boldsymbol{u})\cdot(\nabla\times\boldsymbol{u})\,dV - \int_{CS}\frac{1}{2}\rho(\boldsymbol{u}\cdot\boldsymbol{u})(\boldsymbol{u}\cdot\boldsymbol{n})\,dA \right\}. \quad (6.147)$$

Similarly, summation of viscous terms in Eq. 6.145 yields

$$\frac{D^C}{Dt}\int_{CV}\frac{1}{2}\rho\boldsymbol{u}\cdot\boldsymbol{u}dV + \int_{CS}\left(\frac{1}{2}\rho\boldsymbol{u}\cdot\boldsymbol{u}\right)(\boldsymbol{u}-\boldsymbol{v}_{CS})\cdot\boldsymbol{n}dA$$

$$= \int_{CS}[-p\,\boldsymbol{u}\cdot\boldsymbol{n} + \mu\boldsymbol{u}\times(\nabla\times\boldsymbol{u})\cdot\boldsymbol{n}\,]dA$$

$$-\int_{CV}\mu(\nabla\times\boldsymbol{u})\cdot(\nabla\times\boldsymbol{u})\,dV - \int_{CS}\frac{1}{2}\rho(\boldsymbol{u}\cdot\boldsymbol{u})(\boldsymbol{u}\cdot\boldsymbol{n})\,dA. \quad (6.148)$$

Comparing Eqs. 6.147 and 6.148, we notice a difference regarding the viscous terms on their second lines. For many FSI problems where the fluid viscosity is negligible, the *boundary layer approximation* method has been widely used in modeling the flow [9]. In the boundary layer method, the viscosity is neglected everywhere in the fluid domain except in the vicinity of the structure. Similarly, if we neglect the dissipation inside the control volume, the only terms remaining are $\frac{1}{2}\mu\nabla(\boldsymbol{u}\cdot\boldsymbol{u})\cdot\boldsymbol{n}$ in Eq. 6.147 and $\mu\boldsymbol{u}\times(\nabla\times\boldsymbol{u})\cdot\boldsymbol{n}$ in Eq. 6.148. This difference makes the variational energy rate equation preferable over the energy rate equation when it comes to reduced-order modeling, since the kinetic energy term can readily be obtained as $\frac{1}{2}\mu\nabla(\boldsymbol{u}\cdot\boldsymbol{u})\cdot\boldsymbol{n} = \frac{\mu}{\rho}\nabla\left(\frac{1}{2}\rho\boldsymbol{u}\cdot\boldsymbol{u}\right)\cdot\boldsymbol{n}$, whereas the term $\mu\boldsymbol{u}\times(\nabla\times\boldsymbol{u})\cdot\boldsymbol{n}$ in Eq. 6.148 makes the manipulations challenging. This fact and observation is utilized in applying these equations to the reduced-order modeling of vortex-induced vibration problems in [17] and Chap. 7.

The next chapter will utilize the results of this chapter, which focused on the fluid, and continue the formulations and derivations for a coupled fluid–structure system. This includes consideration of the coupling properties based on the no-slip condition. We show how to extract single DOF models as well as coupled flow-oscillator models, with comparisons made to several published flow-oscillator models.

References

1. Baruh H (1999) Analytical dynamics. WCB/McGraw-Hill, Boston
2. Bateman H (1931) On dissipative systems and related variational principles. Phys Rev 38:815–819

3. Cengel YA, Cimbala JM (2006) Fluid mechanics: fundamentals and applications. McGraw-Hill series in mechanical engineering. McGraw-Hill, New York City
4. Dill EH (2006) Continuum mechanics: elasticity, plasticity, viscoelasticity. CRC Press, Boca Raton
5. Gelfand IM, Fomin SV (1963) Calculus of variations. Prentice-Hall Inc, Englewood Cliffs
6. Goldstein H, Poole C, Safko J (2002) Classical mechanics, 3rd edn. Addison-Wesley, Boston
7. Jourdain PEB (1909) Note on an analogue of gauss principle of least constraint. Q J Pure Appl Math 40:153–157
8. Kövecses J, Cleghorn WL (2003) Finite and impulsive motion of constrained mechanical systems via Jourdain's principle: discrete and hybrid parameter models. Int J Non-Linear Mech 38(6):935–956
9. Kundu PK, Cohen IM (2008) Fluid mechanics, 4th edn. Elsevier Inc., Oxford
10. Lamb H (1963) Hydrodynamics. Cambridge University Press, Cambridge
11. Lanczos C (1970) The variational principles of mechanics, 4th edn. Courier Dover Publications, Mineola
12. Leech CM (1977) Hamilton's principle applied to fluid mechanics. Q J Mech Appl Math 30:107–130
13. McIver DB (1973) Hamilton's principle for systems of changing mass. J Eng Mech 7(3):249–261
14. Millikan CB (1929) On the steady motion of viscous, incompressible fluids; with particular reference to a variation principle. Philos Mag Ser 7, 7(44):641–662
15. Moon FC (1998) Applied dynamics: with applications to multibody and mechatronic systems. Wiley, New York
16. Mottaghi S (2018) Modeling vortex-induced fluid-structure interaction using an extension of Jourdain's principle. PhD dissertation, Rutgers, the State University of New Jersey, New Brunswick
17. Mottaghi S, Benaroya H (2016) Reduced-order modeling of fluid-structure interaction and vortex-induced vibration systems using an extension of Jourdain's principle. J Sound Vib 382(1):193–212
18. Papastavridis JG (1992) On Jourdain's principle. Int J Eng Sci 30(2):135–140
19. Price JF (2006) Lagrangian and Eulerian representations of fluid flow: kinematics and the equations of motion. Woods Hole Technical Report
20. Riewe F (1997) Mechanics with fractional derivatives. Phys Rev E 55:3581–3592
21. Stokes GG (1847) On the theory of oscillatory waves. Trans Camb Philos Soc 8:441–455
22. Vujanovic B, Atanackovic T (1978) On the use of Jourdain's variational principle in nonlinear mechanics and transport phenomena. Acta Mech 29:229–238
23. Wang L-S, Pao Y-H (2003) Jourdain's variational equation and Appell's equation of motion for nonholonomic dynamical systems. Am J Phys 71(1):72–82
24. Xing JT, Price WG (2000) The theory of non-linear elastic ship-water interaction dynamics. J Sound Vib 230(4):877–914

Chapter 7
Eulerian Flow-Oscillator Models

Abstract We apply the Eulerian formulations of the last chapter to derive a general variational formulation of a flow-oscillator modeling framework. A brief review of the application of variational principles to fluid–structure interactions is given. A summary is provided of Jourdain's principle for fluid systems. Boundary conditions are discussed, in particular the no-slip condition and its interpretations. The control volume is expanded upon. Fluid–structure interaction is then modeled in two ways: (i) as a single governing equation of motion for a translating cylinder and for an inverted pendulum, and (ii) as coupled equations of motion utilizing the concept of a wake oscillator. For the wake oscillator, the no-slip condition is further examined and implemented. Experimental data is used to derive a more specific reduced-order model that can be compared with some of the models found in the literature: McIver, Benaroya and Wei, and Hartlen and Currie. A primary conclusion is that the derived framework is an excellent basis for the development of flow-oscillator models, where assumptions are explicitly identified.

7.1 Introduction

The problem of fluid–structure interaction (FSI) has long been one of the great challenges of engineering. FSI is a crucial consideration in the design of many engineering systems, such as offshore structures, aircraft, and bridges. While the importance of the subject has been understood for over a century, it has only been in the past half century that efforts have been made to analytically model the general behavior of such systems. Parallel to analytical attempts, many experiments have been devoted to gathering data and interpreting such interactions. Consequently, analytical dynamics modeling of such problems have evolved with coupling to experimental data resulting in various semi-analytical representations. Generally, attempts have been made specifically to model vortex-induced vibration (VIV) problems by few-degree-of-freedom (DOF) oscillatory models; therefore, they are referred to as *reduced-order* models.

In experimental studies of VIV, certain types of structural configurations have been preferred in the literature, where a rigid solid body with one or two degree(s)

S. Mottaghi et al., *An Analytical Mechanics Framework for Flow-Oscillator Modeling of Vortex-Induced Bluff-Body Oscillations*, Solid Mechanics and Its Applications 260,
https://doi.org/10.1007/978-3-030-26133-7_7

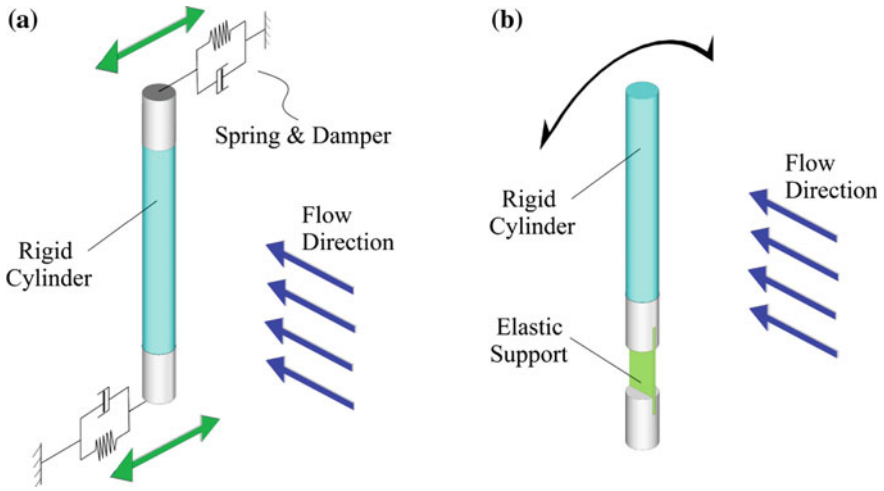

Fig. 7.1 Representative configuration of the *model problem:* **a** translating cylinder, and **b** inverted pendulum

of freedom is immersed in a flow. While experiments have been conducted on a variety of solid shapes (and occasionally on flexible bodies), *reduced-order semi-analytical models* have been generally developed for single DOF rigid bluff bodies, specifically for circular cylinders. The most commonly used model, here called the *model problem*, is a type of translating cylinder or an inverted pendulum that is immersed in a flow, resting on elastic supports, and constrained to move transversely to the flow direction [8]. Schematic diagrams of elements of the two representative configurations of the *model problem* are shown in Fig. 7.1.

The *model problem* has been widely used since it possesses a simple geometric configuration, and yet, it exhibits the majority of the nonlinear behavior characteristics of VIV systems. Consequently, the majority of VIV experiments have been conducted on the *model problem*. Both in experimental and analytical studies, the flow is controlled and generally considered to be two dimensional for all time, as are the shedding vortices.

This chapter applies the theoretical framework of the last chapter to the derivation of reduced-order models from first principles, where assumptions are explicitly stated. A few key features observed in experimental studies are summarized, with more details found in [7, 21].

Starting with the stagnant fluid, if the speed of the flow past the cylinder is increased, three different behavioral regimes are identified: *pre-synchronization*, *resonant synchronization*, and *classical lock-in*. *Pre-synchronization* is the first regime where the structure starts oscillating and vortices are first observed. The amplitudes of the structural oscillations are low and the vortices' strength range from weak to moderate. Observed in this range is a beating behavior, that is, the amplitude

of structural response increases and decreases gradually as the structure oscillates. Moreover, the flow drives the structure in this range.

As the average velocity of the flow is increased, vortices become stronger until the frequency of the vortex shedding reaches the natural frequency of the structure, where near-resonant behavior is observed. Thus, the structural response reaches a maximum in the so-called the *resonant synchronization* region. Similarly to the *pre-synchronization* region, beating behavior is noticeable but weaker, and the structure remains driven by the flow.

If the flow velocity is increased further, constant structural oscillation amplitude and frequency are observed for a range of flow velocities. This phenomenon is called the *classical lock-in*. Unlike the other two regions, the flow is modulated by the structure and the vortices observed are the least organized. The existence of three distinct regimes in the frequency–amplitude response curves of an inverted pendulum is shown in Fig. 7.2.

Also observed in many of the experiments is the existence of hysteretic behavior, that is, the maximum amplitudes of the oscillations are larger as the velocity is increased than when it is decreased, as shown in Fig. 7.3. VIV is a complicated phenomenon. The structural response depends on many factors, such as shedding frequency, Reynolds number, material damping, structural stiffness, surface roughness, cylinder length, density of the fluid and mass of the cylinder, [7, 21]. Therefore, *reduced-order* modeling of VIV has evolved in parallel to experiments in order to help increase our understanding of this phenomenon, as well as to provide a predictive design tool.

Efforts to model VIV as reduced-order systems can be divided into two categories: empirical models and first-principles models. Moreover, the empirical models can be divided into two subcategories: wake-oscillator (wake-body) models and experimental force-coefficient models.

The wake-oscillator models are based on the assumption that an immersed structure in a flow experiences hydrodynamic forces that are similar to those of nonlinear oscillator systems. Therefore, the aim is to obtain nonlinear fluid force equations from the experimentally acquired data that can be coupled with the structural equation of motion (EOM). One significant example of these types of models is that proposed by Hartlen and Currie [11], which is reviewed in Sect. 7.2.

The experimental force-coefficient models are single DOF models. They only include a single forcing function obtained experimentally. Generally, empirical models have relative success in capturing the features of VIV. However, these models neglect the dynamics of the flow by only considering the forces as they are seen by the structure. Therefore, they do not provide much understanding of the physics of the problem. Reviews of empirical models can be found in [6, 7].

While variational principles have been known since the times of Euler, and considered for problems of fluid mechanics for about a century, it was not until 1973 that McIver [17] was among the first researchers to propose the use of variational methods in modeling fluid–structure interaction problems. Also, the work by Benaroya and Wei [3] in 2000 is apparently the earliest attempt to use such methods for VIV problems. Consequently, the literature on the subject is very limited. A brief review

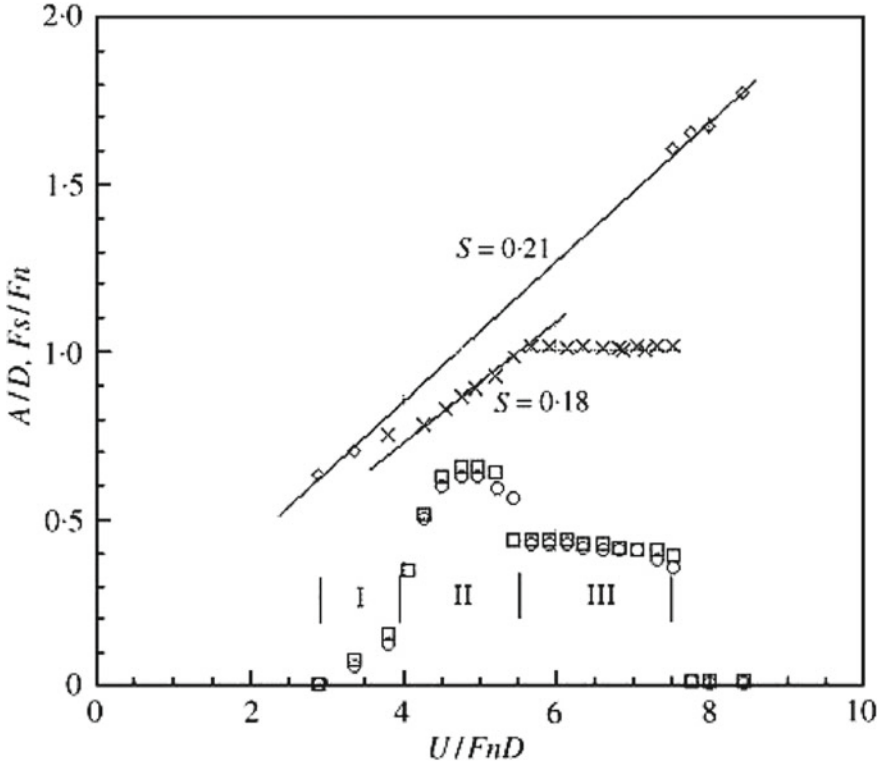

Fig. 7.2 The frequency–amplitude response curves of an inverted pendulum, where A is the amplitude of oscillations, D is the diameter of the cylinder, F_s is the frequency of oscillations, F_n is the natural frequency of the cylinder, U represents the fluid velocity. □, ◯, amplitude of oscillation for two independent but identical experimental runs; ×, frequency of oscillation, and vortex shedding frequency in which VIV was observed; ◊, frequency of vortex shedding where the cylinder was stationary; *I*, pre-synchronization; *II*, resonant synchronization; *III*, classic lock-in [3]. Reprinted with permission

is presented in Sect. 7.3, which is followed by a summary of our extension of Jourdain's principle (Chap. 6) for fluid systems in Sect. 7.4. Then, after a discussion of the selection and implementation of the solid boundary conditions in Sects. 7.5 and 7.6, Jourdain's principle is extended further for FSI systems in Sect. 7.7. Using the extended formulation, reduced-order models in the form of a single governing equation of motion (SEOM) and nonlinear coupled equations of motion (EOM) are obtained for the model problem in Sects. 7.8–7.10, where we also discuss our theoretical methodology for obtaining coupled EOM from the energy rate equations. Then in Sect. 7.11, it is shown that the method developed here can be combined with similarity methods to obtain a lift-oscillator model similar to that proposed by Hartlen and Currie. In Sect. 7.12, comparisons are made between the reduced-order

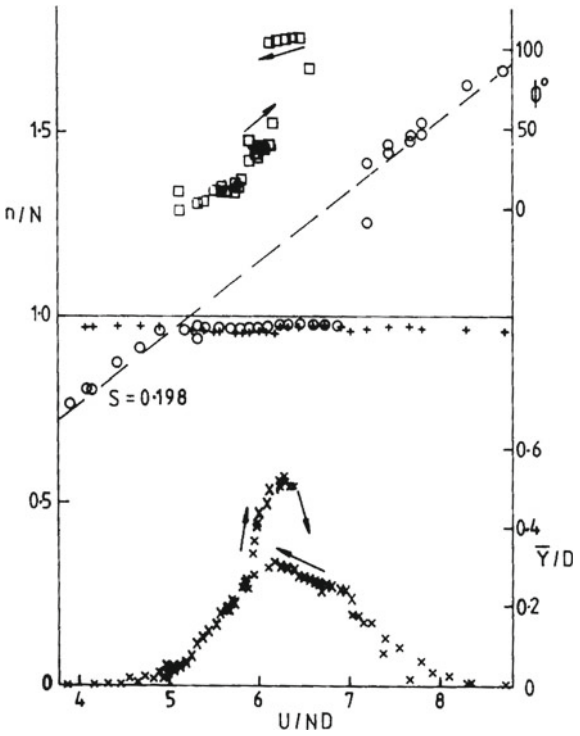

Fig. 7.3 Oscillation characteristics of a vibrating circular cylinder with light damping. n is the frequency of vortex shedding, N is the frequency of oscillations, $\bar{Y}/D$ is the normalized maximum amplitude of oscillation at the reduced velocity U/ND, and ϕ° denotes the phase angle between the fluid force and the cylinder displacement. +, frequency of oscillation; ◯, frequency of vortex shedding; □, phase angle; ×, amplitude of oscillation [2]. Reprinted with permission of the author

model presented in this chapter and those proposed by McIver, Benaroya and Wei, and Hartlen and Currie. Concluding thoughts are given in Sect. 7.13. The outline of the structure of this chapter is shown in Fig. 7.4.

7.2 Hartlen and Currie's *Lift-Oscillator* Model

One of the earliest of the wake-oscillator models is the *lift-oscillator* model proposed by Hartlen and Currie [11], where they considered the model problem in the form of a translating cylinder. Hartlen and Currie considered an instantaneous lift coefficient, c_L, to be a representative variable for the oscillatory lift force. Therefore, they expressed the governing equation of motion for the structure as

$$m\ddot{x}_s + C\dot{x}_s + kx_s = \frac{1}{2}\rho u^2 DLc_L, \tag{7.1}$$

where m is the cylinder mass, C is the structural damping, k is the structural stiffness, ρ denotes the density of the fluid with velocity u, D is the cylinder diameter, L is the

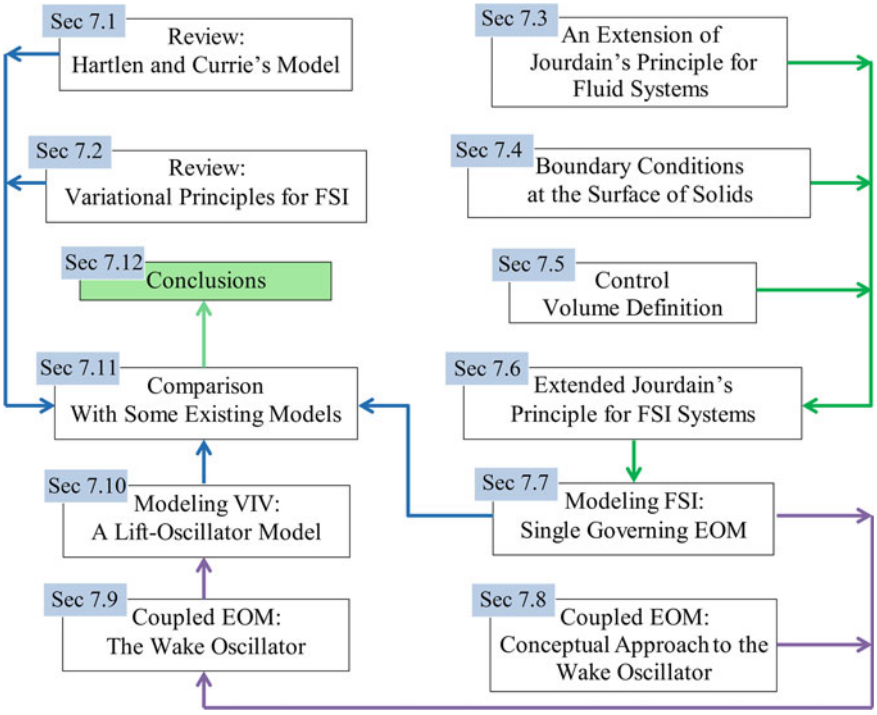

Fig. 7.4 The structure and organization of this chapter

cylinder length, and x_s is the structural displacement transverse to the flow direction. Then, the governing equation was nondimensionalized as

$$\ddot{x}_r + 2\zeta \dot{x}_r + x_r = a\omega_0^2 c_L, \tag{7.2}$$

where x_r is the dimensionless structural displacement, ζ is a reduced damping coefficient, ω_0 is the dimensionless wind speed, and a is a known dimensionless constant. Since the structure exhibits oscillatory behavior, they assumed that the lift coefficient must also behave as an oscillator, in particular, a nonlinear oscillator governed by an equation of the form

$$\ddot{c}_L + (\text{damping term}) + \omega_0^2 c_L = (\text{forcing term})\,. \tag{7.3}$$

Based on the nature of VIV systems, Hartlen and Currie deduced that the oscillator must be a self-excited and self-limited oscillator. Thus, they selected damping terms such that the resulting equation becomes a van der Pol-type oscillator, and so they modified Eq. 7.3 to

$$\ddot{c}_L - \alpha\omega_0\dot{c}_L + \frac{\gamma}{\omega_0}(\dot{c}_L)^3 + \omega_0^2 c_L = (\text{forcing term}), \tag{7.4}$$

where α and γ are found experimentally. The forcing term was selected arbitrarily to be $\beta\dot{x}_r$, where β is a constant to be estimated experimentally. Therefore, Hartlen and Currie expressed their coupled differential equations as

$$\begin{cases} \ddot{x}_r + 2\zeta\dot{x}_r + x_r = a\omega_0^2 c_L \\ \ddot{c}_L - \alpha\omega_0\dot{c}_L + \dfrac{\gamma}{\omega_0}(\dot{c}_L)^3 + \omega_0^2 c_L = \beta\dot{x}_r, \end{cases} \tag{7.5}$$

where only two of the unknown fluid parameters, α, β, and γ, must be selected in order to obtain the best fit to an experimental data set.

It is obvious from the summary above that the model proposed by Hartlen and Currie does not provide any insights into the fluid dynamics and its effects on the structural response. Moreover, Hartlen and Currie's model does not permit a description of the beating behavior [5] that is usually observed in VIV problems. However, their model is one of the most successful attempts at reduced-order modeling of VIV and, perhaps, the most noteworthy of all such approaches.

Next, we summarize several relevant applications of variational principles for reduced-order modeling of FSI and VIV systems.

7.3 A Review: Variational Principles for FSI Systems

While variational principles have been known and utilized in modeling the dynamics of solid systems for well over a century, it has only been during the past few decades that a few attempts have been devoted to applying variational methods to FSI and VIV problems. Next, we review a few such attempts which, we believe, are good representative works.

7.3.1 McIver's Extension of Hamilton's Principle

An important approach to modeling fluid dynamics using variational principles is by McIver [17]. He presented his extended form of Hamilton's principle for problems involving fluid–structure interactions. Having considered Hamilton's principle for a system of continuous particles, McIver utilized Reynolds transport theorem (RTT) to modify the principle for a system of changing mass (control volume, CV). For a moving control volume, it is customary to consider the relative velocities of the fluid particles with respect to the control volume. However, McIver considered the velocity of the control volume with respect to the fluid particles, $\boldsymbol{u}_r$, for which he did not provide any justification. Perhaps McIver's aim was to introduce the backtracking

concept, that has been usually used in applying variational methods to fluid systems, at this stage of his formulation. Also, he assumed that the virtual work performed on a control volume is purely due to the surface tractions at the control surface, that is, he neglected the viscous dissipation of energy inside the control volume. Therefore, using the stress dyadic, $\bar{\boldsymbol{\sigma}}$, he considered the virtual work to be

$$\delta W = \int_{CS} \delta \boldsymbol{r} \cdot \bar{\boldsymbol{\sigma}} \cdot \boldsymbol{n} \, dA, \tag{7.6}$$

where $\delta \boldsymbol{r}$ is the virtual displacement, $\boldsymbol{n}$ is the vector normal to the differential surface element dA, and CS is the control surface. For fluid–structure interaction problems, the control volume can be chosen so that some portions of the control surface match the structural surfaces. Denoting the portions of the CS where the flow cannot pass through by CS_C (closed CS), and representing the rest of the CS by CS_O (open CS), McIver's extension of Hamilton's principle is given by

$$\delta \int_{t_1}^{t_2} (T - \Pi)_{CV} dt + \int_{t_1}^{t_2} \int_{CS_O} \left[\delta \boldsymbol{r} \cdot \bar{\boldsymbol{\sigma}} \cdot \boldsymbol{n} + \rho \left(\boldsymbol{u} \cdot \delta \boldsymbol{r} \right) \left(\boldsymbol{u}_r \cdot \boldsymbol{n} \right) \right] dA dt + \int_{t_1}^{t_2} \int_{CS_C} \delta \boldsymbol{r} \cdot \bar{\boldsymbol{\sigma}} \cdot \boldsymbol{n} dA dt = 0, \tag{7.7}$$

where $\boldsymbol{u}$ is the absolute velocity of the fluid particles, T is the kinetic energy, and Π is the potential energy.

Equation 7.7 represents a stationary process if the integrand of the second term always disappears at the CS_O, that is,

$$\bar{\boldsymbol{\sigma}} + \rho \boldsymbol{u} \boldsymbol{u}_r = 0, \quad \text{or} \quad (\bar{\boldsymbol{\sigma}} + \rho \boldsymbol{u} \boldsymbol{u}_r) \cdot \boldsymbol{n} = 0 \quad \text{at } CS_O. \tag{7.8}$$

Therefore, the applicability of McIver's equation is restricted to the cases where such a control volume can be distinguished from the physics of the problem, where the fluid is bounded by the structure. McIver considered two simple problems as examples, a rocket problem and a flexible pipe problem.

7.3.2 *Xing and Price's Extension of Hamilton's Principle*

Xing and Price [24] modified Hamilton's principle for nonlinear ship–water interactions. They considered that imposing virtual displacements cause the particles to be virtually transported across an assumed control volume. They defined a general integral function of interest, H,

$$H[\phi] = \int_{t_1}^{t_2} \int_{CV} F\left(\phi, \frac{\partial \phi}{\partial t} \right) dV dt, \tag{7.9}$$

where ϕ is a continuous differentiable function of displacement, $\boldsymbol{x}$, and time, t. Denoting the local variation (Eulerian) by $\bar{\delta}$ and the material variation (Lagrangian) by δ, they obtained the local variation of H to be

$$\bar{\delta}H = \int_{t_1}^{t_2} \left\{ \int_{CV} \bar{\delta} F dV + \int_{CS} F \left(\phi, \frac{\partial \phi}{\partial t} \right) (\delta \boldsymbol{x} \cdot \boldsymbol{n}) \, dA \right\} dt. \tag{7.10}$$

Therefore, the variation of H is twofold: the Eulerian variation inside the control volume and the flux of H due to Lagrangian virtual displacements. Then, their model was applied to a rigid ship traveling in calm water and in waves. Xing and Price's method requires further simplifications and assumptions as it contains both Lagrangian and Eulerian variations.

7.3.3 *Benaroya and Wei's Extension of Hamilton's Principle*

Benaroya and Wei [3] considered FSI problems where the fluid contains the structure; for details, see Chap. 4. They showed that Hamilton's principle becomes the balance of energy rates when the configuration is not known at any time. Similar to McIver's approach, they used the RTT to relate Hamilton's principle to a control volume. However, unlike McIver's use of RTT, they chose the conventional form of RTT where the relative velocities, $\boldsymbol{u}_r$, are the relative fluid particle velocities with respect to the control volume. They presented their governing equation as

$$\begin{aligned} \frac{d}{dt} \left(T_{\text{structure}} + \Pi_{\text{structure}} \right)_{CV} &= \int_{CS} \frac{1}{2} \rho u^2 \left(\boldsymbol{u}_r \cdot \boldsymbol{n} \right) dA \\ &+ \int_{CS} \left(-p\boldsymbol{n} + \boldsymbol{\tau} \right) \cdot \boldsymbol{u} dA - \left(m_{\text{fluid}} u \dot{u} \right)_{CV}, \end{aligned} \tag{7.11}$$

where m_{fluid} is the mass of fluid contained by the CV, p is the pressure, and $\boldsymbol{\tau}$ is the shear stress. They explained that the terms on left-hand side of Eq. 7.11 are the structural dynamic terms, and the right-hand side terms can be evaluated experimentally. The result is the acceleration of the structure that can be integrated twice to obtain the structure's displacement.

In parallel with their theoretical development, Benaroya and Wei conducted a series of experiments on the VIV of a circular cylinder in uniform flow. The cylinder was free to vibrate transversely to the flow direction. Having input the experimental data to Eq. 7.11, they showed that their model is successful in predicting the frequencies of the structural oscillation as well as in capturing the beating behavior that is usually observed in VIV. However, the predicted response amplitudes were roughly half of the experimental values. Their results are shown in Fig. 7.5. They concluded that these differences are most likely due to the choice of control volume. In their subsequent paper [5], they examined the effect of the choice of the experimental control volume on the predictions of their model. They found that the predictions

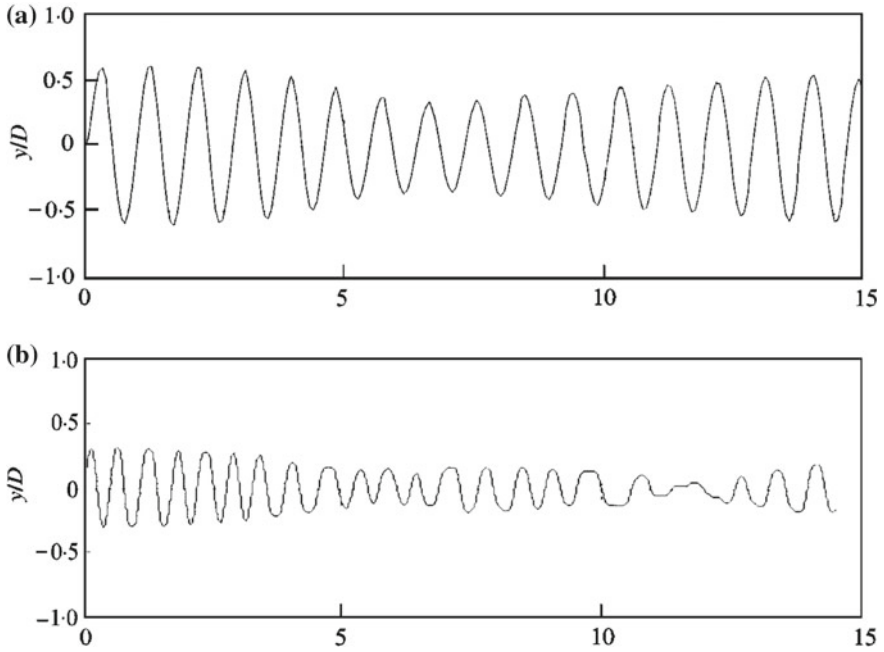

Fig. 7.5 Predicted (bottom) versus experimental (top) amplitudes. Both plots are in seconds [3]. Reprinted with permission

are indeed influenced by the selection of control volume. Having obtained a CV for which the predictions of the model matched the experimental values (shown in Fig. 7.6), they concluded that the control volume must contain both upstream and downstream sections of the flow where the downstream control surface is far enough from the structure as to not pass through the vortex formation region, yet not too far to not capture the true kinetic energy flux due to the dissipation of energy.

As evident from Eq. 7.11, Benaroya and Wei, similar to McIver, neglected the viscous dissipation of energy inside the control volume since their experiments found the viscous forces to be three orders of magnitude smaller than the kinetic energy flux.

7.3.4 Gabbai and Benaroya's Extension of Hamilton's Principle

Benaroya and Wei showed that when the configuration is unknown, which is the case for the majority of fluid and fluid–structure interaction problems, Hamilton's principle is not a variational principle. However, their promising results motivated the research work by Gabbai and Benaroya to modify the same approach so as to obtain

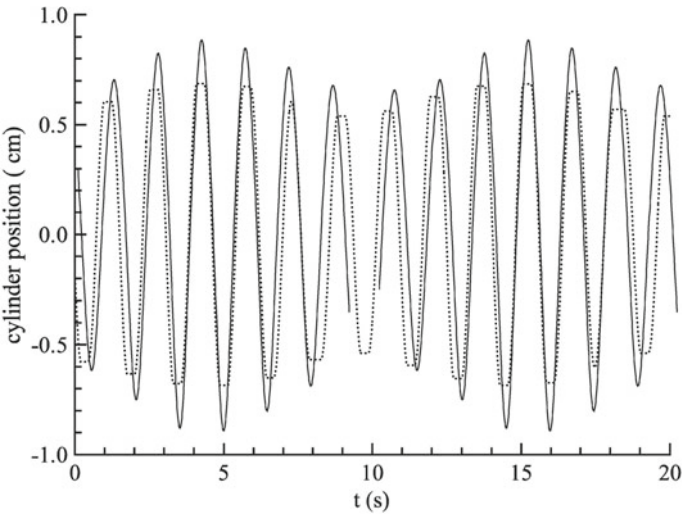

Fig. 7.6 Dong et al. [5] results obtained for the phase-averaged cylinder position versus time, where the solid line represents the experimental result and the dotted line is the computed result for a specific control volume. Reprinted with permission

a variational method [8]. Experiments (see Chap. 4 for details) show the existence of a formation region (cavity) in the vicinity of a cylinder that is immersed in a flow. They assumed that energy is evenly exchanged between the cylinder and the wake in the formation region. Denoting the displacement of this cavity by w, they obtained their variational equation as

$$\int_{t_1}^{t_2} am_{\text{cavity}}\dot{w}\delta\dot{w}dt+\delta\int_{t_1}^{t_2}\frac{1}{2}m\dot{x}^2dt-\delta\int_{t_1}^{t_2}\frac{1}{2}kx^2dt-\int_{t_1}^{t_2}c\dot{x}\delta x dt - \int_{t_1}^{t_2}\delta W\left(\dot{w},\ddot{w},x,\dot{x},\ddot{x},t\right)dt-\delta\int_{t_1}^{t_2}F(w,t)\delta w dt=0, \tag{7.12}$$

where the overdot denotes d/dt, m denotes the mass, x is the displacement of the cylinder, k is the structural stiffness, c is the structural damping, δ is the variational operator, t is time, F is the fluid stiffness, and W represents the instantaneous total work done by the transverse hydrodynamic force acting on the cylinder, $F_{fl/st}$, and by the viscous and pressure forces inside the cavity, $F_{\mu/p}$. Therefore,

$$\delta W\left(\dot{w},\ddot{w},x,\dot{x},\ddot{x},t\right)=-F_{fl/st}\left(\dot{w},\ddot{w},\dot{x},\ddot{x},t\right)\delta x+F_{\mu/p}\left(\dot{w},\ddot{w},\dot{x},\ddot{x},t\right)\delta w. \tag{7.13}$$

Then, based on the literature, the authors proposed some general functions of $\dot{w}$, $\ddot{w}$, $\dot{x}$, $\ddot{x}$, t, and lift coefficient for $F_{fl/st}$ and $F_{\mu/p}$. They showed how three of the existing wake-oscillator models are each a specific case of their more general model.

As evident from the literature, the efforts to apply Hamilton's principle to the problems of fluid–structure interaction have had some success. They have provided more insights into the dynamics of the fluid portion of FSI systems when compared with empirical models. However, these efforts still require additional assumptions regarding the fluid forcing function in order to obtain wake-oscillator type models. Specifically, the coupling mechanism between the structural EOM and that describing the fluid dynamics is the result of assumptions made for a problem at hand rather than being the result of variational operations. Consequently, there exist no general variational approaches for fluid–structure interactions, thus motivating the work that is summarized in this monograph.

In Chap. 6, the application of variational principles to fluid dynamics problems was explored. Among other difficulties, one main challenge was identified to arise from relating variational principles in the Lagrangian frame to the Eulerian frame. It was shown that Jourdain's principle (JP) can be a very effective tool to overcome some of the challenges faced by other variational principles. Consequently, an extension of JP was derived in Chap. 6 for modeling fluid dynamics problems, and this derivation is summarized next for the convenience of the reader.

7.4 An Extension of Jourdain's Principle for Fluid Systems

We consider the application of variational principles for modeling fluid dynamics problems. Variational principles, similar to other first principles, are defined in the Lagrangian frame of reference. However, it has been shown that the equations of motion for fluid systems take on a simpler form in the Eulerian frame of reference. Having reviewed the literature on the subject, one main source of difficulties is identified to be that the concept of virtual displacement (a Lagrangian concept) does not have a Eulerian counterpart, posing many challenges in the application of Hamilton's principle and Lagrange's equation in modeling fluid and FSI systems. This is overcome by utilizing Jourdain's variational principle. The following is a short summary of our derivations in Chap. 6.

Jourdain's principle is based on the *dynamic equilibrium* relation, and for a system of N particles, is given by the relation

$$\sum_{i=1}^{N} \left(m_i \ddot{\boldsymbol{r}}_i - \boldsymbol{F}_i\right) \cdot \delta \dot{\boldsymbol{r}}_i \; = 0, \qquad \text{where} \qquad \delta \boldsymbol{r}_i = 0, \delta t = 0, \tag{7.14}$$

m_i is the mass of particle i moving on the path $\boldsymbol{r}_i$, vector $\boldsymbol{F}_i$ is the force acting on particle i, and $\delta \dot{\boldsymbol{r}}_i$ is the variation of the velocity of particle i (called virtual velocity).

Alternatively, Jourdain's principle can be expressed as

$$\begin{cases} \dfrac{d}{dt}\left[\displaystyle\sum_{i=1}^{N}\frac{d}{dt}\left(m_i\dot{\boldsymbol{r}}_i\right)\cdot\delta\boldsymbol{r}_i\right] = \dfrac{d}{dt}\left[\displaystyle\sum_{i=1}^{N}\boldsymbol{F}_i\cdot\delta\boldsymbol{r}_i\right] \\ \delta t = 0, \quad \delta\boldsymbol{r}_i = 0, \quad \text{and} \quad \dfrac{d}{dt}\left(\delta\boldsymbol{r}_i\right) \neq 0, \end{cases} \tag{7.15}$$

where the first line is the differentiation of d'Alembert's principle with respect to time.

In order to distinguish between Jourdain's and d'Alembert's variational operators, many authors have used the sign δ_1 to denote Jourdain's variation. We prefer to retain the same notation (δ) with Jourdain's constraints where clarity will come from the context. That is, δ in the first line of Eq. 7.15 is d'Alembert's variational operator. Then, both sides of the equation are differentiated using the product rule and use is made of the $\delta\boldsymbol{r}_i = 0$ constraint, where δ in the resulting equation is the Jourdain's variational operator. (In Chap. 6, Eq. 6.58 was used instead of Eq. 6.41 as it is more accessible when extending JP for systems of changing mass.)

In order to extend Jourdain's principle, Eq. 7.15, the relations between the Lagrangian and the Eulerian reference frames are utilized and use is made of a mapping function $\boldsymbol{\Lambda}\left(\boldsymbol{x}, t\right)$ with the properties

$$\boldsymbol{r} = \boldsymbol{\Lambda}\left(\boldsymbol{r}, t\right), \tag{7.16}$$

$$\frac{d}{dt}\boldsymbol{r} = \frac{d}{dt}\boldsymbol{\Lambda}\left(\boldsymbol{r}, t\right) = \left.\frac{D}{Dt}\boldsymbol{\Lambda}\left(\boldsymbol{x}, t\right)\right|_{\boldsymbol{x}=\boldsymbol{r}}, \tag{7.17}$$

and

$$\boldsymbol{u}\left(\boldsymbol{x}, t\right) = \frac{D}{Dt}\boldsymbol{\Lambda}\left(\boldsymbol{x}, t\right), \tag{7.18}$$

where $\boldsymbol{r}$ is the Lagrangian trajectory. For a control volume $CV\left(t\right)$ of a Newtonian incompressible viscous fluid, we showed that Jourdain's principle became (Eq. 6.80, repeated here)

$$\int_{CV(t)}\left(\rho\frac{D\boldsymbol{u}\left(\boldsymbol{x}, t\right)}{Dt} - \boldsymbol{f}_b\left(\boldsymbol{x}, t\right) - \nabla\cdot\bar{\boldsymbol{\sigma}}\right)\cdot\delta\boldsymbol{u}\left(\boldsymbol{x}, t\right)dV\left(t\right) = 0, \tag{7.19}$$

where ρ is the density of the fluid, D/Dt denotes the material derivative, $\boldsymbol{u}\left(\boldsymbol{x}, t\right)$ is the Eulerian velocity of the fluid particle occupying position $\boldsymbol{x}$ at time t, $\boldsymbol{f}_b$ represents the body force per unit volume, $\bar{\boldsymbol{\sigma}}$ is the stress tensor, $\delta\boldsymbol{u}\left(\boldsymbol{x}, t\right)$ is Jourdain's virtual velocity imposed at the spatial position $\boldsymbol{x}$ at time t, and $dV\left(t\right)$ represents the differential volume element.

Using the constitutive relation for Newtonian incompressible fluids,

$$\bar{\boldsymbol{\sigma}} = -p\bar{\boldsymbol{I}} + \mu\left(\nabla \boldsymbol{u} + \nabla^T \boldsymbol{u}\right), \tag{7.20}$$

Equation 7.19 becomes

$$\int_{CV(t)} \left(\rho \frac{D\boldsymbol{u}\,(\boldsymbol{x},t)}{Dt} - \boldsymbol{f}_b\,(\boldsymbol{x},t) + \nabla p\,(\boldsymbol{x},t) - \mu\nabla^2 \boldsymbol{u}\,(\boldsymbol{x},t)\right) \cdot \delta\boldsymbol{u}\,(\boldsymbol{x},t)\,dV\,(t) = 0, \tag{7.21}$$

where p is the thermodynamic pressure, $\bar{\boldsymbol{I}}$ is the identity tensor, and μ is the coefficient of dynamic viscosity. Since $\delta\boldsymbol{u}$ is a nonzero vector, the terms of the integrand inside the parentheses must add to zero, that is, the Navier–Stokes equations are obtained.

Also, the energy rate equation is obtained directly from Jourdain's principle using the relation

$$\delta\dot{L}\,(\dot{\boldsymbol{r}}_i, \boldsymbol{r}_i, t) = \frac{\partial \dot{L}}{\partial \dot{\boldsymbol{r}}_i} \cdot \delta\dot{\boldsymbol{r}}_i, \tag{7.22}$$

if the commutation rule holds and $\dot{L}$ is the rate of Lagrangian function. Having shown that the commutation rule does not hold for the acceleration terms in the Eulerian reference frame, the non-commuting terms are extracted and the energy equation is obtained via JP to be (Eq. 6.143)

$$\overbrace{\delta \int_{CV} \frac{D^C}{Dt}\left(\frac{1}{2}\rho \boldsymbol{u}\cdot\boldsymbol{u}\right) dV}^{\text{rate of kinetic energy}} = \overbrace{\delta \int_{CS} -p\,\boldsymbol{u}\cdot\boldsymbol{n}\,dA + \delta \int_{CV} \{\mu\nabla\cdot[\nabla(\boldsymbol{u}\cdot\boldsymbol{u}) - \boldsymbol{u}\times(\nabla\times\boldsymbol{u})]}^{\text{external loading}}$$
$$\overbrace{-\frac{1}{2}\mu\left\{(\nabla\times\boldsymbol{u})\cdot(\nabla\times\boldsymbol{u}) + \nabla^2(\boldsymbol{u}\cdot\boldsymbol{u}) - 2\nabla\cdot[\boldsymbol{u}\times(\nabla\times\boldsymbol{u})]\right\}}^{\text{viscous dissipation}} dV$$
$$\overbrace{-\delta \int_{CS} \frac{1}{2}\rho\,(\boldsymbol{u}\cdot\boldsymbol{u})\,(\boldsymbol{u}\cdot\boldsymbol{n})\,dA}^{\text{non-commuting term}}, \tag{7.23}$$

or alternatively as (Eq. 6.145)

$$\delta\left\{\overbrace{\frac{D^C}{Dt}\int_{CV}\frac{1}{2}\rho\boldsymbol{u}\cdot\boldsymbol{u}\,dV}^{\text{kinetic energy}} + \overbrace{\int_{CS}\left(\frac{1}{2}\rho\boldsymbol{u}\cdot\boldsymbol{u}\right)(\boldsymbol{u}-\boldsymbol{v}_{CS})\cdot\boldsymbol{n}\,dA}^{\text{flux of kinetic energy}}\right\}$$
$$= \delta\left\{\int_{CS}\overbrace{\{-p\,\boldsymbol{u}\cdot\boldsymbol{n} + \mu[\nabla(\boldsymbol{u}\cdot\boldsymbol{u}) - \boldsymbol{u}\times(\nabla\times\boldsymbol{u})]\cdot\boldsymbol{n}}^{\text{external loads}}\right.$$

$$\overbrace{\left.-\frac{1}{2}\mu\left[\nabla\left(\boldsymbol{u}\cdot\boldsymbol{u}\right)-2\,\boldsymbol{u}\times\left(\nabla\times\boldsymbol{u}\right)\right]\cdot\boldsymbol{n}\right\}dA-\frac{1}{2}\int_{CV}\mu\left(\nabla\times\boldsymbol{u}\right)\cdot\left(\nabla\times\boldsymbol{u}\right)dV}^{\text{viscous dissipation}}$$
$$\left.-\overbrace{\int_{CS}\frac{1}{2}\rho\left(\boldsymbol{u}\cdot\boldsymbol{u}\right)\left(\boldsymbol{u}\cdot\boldsymbol{n}\right)dA}^{\text{non-commuting term}}\right\}, \tag{7.24}$$

where $\boldsymbol{v}_{CS}$ denotes the velocity of the control surface element dA, and the last integral on the right-hand side is due to the non-commuting part of acceleration term. Also, body forces have been neglected. If the only body force present is due to gravity, its potential function can be easily obtained, since gravitational forces are conservative and independent of the fluid velocity field.

For the model problem introduced earlier, gravitational forces can be neglected. Moreover, Eqs. 7.23 and 7.24 represent the energy rate equation in a variational format. In order to obtain the actual energy rate equation, the integrals labeled as "viscous dissipation" must be multiplied by a factor of two, since they are Rayleigh's dissipation function, ϕ, obtained from the relation

$$\delta\phi=\nabla_{\boldsymbol{u}}\phi\cdot\delta\boldsymbol{u}, \tag{7.25}$$

where $\nabla_{\boldsymbol{u}}\phi$ denotes the differentiation of ϕ with respect to $\boldsymbol{u}$ in the direction of $\boldsymbol{u}$. Rayleigh's dissipation function states that if a function ϕ could be found such that $\nabla_{\boldsymbol{u}}\,\phi=\boldsymbol{F}$, then the term $\boldsymbol{F}\cdot\,\delta\boldsymbol{u}$ in the variational formulation can be replaced by $\delta\phi$.

Equations 7.23 and 7.24 can both be used in modeling fluid dynamic systems and FSI, as they are essentially the same. The advantages of one over the other mainly rely on the choice of the control volume and how the boundary conditions are implemented.

Modeling the dynamics of a system of fluid particles, alone, is a very challenging problem due to the nonlinear behavior of fluids. For fluid–structure interaction problems, the difficulties increase since the nature of the boundary conditions between the fluid and structure is not fully understood, and are generally just assumptions backed by experimental results. Therefore, a discussion of boundary conditions is necessary next before we expand Eqs. 7.23 and 7.24 for FSI systems.

7.5 Boundary Conditions at the Surface of Solids

From the time of Newton until the early twentieth century, one topic of intensive discussions has been the boundary conditions (BCs) on solid surfaces that are interacting with viscous fluid particles. Many great scientists and engineers, including

Navier, Stokes, and Prandtl, have considered the topic. For a long time, there was no general agreement on the type of the required BCs with the exception of very slow motion of viscous fluids, where the no-slip condition was accepted [9].

During the past century, many experiments were conducted and compared with theoretical and numerical results using the no-slip condition, leading to almost unified agreement on the no-slip condition [22]. Yet, the no-slip condition remains an assumption (for fluid systems) since it cannot be proven using a first-principles approach. The general understanding is that some intermolecular interactions result in zero relative velocity, $\boldsymbol{u}_r$, of fluid particles at a solid surface [13, pp. 295–296], that is,

$$\boldsymbol{u}_r = \boldsymbol{u} - \boldsymbol{v} = \boldsymbol{0}, \tag{7.26}$$

where $\boldsymbol{u}$ is the velocity of the fluid at the surface of a solid moving with the velocity $\boldsymbol{v}$.

Alternatively, another definition of the no-slip condition is that the tangential components of the relative velocity must vanish [16], that is,

$$\boldsymbol{u}_r \cdot \boldsymbol{t} = (\boldsymbol{u} - \boldsymbol{v}) \cdot \boldsymbol{t} = \boldsymbol{0}, \tag{7.27}$$

or,

$$\boldsymbol{u}_r - (\boldsymbol{u}_r \cdot \boldsymbol{n})\, \boldsymbol{n} = \boldsymbol{0}, \tag{7.28}$$

where $\boldsymbol{t}$ is the unit tangent vector to the surface of the solid. This condition must be considered together with the no-penetration condition for the normal direction, that is, no fluid particles can penetrate the solid.

While the no-slip condition seems to be compatible with many experimental observations on macroscopic scales, some experiments have shown that it is violated at microscopic scales for Newtonian fluids. The wetting property of the surface, the velocity of the flow, surface roughness and gas bubbles are among the factors shown to affect the no-slip boundary condition [1, 12, 20, 25]. More discussion can be found in [22, p. 1222].

The applicability of the no-slip condition, or any other condition, must be justified by a comparison with experimental observations. The no-slip condition, in its most complete form as expressed by Eq. 7.26, satisfies the no-penetration conditions as well. Therefore, for reduced-order models, care must be exercised so that the reduced number of equations can capture the main characteristics of the FSI. For example, if the no-slip condition is strongly imposed, then the resulting reduced-order model most likely cannot model the separation of the vortices from the solid structure, unless additional assumptions are made. Consequently, it might be necessary to relax the no-slip condition to some extent in analytical or numerical modeling. In fact, the no-slip condition has not been applied in its most complete form in many computational simulations or analytical models of FSI. It is implicitly implemented, for example, via other constraints in the system [4] or through an assumed force field [10]. Moreover, the no-slip condition is often explicitly implemented and then is relaxed or corrected in later steps in the modeling process [23]. Alternatively, some weakly impose the no-slip condition [16].

For reduced-order models, the difficulties increase since they are less flexible with respect to the choice of boundary conditions. We continue our derivation by considering the no-slip boundary condition as it is widely accepted in the literature. We will also define explicit and implicit no-slip conditions.

The control volume of interest is described next.

7.6 Control Volume Definition

Generally, care must be exercised in the selection of the control volume, as it greatly affects the applicability of the analytical formulations. Moreover, if the analytical formulations are to be coupled with experimental results, the choice of control volume may be restricted due to experimental limitations, for example, the measurement equipment used and wind/water tunnel dimensions.

Equations 7.23 and 7.24 were obtained for a general control volume, that is, a control volume that can deform and move. Therefore, the derived variational formulations did not face any restrictions in the selection of the control volume. For FSI and VIV problems, the methodology used later imposes a limitation on the selection of the CV in that some portions of the control surface must be comprised of solid surfaces. Since no fluid can cross the solid surface, these control surfaces are referred to as closed control surfaces, CS_C. The other surfaces, where fluid can cross, are called open control surfaces, CS_O.

Since we are interested in reduced-order modeling of the *model problem*, we start by defining control volumes for the two types of *model problem* shown in Fig. 7.1. While our efforts in this chapter are to derive the EOM for a single DOF rigid body coupled to the fluid oscillator, the same method can be used for modeling a general deformable solid as well.

Consider the control volume shown in Fig. 7.7, where the control surface is comprised of three sections, CS_O, CS_C, and the surfaces set apart by the distance α. If $\alpha \to 0$ and if there exist no singularities between the gap, then the surfaces set apart by the distance α can be neglected. Also, we assume that both the rectangular and circular control surfaces move rigidly and independently of each other, as shown in Fig. 7.8.

The shape of the open portion of the control volume is selected to be rectangular for simplicity. Moreover, the rectangular control surface can represent solid surfaces, for instance, they can be chosen to coincide with the walls of a water tunnel.

So far, we have not considered any solid body in our derivations. In order to include a solid structure, we start by considering the original statement of Jourdain's principle for a system volume.

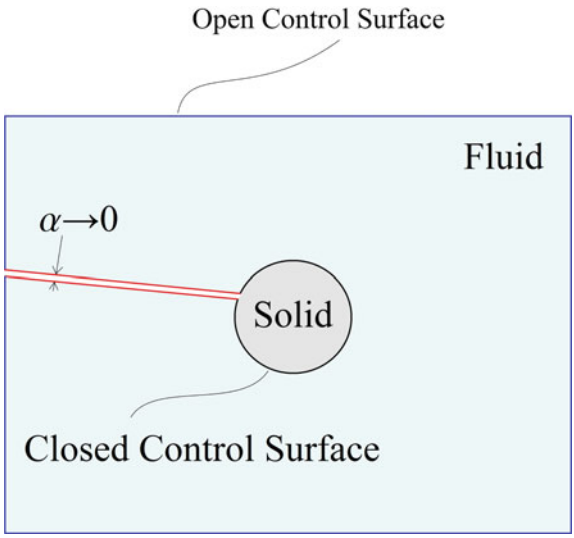

Fig. 7.7 Control volume of interest

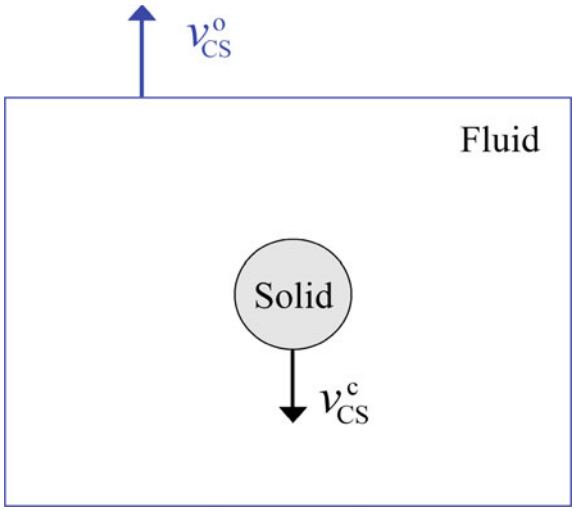

Fig. 7.8 Selected control volume: rectangular and circular control surfaces can move independently

7.7 Extended JP for FSI Systems

Jourdain's variational principle for a set of N fluid plus solid particles is expressed by Eq. 7.14. Consider a continuous system of fluid and solid particles and assume that the system consists of M fluid particles where $M < N$. Jourdain's principle then becomes

$$\sum_{i=1}^{M}\left(m_i\,\ddot{\boldsymbol{r}}_i-\boldsymbol{F}_i\right)\cdot\delta\dot{\boldsymbol{r}}_i+\sum_{j=M+1}^{N}\left(m_j\,\ddot{\boldsymbol{r}}_j-\boldsymbol{F}_j\right)\cdot\delta\dot{\boldsymbol{r}}_j=0,$$

$$\text{where}\quad \delta\boldsymbol{r}_i=0,\,\delta\boldsymbol{r}_j=0 \text{ and } \delta t=0. \tag{7.29}$$

As per the alternative form for Jourdain's principle Eq. 7.15, we can alternatively express Eq. 7.29 as

$$\begin{cases}\dfrac{d}{dt}\left[\displaystyle\sum_{i=1}^{M}\left(m_i\,\ddot{\boldsymbol{r}}_i-\boldsymbol{F}_i\right)\cdot\delta\boldsymbol{r}_i+\sum_{j=M+1}^{N}\left(m_j\,\ddot{\boldsymbol{r}}_j-\boldsymbol{F}_j\right)\cdot\delta\boldsymbol{r}_j\right]=0\\ \delta t=0,\quad \delta\boldsymbol{r}_i=0,\quad \delta\boldsymbol{r}_j=0,\\ \dfrac{d}{dt}\left(\delta\boldsymbol{r}_i\right)\neq 0,\quad \text{and}\quad \dfrac{d}{dt}\left(\delta\boldsymbol{r}_j\right)\neq 0.\end{cases} \tag{7.30}$$

If the set of particles is continuous during some time interval, then Eq. 7.30 can be expressed in integral form as

$$\begin{cases}\dfrac{d}{dt}\displaystyle\int_{V_f}\left[\rho\frac{d\boldsymbol{u}\left(\boldsymbol{r},t\right)}{dt}-\boldsymbol{f}\left(\boldsymbol{r},t\right)\right]\cdot\delta\boldsymbol{\Lambda}\left(\boldsymbol{r},t\right)dV_f\\ +\dfrac{d}{dt}\displaystyle\int_{V_s}\left[\rho_s\frac{d\dot{\boldsymbol{r}}_s}{dt}-\boldsymbol{f}_s\left(\boldsymbol{r}_s\right)\right]\cdot\delta\boldsymbol{r}_s dV_s-\frac{d}{dt}\int_{\substack{\text{Solid}\\ \text{Surface}}}\boldsymbol{f}_s^*\left(\boldsymbol{r}_s\right)\cdot\delta\boldsymbol{r}_s dA_s=0\\ \delta t=0,\quad \delta\boldsymbol{\Lambda}\left(\boldsymbol{r},t\right)=0,\quad \delta\boldsymbol{r}_s=0,\\ \dfrac{d}{dt}\left[\delta\boldsymbol{\Lambda}\left(\boldsymbol{r},t\right)\right]\neq 0,\quad \text{and}\quad \dfrac{d}{dt}\left(\delta\boldsymbol{r}_s\right)\neq 0,\end{cases} \tag{7.31}$$

where V_f is the material volume of the fluid particles, V_s is the material volume of solid particles, ρ_s denotes the density of the solid, $\boldsymbol{r}_s$ is the Lagrangian position of the solid particles, $\boldsymbol{f}_s\left(\boldsymbol{r}_s\right)$ denotes the force density (force per unit volume) in the solid domain at $\boldsymbol{r}_s$, $\boldsymbol{f}_s^*\left(\boldsymbol{r}_s\right)$ is the density of the fluid forces acting at the solid surfaces, $\boldsymbol{r}$ is the Lagrangian position of the fluid particles, and $\boldsymbol{\Lambda}$ is the mapping function introduced earlier. Note that $\boldsymbol{f}_s\left(\boldsymbol{r}_s\right)$ does not include any force due to the fluid dynamics. No constraints are included in deriving Eq. 7.31, except those imposed by Jourdain's principle. The mapping function $\boldsymbol{\Lambda}(\boldsymbol{r},t)$ is introduced so that Lagrangian variables can be related to Eulerian variables.

For the integral over the fluid system in Eq. 7.31, the derivations shown in Chap. 6 remain valid for a Newtonian incompressible viscous fluid. Therefore, the integral over the fluid system can be replaced using Eq. 7.21,

$$\begin{cases} \int_{CV(t)} \left(\rho \dfrac{D\boldsymbol{u}(\boldsymbol{x},t)}{Dt} - \boldsymbol{f}_b(\boldsymbol{x},t) + \nabla p(\boldsymbol{x},t) - \mu \nabla^2 \boldsymbol{u}(\boldsymbol{x},t) \right) \cdot \delta \boldsymbol{u}(\boldsymbol{x},t)\, dV(t) \\ \qquad + \dfrac{d}{dt} \int\limits_{V_s} \left[\rho_s \dfrac{d\dot{\boldsymbol{r}}_s}{dt} - \boldsymbol{f}_s(\boldsymbol{r}_s) \right] \cdot \delta \boldsymbol{r}_s dV_s - \dfrac{d}{dt} \int\limits_{\substack{\text{Solid} \\ \text{Surface}}} \boldsymbol{f}_s^*(\boldsymbol{r}_s) \cdot \delta \boldsymbol{r}_s dA_s = 0 \\ \delta t = 0, \quad \delta \boldsymbol{r}_s = 0, \quad \text{and} \quad \dfrac{d}{dt}(\delta \boldsymbol{r}_s) \neq 0. \end{cases} \tag{7.32}$$

The energy equation for a general control volume of fluid particles was given in Eqs. 7.23 and 7.24. Introducing Eq. 7.24 into Eq. 7.32 results in

$$\begin{cases} \delta \Bigg\{ \dfrac{D^C}{Dt} \int\limits_{CV} \dfrac{1}{2} \rho \boldsymbol{u} \cdot \boldsymbol{u} dV + \int\limits_{CS} \left(\dfrac{1}{2} \rho \boldsymbol{u} \cdot \boldsymbol{u} \right) (\boldsymbol{u} - \boldsymbol{v}_{CS}) \cdot \boldsymbol{n} dA \\ \qquad \overbrace{- \int\limits_{CS} \{ - p\boldsymbol{u} \cdot \boldsymbol{n} + \mu [\nabla (\boldsymbol{u} \cdot \boldsymbol{u}) - \boldsymbol{u} \times (\nabla \times \boldsymbol{u})] \cdot \boldsymbol{n}}^{\text{loading external to the fluid}} \\ \overbrace{- \dfrac{1}{2} \mu [\nabla (\boldsymbol{u} \cdot \boldsymbol{u}) - 2\, \boldsymbol{u} \times (\nabla \times \boldsymbol{u})] \cdot \boldsymbol{n} \Bigg\} dA + \dfrac{1}{2} \int\limits_{CV} \mu (\nabla \times \boldsymbol{u}) \cdot (\nabla \times \boldsymbol{u})\, dV}^{\text{viscous dissipation}} \\ \qquad \overbrace{+ \int\limits_{CS} \dfrac{1}{2} \rho (\boldsymbol{u} \cdot \boldsymbol{u})(\boldsymbol{u} \cdot \boldsymbol{n}) dA \Bigg\}}^{\text{non-commuting term}} \\ \qquad + \dfrac{d}{dt} \int\limits_{V_s} \left[\rho_s \dfrac{d\dot{\boldsymbol{r}}_s}{dt} - \boldsymbol{f}_s(\boldsymbol{r}_s) \right] \cdot \delta \boldsymbol{r}_s\, dV_s - \dfrac{d}{dt} \int\limits_{\substack{\text{Solid} \\ \text{Surface}}} \boldsymbol{f}_s^*(\boldsymbol{r}_s) \cdot \delta \boldsymbol{r}_s dA_s = 0 \\ \delta t = 0, \quad \delta \boldsymbol{r}_s = 0, \quad \text{and} \quad \dfrac{d}{dt}(\delta \boldsymbol{r}_s) \neq 0, \end{cases} \tag{7.33}$$

where body forces are neglected for fluid particles.

Equation 7.33 represents a general variational formulation for a control volume of a Newtonian incompressible viscous fluid and a general solid body. In order to specialize this equation further, boundary conditions must be considered and the stress–strain relation is required for elastic solid bodies. If the structure is assumed to be rigid, such as the model problem, forces acting at the elastic boundaries must be known.

We continue by considering the model problem to illustrate the required procedure. In the following section, Eq. 7.33 is modified further to obtain a single governing EOM describing the dynamics of the FSI system.

7.8 Modeling FSI: Single Governing EOM

In deriving Eq. 7.33, we have not considered the boundary conditions on the solid surface. Therefore, we continue our derivation by considering the no-slip condition in its most complete form.

To include the no-slip condition, we consider the second line of Eq. 7.33 and divide it into integrals over the closed and the open portions of the control surface,

$$\begin{aligned}\delta \int_{CS} \{-p\boldsymbol{u}\cdot\boldsymbol{n} + \mu\left[\nabla(\boldsymbol{u}\cdot\boldsymbol{u}) - \boldsymbol{u}\times(\nabla\times\boldsymbol{u})\right]\cdot\boldsymbol{n}\}\,dA \\ = \delta \int_{CS_C} \{-p\boldsymbol{u}\cdot\boldsymbol{n} + \mu\left[\nabla(\boldsymbol{u}\cdot\boldsymbol{u}) - \boldsymbol{u}\times(\nabla\times\boldsymbol{u})\right]\cdot\boldsymbol{n}\}\,dA \\ + \delta \int_{CS_O} \{-p\boldsymbol{u}\cdot\boldsymbol{n} + \mu\left[\nabla(\boldsymbol{u}\cdot\boldsymbol{u}) - \boldsymbol{u}\times(\nabla\times\boldsymbol{u})\right]\cdot\boldsymbol{n}\}\,dA.\end{aligned} \tag{7.34}$$

Considering Fig. 7.9, we denote the virtual power corresponding to the resultant of the forces acting on the closed control surface, $\boldsymbol{F}$, with δP, and define it as

$$\delta P = \delta \int_{CS_C} \{-p\boldsymbol{u}\cdot\boldsymbol{n} + \mu\left[\nabla(\boldsymbol{u}\cdot\boldsymbol{u}) - \boldsymbol{u}\times(\nabla\times\boldsymbol{u})\right]\cdot\boldsymbol{n}\}\,dA. \tag{7.35}$$

Also, denoting the virtual power of the resultant fluid dynamic forces applied to the solid structure, $\boldsymbol{F}^*$ by δP^*, we define

$$\delta P^* = \frac{d}{dt}\int_{\substack{\text{Solid}\\\text{Surface}}} \boldsymbol{f}_s^*(\boldsymbol{r}_s)\cdot\delta\boldsymbol{r}_s\,dA_s = \int_{\substack{\text{Solid}\\\text{Surface}}} \boldsymbol{f}_s^*(\boldsymbol{r}_s)\cdot\frac{d}{dt}(\delta\boldsymbol{r}_s)\,dA_s, \tag{7.36}$$

where we considered Jourdain's constraint, $\delta\boldsymbol{r}_s = 0$.

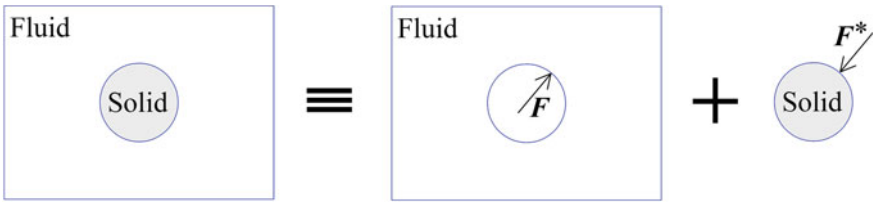

Fig. 7.9 Schematics of FSI between a rigid solid and a fluid, where $\boldsymbol{F}$ denotes the resultant of the forces applied to the fluid by the solid structure and $\boldsymbol{F}^*$ is the resultant of forces applied to the solid structure by the flow

Assuming the no-slip condition, and considering that Jourdain's principle does not permit any displacement, the particles at the solid surface remain in the same relative position. Moreover, the shear terms of Eq. 7.35 (terms containing μ) are representative of external loads and are not dissipative. Therefore, in the absence of dissipative terms, the power lost by the structure must be absorbed by the fluid and vice versa. Therefore, $\delta P = -\delta P^*$.

Moreover, the virtual velocities must be compatible with the system's constraints, thus $\delta \dot{\boldsymbol{r}}_s = \delta \boldsymbol{u}$ at the closed control surface. Therefore, the external fluid forces and $\boldsymbol{f}_s^*(\boldsymbol{r}_s)$ are action and reaction forces at any point on the solid surface. Then, using the terms for external load from Eq. 7.23, we obtain

$$\frac{d}{dt}\int\limits_{\substack{\text{Solid}\\ \text{Surface}}} \boldsymbol{f}_s^*(\boldsymbol{r}_s)\cdot\delta\boldsymbol{r}_s dA_s = -\delta\int\limits_{CS_C}\{-p\boldsymbol{u}\cdot\boldsymbol{n} + \mu\left[\nabla(\boldsymbol{u}\cdot\boldsymbol{u}) - \boldsymbol{u}\times(\nabla\times\boldsymbol{u})\right]\cdot\boldsymbol{n}\}\,dA. \tag{7.37}$$

Substituting Eq. 7.37 into Eq. 7.34, and introducing it into Eq. 7.33, we obtain

$$\left\{\begin{array}{l}
\delta\left\{\dfrac{D^C}{Dt}\displaystyle\int_{CV}\frac{1}{2}\rho\boldsymbol{u}\cdot\boldsymbol{u}dV + \int_{CS}\left(\frac{1}{2}\rho\boldsymbol{u}\cdot\boldsymbol{u}\right)(\boldsymbol{u}-\boldsymbol{v}_{CS})\cdot\boldsymbol{n}dA\right.\\
\qquad\overbrace{-\displaystyle\int_{CS_O}\{-p\boldsymbol{u}\cdot\boldsymbol{n} + \mu\left[\nabla(\boldsymbol{u}\cdot\boldsymbol{u}) - \boldsymbol{u}\times(\nabla\times\boldsymbol{u})\right]\cdot\boldsymbol{n}\}\,dA}^{\text{loading external to the fluid}}\\
\overbrace{+\displaystyle\int_{CS}\frac{1}{2}\mu\left[\nabla(\boldsymbol{u}\cdot\boldsymbol{u}) - 2\,\boldsymbol{u}\times(\nabla\times\boldsymbol{u})\right]\cdot\boldsymbol{n}dA + \frac{1}{2}\int_{CV}\mu\,(\nabla\times\boldsymbol{u})\cdot(\nabla\times\boldsymbol{u})\,dV}^{\text{viscous dissipation}}\\
\qquad\overbrace{\left.+\displaystyle\int_{CS}\frac{1}{2}\rho\,(\boldsymbol{u}\cdot\boldsymbol{u})\,(\boldsymbol{u}\cdot\boldsymbol{n})\,dA\right\}}^{\text{non-commuting term}}\\
\qquad\qquad +\dfrac{d}{dt}\displaystyle\int_{V_s}\left[\rho_s\frac{d\dot{\boldsymbol{r}}_s}{dt} - \boldsymbol{f}_s(\boldsymbol{r}_s)\right]\cdot\delta\boldsymbol{r}_s dV_s = 0\\
\delta t = 0, \quad \delta\boldsymbol{r}_s = 0, \quad \text{and} \quad \dfrac{d}{dt}(\delta\boldsymbol{r}_s) \neq 0.
\end{array}\right. \tag{7.38}$$

Equation 7.38 is valid for any control volume of a Newtonian incompressible viscous fluid and any solid body (rigid or deformable). We next continue our derivation for the *model problem*, which assumes the solid body to be rigid. For a deformable solid body, similar manipulations need to be performed, given that the stress–strain relations $\boldsymbol{f}_s(\boldsymbol{r}_s, t)$ are known.

7.8.1 Single Governing EOM for the Translating Cylinder

Consider the model problem in the form of the translating cylinder shown in Fig. 7.1a. One generalized coordinate is required to fully describe the motion of the cylinder. Let the generalized coordinate be the Lagrangian coordinate $\boldsymbol{x}_s(t)$ measured from the center of the cylinder when it is at rest, perpendicular to the axis of symmetry of the cylinder and transverse to the flow direction.

Setting $\boldsymbol{r}_s(t) = \boldsymbol{x}_s(t)$ and $\boldsymbol{f}_s(\boldsymbol{x}_s) = \frac{1}{V_s}(-C\dot{\boldsymbol{x}}_s - k\boldsymbol{x}_s)$ in Eq. 7.38, the corresponding terms can be replaced as follows:

$$\frac{d}{dt}\int_{V_s}\left[\rho_s\frac{d\dot{\boldsymbol{r}}_s}{dt} - \boldsymbol{f}_s(\boldsymbol{r}_s)\right]\cdot\delta\boldsymbol{r}_s dV_s = \frac{d}{dt}\left[\left(m_s\ddot{\boldsymbol{x}}_s + C\dot{\boldsymbol{x}}_s + k\boldsymbol{x}_s\right)\cdot\delta\boldsymbol{x}_s\right]$$
$$= \left(m_s\ddot{\boldsymbol{x}}_s + C\dot{\boldsymbol{x}}_s + k\boldsymbol{x}_s\right)\cdot\delta\dot{\boldsymbol{x}}_s, \tag{7.39}$$

where C is the net support damping constant and k denotes the net support spring constant. In deriving Eq. 7.39, the structural terms are differentiated and the variational constraint ($\delta\boldsymbol{x}_s = 0$) is imposed. Also, the rigidity of the cylinder is considered in the integration over the solid volume.

Similar to the energy rate terms obtained for the control volume of fluid particles, Eqs. 7.23 and 7.24, we seek the energy rate terms corresponding to the structural terms using Eq. 7.22. The structural parameter $\boldsymbol{x}_s$ is a Lagrangian coordinate. Therefore, Eq. 7.22 can be used to obtain the energy rate equation for the conservative structural terms,

$$\begin{aligned}\left(m_s\,\ddot{\boldsymbol{x}}_s + k\,\boldsymbol{x}_s\right)\cdot\delta\dot{\boldsymbol{x}}_s &= m_s\,\ddot{\boldsymbol{x}}_s\cdot\delta\dot{\boldsymbol{x}}_s + k\,\boldsymbol{x}_s\cdot\delta\dot{\boldsymbol{x}}_s\\ &= \frac{\partial\left(m_s\,\ddot{\boldsymbol{x}}_s\cdot\dot{\boldsymbol{x}}_s\right)}{\partial\dot{\boldsymbol{x}}_s}\cdot\delta\dot{\boldsymbol{x}}_s + \frac{\partial\left(k\,\boldsymbol{x}_s\cdot\dot{\boldsymbol{x}}_s\right)}{\partial\dot{\boldsymbol{x}}_s}\cdot\delta\dot{\boldsymbol{x}}_s\\ &= \delta\left(m_s\,\ddot{\boldsymbol{x}}_s\cdot\dot{\boldsymbol{x}}_s + k\,\boldsymbol{x}_s\cdot\dot{\boldsymbol{x}}_s\right).\end{aligned} \tag{7.40}$$

For the nonconservative linear damper, we use Rayleigh's dissipation function, $\frac{1}{2}C\,\dot{\boldsymbol{x}}_s\cdot\dot{\boldsymbol{x}}_s$, and obtain its directional derivative with respect to $\dot{\boldsymbol{x}}_s$ in the direction of $\dot{\boldsymbol{x}}_s$,

$$\nabla_{\dot{\boldsymbol{x}}_s}\left(\frac{1}{2}C\dot{\boldsymbol{x}}_s\cdot\dot{\boldsymbol{x}}_s\right) = C\dot{\boldsymbol{x}}_s. \tag{7.41}$$

Therefore, the variation of the function above can be obtained using Eq. 7.25,

$$\delta\left(\frac{1}{2}C\dot{\boldsymbol{x}}_s\cdot\dot{\boldsymbol{x}}_s\right) = C\dot{\boldsymbol{x}}_s\cdot\delta\dot{\boldsymbol{x}}_s. \tag{7.42}$$

Substituting Eqs. 7.40 and 7.42 into Eq. 7.39, and introducing the resulting relation into Eq. 7.38, we find the energy rate equation for the translating cylinder problem,

$$\delta \left\{ \frac{D^C}{Dt} \int_{CV} \frac{1}{2}\rho \boldsymbol{u}\cdot\boldsymbol{u}\, dV + \int_{CS} \left(\frac{1}{2}\rho \boldsymbol{u}\cdot\boldsymbol{u}\right)(\boldsymbol{u}-\boldsymbol{v}_{CS})\cdot \boldsymbol{n} dA \right.$$
$$- \int_{CS_O} \{-p\boldsymbol{u}\cdot\boldsymbol{n} + \mu\left[\nabla(\boldsymbol{u}\cdot\boldsymbol{u}) - \boldsymbol{u}\times(\nabla\times\boldsymbol{u})\right]\cdot\boldsymbol{n}\} dA$$
$$+ \int_{CS} \left\{\frac{1}{2}\mu\left[\nabla(\boldsymbol{u}\cdot\boldsymbol{u}) - 2\,\boldsymbol{u}\times(\nabla\times\boldsymbol{u})\right]\cdot\boldsymbol{n}\right\} dA$$
$$\left. + \frac{1}{2}\int_{CV} \mu(\nabla\times\boldsymbol{u})\cdot(\nabla\times\boldsymbol{u})\, dV + \int_{CS}\frac{1}{2}\rho(\boldsymbol{u}\cdot\boldsymbol{u})(\boldsymbol{u}\cdot\boldsymbol{n})\, dA \right\}$$
$$+ \delta\left(m_s\ddot{\boldsymbol{x}}_s\cdot\dot{\boldsymbol{x}}_s + \frac{1}{2}C\dot{\boldsymbol{x}}_s\cdot\dot{\boldsymbol{x}}_s + k\boldsymbol{x}_s\cdot\dot{\boldsymbol{x}}_s\right) = 0. \tag{7.43}$$

In deriving Eq. 7.43, we did not add any constraints regarding the nature of solid–fluid interaction other than the action and reaction forces. In order to include the boundary conditions, we next separate the integrals over the control surface into integrals over its open and closed portions. For the flux of kinetic energy, we have

$$\int_{CS}\left(\frac{1}{2}\rho\boldsymbol{u}\cdot\boldsymbol{u}\right)(\boldsymbol{u}-\boldsymbol{v}_{CS})\cdot\boldsymbol{n}dA$$
$$= \int_{CS_C}\left(\frac{1}{2}\rho\boldsymbol{u}\cdot\boldsymbol{u}\right)(\boldsymbol{u}-\boldsymbol{v}^c_{CS})\cdot\boldsymbol{n}dA + \int_{CS_O}\left(\frac{1}{2}\rho\boldsymbol{u}\cdot\boldsymbol{u}\right)(\boldsymbol{u}-\boldsymbol{v}^o_{CS})\cdot\boldsymbol{n}dA, \tag{7.44}$$

where $\boldsymbol{v}^o_{CS}$ and $\boldsymbol{v}^c_{CS}$ are the velocities of the open and closed portions of the control volume, respectively. The first integral on the right-hand side of Eq. 7.44 is equal to zero due to the *no-penetration* condition, therefore,

$$\int_{CS}\left(\frac{1}{2}\rho\boldsymbol{u}\cdot\boldsymbol{u}\right)(\boldsymbol{u}-\boldsymbol{v}_{CS})\cdot\boldsymbol{n}dA = \int_{CS_O}\left(\frac{1}{2}\rho\boldsymbol{u}\cdot\boldsymbol{u}\right)(\boldsymbol{u}-\boldsymbol{v}^o_{CS})\cdot\boldsymbol{n}dA. \tag{7.45}$$

For the fluid dissipative forces at the control surfaces, we expand the fourth integral in Eq. 7.43 as follows:

$$\int_{CS} \frac{1}{2}\mu \left[\nabla (\boldsymbol{u}\cdot\boldsymbol{u}) - 2\,\boldsymbol{u}\times(\nabla\times\boldsymbol{u})\right]\cdot\boldsymbol{n}dA$$
$$= \int_{CS_O} \frac{1}{2}\mu \left[\nabla (\boldsymbol{u}\cdot\boldsymbol{u}) - 2\,\boldsymbol{u}\times(\nabla\times\boldsymbol{u})\right]\cdot\boldsymbol{n}dA$$
$$+ \int_{CS_C} \frac{1}{2}\mu \left[\nabla (\boldsymbol{u}\cdot\boldsymbol{u}) - 2\,\boldsymbol{u}\times(\nabla\times\boldsymbol{u})\right]\cdot\boldsymbol{n}dA. \quad (7.46)$$

The second integral on the right-hand side, over the closed control surface, can be interpreted in multiple ways. We expect energy to be dissipated at higher rates near the structure due to a larger velocity gradient. Even though the no-slip condition implies that no energy is lost due to friction because of zero relative motion between the fluid and solid, viscous dissipation can be envisioned between the fluid particles at the solid surface and those particles adjacent to them. So, we choose to keep the dissipative terms at the closed control surfaces and continue our derivations.

We make two clarifications regarding the viscous terms. First, for a solid structure that does not move, the dissipative terms at the closed boundary disappear [14, article 329]. Therefore, one choice seems to be that $\boldsymbol{u}$ in Eq. 7.46 can be replaced with $\boldsymbol{u}_r$, especially when experimental data is considered. Second, the same discussion as that made for dissipative terms applies to viscous forces acting external to the fluid, and one may decide to keep these in the energy equation. However, the pressure terms are conservative forces for incompressible fluids and they can be neglected.

Finally, regarding the non-commuting terms, we also consider the no-slip condition, which states that at the closed control surface $\boldsymbol{u} = \dot{\boldsymbol{x}}_s$ for all time. Replacing $\boldsymbol{u}$ by $\dot{\boldsymbol{x}}_s$ at the closed surfaces and considering that the commutation rule holds for $\dot{\boldsymbol{x}}_s$, the non-commuting terms disappear. Therefore, in Eq. 7.43 we have

$$\int_{CS} \frac{1}{2}\rho\,(\boldsymbol{u}\cdot\boldsymbol{u})\,(\boldsymbol{u}\cdot\boldsymbol{n})\,dA = \int_{CS_O} \frac{1}{2}\rho\,(\boldsymbol{u}\cdot\boldsymbol{u})\,(\boldsymbol{u}\cdot\boldsymbol{n})\,dA. \quad (7.47)$$

Having specified the boundary condition, the variational energy rate equation for the translating cylinder problem is obtained by substituting Eqs. 7.45–7.47 into Eq. 7.43, resulting in

$$\delta\left\{\frac{D^C}{Dt}\int_{CV}\frac{1}{2}\rho\boldsymbol{u}\cdot\boldsymbol{u}\,dV + \int_{CS_O}\left(\frac{1}{2}\rho\,\boldsymbol{u}\cdot\boldsymbol{u}\right)\left(\boldsymbol{u}-\boldsymbol{v}^o_{CS}\right)\cdot\boldsymbol{n}dA\right.$$
$$\left. - \int_{CS_O}\overbrace{\{-p\boldsymbol{u}\cdot\boldsymbol{n} + \mu\left[\nabla(\boldsymbol{u}\cdot\boldsymbol{u}) - \boldsymbol{u}\times(\nabla\times\boldsymbol{u})\right]\cdot\boldsymbol{n}}^{\text{external load at open CS}}\right.$$

$$
\begin{aligned}
&\overbrace{-\frac{1}{2}\mu\left[\nabla\left(\boldsymbol{u}\cdot\boldsymbol{u}\right)-2\boldsymbol{u}\times\left(\nabla\times\boldsymbol{u}\right)\right]\cdot\boldsymbol{n}}^{\text{viscous dissipation at open CS}}\Bigg\}dA\\
&+\overbrace{\int\limits_{CS_C}\frac{1}{2}\mu\left[\nabla\left(\boldsymbol{u}\cdot\boldsymbol{u}\right)-2\boldsymbol{u}\times\left(\nabla\times\boldsymbol{u}\right)\right]\cdot\boldsymbol{n}\,dA}^{\text{viscous dissipation at solid surface}}\\
&+\overbrace{\int\limits_{CV}\frac{1}{2}\mu\left(\nabla\times\boldsymbol{u}\right)\cdot\left(\nabla\times\boldsymbol{u}\right)dV}^{\text{viscous dissipation inside the CV}}+\int\limits_{CS_O}\frac{1}{2}\rho\left(\boldsymbol{u}\cdot\boldsymbol{u}\right)\left(\boldsymbol{u}\cdot\boldsymbol{n}\right)\,dA\\
&+m_s\,\ddot{\boldsymbol{x}}_s\cdot\dot{\boldsymbol{x}}_s+\frac{1}{2}C\,\dot{\boldsymbol{x}}_s\cdot\dot{\boldsymbol{x}}_s+k\,\boldsymbol{x}_s\cdot\dot{\boldsymbol{x}}_s\Bigg\}=0.
\end{aligned}
\tag{7.48}
$$

Rayleigh's dissipation function must be multiplied by a factor of two in order to obtain the energy rate equation [18]. Therefore, the energy rate equation for the translating cylinder problem is

$$
\begin{aligned}
&\frac{D^C}{Dt}\int\limits_{CV}\frac{1}{2}\rho\boldsymbol{u}\cdot\boldsymbol{u}\,dV+\int\limits_{CS_O}\left(\frac{1}{2}\rho\,\boldsymbol{u}\cdot\boldsymbol{u}\right)\left(\boldsymbol{u}-\boldsymbol{v}^o_{CS}\right)\cdot\boldsymbol{n}\,dA\\
&\quad-\int\limits_{CS_O}\left[-\,p\,\boldsymbol{u}\cdot\boldsymbol{n}\,+\mu\boldsymbol{u}\times\left(\nabla\times\boldsymbol{u}\right)\cdot\boldsymbol{n}\right]dA\\
&\quad+\int\limits_{CS_C}\mu\left[\nabla\left(\boldsymbol{u}\cdot\boldsymbol{u}\right)-2\boldsymbol{u}\times\left(\nabla\times\boldsymbol{u}\right)\right]\cdot\boldsymbol{n}\,dA\\
&+\int\limits_{CV}\mu\left(\nabla\times\boldsymbol{u}\right)\cdot\left(\nabla\times\boldsymbol{u}\right)dV+\int\limits_{CS_O}\frac{1}{2}\rho\left(\boldsymbol{u}\cdot\boldsymbol{u}\right)\left(\boldsymbol{u}\cdot\boldsymbol{n}\right)\,dA\\
&\quad+m_s\,\ddot{\boldsymbol{x}}_s\cdot\dot{\boldsymbol{x}}_s+C\,\dot{\boldsymbol{x}}_s\cdot\dot{\boldsymbol{x}}_s+k\,\boldsymbol{x}_s\cdot\dot{\boldsymbol{x}}_s=0,
\end{aligned}
\tag{7.49}
$$

where we summed the viscous terms at the open control surface.

The *model problem* in the form of the inverted pendulum is considered in the following section.

7.8.2 Single Governing EOM for the Inverted Pendulum

Similarly to the translating cylinder problem, the inverted pendulum problem (Fig. 7.1b) is a single DOF structure. The single generalized coordinate is selected

to be the angle of rotation of the rigid cylinder θ (radians) about its support. Also, the same assumptions as those made by Benaroya and Wei [3] are used, which are three-dimensional effects can be ignored (vortices remain two dimensional), weight and buoyancy forces must be included for the structure, and the resultant of all the forces act at the geometric center of the circular cylinder. Moreover, the horizontal plane passing through the center of geometry contains the two dimensional vortices.

Therefore, by replacing the last term in Eq. 7.38 by

$$\left[I_0\ddot{\theta} + C_T\dot{\theta} + k_T\theta - (m_s g - B)\,\frac{L}{2}\sin\theta \mathbf{e}_\theta \right] \cdot \delta\theta \mathbf{e}_\theta,$$

the energy rate equation is found to be

$$\begin{aligned}
\frac{D^C}{Dt}\int_{CV} \frac{1}{2}\rho \boldsymbol{u}\cdot\boldsymbol{u}dV + \int_{CS_O}\left(\frac{1}{2}\rho \boldsymbol{u}\cdot\boldsymbol{u}\right)\left(\boldsymbol{u}-\boldsymbol{v}^o_{CS}\right)\cdot\boldsymbol{n}dA \\
- \int_{CS_O}\left[-p\boldsymbol{u}\cdot\boldsymbol{n} + \mu\boldsymbol{u}\times(\nabla\times\boldsymbol{u})\cdot\boldsymbol{n}\right]dA \\
+ \int_{CS_C}\mu\left[\nabla(\boldsymbol{u}\cdot\boldsymbol{u}) - 2\boldsymbol{u}\times(\nabla\times\boldsymbol{u})\right]\cdot\boldsymbol{n}dA \\
+ \int_{CV}\mu(\nabla\times\boldsymbol{u})\cdot(\nabla\times\boldsymbol{u})\,dV + \int_{CS_O}\frac{1}{2}\rho(\boldsymbol{u}\cdot\boldsymbol{u})(\boldsymbol{u}\cdot\boldsymbol{n})\,dA \\
+ I_0\ddot{\theta}\dot{\theta} + C_T\dot{\theta}^2 + k_T\theta\dot{\theta} - \left[(m_s g - B)\,\frac{L}{2}\sin\theta\right]\dot{\theta}\Bigg\} = 0.
\end{aligned} \tag{7.50}$$

The derivations required to obtain this equation are not presented here since they are similar to those shown in the last section. Detailed derivations can be found in [19].

Having obtained a single degree-of-freedom equation for the model problem, we next seek reduced-order models that are two coupled EOM. We begin by explaining our methodology based on some of the fundamental concepts of the variational calculus.

7.9 Coupled Equations of Motion: Conceptual Approach to the Wake Oscillator

We have obtained the variation of the rate of the Lagrangian function L (Eq. 7.48 and the variational equation corresponding to Eq. 7.50). Our next goal is to derive two nonlinear coupled equations that can fully describe the main characteristics of the dynamics of a FSI system.

In analytical mechanics, the partial derivatives of the Lagrangian function with respect to velocities results in a fundamental concept called the *generalized momentum* [15], p_i, defined as

$$p_i = \frac{\partial L}{\partial \dot{q}_i}, \tag{7.51}$$

where $\dot{q}_i$ is the generalized velocity that can be selected to be either the Lagrangian or the Eulerian velocities.

The following derivations are similar in many ways to that concept as a result of the definition of Jourdain's variational operator:

$$\delta\psi = \lim_{\varepsilon \to 0} \frac{1}{\varepsilon} \left[\psi \left(\boldsymbol{u} + \varepsilon \, \delta \boldsymbol{u} \right) - \psi \left(\boldsymbol{u} \right) \right], \tag{7.52}$$

and

$$\delta\psi = \frac{\partial \psi}{\partial \boldsymbol{u}} \cdot \delta \boldsymbol{u}, \tag{7.53}$$

where ψ is a potential function, $\boldsymbol{u}$ is the velocity field and $\delta \boldsymbol{u}$ is the variation of the velocity field. However, here we are dealing with the rate of the Lagrangian function, $\dot{L}$ (or in the Eulerian reference frame, DL/Dt), instead of the Lagrangian L. Therefore, applying Eq. 7.53 would result in the *rate of generalized momenta.*

A fundamental concept of variational calculus, called *Noether's principle*, states that any infinitesimal transformation of either the action variables, or the independent variable, involving a constant parameter results in a conservation law if the Lagrangian remains unchanged [15]. In Chap. 6 and [19], we showed that the energy rate equation ($\dot{L} = 0$) can be directly obtained from Jourdain's principle using Eq. 7.53. That is, the corresponding differential equations can be obtained by using the definition of Jourdain's principle and by choosing $\boldsymbol{u}$ and $\dot{\boldsymbol{r}}_s$ to be the independent generalized velocities. Thus,

$$\delta\dot{L} = \frac{\partial \dot{L}}{\partial \boldsymbol{u}} \cdot \delta \boldsymbol{u} + \frac{\partial \dot{L}}{\partial \dot{\boldsymbol{r}}_s} \cdot \delta \dot{\boldsymbol{r}}_s = 0, \tag{7.54}$$

where $\partial \dot{L}/\partial \boldsymbol{u}$ and $\partial \dot{L}/\partial \dot{\boldsymbol{r}}_s$ are defined as

$$\begin{aligned} \frac{\partial \dot{L}}{\partial \boldsymbol{u}} \cdot \delta \boldsymbol{u} &= \left. \frac{\partial \dot{L} \left(\boldsymbol{u} + \varepsilon \delta \boldsymbol{u} \right)}{\partial \varepsilon} \right|_{\varepsilon = 0} \\ &\equiv \lim_{\varepsilon \to 0} \frac{1}{\varepsilon} \left[\dot{L} \left(\boldsymbol{u} + \varepsilon \, \delta \boldsymbol{u} \right) - \dot{L} \left(\boldsymbol{u} \right) \right], \end{aligned} \tag{7.55}$$

and

$$\frac{\partial \dot{L}}{\partial \dot{\boldsymbol{r}}_s} \cdot \delta \dot{\boldsymbol{r}}_s = \left. \frac{\partial \dot{L}\left(\dot{\boldsymbol{r}}_s + \varepsilon \delta \dot{\boldsymbol{r}}_s\right)}{\partial \varepsilon} \right|_{\varepsilon=0}$$
$$\equiv \lim_{\varepsilon \to 0} \frac{1}{\varepsilon} \left[\dot{L}\left(\dot{\boldsymbol{r}}_s + \varepsilon \delta \dot{\boldsymbol{r}}_s\right) - \dot{L}\left(\dot{\boldsymbol{r}}_s\right) \right]. \tag{7.56}$$

Since $\delta \boldsymbol{u}$ and $\delta \dot{\boldsymbol{r}}_s$ are arbitrary, independent, nonzero vectors, Eq. 7.54 results in

$$\frac{\partial \dot{L}}{\partial \boldsymbol{u}} = 0 \tag{7.57}$$
$$\frac{\partial \dot{L}}{\partial \dot{\boldsymbol{r}}_s} = 0. \tag{7.58}$$

For the model problem, these are four coupled equations: Eq. 7.58 is a single differential equation (since the structure has a single DOF) representing the solid structure, and Eq. 7.57 are three differential equations describing the flow.

Consequently, if we use $\partial \dot{L}/\partial \dot{\boldsymbol{r}}_s = 0$ to obtain the structural governing equation and substitute it into Eq. 7.54, we are left with

$$\frac{\partial \dot{L}}{\partial \boldsymbol{u}} \cdot \delta \boldsymbol{u} = 0. \tag{7.59}$$

Defining the partial scalar potential function $\delta \dot{L}_{\boldsymbol{u}}$ as

$$\delta \dot{L}_{\boldsymbol{u}} = \frac{\partial \dot{L}}{\partial \boldsymbol{u}} \cdot \delta \boldsymbol{u}, \tag{7.60}$$

the coupled set of equations represented by Eqs. 7.57 and 7.58 becomes

$$\begin{cases} \delta \dot{L}_{\boldsymbol{u}} = 0 \\ \dfrac{\partial \dot{L}}{\partial \dot{\boldsymbol{r}}_s} = 0. \end{cases} \tag{7.61}$$

Since $\dot{L}_{\boldsymbol{u}}$ is a set of potential functions satisfying $\delta \dot{L}_{\boldsymbol{u}} = 0$, then $\dot{L}_{\boldsymbol{u}} = 0$ is the corresponding balance of energy (conservation) equation. Therefore, Eq. 7.61 become

$$\begin{cases} \dot{L}_{\boldsymbol{u}} = 0 \\ \dfrac{\partial \dot{L}}{\partial \dot{\boldsymbol{r}}_s} = 0. \end{cases} \tag{7.62}$$

These are two coupled equations: $\partial \dot{L}/\partial \dot{\boldsymbol{r}}_s = 0$ is an ordinary differential equation representing the structural oscillation, and $\dot{L}_{\boldsymbol{u}} = 0$ is an integral equation representing the fluid dynamics.

Generally, variational methods are powerful tools for conservative systems. The approach explained here requires monogenic forces and a scleronomic system.

Frictional forces (structural damping and viscous forces) are polygenic and the corresponding energy rate terms are obtained using Rayleigh's dissipation function. Therefore, the first line of Eq. 7.62 alone is not a conservation equation but rather it is a power equation representing the dynamics of the fluid system as coupled to the structural EOM. These concepts will become clearer in application below.

7.10 Coupled Equations of Motion: The Wake Oscillator

In this section, we wish to obtain reduced-order wake-oscillator models comprised of two coupled EOM (in the form of the wake-oscillator model) using the methodology explained in the previous section. In Sect. 7.8, we obtained a single governing EOM for FSI systems in the general form of Eq. 7.38. For the single degree-of-freedom model, the boundary conditions are important but are not crucial to the modeling process since the structural response is estimated via averaging the energy that must be transferred to the structure. On the other hand, when obtaining a reduced-order model in the form of a wake-oscillator model, the boundary conditions are extremely important as these essentially determine the nature of the coupling between the two governing equations of motion.

In Sect. 7.5, we discussed that imposing the no-slip condition in its most complete form may weaken the reduced-order model's ability to capture the true dynamics of the FSI system, and that weak forms of no-slip conditions have generally been applied in many computational simulations or analytical models of FSI. Therefore, we start the modeling process from the variational formulation expressed by Eq. 7.38. For these reasons, we wish to reintroduce the no-slip condition into Eq. 7.38. This is done explicitly and implicitly in the following two sections, where this terminology will become clear.

For simplicity, only the model problem in the form of the translating cylinder is considered. We apply Gauss' divergence theorem to Eq. 7.43 in order to take the non-commuting term inside the control volume and neglect the changes that resulted from the no-slip condition in deriving Eq. 7.43, resulting in

$$\delta\left\{\frac{D^C}{Dt}\int_{CV}\frac{1}{2}\rho\boldsymbol{u}\cdot\boldsymbol{u}dV+\int_{CS}\left(\frac{1}{2}\rho\boldsymbol{u}\cdot\boldsymbol{u}\right)(\boldsymbol{u}-\boldsymbol{v}_{CS})\cdot\boldsymbol{n}dA\right.$$
$$\overbrace{-\int_{CS}\{-p\boldsymbol{u}\cdot\boldsymbol{n}+\mu\left[\nabla(\boldsymbol{u}\cdot\boldsymbol{u})-\boldsymbol{u}\times(\nabla\times\boldsymbol{u})\right]\cdot\boldsymbol{n}}^{\text{loading external to the fluid}}$$
$$\left.\overbrace{-\frac{1}{2}\mu\left[\nabla(\boldsymbol{u}\cdot\boldsymbol{u})-2\,\boldsymbol{u}\times(\nabla\times\boldsymbol{u})\right]\cdot\boldsymbol{n}}^{\text{viscous dissipation}}\right\}dA+\frac{1}{2}\int_{CV}\mu\,(\nabla\times\boldsymbol{u})\cdot(\nabla\times\boldsymbol{u})\,dV$$

$$\left. \overbrace{+\int_{CV} \nabla \cdot \left[\frac{1}{2}\rho\,(\boldsymbol{u}\cdot\boldsymbol{u})\,\boldsymbol{u}\right] dV}^{\text{non-commuting term}} \right\} + \delta\left(m_s \ddot{\boldsymbol{x}}_s \cdot \dot{\boldsymbol{x}}_s + \frac{1}{2} C \dot{\boldsymbol{x}}_s \cdot \dot{\boldsymbol{x}}_s + k \boldsymbol{x}_s \cdot \dot{\boldsymbol{x}}_s\right) = 0. \tag{7.63}$$

Equation 7.63 can also be expressed as

$$\delta \left\{ \int_{CV} \frac{D^C}{Dt}\left(\frac{1}{2}\rho \boldsymbol{u}\cdot\boldsymbol{u}\right) dV \overbrace{-\int_{CS} \{-p\boldsymbol{u}\cdot\boldsymbol{n} + \mu\left[\nabla(\boldsymbol{u}\cdot\boldsymbol{u}) - \boldsymbol{u}\times(\nabla\times\boldsymbol{u})\right]\cdot\boldsymbol{n}}^{\text{loading external to the fluid}} \right.$$
$$\overbrace{-\frac{1}{2}\mu\left[\nabla(\boldsymbol{u}\cdot\boldsymbol{u}) - 2\,\boldsymbol{u}\times(\nabla\times\boldsymbol{u})\right]\cdot\boldsymbol{n}}^{\text{viscous dissipation}} \left.\right\} dA + \frac{1}{2}\int_{CV} \mu\,(\nabla\times\boldsymbol{u})\cdot(\nabla\times\boldsymbol{u})\,dV$$
$$\left. \overbrace{+\int_{CV} \nabla \cdot \left[\frac{1}{2}\rho\,(\boldsymbol{u}\cdot\boldsymbol{u})\,\boldsymbol{u}\right] dV}^{\text{non-commuting term}} \right\} + \delta\left(m_s \ddot{\boldsymbol{x}}_s \cdot \dot{\boldsymbol{x}}_s + \frac{1}{2} C \dot{\boldsymbol{x}}_s \cdot \dot{\boldsymbol{x}}_s + k \boldsymbol{x}_s \cdot \dot{\boldsymbol{x}}_s\right) = 0, \tag{7.64}$$

where we used Eq. 7.23 instead of Eq. 7.24 for the fluid terms. Equations 7.63 and 7.64 are similar equations, yet each has different advantages depending on the selection of the control volume. Note that no boundary condition has yet been applied in deriving Eqs. 7.63 and 7.64.

7.10.1 *Reduced-Order Model with Implicit Implementation of the No-Slip Condition*

The applicability of an analytical formulation is greatly affected by the selection of the control volume. For reasons that will become apparent, we consider the more restricted form of the control volume shown in Fig. 7.10, where the control volume moves rigidly with the structure. Therefore,

$$\boldsymbol{v}_{CS} = \boldsymbol{v}_{\text{structure}}. \tag{7.65}$$

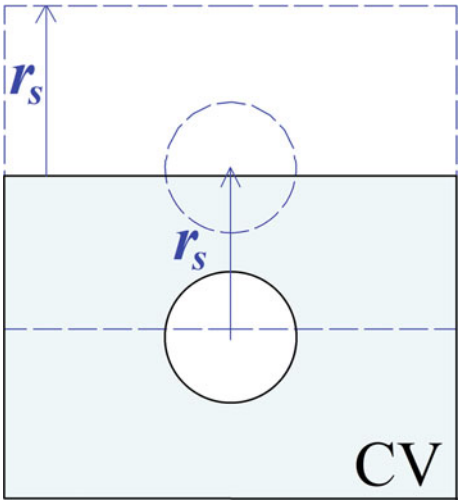

Fig. 7.10 The selected control volume where the control volume moves rigidly with the structure. $\boldsymbol{r}_s$ denotes the displacement of the structure

No other requirements are necessary other than some portions of the control surface must be the solid surfaces. In Fig. 7.10, the open portion of the control volume is selected to be rectangular in shape for simplicity. Moreover, we denote the velocity of the structure by $\dot{\boldsymbol{x}}_s$, resulting in $\dot{\boldsymbol{x}}_s = \boldsymbol{v}_{CS}$.

In Sect. 7.7, we discussed that by excluding the dissipative terms the remaining viscous terms together with the pressure represent the external loads on the closed surface, and they can be viewed as conservative action and reaction forces where the no-slip condition is considered. Therefore, going through the same steps shown there, Eq. 7.63 becomes

$$\begin{aligned}\delta\Bigg\{\frac{D^C}{Dt}\int_{CV}\frac{1}{2}\rho\boldsymbol{u}\cdot\boldsymbol{u}\,dV+\int_{CV}\nabla\cdot\left[\left(\frac{1}{2}\rho\boldsymbol{u}\cdot\boldsymbol{u}\right)\left(\boldsymbol{u}-\dot{\boldsymbol{x}}_s\right)\right]dV\\ -\int_{CS_O}\left[-p\boldsymbol{u}\cdot\boldsymbol{n}+\frac{1}{2}\mu\nabla\left(\boldsymbol{u}\cdot\boldsymbol{u}\right)\cdot\boldsymbol{n}\right]dA\\ +\int_{CS_C}\frac{1}{2}\mu\left[\nabla\left(\boldsymbol{u}\cdot\boldsymbol{u}\right)-2\,\boldsymbol{u}\times\left(\nabla\times\boldsymbol{u}\right)\right]\cdot\boldsymbol{n}\,dA\\ +\frac{1}{2}\int_{CV}\mu\left(\nabla\times\boldsymbol{u}\right)\cdot\left(\nabla\times\boldsymbol{u}\right)dV+\int_{CV}\nabla\cdot\left[\frac{1}{2}\rho\left(\boldsymbol{u}\cdot\boldsymbol{u}\right)\boldsymbol{u}\right]dV\Bigg\}\\ +\delta\left(m_s\ddot{\boldsymbol{x}}_s\cdot\dot{\boldsymbol{x}}_s+\frac{1}{2}C\dot{\boldsymbol{x}}_s\cdot\dot{\boldsymbol{x}}_s+k\boldsymbol{x}_s\cdot\dot{\boldsymbol{x}}_s\right)=0,\end{aligned}\tag{7.66}$$

where the term $\left(\frac{1}{2}\rho \boldsymbol{u}\cdot\boldsymbol{u}\right)\left(\boldsymbol{u}-\dot{\boldsymbol{x}}_s\right)$ is taken inside the control volume, assuming that the fluid particles can shed from the structure. Thus, the no-slip condition is implemented by neglecting the viscous and pressure forces at the solid structure in Eq. 7.66. The no-penetration condition will be satisfied by integration over the appropriate control volume.

Having obtained the variational energy rate equation, we wish to obtain two coupled governing equations via the methodology explained in Sect. 7.9. We start by applying Eqs. 7.55–7.66 in order to obtain the rate of generalized momentum associated with $\boldsymbol{u}$. However, we are just interested in the partial scalar potential $\dot{L}_{\boldsymbol{u}}$. The potential terms not containing the flow velocity $\boldsymbol{u}$ will drop out and the terms expressed purely by $\boldsymbol{u}$ remain the same. Moreover, the potential functions of both velocities $\boldsymbol{u}$ and $\dot{\boldsymbol{x}}_s$ remain the same. Therefore, $\delta\dot{L}_{\boldsymbol{u}}$ is found to be

$$\begin{aligned}\delta\dot{L}_{\boldsymbol{u}} = \delta\Bigg\{ &\frac{D^C}{Dt}\int_{CV}\frac{1}{2}\rho\boldsymbol{u}\cdot\boldsymbol{u}\,dV + \int_{CV}\nabla\cdot\left[\left(\frac{1}{2}\rho\boldsymbol{u}\cdot\boldsymbol{u}\right)\left(\boldsymbol{u}-\dot{\boldsymbol{x}}_s\right)\right]dV \\ &- \int_{CS_O}\left[-p\boldsymbol{u}\cdot\boldsymbol{n} + \frac{1}{2}\mu\nabla\left(\boldsymbol{u}\cdot\boldsymbol{u}\right)\cdot\boldsymbol{n}\right]dA \\ &+ \int_{CS_C}\frac{1}{2}\mu\left[\nabla\left(\boldsymbol{u}\cdot\boldsymbol{u}\right) - 2\,\boldsymbol{u}\times\left(\nabla\times\boldsymbol{u}\right)\right]\cdot\boldsymbol{n}\,dA \\ &+ \frac{1}{2}\int_{CV}\mu\left(\nabla\times\boldsymbol{u}\right)\cdot\left(\nabla\times\boldsymbol{u}\right)dV + \int_{CV}\nabla\cdot\left[\frac{1}{2}\rho\left(\boldsymbol{u}\cdot\boldsymbol{u}\right)\boldsymbol{u}\right]dV\Bigg\}.\end{aligned} \tag{7.67}$$

The equation representing the participation of the fluid dynamic parameters is obtained from Eqs. 7.62 by setting $\dot{L}_{\boldsymbol{u}} = 0$.

For the structural terms, we apply Eq. 7.56 to the remaining terms of the energy equation (Eq. 7.66), which are

$$\delta\int_{CV}\nabla\cdot\left[\left(\frac{1}{2}\rho\boldsymbol{u}\cdot\boldsymbol{u}\right)\left(-\dot{\boldsymbol{x}}_s\right)\right]dV + \delta\left(m_s\ddot{\boldsymbol{x}}_s\cdot\dot{\boldsymbol{x}}_s + \frac{1}{2}C\dot{\boldsymbol{x}}_s\cdot\dot{\boldsymbol{x}}_s + k\boldsymbol{x}_s\cdot\dot{\boldsymbol{x}}_s\right) = 0. \tag{7.68}$$

Considering the structural terms, we have

$$\delta\left(m_s\ddot{\boldsymbol{x}}_s\cdot\dot{\boldsymbol{x}}_s + \frac{1}{2}C\dot{\boldsymbol{x}}_s\cdot\dot{\boldsymbol{x}}_s + k\boldsymbol{x}_s\cdot\dot{\boldsymbol{x}}_s\right) = \left(m_s\ddot{\boldsymbol{x}}_s + C\dot{\boldsymbol{x}}_s + k\boldsymbol{x}_s\right)\cdot\delta\dot{\boldsymbol{x}}_s \tag{7.69}$$

$$= \left(m_s\ddot{x}_s + C\dot{x}_s + kx_s\right)\delta\dot{x}_s. \tag{7.70}$$

Manipulating the flux of the kinetic energy term using Gauss' theorem, we obtain

$$\begin{aligned}\delta \int_{CV} \nabla \cdot \left[\left(\frac{1}{2}\rho \boldsymbol{u} \cdot \boldsymbol{u} \right) \dot{\boldsymbol{x}}_s \right] dV &= \delta \int_{CS} \left(\frac{1}{2}\rho \boldsymbol{u} \cdot \boldsymbol{u} \right) \left(\dot{\boldsymbol{x}}_s \cdot \boldsymbol{n} \right) dA \\ &= \int_{CS} \left(\frac{1}{2}\rho \boldsymbol{u} \cdot \boldsymbol{u} \right) \left(\delta \dot{\boldsymbol{x}}_s \cdot \boldsymbol{n} \right) dA \\ &= \delta \dot{x}_s \left\{ \int_{CV} \nabla \left(\frac{1}{2}\rho \boldsymbol{u} \cdot \boldsymbol{u} \right) \cdot \mathbf{e}_x dV \right\}, \end{aligned} \tag{7.71}$$

where $\mathbf{e}_x$ is the unit vector in the direction of $\dot{\boldsymbol{x}}_s$. Substituting Eqs. 7.70 and 7.71 into Eq. 7.68, we have

$$-\delta \dot{x}_s \left\{ \int_{CV} \nabla \left(\frac{1}{2}\rho \boldsymbol{u} \cdot \boldsymbol{u} \right) \cdot \mathbf{e}_x dV \right\} + \left(m_s \ddot{x}_s + C \dot{x}_s + k x_s \right) \delta \dot{x}_s = 0. \tag{7.72}$$

Considering that $\delta \dot{x}_s$ is arbitrary, the structural EOM is found to be

$$m_s\, \ddot{x}_s + C\, \dot{x}_s + k\, x_s = \int_{CV} \nabla \left(\frac{1}{2}\rho \boldsymbol{u} \cdot \boldsymbol{u} \right) \cdot \mathbf{e}_x dV. \tag{7.73}$$

Finally, the general coupled equations of motion are obtained from Eqs. 7.67 and 7.73 to be

$$\begin{cases} m_s \ddot{x}_s + C \dot{x}_s + k x_s = \displaystyle\int_{CV} \nabla \left(\frac{1}{2}\rho \boldsymbol{u} \cdot \boldsymbol{u} \right) \cdot \mathbf{e}_x dV, \\ \dfrac{D^C}{Dt} \displaystyle\int_{CV} \frac{1}{2}\rho \boldsymbol{u} \cdot \boldsymbol{u}\, dV + \int_{CV} \nabla \left(\frac{1}{2}\rho \boldsymbol{u} \cdot \boldsymbol{u} \right) \cdot \boldsymbol{u} dV \\ \qquad - \displaystyle\int_{CS_O} \left[-p \boldsymbol{u} \cdot \boldsymbol{n} + \frac{1}{2}\mu \nabla \left(\boldsymbol{u} \cdot \boldsymbol{u} \right) \cdot \boldsymbol{n} \right] dA \\ \qquad + \displaystyle\int_{CS_C} \frac{1}{2}\mu \left[\nabla \left(\boldsymbol{u} \cdot \boldsymbol{u} \right) - 2\, \boldsymbol{u} \times \left(\nabla \times \boldsymbol{u} \right) \right] \cdot \boldsymbol{n}\, dA \\ + \displaystyle\int_{CV} \frac{1}{2}\mu \left(\nabla \times \boldsymbol{u} \right) \cdot \left(\nabla \times \boldsymbol{u} \right) dV + \int_{CV} \nabla \left[\frac{1}{2}\rho \left(\boldsymbol{u} \cdot \boldsymbol{u} \right) \right] \cdot \boldsymbol{u}\, dV \\ \qquad = \displaystyle\int_{CV} \nabla \left(\frac{1}{2}\rho \boldsymbol{u} \cdot \boldsymbol{u} \right) \cdot \dot{\boldsymbol{x}}_s dV. \end{cases} \tag{7.74}$$

Having obtained the coupled equations for the model problem, we next show that a different set of equations can be obtained using a different approach to implementing the boundary conditions.

7.10.2 Reduced-Order Model with Explicit Implementation of the No-Slip Condition

In the previous section, we obtained a reduced-order model by implementing the no-slip condition implicitly, that is, by assuming that the fluid forces at the solid surface have an equal and opposite reaction. Therefore, they do not affect the total energy of a system (based on d'Alembert's principle). Alternatively, in this section, we show that a different approach can be used if we wish to keep the interacting forces at the solid surface. Similarly to the previous section, we assume that the no-slip condition holds. (Note that Dong et al. [5] did not consider any boundary conditions and yet they obtained a control volume where the predictions of their analytical model matched the experimental observation with very good accuracy.) We choose the control volume shown in Fig. 7.8. The open portion of the control volume can contain closed surfaces and it may be selected to have shapes other than the rectangle shown in that figure.

The no-slip condition implies that

$$\boldsymbol{u} - \dot{\boldsymbol{x}}_s = \boldsymbol{0}, \quad \text{or,} \quad \dot{\boldsymbol{x}}_s - \boldsymbol{u} = \boldsymbol{0}, \quad \text{at the solid surface.} \tag{7.75}$$

Therefore, we wish to introduce Eq. 7.75 into Eq. 7.64. Since the virtual velocities must be compatible with the system constraints, and the no-slip condition is simply a nonholonomic constraint, we have

$$\delta\boldsymbol{u} - \delta\dot{\boldsymbol{x}}_s = \boldsymbol{0}, \quad \text{or,} \quad \delta\dot{\boldsymbol{x}}_s - \delta\boldsymbol{u} = \boldsymbol{0}, \quad \text{at the solid surface.} \tag{7.76}$$

From the derivations of Sect. 7.8, and by dimensional considerations, we choose a no-slip condition of the form

$$\delta \int_{CS_C} \left(\frac{1}{2}\rho \boldsymbol{u}\cdot\boldsymbol{u}\right)\left(\dot{\boldsymbol{x}}_s - \boldsymbol{u}\right)\cdot\boldsymbol{n}\,dA = 0. \tag{7.77}$$

Since Eq. 7.77 equals zero for all time, we can add it to Eq. 7.64 to obtain

$$\delta\left\{\int_{CV}\frac{D^C}{Dt}\left(\frac{1}{2}\rho\boldsymbol{u}\cdot\boldsymbol{u}\right)dV + \overbrace{\int_{CS_C}\left(\frac{1}{2}\rho\boldsymbol{u}\cdot\boldsymbol{u}\right)\left(\dot{\boldsymbol{x}}_s-\boldsymbol{u}\right)\cdot\boldsymbol{n}\,dA}^{\text{no-slip condition}}\right.$$
$$\left.\overbrace{-\int_{CS}\left\{-p\boldsymbol{u}\cdot\boldsymbol{n} + \mu\left[\nabla\left(\boldsymbol{u}\cdot\boldsymbol{u}\right) - \boldsymbol{u}\times\left(\nabla\times\boldsymbol{u}\right)\right]\cdot\boldsymbol{n}}^{\text{loading external to the fluid}}\right.$$

$$\overbrace{-\frac{1}{2}\mu\left[\nabla\left(\boldsymbol{u}\cdot\boldsymbol{u}\right)-2\,\boldsymbol{u}\times\left(\nabla\times\boldsymbol{u}\right)\right]\cdot\boldsymbol{n}}^{\text{viscous dissipation}}\Bigg\}dA+\int\limits_{CV}\frac{1}{2}\mu\left(\nabla\times\boldsymbol{u}\right)\cdot\left(\nabla\times\boldsymbol{u}\right)dV$$

$$+\overbrace{\int\limits_{CV}\nabla\cdot\left[\frac{1}{2}\rho\left(\boldsymbol{u}\cdot\boldsymbol{u}\right)\boldsymbol{u}\right]dV}^{\text{non-commuting term}}\Bigg\}$$

$$+\delta\left(m_s\ddot{\boldsymbol{x}}_s\cdot\dot{\boldsymbol{x}}_s+\frac{1}{2}C\dot{\boldsymbol{x}}_s\cdot\dot{\boldsymbol{x}}_s+k\boldsymbol{x}_s\cdot\dot{\boldsymbol{x}}_s\right)=0. \quad (7.78)$$

Summation of the viscous terms and expansion of the second and last integrals of Equation 7.78 yields, for the problem at hand,

$$\delta\Bigg\{\int\limits_{CV}\rho\frac{D^C}{Dt}\left(\frac{1}{2}u^2\right)dV+\int\limits_{CS_C}\rho\left(\frac{1}{2}u^2\right)\left(\dot{\boldsymbol{x}}_s\cdot\boldsymbol{n}\right)dA-\int\limits_{CS_C}\rho\left(\frac{1}{2}u^2\right)\left(\boldsymbol{u}\cdot\boldsymbol{n}\right)dA$$

$$-\int\limits_{CS}\left[-p\boldsymbol{u}\cdot\boldsymbol{n}+\mu\nabla\left(\frac{1}{2}u^2\right)\cdot\boldsymbol{n}\right]dA+\int\limits_{CV}\frac{1}{2}\mu\left(\nabla\times\boldsymbol{u}\right)\cdot\left(\nabla\times\boldsymbol{u}\right)dV$$

$$+\int\limits_{CS_C}\rho\left(\frac{1}{2}u^2\right)\left(\boldsymbol{u}\cdot\boldsymbol{n}\right)\,dA+\int\limits_{CS_O}\rho\left(\frac{1}{2}u^2\right)\left(\boldsymbol{u}\cdot\boldsymbol{n}\right)\,dA\Bigg\}$$

$$+\delta\left(m_s\ddot{\boldsymbol{x}}_s\cdot\dot{\boldsymbol{x}}_s+\frac{1}{2}C\dot{\boldsymbol{x}}_s\cdot\dot{\boldsymbol{x}}_s+k\boldsymbol{x}_s\cdot\dot{\boldsymbol{x}}_s\right)=0. \quad (7.79)$$

Summing terms of the form $\int_{CS_C}\rho\left(\frac{1}{2}u^2\right)\left(\boldsymbol{u}\cdot\boldsymbol{n}\right)dA$ and applying Gauss' theorem to the viscous terms in the integrand of the fourth integral,

$$\int\limits_{CS}\frac{1}{2}\mu\nabla\left(u^2\right)\cdot\boldsymbol{n}dA=\int\limits_{CV}\mu\nabla^2\left(\frac{1}{2}u^2\right)dV, \quad (7.80)$$

we obtain,

$$\delta\Bigg\{\int\limits_{CV}\rho\frac{D^C}{Dt}\left(\frac{1}{2}u^2\right)dV+\int\limits_{CS_C}\rho\left(\frac{1}{2}u^2\right)\left(\dot{\boldsymbol{x}}_s\cdot\boldsymbol{n}\right)dA+\int\limits_{CS_O}\rho\left(\frac{1}{2}u^2\right)\left(\boldsymbol{u}\cdot\boldsymbol{n}\right)\,dA$$

$$+\int\limits_{CV}\left[\nabla p\cdot\boldsymbol{u}-\mu\nabla^2\left(\frac{1}{2}u^2\right)\cdot\boldsymbol{n}+\frac{1}{2}\mu\left(\nabla\times\boldsymbol{u}\right)\cdot\left(\nabla\times\boldsymbol{u}\right)\right]dV$$

$$+m_s\ddot{\boldsymbol{x}}_s\cdot\dot{\boldsymbol{x}}_s+\frac{1}{2}C\dot{\boldsymbol{x}}_s\cdot\dot{\boldsymbol{x}}_s+k\boldsymbol{x}_s\cdot\dot{\boldsymbol{x}}_s\Bigg\}=0. \quad (7.81)$$

Applying Eqs. 7.62–7.81 results in

$$\begin{cases} m_s\ddot{x}_s + C\dot{x}_s + kx_s = -\int\limits_{CS_C} \rho\left(\frac{1}{2}u^2\right)(\mathbf{e}_x \cdot \boldsymbol{n})\, dA \\ \int\limits_{CV} \rho\frac{D^C}{Dt}\left(\frac{1}{2}u^2\right) dV + \int\limits_{CS_O} \rho\left(\frac{1}{2}u^2\right)(\boldsymbol{u}\cdot\boldsymbol{n})\ dA \\ +\int\limits_{CV}\left[\nabla p\cdot\boldsymbol{u} - \mu\nabla^2\left(\frac{1}{2}u^2\right) + \frac{1}{2}\mu\,(\nabla\times\boldsymbol{u})\cdot(\nabla\times\boldsymbol{u})\right] dV \\ \qquad\qquad = -\dot{x}_s\int\limits_{CS_C}\rho\left(\frac{1}{2}u^2\right)(\mathbf{e}_x\cdot\boldsymbol{n})\, dA, \end{cases} \tag{7.82}$$

where $\boldsymbol{u}^2 = \boldsymbol{u}\cdot\boldsymbol{u}$, and the required steps are similar to those of Sect. 7.10.1.

Thus far, we have obtained two possible reduced-order governing equations of the model problem in the form of a translating cylinder. Similar reduced-order models for the inverted pendulum problem can be obtained [19].

As evident from our derivations thus far, depending on our interpretation of the boundary conditions, and on how we choose to implement it, the resulting reduced-order model would differ to some extent. Both Eqs. 7.74 and 7.82, or any other models obtained by implementing the boundary conditions differently than those shown, can be simplified further by dimensional analysis, similarity methods or perturbation techniques. However, experimental data and observations are required for further simplifications.

In order to show the steps required, as an example, we consider the experimental observations of Benaroya and Wei [3] and Dong et al. [5] to obtain a model similar to the wake oscillator proposed by Hartlen and Currie. To accomplish this, we will not use similarity methods in a traditional way. However, we will make a few assumptions based on experimental observations.

It is emphasized that the next section is an example where we specialize the above equations only to demonstrate that the above-derived equations embody the flow-oscillators of the literature. The example does not limit the applicability of those equations.

7.11 Modeling VIV: A *Lift-Oscillator* Model

Our main goal in this chapter has been to obtain first-principle-based equations governing vortex-induced structural oscillations, which we accomplished in the previous sections with Eqs. 7.74 and 7.82. These results are two coupled governing equations, one a differential equation representing the structure and the other an integral equation representing the fluid dynamics.

However, wake-oscillator models in the literature are generally two coupled differential equations, one linear and one nonlinear. In order to show that such equations can be obtained from, for example, Eq. 7.82, we seek a reduced-order model similar to the *lift-oscillator* model of Hartlen and Currie [11]. Their model has been chosen since it is one of the earliest and, perhaps, the most noteworthy of the wake-oscillator models.

We start our manipulations with some general assumptions that can be made for many VIV problems and apply these to the reduced-order model Eq. 7.82.

For fluids with very low viscosity, the *boundary layer approximation method,* proposed by Prandtl, assumes that viscosity only exists in the vicinity of the solid structure, and is neglected elsewhere. In Eq. 7.82 the term $\mu\nabla^2\left(\frac{1}{2}u^2\right)$ represents the sum of the viscous forces acting as external loads, and those dissipating energy on the surface of the structure and on the open control surfaces. Therefore, following Prandtl's hypothesis, we neglect the viscous dissipation inside the control volume, (see Eq. 7.48),

$$\int_{CV} \frac{1}{2}\mu\left(\nabla\times\boldsymbol{u}\right)\cdot\left(\nabla\times\boldsymbol{u}\right)dV \approx 0. \tag{7.83}$$

Applying Eq. 7.83 to Eq. 7.82 results in

$$\begin{cases} m_s\ddot{x}_s + C\dot{x}_s + kx_s = -\displaystyle\int_{CS_C}\rho\hat{T}\left(\mathbf{e}_x\cdot\boldsymbol{n}\right)dA \\ \displaystyle\int_{CV}\rho\frac{D^C\hat{T}}{Dt}dV + \int_{CS_O}\rho\hat{T}\left(\boldsymbol{u}\cdot\boldsymbol{n}\right)\,dA + \int_{CV}\left(\nabla p\cdot\boldsymbol{u} - \mu\nabla^2\hat{T}\right)dV \\ \qquad\qquad = -\dot{x}_s\displaystyle\int_{CS_C}\rho\hat{T}\left(\mathbf{e}_x\cdot\boldsymbol{n}\right)dA, \end{cases} \tag{7.84}$$

where the kinetic energy density function is $\hat{T} = u^2/2$. In order to simplify Eq. 7.84 further, we consider some experimental observations of Dong et al. [5].

Dong et al. performed a series of experiments on the VIV model problem in the form of an inverted pendulum. They found an optimum control volume for which the analytical model proposed by Benaroya and Wei [3] predicted the structural response with excellent accuracy. The phase-averaged terms of Benaroya and Wei's energy rate equation obtained by their experiments are shown in Fig. 7.11, where the figure depicts the results for the optimum control volume. The corresponding spectra of the fluid energy transport terms (of Fig. 7.11) are shown in Fig. 7.12.

Considering Fig. 7.12, Dong et al. reported that their careful examination indicates that the flux of the fluid kinetic energy across the open control surface and the work done by the pressure were correlated with the vortex shedding while the flux of the kinetic energy around the cylinder was correlated with the cylinder oscillation. We expect that the last statement is a result of the no-slip condition.

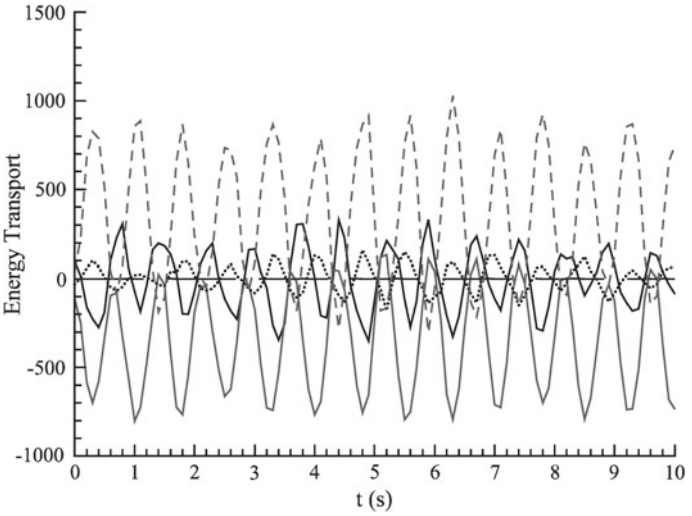

Fig. 7.11 Phase-averaged terms of Eq. 7.124 for the inverted pendulum model where the dark solid line denotes the time rate of change of the fluid kinetic energy in CV, the light solid line is the flux of kinetic energy, the dashed lined is the rate of work done on the cylinder by pressure forces, and the dotted line is the time rate of change of mechanical energy of the cylinder. The work done by the viscous forces are included in the figure, however, they are too small to be visible ([5], reprinted with permission)

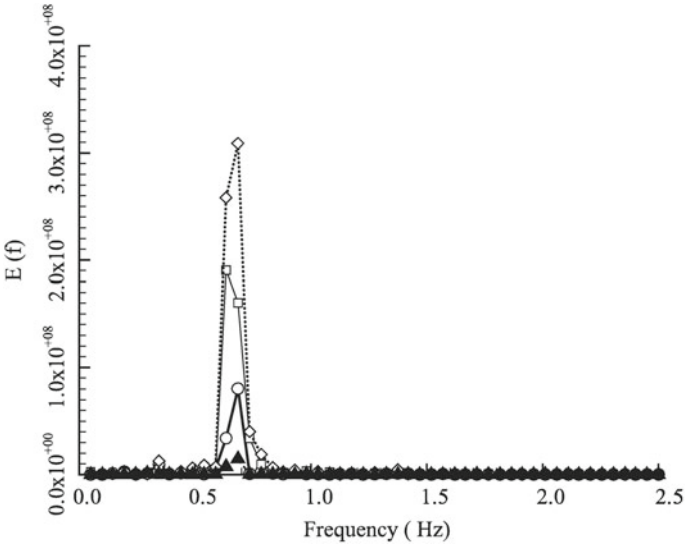

Fig. 7.12 Spectra of the energy terms shown in Fig. 7.11, where —◯— corresponds to the time rate of change of the fluid kinetic energy inside the CV, · · · ◇ · · · is for the flux of kinetic energy, —□— is for the rate of work done by pressure on the structure, - -▲- - represents the rate of mechanical energy of the cylinder ([5], reprinted with permission)

These experiments were conducted on an inverted pendulum, while we have considered the model problem in the form of a translating cylinder. However, due to similarities between the two problems, we assume similar results would be found for the problem at hand. Moreover, the control volume of their experiments was selected such that the downstream control surface views the structured vortices, that is, it was close enough to the structure so that the shed vortices had not yet broken down into smaller eddies.

Since Dong et al. considered the rate of kinetic energy to be $\int_{CV} \frac{\partial T}{\partial t} dV$, we extract the same integral from the first integral in the second equation of Eq. 7.84 and obtain

$$\begin{cases} m_s \ddot{x}_s + C\dot{x}_s + kx_s = -\int\limits_{CS_C} \rho \hat{T} \left(\mathbf{e}_x \cdot \boldsymbol{n}\right) dA \\ \int\limits_{CV} \rho \dfrac{\partial \hat{T}}{\partial t} dV + \int\limits_{CS_C} \rho \hat{T} \left(\boldsymbol{u} \cdot \boldsymbol{n}\right) dA + 2 \int\limits_{CS_O} \rho \hat{T} \left(\boldsymbol{u} \cdot \boldsymbol{n}\right) dA \\ + \int\limits_{CV} \left(\nabla p \cdot \boldsymbol{u} - \mu \nabla^2 \hat{T}\right) dV = -\dot{x}_s \int\limits_{CS_C} \rho \hat{T} \left(\mathbf{e}_x \cdot \boldsymbol{n}\right) dA. \end{cases} \tag{7.85}$$

Next we interpret the experimental observations of Dong et al. so that they become applicable to Eq. 7.85. Based on their observation that the flux term at the closed surface corresponds to the structural vibration, we assume the relation

$$\int\limits_{CS_C} \rho \hat{T} \left(\boldsymbol{x}, t\right) \left[\boldsymbol{u} \left(\boldsymbol{x}, t\right) \cdot \boldsymbol{n}\right] \, dA = \int\limits_{CS_C} \rho \hat{T} \left(\boldsymbol{x}, t + \frac{1}{f_s}\right) \left[\boldsymbol{u} \left(\boldsymbol{x}, t + \frac{1}{f_s}\right) \cdot \boldsymbol{n}\right] \, dA, \tag{7.86}$$

where f_s (Hz) is the vibration frequency. Equation 7.86 represents a boundary condition, and since we have two coupled equations it must only be applied to one of them. Therefore, the similar term in the other equation becomes relaxed from this boundary condition. Since the no-slip condition is a boundary condition for the fluid and not the structure, we make the substitution in the governing equation of the fluid (second equation) in Eq. 7.85. Moreover, the terms $\int_{CS_C} \rho \hat{T} \left(\boldsymbol{u} \cdot \boldsymbol{n}\right) dA$ and $\dot{x}_s \int_{CS_C} \rho \hat{T} \left(\mathbf{e}_x \cdot \boldsymbol{n}\right) dA$ vary with the same frequency, thus we assume that their superposition also varies with the same frequency. Therefore,

$$\alpha \dot{x}_s \cong \dot{x}_s \int\limits_{CS_C} \rho \hat{T} \left(\mathbf{e}_x \cdot \boldsymbol{n}\right) dA + \int\limits_{CS_C} \rho \hat{T} \left(\boldsymbol{u} \cdot \boldsymbol{n}\right) dA, \tag{7.87}$$

where α is a constant with dimensions of force and the integrals are evaluated from the experimental measurements in the vicinity of the structure. This relaxes the condition on the corresponding term in the structural differential equation. In the last equation,

$$\int_{CS_C} \rho \hat{T}\left(\boldsymbol{x}, t\right)\left(\mathbf{e}_x \cdot \boldsymbol{n}\right) dA \equiv \int_{CS_C} \rho \hat{T}\left(\boldsymbol{x}, t+\frac{1}{f_v}\right)\left(\mathbf{e}_x \cdot \boldsymbol{n}\right) dA, \tag{7.88}$$

where f_v (Hz) is the frequency of vortex shedding.

Considering the second equation in Eq. 7.85, and introducing Eq. 7.87, we have

$$\int_{CV} \rho \frac{\partial \hat{T}}{\partial t} dV + 2 \int_{CS_O} \rho \hat{T}\left(\boldsymbol{u} \cdot \boldsymbol{n}\right)\, dA + \int_{CV} \left(\nabla p \cdot \boldsymbol{u} - \mu \nabla^2 \hat{T}\right) dV = -\alpha \dot{x}_s. \tag{7.89}$$

Applying Gauss' divergence theorem to the pressure and viscous terms, we have

$$\int_{CV} \rho \frac{\partial \hat{T}}{\partial t} dV + 2 \int_{CS_O} \rho \hat{T}\left(\boldsymbol{u} \cdot \boldsymbol{n}\right)\, dA + \int_{CS} \left(p\boldsymbol{u} - \mu \nabla \hat{T}\right) \cdot \boldsymbol{n} dA = -\alpha \dot{x}_s, \tag{7.90}$$

so that no pressure or viscous terms are present inside the control volume. Note that the viscous terms were neglected by the hypothesis of Eq. 7.83. Dong et al. found that the rate of work done by the viscous forces to be so small that its corresponding trace is not visible in Fig. 7.11. They also found that the time rate of change of the kinetic energy of the system was correlated with the vortex shedding frequency. Therefore,

$$\int_{CV} \rho \frac{\partial}{\partial t} \hat{T}\left(\boldsymbol{x}, t\right) dV = \int_{CV} \rho \frac{\partial}{\partial t} \hat{T}\left(\boldsymbol{x}, t+\frac{1}{f_v}\right) dV, \tag{7.91}$$

or,

$$\frac{\partial}{\partial t} \int_{CV} \rho \hat{T}\left(\boldsymbol{x}, t\right) dV = \frac{\partial}{\partial t} \int_{CV} \rho \hat{T}\left(\boldsymbol{x}, t+\frac{1}{f_v}\right) dV. \tag{7.92}$$

At this point, we choose the direction of free-stream flow to be the z axis of the Cartesian coordinate system defined in Fig. 7.13. Therefore, $\hat{T}\left(\boldsymbol{x}, t\right) = \hat{T}\left(x, z, t\right)$.

Since no external or dissipative forces are present inside the control volume in Eq. 7.90, a shed vortex must repeat its pattern periodically as it travels in the direction of the free-stream flow. Therefore, we have

$$\hat{T}\left(x, z, t\right) = \hat{T}\left(x, z - c_v t, t\right), \tag{7.93}$$

where c_v is the velocity of shed vortices.

Considering Eqs. 7.92 and 7.93 together with Fig. 7.11, $\hat{T}\left(\boldsymbol{x}, t\right)$ has the characteristics of a propagating wave with velocity c_v and frequency f_v. Therefore, from the wave equation, we have

$$\frac{\partial^2 \hat{T}\left(\boldsymbol{x}, t\right)}{\partial t^2} \equiv c_v^2 \nabla^2 \hat{T}\left(\boldsymbol{x}, t\right), \tag{7.94}$$

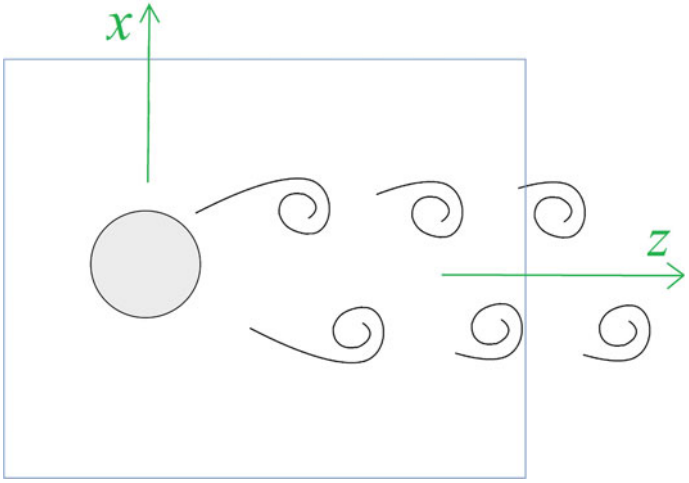

Fig. 7.13 A schematic diagram of the experiments of Dong et al. where the shedded vortices are $P + S$-type vortices. For the classification of vortices refer to [7]

or

$$\nabla^2 \hat{T}(\boldsymbol{x}, t) = \frac{1}{c_v^2} \frac{\partial^2 \hat{T}(\boldsymbol{x}, t)}{\partial t^2}. \tag{7.95}$$

Introducing Eq. 7.95 into Eq. 7.89, yields

$$\int_{CV} \rho \frac{\partial \hat{T}}{\partial t} dV + 2 \int_{CS_O} \rho \hat{T} (\boldsymbol{u} \cdot \boldsymbol{n}) \, dA + \int_{CV} \nabla p \cdot \boldsymbol{u} dV - \int_{CV} \frac{\mu}{c_v^2} \frac{\partial^2 \hat{T}(\boldsymbol{x}, t)}{\partial t^2} dV = -\alpha \dot{x}_s. \tag{7.96}$$

Based on the experiments of Dong et al., the flux of the kinetic energy across the open control volume was found to vary with the frequency of the vortex shedding, that is,

$$\int_{CS_O} \rho \hat{T}(\boldsymbol{x}, t) [\boldsymbol{u}(\boldsymbol{x}, t) \cdot \boldsymbol{n}] \, dA = \int_{CS_O} \rho \hat{T} \left(\boldsymbol{x}, t + \frac{1}{f_v} \right) \left[\boldsymbol{u} \left(\boldsymbol{x}, t + \frac{1}{f_v} \right) \cdot \boldsymbol{n} \right] dA. \tag{7.97}$$

However, the kinetic energy inside the control volume must also vary with the same frequency when Eq. 7.92 is considered. Moreover, the flux of the kinetic energy adds and subtracts energy from the system very similarly to a spring. Since, $\hat{T}(\boldsymbol{x}, t)$, $\boldsymbol{u}(\boldsymbol{x}, t)$ and $\hat{T}(\boldsymbol{x}, t) \boldsymbol{u}(\boldsymbol{x}, t)$ have the same frequency, and since the solution of the

velocity field inside the control volume is a function of the boundary conditions, we can write

$$\int_{CS_O} \rho\hat{T}\left(\boldsymbol{x},t\right)\left[\boldsymbol{u}\left(\boldsymbol{x},t\right)\cdot\boldsymbol{n}\right]\,dA \underset{\sim}{\propto} -\int_{CV} \rho f_v \hat{T}\left(\boldsymbol{x},t\right)dV, \tag{7.98}$$

where $\underset{\sim}{\propto}$ means they are approximately proportional and the negative sign is introduced to show that the right-hand side is positive when the left-hand side is negative. Assuming proportionality, we can write

$$\int_{CS_O} \rho\hat{T}\left(\boldsymbol{x},t\right)\left[\boldsymbol{u}\left(\boldsymbol{x},t\right)\cdot\boldsymbol{n}\right]\,dA = -\int_{CV} \beta\rho f_v \hat{T}\left(\boldsymbol{x},t\right)dV, \tag{7.99}$$

where β is a constant to be determined. Substituting Eq. 7.99 into Eq. 7.96, we obtain

$$-\frac{\mu}{c_v^2}\int_{CV}\frac{\partial^2\hat{T}\left(\boldsymbol{x},t\right)}{\partial t^2}dV + \int_{CV}\rho\frac{\partial\hat{T}}{\partial t}dV - \int_{CV} 2\beta f_v\rho\hat{T}dV + \int_{CV}\nabla p\cdot\boldsymbol{u}dV = -\alpha\dot{x}_s. \tag{7.100}$$

From Gauss' divergence theorem, we expect that the term $\int_{CS_C}\rho\hat{T}\left(\mathbf{e}_x\cdot\boldsymbol{n}\right)dA$ in Eq. 7.85 can be related in the following way,

$$\int_{CS_C}\rho\hat{T}\left(\mathbf{e}_x\cdot\boldsymbol{n}\right)dA \underset{\sim}{\propto} \int_{CV}\nabla\left(\rho\hat{T}\right)\cdot\mathbf{e}_x dV, \tag{7.101}$$

and, since $\hat{T}\left(\boldsymbol{x},t\right)$ has the characteristics of a propagating wave

$$\frac{\partial\hat{T}\left(\boldsymbol{x},t\right)}{\partial t} \equiv -c_v\nabla\hat{T}\left(\boldsymbol{x},t\right). \tag{7.102}$$

Equation 7.101 becomes

$$\int_{CS_C}\rho\hat{T}\left(\mathbf{e}_x\cdot\boldsymbol{n}\right)dA \underset{\sim}{\propto} -\int_{CV}\frac{1}{c_v}\rho\frac{\partial\hat{T}\left(\boldsymbol{x},t\right)}{\partial t}dV. \tag{7.103}$$

Therefore, we assume proportionality and obtain

$$\int_{CS_C}\rho\hat{T}\left(\mathbf{e}_x\cdot\boldsymbol{n}\right)dA = -\int_{CV}\gamma\frac{1}{c_v}\rho\frac{\partial\hat{T}\left(\boldsymbol{x},t\right)}{\partial t}dV, \tag{7.104}$$

where γ is a constant to be determined. It is important to note that in Eqs. 7.99 and 7.104, constants β and γ can more generally be replaced with functions of f_v and

f_v/c_v, respectively, if the vortices are not structured in a velocity range of interest. However, the vortices were fairly structured at the examined flow velocity [3, 5].

Substituting Eqs. 7.100 and 7.104 into Eq. 7.85 yields

$$\begin{cases} m_s\ddot{x}_s + C\dot{x}_s + kx_s = \int\limits_{CV} \gamma \dfrac{1}{c_v}\rho \dfrac{\partial \hat{T}\left(\boldsymbol{x},t\right)}{\partial t} dV \\ -\dfrac{\mu}{c_v^2}\int\limits_{CV} \dfrac{\partial^2 \hat{T}\left(\boldsymbol{x},t\right)}{\partial t^2} dV + \int\limits_{CV} \rho \dfrac{\partial \hat{T}}{\partial t} dV - \int\limits_{CV} 2\beta f_v \rho \hat{T} dV + \int\limits_{CV} \nabla p \cdot \boldsymbol{u} dV = -\alpha \dot{x}_s. \end{cases} \tag{7.105}$$

Thus far, we have not considered the pressure terms, since they are perhaps the most complex and challenging terms. The pressure is the thermodynamic pressure, generally assumed to be independent of velocity in the derivation of the constitutive relation for Newtonian incompressible fluids. Yet, its distribution is often found to be a function of velocity. For example, for problems with steady low speed flow, the pressure distribution is found via Bernoulli's equation to be

$$p + \frac{1}{2}\rho u^2 = p_\infty + \frac{1}{2}\rho u_\infty^2, \tag{7.106}$$

which leads to defining a nondimensional excess pressure, called the *pressure coefficient* C_p,

$$C_p \equiv \frac{p - p_\infty}{\frac{1}{2}\rho u_\infty^2}, \tag{7.107}$$

where p_∞ and u_∞ are the pressure and velocity at infinity.

While the pressure coefficient was originally defined for steady flow, it has been used extensively in similarity analyses of complicated nonlinear problems. For example, it is used to relate the local pressure at a point, $p\left(\boldsymbol{x}\right)$, to other parameters of the nondimensional Navier–Stokes equations via the relation

$$\frac{p\left(\boldsymbol{x}\right) - p_\infty}{\frac{1}{2}\rho u_\infty^2} = f\left(\text{Fr}, \text{Re}; \frac{\boldsymbol{x}}{l}\right), \tag{7.108}$$

where Fr denotes the Froude number, Re is the Reynolds number, l is a length scale, and $f\left(\ \right)$ is a function [13].

As evident from Eq. 7.105, pressure is an external load to the control volume. Also, since we are seeking a reduced-order model that can be coupled with the experiments, a set of experimental velocities is already the result of the pressure field. In Chap. 6, we argued that the classical energy equation is the zeroth-order approximation to a complete energy accounting. Moreover, when deriving our variational energy equation we assumed that the pressure remains constant with respect to first-order velocities, and there seems no reason why we cannot assume it to vary with first-order velocities. Given the difficulties faced in acquiring

experimental data, we are encouraged to consider an approximation of pressure at least up to first order. However, the zeroth-order terms can be neglected since their effects must be observable from the measured velocities.

The experiments of Dong et al. found that the work done by the pressure was correlated with the rate of kinetic energy, that is,

$$p\left(\boldsymbol{x},t\right)=p\left(\boldsymbol{x},t+\frac{1}{f_v}\right). \tag{7.109}$$

Based on Eq. 7.107, we expect a relation between pressure and kinetic energy of the form

$$p\left(\boldsymbol{x},t\right)=f\left[\rho\hat{T}\left(\boldsymbol{x},t\right)\right], \tag{7.110}$$

where f is a function to be determined. Furthermore, since $\hat{T}\left(\boldsymbol{x},t\right)$ behaves similarly to a wave, that is,

$$\begin{aligned} p\left(\boldsymbol{x},t\right)&=f\left[\rho\hat{T}\left(\boldsymbol{x},t\right)\right]\\ &=f\left[\rho\hat{T}\left(\boldsymbol{x},t+\frac{1}{f_v}\right)\right]\\ &=f\left[\rho\hat{T}\left(\boldsymbol{x}-c_vt,t\right)\right], \end{aligned} \tag{7.111}$$

p itself must be in the form of a wave. Therefore,

$$\frac{\partial p\left(\boldsymbol{x},t\right)}{\partial t}\equiv-c_v\nabla p\left(\boldsymbol{x},t\right). \tag{7.112}$$

Consequently, we can say that $\nabla p\left(\boldsymbol{x},t\right)$ must be a function of $\frac{\partial}{\partial t}\hat{T}\left(\boldsymbol{x},t\right)$, that is,

$$\nabla p\left(\boldsymbol{x},t\right)=-\frac{1}{c_v}\boldsymbol{f}\left[\frac{\partial}{\partial t}\hat{T}\left(\boldsymbol{x},t\right)\right], \tag{7.113}$$

where $\boldsymbol{f}$ is a vector-valued function to be determined. Substituting Eq. 7.113 into Eq. 7.105, we obtain

$$\begin{cases} m_s\ddot{x}_s+C\dot{x}_s+kx_s=\dfrac{\gamma}{c_v}\displaystyle\int_{CV}\rho\frac{\partial\hat{T}\left(\boldsymbol{x},t\right)}{\partial t}dV\\ \dfrac{\mu}{c_v^2}\displaystyle\int_{CV}\frac{\partial^2\hat{T}\left(\boldsymbol{x},t\right)}{\partial t^2}dV-\int_{CV}\rho\frac{\partial\hat{T}}{\partial t}dV+\int_{CV}\frac{1}{c_v}\boldsymbol{f}\left[\frac{\partial\hat{T}\left(\boldsymbol{x},t\right)}{\partial t}\right]\cdot\boldsymbol{u}dV\\ \qquad\qquad+\displaystyle\int_{CV}2\beta f_v\rho\hat{T}dV=\alpha\dot{x}_s. \end{cases} \tag{7.114}$$

Defining an instantaneous kinetic energy function for the control volume of an incompressible fluid by

$$T(t) = \int_{CV} \rho \hat{T} dV, \tag{7.115}$$

and introducing it into Eq. 7.114, we obtain

$$\begin{cases} m_s \ddot{x}_s + C\dot{x}_s + kx_s = \dfrac{\gamma}{c_v}\dot{T} \\ \dfrac{\mu}{\rho c_v^2}\ddot{T} - \dot{T} + f\left(\dot{T}\right) + 2\beta f_v T = \alpha \dot{x}_s, \end{cases} \tag{7.116}$$

where α, β, and γ are defined by Eqs. 7.87, 7.99 and 7.104, respectively; $f\left(\dot{T}\right)$ is a function with an order higher than one with respect to $\dot{T}$, and an appropriate form of $f\left(\dot{T}\right)$ must be selected based on experimental considerations. Since the sign of $f\left(\dot{T}\right)$ must be positive, Eq. 7.116 is a van der Pol-type oscillator.

For comparison with Hartlen and Currie, we may assume that $f\left(\dot{T}\right)$ is the first-order term of the Taylor series of a sine function. We select

$$f\left(\dot{T}\right) = \frac{\eta}{\rho f_v c_v^4}\dot{T}^3, \tag{7.117}$$

where the negative sign is eliminated since $f\left(\dot{T}\right)$ must be a positive-valued function, and η is a constant found experimentally. Based on this choice, the reduced-order model becomes

$$\begin{cases} m_s \ddot{x}_s + C\dot{x}_s + kx_s = \dfrac{\gamma}{c_v}\dot{T} \\ \dfrac{\mu}{\rho c_v^2}\ddot{T} - \dot{T} + \dfrac{\eta}{\rho f_v c_v^4}\dot{T}^3 + 2\beta f_v T = \alpha \dot{x}_s. \end{cases} \tag{7.118}$$

It is worth noting that one may choose to keep the zeroth-order term of the $f\left(\dot{T}\right)$ due to experimental considerations. This will introduce another constant that must be evaluated together with η from curve fitting to particular experimental measurements.

Thus far, we have obtained reduced-order models in the form of single governing EOM and two coupled EOM. Next, a comparison is made between our derived equations and some of the existing models in the literature.

7.12 Comparison with Some Existing Models

7.12.1 Comparison with McIver's Extension of Hamilton's Principle

McIver's extended Hamilton's principle for systems involving fluid–structure interaction [17], specifically systems where the fluid is internal to the structure. In this section, we compare our derivations to those of McIver, even though we recognize the significant differences in our two physical systems.

The first difference is due to McIver's assumption that the only virtual work applied to a control volume is due to the surface traction over the control surfaces [17, p. 251]. Therefore, McIver started his derivations by assuming that there is no dissipation of energy due to viscosity. If we had made the same assumption, the terms marked *viscous dissipation* would not be present in Eq. 7.23.

In his paper, McIver also presented his energy rate equation in the absence of any interacting system as [17, Eq. 23]

$$\frac{d}{dt}\left(T+\Pi\right)_{CV} = \iint\limits_{CV_O}\left[\boldsymbol{u}\cdot\bar{\boldsymbol{\sigma}} + \rho\left(\frac{1}{2}u^2+e\right)\left(\boldsymbol{v}_{CV}-\boldsymbol{u}\right)\right]\cdot\boldsymbol{n}dA, \tag{7.119}$$

where e denotes the density of the potential Π, and we have changed McIver's notations to match ours to avoid confusion. Neglecting the potential energy terms (as we did) and substituting the terms T and $\bar{\boldsymbol{\sigma}}$, Eq. 7.119 becomes

$$\frac{d}{dt}\int\limits_{CV}\frac{1}{2}\rho u^2 dV = \int\limits_{CS}\left\{\boldsymbol{u}\cdot\left[-p\bar{\boldsymbol{I}}+\mu\left(\nabla\boldsymbol{u}+\nabla^T\boldsymbol{u}\right)\right]+\left(\frac{1}{2}\rho u^2\right)\left(\boldsymbol{v}_{CS}-\boldsymbol{u}\right)\right\}\cdot\boldsymbol{n}dA. \tag{7.120}$$

For comparison, if we neglect the terms corresponding to viscous dissipation in Eq. 7.24 and manipulate the other terms to match those of McIver's equation, the energy rate equation becomes

$$\begin{aligned}&\frac{D^C}{Dt}\int\limits_{CV}\frac{1}{2}\rho u^2 dV\\ &=\int\limits_{CS}\left\{\boldsymbol{u}\cdot\left[-p\bar{\boldsymbol{I}}+\mu\left(\nabla\boldsymbol{u}+\nabla^T\boldsymbol{u}\right)\right]+\left(\frac{1}{2}\rho u^2\right)\left(\boldsymbol{v}_{CS}-\boldsymbol{u}\right)+\left(\frac{1}{2}\rho u^2\right)\boldsymbol{u}\right\}\cdot\boldsymbol{n}dA.\end{aligned} \tag{7.121}$$

Comparing Eq. 7.121 with Eq. 7.120, another important difference becomes clear, that is, there is the additional term of power due to the non-commuting part of the rate of kinetic energy, $\left(\frac{1}{2}\rho u^2\right)\boldsymbol{u}$. As mentioned earlier, this term was obtained after examining the commutation rule in the Eulerian reference frame in Chap. 6. However,

McIver assumed the commutation rule holds. Moreover, he did not consider the relations between the Lagrangian and the Eulerian reference frames.

For an incompressible fluid, the thermodynamic pressure can be considered to be a conservative force. McIver considered the energy equation for a control volume of fluid particles in the absence of a solid system to be Eq. 7.119, and he discussed that the energy of the control volume would be conserved if the control volume is selected such that the terms on the right-hand side of Eq. 7.119 disappear for all time. For this, the control surface must satisfy the relation

$$\boldsymbol{v}_{CS} \cdot \boldsymbol{n} = -\frac{\boldsymbol{u} \cdot \bar{\boldsymbol{\sigma}} \cdot \boldsymbol{n}}{\rho\left(\frac{1}{2}u^2 + e\right)} + \boldsymbol{u} \cdot \boldsymbol{n}. \tag{7.122}$$

For FSI and VIV, the selection of a control volume such that it satisfies this relation is very challenging. It might be easily recognizable for systems where an approximately laminar flow is internal to the structure, but it is ambiguous otherwise. Thus, it is very challenging to compare McIver's method with ours any further since McIver's appropriate control volume cannot be distinguished without knowing the velocity field of the flow.

Another interesting extension of Hamilton's principle was by Benaroya and Wei [3], which is considered in the following section.

7.12.2 Comparison with Benaroya and Wei's Extension of Hamilton's Principle

In the previous section, we discussed that the applicability of McIver's approach is greatly limited by the constraint it imposes on selecting the appropriate control volume. Having considered McIver's method, Benaroya and Wei ([3], and Chap. 4) took on a more challenging task to extend Hamilton's principle for VIV problems where the flow is external to the structure. In this chapter, we used their methodology in obtaining the single governing EOM for the model problem. Thus, a short summary of their work suffices.

Benaroya and Wei discussed in detail that in the absence of known particle trajectories for the fluid flow, stationarity cannot be ensured. Thus, setting $\delta \boldsymbol{r} = \boldsymbol{u} dt$ would lead to the conservation of energy equation. Based on their experimental measurements, they neglected the viscous dissipation of energy inside the control volume and obtained the energy equation for the translating cylinder problem (Fig. 7.1a) to be,

$$\begin{aligned} &\dot{\boldsymbol{x}}_s \left(m_s \ddot{\boldsymbol{x}}_s + k\boldsymbol{x}_s\right) + \left(m_{fluid} u\dot{u}\right)_{CV} \\ &= \int_{CS} \frac{1}{2}\rho u^2 \left(\boldsymbol{u}_r \cdot \boldsymbol{n}\right) dA + \int_{CS_O} (-p\boldsymbol{n} + \boldsymbol{\tau}) \cdot \boldsymbol{u}\, dA + \int_{CS_C} (-p\boldsymbol{n} + \boldsymbol{\tau}) \cdot \boldsymbol{u}\, dA, \end{aligned} \tag{7.123}$$

and for the inverted pendulum problem, they derived the governing EOM

$$\dot{\theta}\left[I_0\,\ddot{\theta}+k_T\theta\;-(m_s g-B)\,\frac{L}{2}\sin\theta\;\right]+\left(m_{fluid}u\dot{u}\right)_{CV}$$
$$=\int_{CS}\frac{1}{2}\rho u^2\,(\boldsymbol{u}_r\cdot\boldsymbol{n})\,dA+\int_{CS_O}(-p\boldsymbol{n}+\boldsymbol{\tau})\cdot\boldsymbol{u}\,dA+\int_{CS_C}(-p\boldsymbol{n}+\boldsymbol{\tau})\cdot\boldsymbol{u}\,dA, \tag{7.124}$$

where they have ignored the structural damping.

Comparing Benaroya and Wei's results (Eqs. 7.123 and 7.124) to Eqs. 7.49 and 7.50, we notice that the sign of the flux of kinetic energy in our equation is different than theirs. The reason is that Benaroya and Wei used the RTT to relate the integration over the control system to that over the control volume while we used the RTT twice when deriving our energy equation in Chap. 6; once for the same purpose and once to relate the change of control volume to itself.

Moreover, Benaroya and Wei consider the pressure and shear forces at the closed surface which we neglect by considering them to be action and reaction forces that do not appear in the energy equation. Regarding these terms, their equation also differs from that obtained by McIver.

Additionally, we notice similar differences to those observed in Sect. 7.12.1, that is, the dissipation terms and the non-commuting term of the rate of kinetic energy are not present in their formulation.

Next, we compare our lift-oscillator model with the one proposed by Hartlen and Currie.

7.12.3 *Comparison with Hartlen and Currie's Lift-Oscillator Model*

The *lift-oscillator* model proposed by Hartlen and Currie was not derived from a first-principles approach. In Sect. 7.11, our aim was to obtain a model similar to their lift-oscillator model since it is one of the most popular empirical models. Comparison of our result, Eq. 7.118, to Hartlen and Currie's model expressed by Eq. 7.5 reveals a few differences that are worth noting, as follows.

The first difference is that the constants of Hartlen and Currie's model (α, β, and γ) are meant to be used to fit the EOM to a particular dataset. These constants do not correspond to any dynamical parameter of the fluid flow, and therefore, cannot provide any physical insights. Contrary to their model, the constants α, β, γ and η of the model developed here are obtained from specific assumptions made regarding fluid dynamic behavior.

As mentioned earlier, only two of the unknown fluid parameters of Hartlen and Currie's model must be selected in order to obtain the best fit to an experimental

data set [5]. However, in our model, only the constant η is obtained by curve fitting, where its physical meaning is well understood from Eq. 7.117.

Another difference observed between the two models is how the two EOMs are coupled. To clarify this statement, let us assume that the nonlinear EOM representing the fluid flow is a second oscillator coupled with the structure. In Hartlen and Currie's model, the structural EOM observes the forcing function due to c_L, that is, the displacement of the oscillator. However, in our model the structural EOM is coupled to the second oscillator via the velocity, $\dot{T}$, i.e., the rate of kinetic energy. As has been discussed, Hartlen and Currie's model cannot represent beating behavior [5]. The beating behavior can be envisioned to be a result of the superposition of two waves with different frequencies. If Hartlen and Currie's model does not permit beating behavior, then the two oscillators are in phase. Since velocity is out of phase with respect to displacement, then coupling via velocity allows a beating behavior.

Having compared our method with three existing models, the chapter is concluded next.

7.13 Discussion

While the importance of fluid–structure interaction has been well understood for many years, there exist no compelling analytical methods where the reduced-order models are derived from first principles. In the past few decades, few attempts to utilize variational principles in modeling FSI systems have had any success. These models were not directly obtained from variational operations and they required ad hoc assumptions. To overcome this difficulty, we extended Jourdain's principle for the modeling of FSI systems for a Newtonian incompressible viscous fluid. As examples, we considered the model problem first as a translating cylinder and then as an inverted pendulum (shown in Fig. 7.1), and obtained two types of reduced-order models, first in the form of a single governing EOM (SEOM), and then in the form of two coupled EOMs.

For the SEOM model, we used Benaroya and Wei's methodology to extend our energy rate equation for such systems. This method requires the pressure to be known at the surface of the structure. PIV and DPIV methods only estimate the velocity field. Thus, the pressure term is problematic. To obtain the pressure, Benaroya and Wei integrated the Navier–Stokes equation numerically. In our derivations, we neglect the pressure terms by considering them to be action and reaction forces. However, the pressure remains a requirement for the open sections of the control surface.

Our method, based on the important concept of generalized momentum in analytical mechanics, uses the rate of generalized momenta to obtain reduced-order coupled governing equations from the variational energy rate equation (extended JP). Depending on the type of equations required, two possible methods are those expressed by Eqs. 7.57, 7.58, and by Eq. 7.62.

For the model problem, we chose Eq. 7.62 and obtained two coupled equations, one a differential equation and the other an integral equation. We showed the

importance of boundary conditions and their implementation by obtaining two different possible reduced-order governing equations for the translating cylinder model problem (Eqs. 7.74 and 7.82).

The wake-oscillator models available in the literature are ad hoc models, obtained by guessing a function that can capture some characteristics of a system. Therefore, they do not provide any insights into the fluid dynamic parameters that can affect the outcome. Nevertheless, they are valuable for engineering applications. As an example, we considered the model proposed by Hartlen and Currie. Their *lift-oscillator* model captures many features of the structural response without addressing the fluid dynamics.

Referring to Eq. 7.116, the method developed in this chapter has the advantage that the resulting reduced-order model is expressed in terms of the kinetic energy of the control volume. Each of the terms in Eq. 7.116 has a specific meaning and can be traced back to the energy equation, and even further back to the Navier–Stokes equation.

There exist no reduced-order models in the literature that are obtained without an assumed lift or drag coefficient function. The reduced-order modeling method proposed here does not require any such ad hoc assumptions. The coupled equations are obtained directly from the energy equation by using a variational method based on first principles, but we recognize that the specific derivation of our actual flow-oscillator equations required a prior knowledge of the particular physical problem. While there are assumptions at this stage of the work, these are chosen based on a reading of experimental data. The primary contributions of this chapter are the general derivations surrounding Jourdain's principle and the formulation in Eulerian form, along with application to fluid–structure systems.

We expect that the method developed here can be extended to compressible flows and elastic structures, albeit with a major effort.

Our summary of the whole monograph is given in the next chapter.

References

1. Barrat J-L, Bocquet L (1999) Influence of wetting properties on hydrodynamic boundary conditions at a fluid/solid interface. Faraday Discuss 112:119–128
2. Bearman PW (1984) Vortex shedding from oscillating bluff bodies. Annu Rev Fluid Mech 16:195–222
3. Benaroya H, Wei T (2000) Hamilton's principle for external viscous fluid structure interactions. J Sound Vib 238(1):113–145
4. De Hart J, Peters GWM, Schreurs PJG, Baaijens FPT (2000) A two-dimensional fluid-structure interaction model of the aortic value. J Biomech 33(9):1079–1088
5. Dong P, Benaroya H, Wei T (2004) Integrating experiments into an energy-based reduced-order model for vortex-induced-vibrations of a cylinder mounted as an inverted pendulum. J Sound Vib 276(1–2):45–63
6. Gabbai RD (2006) Hamilton's principle for fluid-structure interaction and applications to the free-vibration of an elastically-mounted cylinder. PhD dissertation, Rutgers, the State University of New Jersey, New Brunswick, NJ

7. Gabbai RD, Benaroya H (2005) An overview of modeling and experiments of vortex-induced vibration of circular cylinders. J Sound Vib 282:575–616
8. Gabbai RD, Benaroya H (2008) A first-principles derivation procedure for wake-body models in vortex-induced vibration: proof-of-concept. J Sound Vib 312:19–38
9. Goldstein S (1969) Fluid mechanics in the first half of this century. Annu Rev Fluid Mech 1(1):1–29
10. Goldstein D, Handler R, Sirovich L (1993) Modeling a no-slip flow boundary with an external force field. J Comput Phys 105(2):354–366
11. Hartlen RT, Currie IG (1970) Lift-oscillator model of vortex induced vibration. J Eng Mech 96(5):577–591
12. Hocking LM (1976) A moving fluid interface on a rough surface. J Fluid Mech 76(04):801–817
13. Kundu PK, Cohen IM (2008) Fluid mechanics, 4th edn. Elsevier Inc., Oxford
14. Lamb H (1963) Hydrodynamics. Cambridge University Press, Cambridge
15. Lanczos C (1970) The variational principles of mechanics, 4th edn. Courier Dover Publications, New York
16. Layton W (1999) Weak imposition of "no-slip" conditions in finite element methods. Comput Math Appl 38:129–142
17. McIver DB (1973) Hamilton's principle for systems of changing mass. J Eng Mech 7(3):249–261
18. Millikan CB (1929) On the steady motion of viscous, incompressible fluids; with particular reference to a variation principle. Philos Mag Ser 7, 7(44):641–662
19. Mottaghi S (2015) Modeling vortex-induced fluid-structure interaction using an extension of Jourdain's principle. PhD dissertation, Rutgers, the State University of New Jersey, New Brunswick, NJ
20. Pit R, Hervet H, Leger L (1999) Friction and slip of a simple liquid at a solid surface. Tribol Lett 7(2–3):147–152
21. Sarpkaya T (2004) A critical review of the intrinsic nature of vortex-induced vibrations. J Fluids Struct 19(4):389–447
22. Tropea C, Yarin AL, Foss JF (eds) (2007) Springer Handbook of Experimental Fluid Mechanics, vol 1. Springer, Berlin
23. van Loon R, Anderson PD, van de Vosse FN (2006) A fluid-structure interaction method with solid-rigid contact for heart valve dynamics. J Comput Phys 217(2):806–823
24. Xing JT, Price WG (2000) The theory of non-linear elastic ship-water interaction dynamics. J Sound Vib 230(4):877–914
25. Zhu Y, Granick S (2002) Limits of the hydrodynamic no-slip boundary condition. Phys Rev Lett 88:106102

Chapter 8
Concluding Thoughts

The problem of fluid–structure interaction (FSI) has long been one of the great challenges in engineering. It is a crucial consideration in the design of many engineering systems such as offshore structures, skyscrapers, aircraft, and bridges. This monograph has focused on incompressible flows and bluff bodies. There is also a vast literature and research effort on compressible flows over aerodynamic bodies.

While the importance of the subject has been understood for well over a century, it has been only in the past few decades that efforts have been made to analytically model the general behavior of such systems. Parallel to analytical attempts, many experiments have been devoted to gathering data and interpreting such interactions. Generally, attempts have been made to model vortex-induced vibration (VIV) problems as few degrees-of-freedom (DOF) oscillatory models; therefore, they are referred to as reduced-order models.

Due to the complexity of the interactions between fluid and structure, in particular for vortex-induced vibration, a variety of efforts have been undertaken to explain the physics of this coupling. Initially, the efforts were experimental so that "reality" could be visualized, and then explained. Tremendous efforts have led to impressive results by numerous experimentalists along with extensive phenomenological understanding of this behavior. The practical needs of industry required more than just understanding, it required designs of structures and machines that could operate safely for long periods of time in fluid environments where complex interactions occur. For vortex-induced oscillations, this led to the need for design equations that were representative of the experimental data. Physical theory lagged experimental data, of course, but the need for governing design equations was there, resulting in the formulation of governing equations that qualitatively mimicked the data and could be made to fit the data in specific instances by the use of parameters. Such semi-empirical equations have formed the backbone of reduced-order modeling for VIV.

Only recently, analytical dynamics-based modeling of such problems has evolved with coupling to experimental data, resulting in various semi-analytical representations. Our monograph represents a line of work with the goal of laying a fundamental foundation for such reduced-order modeling. This effort is based on the variational

S. Mottaghi et al., *An Analytical Mechanics Framework for Flow-Oscillator Modeling of Vortex-Induced Bluff-Body Oscillations*, Solid Mechanics and Its Applications 260,
https://doi.org/10.1007/978-3-030-26133-7_8

principles of mechanics. In Chap. 2, we provided a representative review of the literature. While the review does not include all published works, of course, as there are thousands of such publications, we have endeavored to review the highlights of such work as exemplified by the better known papers. We believe that this chapter well represents the state of the art as it relates to the work presented in this monograph, emphasizing analytical approaches. There are numerous papers on experimental and numerical approaches to this class of problems, both of a fundamental nature, and with dozens of application-specific studies.

In Chap. 3, we summarized analytical mechanics. The analytical approaches are based on variational principles. The term variational is from the calculus of variations, the foundation for such techniques. An important advantage of the analytical method is that the equations of motion are coordinate independent, and the derivations of the governing equations proceed in parallel with a consideration of the boundary conditions. Newton's second law of motion is vectorial, and boundary conditions are generally considered separately from the derivations of the governing equations. We have included this chapter in order to provide the opportunity for the interested and motivated reader to gain the needed background for the remaining chapters of the book, and thus make the book relatively self-contained. We also introduce more advanced concepts related to Jourdain's Principle in Chaps. 6 and 7, as they are needed.

Chapter 4 summarizes our initial foray into this approach to the analytical modeling of VIV. Our motivation was to move beyond phenomenological approaches that, while valuable, are limited in their ability to explain VIV in terms of fundamental physical principles. This part of the work is based on Hamilton's Principle in conjunction with Reynolds Transport Theorem. Hamilton's principle in analytical dynamics is a great intellectual achievement. As with Lagrange's equations, Hamilton's principle is derived from the Principle of Virtual Work. Our work in this chapter is an extension of the fundamental work of McIver for systems of changing mass. In particular, the development by McIver was a successful attempt to model structures with internal moving fluid. We built on his ideas and extended Hamilton's principle for structures vibrating in an incompressible fluid. There were challenges, one of which was the definition of the control volume around the structure and its location and extension. Our result was a single energy equation for the structural vibration, coupled to experimental results.

Chapter 5 reexamines the approach taken in Chap. 4, again by utilizing Hamilton's Principle in conjunction with Reynolds Transport Theorem. After general derivations based on these, a transversely oscillating circular cylinder is modeled as a 2D problem. Terms in the derived equations are related to the various energies in the system, both fluid and structural. Two coupled governing equations of motion are derived, one for the fluid wake-oscillator and the second for the rigid structural dynamics. These general equations are then compared to wake- oscillator models that are well known: Krenk and Nielsen, Hall, Berger, and Tamura and Matsui. Nonlinear wake-oscillator models have been shown to be leading-order approximations for the vortex shedding instability from a fixed cylinder in uniform flow, while wake-body models have been shown to represent the same type of leading-order approximation for

forced oscillations of circular cylinders in uniform flows. These findings imply that these models have, at least to some degree, fluid dynamical origins. It is precisely because of these fluid dynamical origins that wake-body models have been successful.

However, by the very nature of being leading-order approximations to very complex interactions, they have limitations. The methodology presented in this chapter serves to address these. The fluid dynamical origins can be accounted for since the starting variational principle is rigorous. The limitations are accounted for because any assumptions made in reducing the variational principle are explicitly stated. It has been shown that the wake-body model derived from the proposed methodology shares many qualitative features with the three comparison models chosen from the literature. We can argue that the comparison models are special cases of our derived models. This follows from the fact that the derived model is found to involve terms that do not appear in the comparison models. These additional terms are, for the most part, the autoparametric terms. It is not the aim of this paper to weigh in on the issue of whether or not these terms should be retained. Suffice it to say that many authors have previously addressed the inadequacy of linear coupling terms in wake-body models. There are terms in the comparison models that are not captured in the derived model. This is simply a manifestation of the assumed forms in the derived equations. Subject to a different set of assumptions, these equations could conceivably be modified such that the "missing" terms appear in the derived model. It cannot be stressed enough that these modifications would need to be justified. This is, in essence, the embodiment of the advantage of the method presented in this chapter and this book generally: That while the wake-body models still contain arbitrary coefficients, their forms are arrived at by a line of reasoning, rather than a "hit or miss" approach.

We believe that this approach can be implemented in other fluid–structure interaction problems. The possibility of applying it to derive wake-body models for elastic structures in uniform and shear flows is something that is possible with much work. The current chapter was based on variational methods, where the variation was a virtual displacement. Based on these derivations, a flow-oscillator set of equations was formulated. In the next two chapters, a variational approach based on virtual velocities is formulated, where we first relate Lagrangian variables to Eulerian variables.

Chapters 6 and 7 are coupled, with the first laying the Jourdain's Principle basis for transforming Lagrangian variables and equations into an Eulerian frame of reference. First Lagrangian and Eulerian displacement fields are related. Then velocity fields, and then the time derivatives of the system properties are related. In order to set up a variational principle, it became necessary to relate variations in both frames of reference. Since virtual displacements are not easily suited to fluids, Jourdain's Principle is introduced and discussed as an alternative framework, and derived from d'Alembert's Principle. Jourdain's Principle is then derived for an Eulerian frame of reference. Then energy and energy-rate equations are derived in the Eulerian frame. The Rayleigh dissipation function is introduced and discussed, since we are interested in applications to incompressible but viscous fluids.

Chapter 7 begins with a summary of the key results from Chap. 6, as well as a summary of the key experimental results and the essential flow-oscillator mathematical models. The introduction of the structure into the fluid required a discussion of boundary conditions, in particular, the no-slip condition and how it can be introduced. Jourdain's Principle is extended for fluid–structure interacting systems. A general variational formulation for a control volume of a Newtonian incompressible viscous fluid and an internal general solid body is derived. It is then used to derive a single degree-of-freedom model of fluid–structure interaction, and then for a wake-oscillator model with two coupled equations. Two approaches are taken in order to show that depending on the assumptions made, a different set of equations is derived. This is acceptable, and demonstrates the power and usefulness of the variational framework that has been created. The key advantage over the phenomenological approaches is that instead of implicit assumptions, we are able to identify (and modify if necessary) the assumptions made explicitly. In order to compare the derived framework, with specific mathematical models, experimental results are used in order to reduce the general framework models to wake-oscillator models published in the literature. These are compared to the models of: McIver, Benaroya and Wei, and Hartlen and Currie.

While it is theoretically possible to extend the current work to compressible and/or elastic structures, this would be a significant endeavor and challenge. It is unclear what would be accomplished by doing this, but the theoretical issues to be resolved can be of interest more generally.

Index

S. Mottaghi et al., *An Analytical Mechanics Framework for Flow-Oscillator Modeling of Vortex-Induced Bluff-Body Oscillations*, Solid Mechanics and Its Applications 260,
https://doi.org/10.1007/978-3-030-26133-7